Control Engineering Perspective on Genome-Scale Metabolic Modeling

by

Andrew Louis Damiani

A dissertation submitted to the Graduate Faculty of
Auburn University
in partial fulfillment of the
requirements for the Degree of
Doctor of Philosophy

Auburn, Alabama
December 12, 2015

Key words: *Scheffersomyces stipitis*, Flux Balance Analysis, Genome-scale metabolic models, System Identification Framework, Model Validation, Phenotype Phase Plane Analysis

Approved by

Jin Wang, Chair, Associate Professor of Chemical Engineering
Q. Peter He, Associate Professor of Chemical Engineering, Tuskegee University
Thomas W. Jeffries, Professor of Bacteriology, Emeritus; University of Wisconsin-Madison
Allan E. David, Assistant Professor of Chemical Engineering
Yoon Y. Lee, Professor of Chemical Engineering

Abstract

Fossil fuels impart major problems on the global economy and have detrimental effects to the environment, which has caused a world-wide initiative of producing renewable fuels. Lignocellulosic bioethanol for renewable energy has recently gained attention, because it can overcome the limitations that first generation biofuels impose. Nonetheless, in order to have this process commercialized, the biological conversion of pentose sugars, mainly xylose, needs to be improved. *Scheffersomyces stipitis* has a physiology that makes it a valuable candidate for lignocellulosic bioethanol production, and lately has provided genes for designing recombinant *Saccharomyces cerevisiae*.

In this study, a system biology approach was taken to understand the relationship of the genotype to phenotype, whereby genome-scale metabolic models (GSMMs) are used in conjunction with constraint-based modeling. The major restriction of GSMMs is having an accurate methodology for validation and evaluation. This is due to the size and complexity of the models. A new system identification based (SID-based) framework was established in order to enable a knowledge-matching approach for GSMM validation. The SID framework provided an avenue to extract the metabolic information embedded in a GSMM, through designed *in silico* experiments, and model validation is done by matching the extracted knowledge with the existing knowledge. Chapter 2 provides the methodology of the SID framework and illustrates the usage through a simple metabolic network.

In Chapter 3, a comprehensive examination was carried out on two published GSMMs of *S. stipitis*, iSS884 and iBB814, in order to find the superior model

The conventional validation experiments proved to be unreliable, since iSS884 performed better on the quantitative experiments, while iBB814 was better on the qualitative experiments. The uncertainty of which model was superior was brought to light through the SID framework. iBB814 showed that it agreed with the existing metabolic knowledge on *S. stipitis* better than iSS884.

Chapter 4 showed that the errors in iBB814 were eliminated by refining iBB814 to construct a modified model known as iAD828. The SID framework was used to guide model refinement, which is typically a labor some and time intensive process. SID framework eradicates the trial-and-error approach, but rather has the power to uncover the reaction errors. iAD828 predicts xylitol production under oxygen-limited conditions, which is in agreement with experimental reports. This was a significant improvement, since iSS884 and iBB814 does not have this capability and now iAD828 can be used to properly engineer recombinant strains. Also the SID framework results of iAD828 show noteworthy improvement relative to iSS884 and iBB814.

The superior performance of iAD828 propelled the use of this model for strategies to increase ethanol production. Understanding cofactor balance during fermentation is crucial in obtaining high quality strains for ethanol overproduction. Recently much work has been done on cofactor imbalance of the first two reactions of xylose metabolism-xylose reductase and xylitol dehydrogenase. There is not a clear understanding in *S. stipitis* how the cofactor preference of xylose reductase affects the metabolism. The cofactor preference of xylose reductase was varied and an optimal phenotype was determined. Analysis from this guided *in silico* metabolic engineering strategies resulted in elevated production of ethanol. This information can be found in Chapter 5.

In Chapter 6, SID enhanced PhPP analysis was developed as a tool to overcome the limitations that PhPP analysis imposed. The power of this tool was shown by applying it to an illustrated example and an *E. coli* core model. Here the traditional PhPP analysis was unable to uncover the metabolic knowledge that the SID enhanced PhPP analysis was able to accomplish. The traditional PhPP analysis used shadow prices to determine the different phenotypes. This proved to be problematic for the *E. coli* core model. SID enhanced PhPP analysis was able to detect a "missing" phenotype that PhPP analysis failed to uncover. Also as the size of the metabolic model increases, the shadow price from PhPP analysis decreases to the point of having only miniscule meaning. Error was shown in the shadow price of the formate exchange flux. SID enhanced PhPP analysis provides a powerful tool for understanding metabolic phenotypes. Chapter 7 describes the conclusions and the future work of this study.

Acknowledgments

First and foremost, I like to thank Jesus who gave me new life in Him, who called me out of darkness and into the marvelous light while at Auburn. Thank you for the riches of grace and patience to complete this work: 2 Corinthians 12:9 "My grace is sufficient for you, for My strength is made perfect in weakness."

I would like to express my appreciation for my advisor, Dr. Wang, for her persistent support and her congenial concern throughout my graduate time. She is an exemplary mentor and always takes the time to have a meeting for discussion. Dr. He, for his patience and support when mentoring me on computational work and writing, awesome skills! Dr. Jeffries for his valuable discussion and guidance, Dr. David for his thoughtfulness and asking challenging questions, and to Dr. Lee and Dr. Goodwin for their support. I would also like to acknowledge Dr. Ogunnaike, who encouraged me in applying for graduate school, and Dr. Eden for recruiting me.

I would like to thank my group members: Hector Galicia, Meng Liang, Min Kim, Zi Xiu Wang, Kyle Stone, Matthew Hillard, Devarshi Shah, Alyson Charles, Jeff Liu, Tomi Adekoya and Rong Walburg for their support and valuable disscusions. Also I would like to thank the rest of my fellow graduate students and staff at Auburn.

Special thanks to my parents, Andrew Damiani and Mary Jo Damiani, for their sacrificing, love, and patience throughout the years. Also like to thank my sister and her brother-in law, Melissa and Stephen Merced, and brother Nick for their love and support. Also to my grandparents: Giselle and Vincent Damiani, and Ed and Carol Szumowski for their love and encouragement. Also to my brothers and sisters in Christ who helped me get my footing in my Christian walk. Jeff Cooling aka "the Guru" for his spiritual wisdom and guidance, and being an

exemplary disciple of Jesus. Thanks to: Jeremy and AnneCatherine Crompton for their friendship and encouragement, and to my church family at Fire and Grace Church. Thanks to: Peter and Louis Morchen for our great discussions at Burger King. Thanks to: the prayer group of Norma Stibbs for their love and unity, had many awesome times.

Table of Contents

List of Tables

List of Figures

Chapter 1: Introduction

1.1 Renewable energy derived from biomass

Fossil fuels impose major worldwide economic concerns and environmental pressures, due to there being a limited supply that needs to be able to foster an increasing energy requirement of the industrialized world, and the adverse effects of the production of greenhouse gases (Cherubini, 2010; Gupta and Verma, 2015). The strong dependency on petroleum based fuels intensifies the problem, where it accounts for 80% of the energy needs and 73% of carbon dioxide emissions worldwide. With the oil demand of world in 2013 being approximately 90 million barrels a day (Hufbauer and Charnovitz, 2009) and it is projected that in 2030 that it reaches 116 million barrels a day, with the transportation sector accounting for 60% of this total. Therefore there is an imperative mandate for alternative energy source (IEA, 2007). Using biomass as an energy source to produce biofuels provides an attractive options in following ways: (1) economic potential due to the increasing prices of fossil fuels, (2) provides a sustainable source for energy in the future, and (3) affords favorable environmental conditions due to no net carbon dioxide emissions and very low amount of sulfur (Balkema and Pols, 2015; Eisentraut, 2010; Sobrino and Monroy, 2010).

1.1.1 Production of sustainable fuels

Bioethanol is the primary transportation fuel substitute for gasoline. It has many favorable properties, one being that it comes from a renewable source and can be used as an octane enhancer, since it is a high octane fuel. On the environment spectrum, it has low toxicity, it is biodegradable, and minimal pollution is emitted. It also has the ability to diminish greenhouse gas emissions, where it has been shown to decrease greenhouse gas compared to

fossil fuels 18% and 88% when using corn derived and cellulosic feedstock respectively (Service, 2007). Also leading oil producing countries have a stronghold on importing countries, thus blending bioethanol with gasoline provides a greater fuel security for countries. Another benefit is that entirely new infrastructure is created that opens the doors for employment (Balat and Balat, 2009; Evans, 1997). The last couple of decades have shown an increasing inclination for bioethanol production with 31 billion liters in 2001 (Berg, 2001) to 39 billion liters in 2006 and it is projected to go to 100 billion liters in 2015 (Licht et al., 2006). The U.S. (United States) is the leading producer, and the U.S. Department of Energy (DOE) and the U.S. Department of Agriculture (USDA) have recently mandated that 36 billion gallons of biofuels be produced by 2022. The U.S. being the top producer in bioethanol is due to the strong governmental support, which started back in 1978 with the Energy Tax Act that granted tax credits for ethanol usage. Recently in 2007, congress passed the Energy Independence and Security Act, which mandated the supply of 12 billion gallons of bioethanol by 2010 and this would increase to 15 billion gallons for 2015. Figure 1.1 shows the production of biofuels, specifically hydrotreated vegetable oil (HVO) known as "green diesel", biodiesel, and bioethanol through the years of 2000 - 2013. Bioethanol remains the top biofuel being produced with 75% of the total biofuel production, and U.S. production is around 50 billion liters, where almost all was from corn feedstock. Brazil is the next largest producer; together the U.S. and Brazil produce 62% of the bioethanol in the world, from sugar cane and corn. European countries are getting involved, where the European Union has set similar goals as the U.S. (Cherubini, 2010).

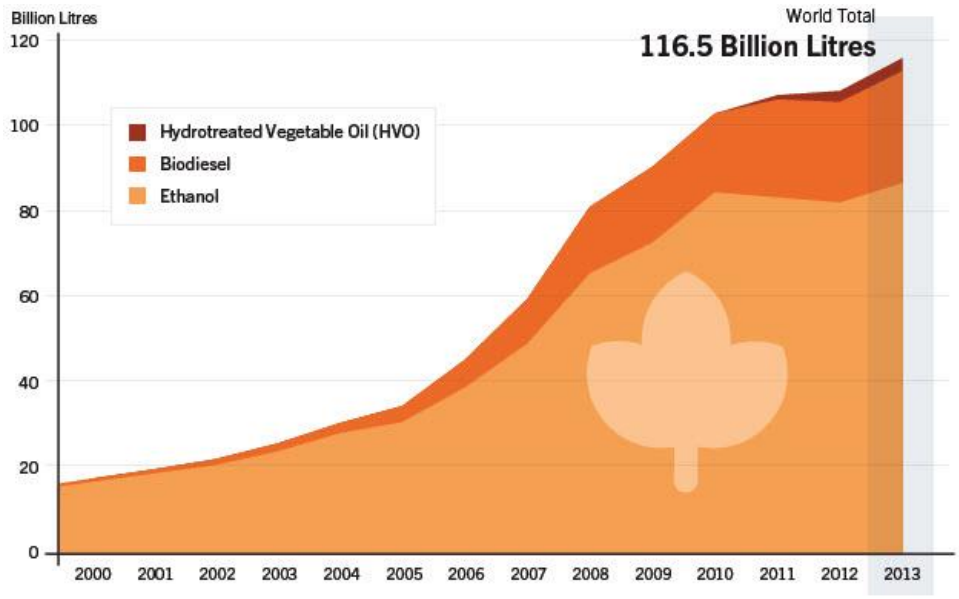

Figure 1.1: Global production of hydrotreated vegetable oil, biodiesel, and bioethanol for 2000 – 2013 (Global Status Report - REN21, 2014)

1.1.1.1 First generation biofuels

First generation biofuels are produced from feedstocks that are derived from food crops. Some of the commonly used raw materials are sugar cane, corn, animal fats, and vegetable oil (Naik et al., 2007). Conventional methods are used for production of first generational bioethanol, and production of first generation biofuels are considered a well-established industry. Despite the need to reduce greenhouse gas emission, first generational biofuels provides limited reduction (Collins, 2007). Another major drawback of first generation feedstocks is the competition with the food industry (Marris, 2006).

1.1.1.2 Second generation biofuels

This has brought the incipient of second generation biofuels, which are based on nonfood crops or crop resdiues. Unlike corn feedstock, which is composed of a starchy material, ligonocellulosic biomass comes from the fibrous part of plant that is non-starchy. Lignocellulosic

biomass are divided into five groups of feedstocks: 1) agricultural residues (leftover material from crops, such as corn stover and wheat straw); 2) forestry wastes (chips and sawdust from lumber mills, dead trees, and tree branches); 3) municipal solid wastes (household garbage and paper products); 4) food processing and other industrial wastes (black liquor, a paper manufacturing by-product); and 5) energy crops (fast-growing trees and grasses, such as switchgrass, poplar and willow) (Mansfield et al., 2006). Hexose and pentose sugars comprise about 50 – 80% of the carbohydrates in lignocellulosic biomass. The carbohydrates are biologically converted to bioethanol through fermentation (Mousdale, 2006). The carbohydrates are broken down in two groups, cellulose and hemicellulose. Cellulose is composed of linear glucose polymers that are β linked together. Hemicellulose is an extensive branched polymer that is comprised of five-carbon sugars: arabinose and xylose, and a six-carbon sugar: galactose, glucose, and mannose. There is a non-carbohydrate group, lignin, which provides the structural foundation of the plant, where this part cannot be fermented (Sindu et al., 2015).

Lignocellulosic biomass is known as a green gold raw material, because it has many advantages: (1) renewable and sustainable, (2) reduction of air pollutions that result from burning and rotting of biomass in fields, (3) alleviating greenhouse gases, (4) provides economic benefits locally through development and simulation, (5) halting energy dependence on countries that rely on importing oil, and (6) generating technical jobs (Bjerre et al., 1996). It has been calculated that lignocellulosic biomass has the potential to produce 442 billion liters of bioethanol, which is due having the world's largest renewable source of bioethanol (Hakeem, 2014). The two routes for conversion of lignocellulosic biomass to biofuels are done through thermochemical and biochemical conversion. Thermochemical conversion first involves the production of synthesis gas (blend of carbon monoxide and hydrogen) through gasification or

pyrolysis, then reformation of fuel through a catalytic process, such as the commonly used one of the Fischer-Tropsch reaction or by a biological reaction. Biochemical conversion involves first breaking down the sugar polymer to sugar monomers through pretreatment processing, and then microorganisms are used to ferment the sugar into biofuels (Mckendry, 2002). A recent study showed that production costs of second generation biofuels is two to three times more expensive than petroleum based fuel production costs (Balan, 2014).

1.1.2 Microbial strains for biofuels

Present research efforts focus on fermenting glucose and xylose. Cofermentation is one route that ferments the sugars simultaneously, and it is believed to have fewer costs then solely fermenting the individual sugars (Ohgren et al., 2007; Zhao et al., 2008). There are a collection of microorganisms available, such as *Saccharomyces cerevisiae*, *Scheffersomyces stipitis*, *Kluyveromyces marxianus*, *Candida shehatate*, *Zymomonas mobilis* and *Escherichia coli* (Gírio et al., 2010). Prokaryotes (*E. coli*) and lower eukaryotes are strains that have been used to produce ethanol from biomass feedstocks. Yeast has enhanced properties, because they have higher ethanol tolerance, resistance to contamination, growth at low pH, and have thicker cell walls (Jeffries, 2006). Also yeast has already been in industrial applications, therefore there is an established production facility (Hahn-Hägerdal et al., 2007).

1.1.2.1 Saccharomyces cerevisiae

S. cerevisiae is the most common microorganism used for ethanol production, which is accomplished through fermentation of hexose sugars. When pentose sugars are present in the feedstock the productivity diminishes. It has the capability only to metabolize phosphorylated pentose sugars, like ribose 5-phosphate, but assimilation of pentoses such as xylose is problematic. *S. stipitis* and *E. coli* can natively ferment xylose (Kim et al., 2007), however

ethanol productivity is still low so metabolic engineering to create recombinant strains, such as *S. cerevisiae* or *Z. mobilis* has been a major focus on research (Joachimsthal and Rogers, 2000; Martín et al., 2002; Jeppsson et al, 2002). The recombinant strains also have limitations, mainly the one being a cofactor imbalance of the engineered pathway of the xylose metabolism, which are xylose reductase and xylitol dehydrogenase (Roca et al., 2003; Matsushika et al, 2008; Matsushika et al, 2009a). Another approach that has been used to bypass the cofactor imbalance problem is to implement xylose isomerase; however most strains metabolized in this manner have low xylose consumption rates (Van Maris et al, 2007; Kuyper et al, 2005; Karhumaa et al., 2007). Other factors limiting xylose utilization in recombinant cells are inefficient xylose transporters (Kötter and Ciriacy, 2003), lower capacity for the pentose phosphate pathway (PPP) (Walfridsson et al, 1995) and inappropriate regulatory mechanisms (Jeffries and Van Vleet et al., 2009). Efforts were made to increase the affinity of the xylose transporter. Sut1 increased ethanol productivity; however capacity of the yeast was still limited (Katahira et al., 2008). Knowledge of how yeasts such as *S. stipitis* natively ferment xylose is still limited in terms of relavant biochemical reactions, thermodynamics, enzyme kinetics, and mechanistic understandings. These factors all limit the extent to which could be the main reason that metabolic engineering can succeed. Part of my research focuses on using genome-scale metabolic modeling of *S. stipitis* to gain a better understanding of its cellular metabolism in order to understand which key steps to change in order to improve both *S. stipitis* and engineered *S. cerevisiae* for lignocellulosic ethanol production. Specifically, a genome-level understanding of xylose metabolism in *S. stipitis* would help identify effective strategies for metabolic engineering design.

1.1.2.2 Scheffersomyces stipitis

1.1.2.2.1 Introduction

Scheffersomyces stipitis previously called *Pichia stipitis* that was first isolated from the excreted frass of wood-ingesting beetles (Shi et al., 2002). Due to its important role in the production of lignocellulosic ethanol, a second generation biofuel (Naik et al., 2010), *S. stipitis* has drawn increasing research interest in the last few decades (Eisentraut, 2010). Currently efficient pentose utilization remains one of the economic barriers to producing cost-effective lignocellulosic ethanol through biological conversion (Margeot et al., 2009), and *S. stipitis* has the highest native capacity to ferment xylose into ethanol (Van Dijken et al., 1986; Du Preez et al., 1989). The concentration of ethanol can be up to 61 g/L in media containing xylose and nutrients (Slininger et al., 2006). The ethanol yield spans between 0.31 – 0.48 g/g, which makes this yeast strain one of the most effective for xylose fermentation for ethanol production (Agbogbo and Coward-Kelly et al., 2008). Other reports that used a fed-batch setup were able to produce up to 47 g/L of ethanol from xylose (Du Preez et al., 1989) with ethanol yields of 0.35 – 0.44 g/g (Hahn-Hägerdal and Pamment, 2004). With most of the carbon flux going toward ethanol production, this leaves very little xylitol being produced. Nonetheless, fermentation rate is still low on xylose when compared to glucose fermentation of *S. cerevisiae*.

It also has the capability to digest a spectrum of sugars that in are comprised in the hydrolysate, such as glucose, galactose, mannose, and cellobiose. A recent study showed that *S. stipitis* outperformed industrial strains in terms of fermentation (Matsushika et al., 2009b). Under xylose fermentation conditions most of the carbon flux goes to ethanol production, while a small amount goes to xylitol. The fermentation rate of glucose on *S. cerevisiae* is a lot higher than xylose fermentation of *S. stipitis*. *S. stipitis* can produce ethanol at a yield close to the

theoretical maximum under oxygen-limitation. In addition, low ethanol tolerance and no growth under anaerobic condition are also limitations that complicate utilization in industrial applications. (Du Preez et al., 1989; Grootjen et al., 1990; Shi & Jeffries, 1998). To address these limitations, attempts have been made to improve the xylose uptake rate of *S. stipitis* under oxygen-limitation, as well as to introduce enzymes for the xylose fermentation pathways from *S. stipitis* into engineered *S. cerevisiae* (Johansson & Hahn-Hagerdal, 2002; Karhumaa et al., 2005). Many metabolic engineering and adaptive evolution strategies that been used with *S. cerevisiae* (Harhangi et al., 2003; Sonderegger et al., 2004). However, these attempts have not been entirely successful (Kotter & Ciriacy, 1993; Eliasson et al., 2000; De Deken, 1966; Bruinenberg, et al. 1983), which is due redox balance, lack of sugar transports and digestion genes. It is important to gain further understanding to either improve it as a host strain or even as a gene provider for other strains.

1.1.2.2.2 Xylose metabolism

Figure 1.2 shows the xylose metabolism for *S. stipitis*, where xylose is converted into xylitol by a xylose reductase (XR), that has the ability to use both NADH and NADPH with an activity ratio of 0.7 for NADH/NADPH (Jeffries et al., 1999). Xylitol is then oxidized to xylulose by xylitol dehydrogenase (XDH), where NAD is used as the cofactor. NADP is given a dashed line, since there have been reports that this cofactor has also been used for this reaction (Matsushika et al., 2008; Yablochkova et al., 2004). Xylulose is phosphorylated to xylulose 5-phosphate, which then enters the non-oxidative branch of PPP. The end products of the non-oxidative branch of PPP is carbon compounds of fructose 6-phosphate and glyceraldehyde 3-phosphate (Jeffries, 2006).

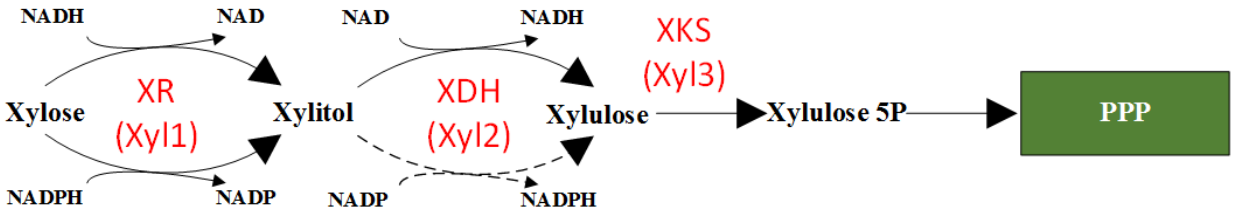

Figure 1.2: Xylose Metabolism of *S. stipitis*. Red letters without parenthesis represent enzymes. Red letters in parenthesis represent genes that encode the enzymes

Diauxic behavior is shown for *S. stipitis*, when glucose and xylose are incorporated into the same media (Grootjen et al., 1991; Slininger et al., 2011). Gene expression data showed that Xyl1, Xyl2, and Xyl3 were upregulated for both oxygen-limited and aerobic conditions, when xylose was used as the substrate, but these genes where downregulated when glucose was used (Jeffries et al., 2007). When Xyl1 expression was increased (Takuma et al., 1991) this resulted in enzymatic activity increasing two-fold, however this had no profit for ethanol production (Dahn, et al., 1996).

1.1.2.2.3 Oxygenation characteristics

S. stipitis is a Crabtree-negative yeast, meaning that the presence or abesnce of oxygen regulates the fermentation rate, as opposed to the Crabtree-positive yeast (*S. cerevisiae*), where fermentation is regulated by the level of the sugar concentration present, such as glucose, making it independent of oxygen uptake rate. Respiro-fermentative behavior is seen only under oxygen-limited condition for *S. stipitis* (Klinner et al., 2005). Under oxygen-limitation, the enzymes pyruvate decarboxylase and alcohol dehydrogenase show increased activity (Skoog and Hahn-Hägerdal, 1990; Skoog et al., 1992) as well as their corresponding genes (Jeffries et al., 2007). These are the enzymes that catalyze reactions for ethanol production, where pyruvate decarboxylase (Pdc1 and Pdc5) and alcohol dehydrogenase (Adh1 and Adh2) are shown in Figure 1.3. Alcohol dehydrogenase (Adh1) was ten times higher under oxygen-limited than

aerobic conditions. Also pyruvate decarboxylase was activated when oxygen levels switched from aerobic to oxygen-limited condition (Cho and Jeffries, 1999).

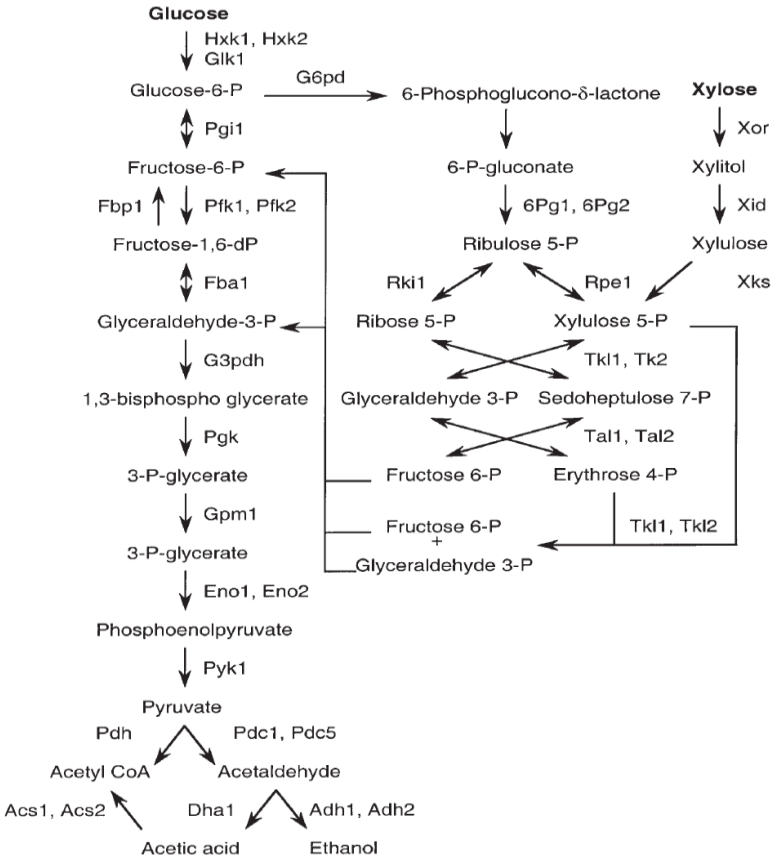

Figure 1.3: Outline of glucose and xylose metabolism in yeasts. Enzyme designations are from assigned loci in *Saccharomyces cerevisiae* or *Pichia stipitis*. *Hxk1* Hexokinase P1; *Hxk2* hexokinase PII; *Glk* glucokinase; *Pgi* phosphoglucose isomerase; *Pfk* phosphofructokinase 1; *Fba*fructose-bisphosphate aldolase; *Tdh* (G3p) glyceraldehyde-3-phosphate dehydrogenase; *Pgk* 3-phosphoglycerate kinase; *Gpm* phosphoglycerate mutase; *Eno* enolase (2 phosphoglycerate dehydratase); *Pyk* pyruvate kinase; *Pdc* pyruvate decarboxylase; *Adh* alcohol dehydrogenase; *Pdh* pyruvate dehydrogenase; *Dha* aldehyde dehydrogenase; *Acs* acety l-coenzyme A synthetase; *6Pg* 6-phosphogluconate dehydrogenase, decarboxylating; *Rpe* ribulose-phosphate 3-epimerase; *Rki* ribose-5-phosphate isomerase; *Tkl* transketolase; *Tal* transaldolase; *Xor* xylose (aldose) reductase; *Xid* xylitol dehydrogenase; *Xks* xylulokinase (Jeffries and Shi, 1999)

One major disadvantage of *S. stipitis* is its inability to grow even though it can produce ethanol under anaerobic conditions (Bruinenberg et al., 1994). It is still unclear why *S. stipitis* cannot grow under anaerobically it needs only minimal oxygen present to achieve optimal ethanol production conditions (Cho and Jeffries, 1999).

1.1.2.2.4 Electron Transport Chain (ETC)

S. stipitis has the standard respiration machinery along with alternative respiratory components that allow the transfer of electron transfer to occur with or without coupling to ATP production. This allows electrons either to enter through Complex I for mitochondrial NADH oxidation or through the external or internal non-proton translocases of NADH or NADPH. A clear depiction of this can be seen in Figure 1.4. At the terminal of the ETC is Complex IV, which is part of the standard machinery or an alternative oxidase, which can be used under very low oxygen conditions and only on xylose not glucose.

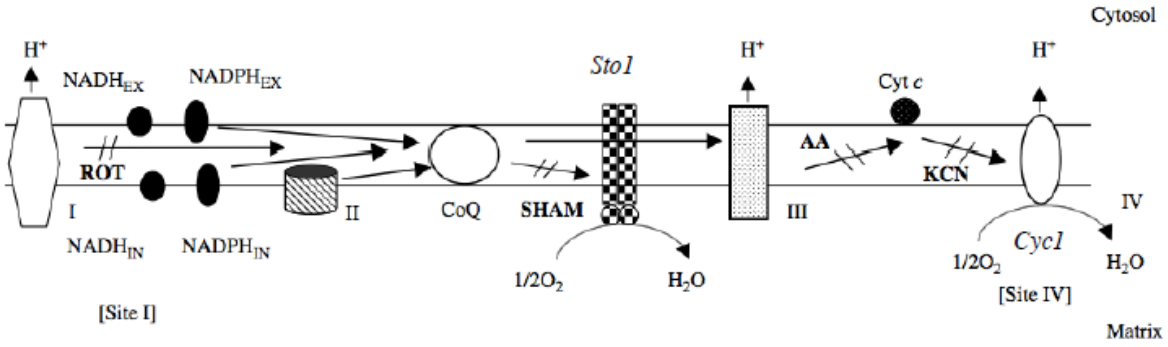

Figure 1.4: ETC of *S. stipitis.* Contains the proton-translocating NADH dehydrogenase (Complex I); internal and external non-proton translocating NADH dehydrogenase ($NADH_{IN}$, $NADH_{EX}$);internal and external non-proton translocating NADPH dehydrogenase ($NADPH_{IN}$, $NADPH_{EX}$); succinate dehydrogenase (Complex II); ubiquinone complex (CoQ); SHAM-sensitive alternative terminal oxidase, cytochrome bc1 (Complex III); cytochrome *c* (Cyt *c*); and cytochrome *c* oxidase (Complex IV) (Joseph-Horne et al., 2004)

1.2 System biology

System biology is a rapidly growing field of study that was primary developed in academia, and is gaining popularity in commercial industries (Ideker et al., 2001). Biological systems present a great challenge to researchers due to the great complexity. Conventionally, scientists have adopted the reductionist point of view, which states that examining the simplest parts of a system are critical in understanding the system as a whole. The system is broken down

to the most reduced state of complexity, and then worked upward in complexity. This separates biological systems into specific parts, and then studies them under isolation (Aderem, 2005; Gallagher et al., 1999). Then once all the parts are understood, then the pieces can put together like a puzzle and the understanding of the system can be established. Scientists have devoted their lives to study one particular gene or protein in order to gain knowledge. Although success has been achieved using the reductionist approach, however when applied to biological system there are great limitations, such that it is a grueling process that makes it pretty much impossible to unravel the mechanisms involved. This is mainly due to gaining a higher level of understanding the interactions between genes, proteins, and their effect on the metabolism. The development of innovative technologies has brought about the production of complex biological datasets. Genetic synthesis technologies and sequencing has emerged in biological research that have reaped the sequencing the first genome and genome-scale metabolic models. System biology provides a comprehensive functionality of biological systems through studying the behavior and relationship of the biological elements simultaneously (Barabasi et al., 2004). Mainly it utilizes a holistic approach from which quantitative data can be extracted. Rather than examining an individual biological entity, it allows for studying the flow of information as a whole on all biological levels, such as on proteins, genomics, regulation networks, and metabolically (Spencer et al., 2008; Tang et al., 2005; Palsson, 2002). Figure 1.5 provides the general concept of system biology versus the traditional reductionist approach. The reductionist approach investigates the individual components of a system, such as the components of a computer network or genes of a specific organ. System biologists integrate information together globally, therefore instead of performing their research to the far left as the reductionist, their research proceeds to the right, where the whole system can be studied together (Galitski, 2012).

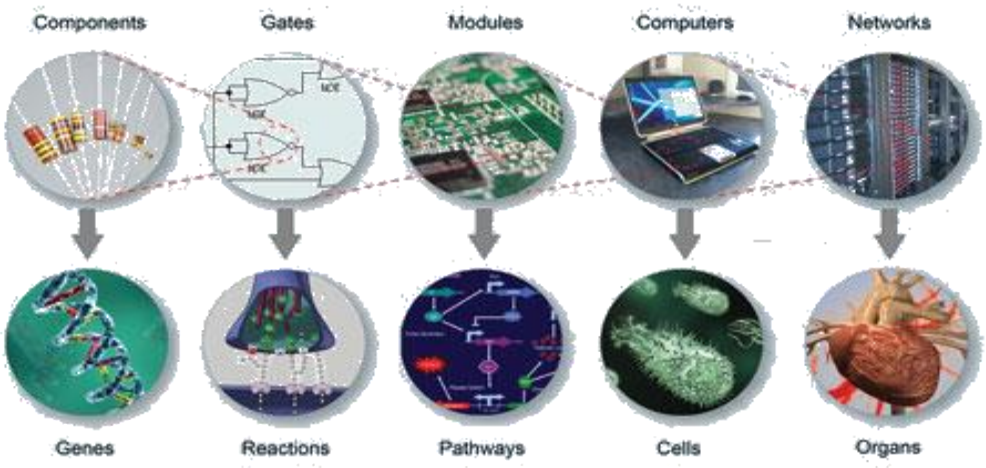

Figure 1.5: Integrative approach of system biology (Galitski, 2012)

A recent paper (Sauer et al., 2007) stressed on the significance of using a system-level approach for studying cellular metabolisms: "Rather than a reductionist viewpoint (that is, a deterministic genetic view), the pluralism of cause and effects in biological networks is better addressed by observing, through quantitative measures, multiple components simultaneously, and by rigorous data integration with mathematical models. Such a system-wide perspective (so-called systems biology) on component interactions is required so that network properties, such as a particular functional state or robustness, can be quantitatively understood and rationally manipulated".

My work used an integrative perspective by comparing, refining, and validating genome-scale metabolic network models in order to gain a systems level understanding. Let us now look at the literatue of the modeling techniques that were employed.

1.2.1 Modeling of metabolic networks

The primary goal of modeling metabolic networks is to deconstruct the complex information of the microorganism into a computational framework with the objective of predicting the cellular phenotype from the genotype (Bordbar et al., 2014). Compared to other biological systems, metabolic networks are relatively well understood, which is attributed to

knowledge of the metabolites and the reactions that convert the biological constituents. The structure of the metabolic reactions and their connectivity is established, thus we have a fundamental understanding of the metabolic network. Metabolism is a key player for regulating the homeostasis of organisms, because of the constant substrate being taken up and conversion into building blocks for biomass and by-products. The size of metabolic networks is typically classified under two camps: central carbon metabolism models (~80 reactions, 40 metabolites) and genome-scale models (>1000 reactions, >500 metabolites) (Krömer et al., 2014). Commonly, there are four primary approaches are taken to model metabolic networks (Stelling, 2004; Zomorrodi et al., 2012): 1. Interaction-based networks – neglect the stoichiometry of the network and emphasize the network connectivity. The main assumption is that the system remains stationary. Are used in large-scale systems (transcription of genes and proteomics) that focus on how information is propagated. 2. Dynamic models – ordinary differential equations with kinetic information are used to depict the dynamics of the system. 3. Stoichiometric models – examine fundamental cellular biochemistry that is used to quantify the intracellular mass flow at steady state, where the system is used to be stationary. 4. Stoichiometric models with kinetic information – very similar to type 3 (Stoichiometric models) except now there exists at least one kinetic equation that relates the concentration of a metabolite to the reaction rate.

Modeling that is done in biological systems usually invokes theory-based models, which involves a particular input with a set equation for a specific solution. These types of models are troublesome, because the kinetic parameters need to be determined through expensive experiments (Famili et al., 2005; Segrè et al., 2003). The accurate determination of the parameters can be often questioned, due to the variability and difficulty of their measurements. Parameters need to be quantified usually have significant error or have not even been measured

under *in vivo* conditions (Rizzi et al., 1997; Teusink et al, 2000; Vaseghi et al., 1999; Wright and Kelly, 1981). Due to these shortcomings, there has been no genome-scale theory-based model constructed (Jamshidi and Palsson, 2008). Another common approach is cybernetic modeling, which finds unknown or hidden parameters through various assumptions (Kompala et al, 1984; Young et al, 2008).

Constraint-based models are known as structural metabolic network modeling, which does not require kinetic parameters, but rather defined constraints. They are based on the micro-evolutionary principle that biological systems have adapted to diverse environments over time and as they multiply they are not identical to their parent cells. Palsson describes the phenomena this way: "To survive in a given environment, organisms must satisfy myriad constraints, which limit the range of available phenotypes. All expressed phenotypes resulting from the selection process must satisfy the governing constraints. Therefore, clear identification and statement of constraints to define ranges of allowable phenotypic states provides a fundamental approach to understanding biological systems that is consistent with our understanding of the way in which organisms operate and evolve (Palsson et al, 2006)". Constraint-based models have been around for more than 25 years, since 1986 (Fell and Small, 1986), peaking in the mid-1990's (Savinell and Palsson et al, 1992; Varma et al., 1993) they were used to compute the metabolic flux distribution and cellular growth.

The different types and magnitudes of the constraints will limit the cellular function. A recent paper summarizes the types of constraints in four categories: fundamental physico-chemical constraints, topological constraints, environmental constraints, and regulatory constraints.

(i) Physico-chemical constraints: Numerous constraints govern cellular metabolism and are known as hard constraints. Hard constraints are the laws of conservation of mass, energy, and thermodynamics (Covert et al, 2001; Edwards et al., 2002). These constraints will not change with the environmental pressures.

(ii) Topological constraints: This deals with the crowding of molecules inside the cell. For instance, the length of a bacterial genome is on the magnitude of 1000 times the length of the cell. Thus this means that the DNA must be crammed tightly, but fully accessible in order to be unraveled into cellular machinery.

(iii) Environmental constraints: These constraints are time and condition dependent. Examples of these constraints are availability of nutrients, pH, temperature, and osmolality

(iv) Regulatory constraints: These constraints are different from the three types described above, because they are self-imposed constraints. They can change based on the evolutionary conditions and can vary with time. These constraints are used to eradicate suboptimal phenotype states and improve fitness. Recently, there are regulatory constraints based on transcriptional levels of genes (Reed et al., 2012).

Constraint-based models have become popular among researchers, because they operate under steady-state conditions and only need the network stoichiometry. This has brought about a myriad of tools/algorithms developed for modeling metabolic networks. The main ones are: flux balance analysis (FBA) (Varma et al., 1993; Edwards et al., 1999) metabolic flux analysis (MFA) (Schilling et al, 1999; Varma and Palsson, 1994) elementary mode analysis (EMA) (Schuster et al., 1999), extreme pathway analysis (EPA) (Schilling et al, 1999), robustness analysis (RNA) (Edwards and Palsson, 2000), phenotype phase plane analysis (PhPP) (Edwards et al., 2002), minimization of metabolic adjustment (MOMA) (Segrè et al., 2002), flux variability analysis (FVA) (Mahadevan and Schilling, 2003), and regulatory on-off minimization (ROOM) (Shlomi et al., 2005). More than 100 methods have been developed to predict and analyze metabolic activity through constraint-based models. Figure 1.6 shows the phylogenetic tree of them.

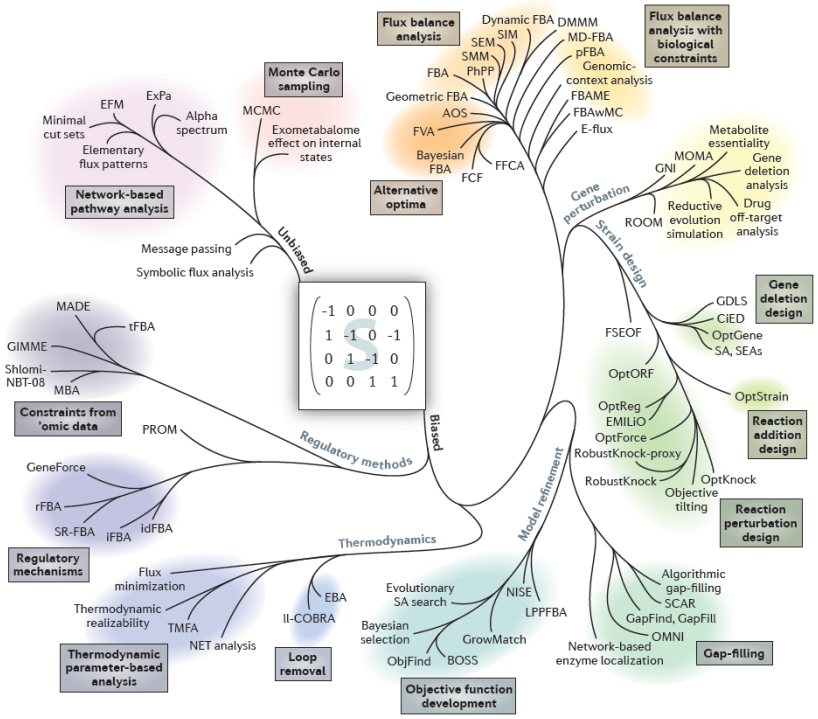

Figure 1.6: Phylogenetic tree of constraint-based tools (Lewis et al., 2012)

Modeling techniques discussed above compute static metabolic states. However, there are disadvantages: the cell's dynamic behavior cannot be determined, there are difficulties on implementing cellular regulation, and most experiments are done in batch and fed-batch cultures, where a dynamic model is required (Antoniewicz, 2013; Kauffman et al., 2003). Presently, the dynamic behavior is modeled through three modeling techniques, which are kinetic modeling, cybernetics, and dynamic FBA. For kinetic modeling and cybernetics require parameters that need to be fitted through designed experiments (Raman and Chandra, 2009; Smallbone et al., 2010). Dynamic FBA is an extension of FBA, however it does require empirical substrate equations, such as using michaelis-menten kinetics (Hanly and Henson, 2011; Hjersted and Henson, 2009). Dynamic modeling is not examined in this work, but is a future step that is needed to improve model prediction.

1.2.2 Flux Balance Analysis

Flux balance analysis (FBA) is a powerful technique that was developed in 1993 (Varma and Palsson, 1993). It was the first optimization-based tool for determining the metabolic flux distribution (Varma and Palsson, 1994). The metabolic network is treated as a linear programming problem, and an objective function, typically growth rate, is used to calculate an optimal solution. Reversibility data for reactions are used for the lower and upper bounds in order to constrain the reaction fluxes, which are the variables in the problem. The other constraints are the extracellular uptake rates of the substrates, such as carbon and oxygen source. This method is used calculate the flow of metabolites in a metabolic network, metabolite of interest (Orth et al., 2010). There are currently more than 35 organisms that have metabolic network models developed, and high-throughput technologies allow the construction of many

more each year, thus FBA is extremely important tool for gaining biological knowledge in these models (Gianchandan et al, 2010; Orth et al, 2011; Schellenberger et al., 2011).

As previously discussed, FBA doesn't require kinetic parameters, but it uses well defined constraints based on fundamental laws of nature. However, there are limitations to this, such that it does not calculate metabolite concentration (Lee et al., 2006). Also the focus is solely on the metabolism, so it does not incorporate regulatory effects of genes or enzyme activity (Ramakrishna et al, 2001). Because it is a steady-state approach, it only uses time-invariant substrate and nutrient consumption rates, thus it is only uses prediction from continuous experiments.

A simplified metabolic network model of 4 reactions and 3 metabolites is displayed in Figure 1.7 to demonstrate how FBA is carried out. This can be thought of a network flow problem in the field linear programming, where the metabolites are nodes and the reactions are the edges. The next section will discuss how genome-scale metabolic network models are construction, but briefly these are generated from an annotated genome and other biochemical and physiological databases. The reconstruction process is extensive, such that it can take months or years to complete (Thiele and Palsson, 2010; Henry, et al., 2010). A mass balance is prescribed on each metabolite in the network and is written in the form of a stoichiometric matrix (S). The rows and columns represent each unique reaction and metabolite, respectively. Each column entry represents the stoichiometric coefficient of each metabolite. The sign determines whether a metabolite is consumed or produced, a positive sign is production and a negative sign is consumption. If the metabolite is not present in the reaction the entry receives a zero. The stoichiometric matrix is mass balanced, meaning the total consumption and production each metabolite is balanced at steady state. It is common for the reactions to exceed the number of

metabolites. This becomes an underdetermined problem, meaning that there is infinite number of solutions. Here the key assumption of a steady state system is made which transforms this from a dynamic problem into a static one. This assumption is justified the assumptions that (1) intracellular metabolites reach thermodynamic equilibrium orders of magnitude faster than enzyme level change or cells double, and (2) in constrast to metabolite flux, intracellular metabolite concentrations change minimally in response to physiological changes in the cell because they are largely determined by enzyme affinities rather than reaction rates. As a result, metabolite levels are balanced kinetically and thermodynamically at each flux. The x term represents the metabolite concentration, where this is shown in the derivative with respect to time, and the v is the matrix of fluxes of individual reactions combined. FBA lessens the computational load by assuming a steady state, where, such is turned into a time-invariant problem, which is essentially like solving for the null space.

Using the assumption of a steady state is a generally acceptable practice in systems biology, which eliminates the convoluted system dynamics of metabolism that takes into consideration the kinetics and enzyme activities. As stated above the justification stems from the fact that the metabolite levels are highly transient relative to the cellular growth and the extracellular environmental changes. Studies showed that the metabolic transients only last a couple of minutes, therefore the metabolic fluxes are in a quasi-steady state in comparison to the growth and process transients (Varma and Palsson, 2004).

From there the reactions are constrained, that are primarly in the pickup and output reactions, such as substrates, oxygen, and byproducts. Intracellular reactions can be constrained if there is supporting experiment information, such as through ^{13}C labeled experiments of the metabolic flux (Sauer, 2006; Wiechert, 2001). The variable v_i represents an individual reaction,

where it is constrained between a lower bound α_i and an upper bound β_i. Implementation of constraints generates a solution space of an n dimensional polytope, which is the allowable solution space of flux distributions. Ingrafting constraints is why researchers have named this approach, constraint-based metabolic models (Llaneras and Picó, 2010).

The final step is to determine an objective function in order to pinpoint a unique solution in the feasible space of the polytope. In the early years of FBA, there were many objective functions selected (Pramanik and Keasling, 1997; Varma and Palsson, 1994), however then the maximization of the biomass objective function emerged as the main one, which it is the stoichiometric yield for biomass. It is contains in equation format the building blocks that make up the biomass component. It has been determined that flux through the biomass reaction rate is directly proportional to the growth of the organism (Stephanopoulos et al., 1998). The micro-evolution principle is applied, which states that surviving microorganisms have gained an advantage over the competing microorganisms by growing in more of an effective way. Therefore optimization guides cellular decision making.

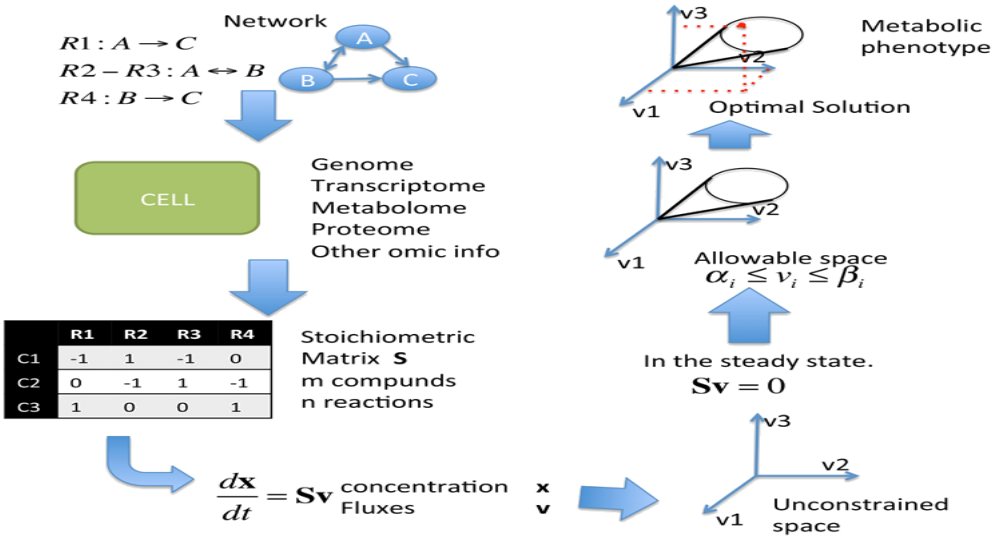

Figure 1.7: FBA construction on a simplified metabolic network model (Patiño et al., 2012)

The biomass growth reaction is based on experimentally determined biomass components (Feist et al., 2010; Schuetz et al., 2007). Other maximization objective functions are metabolite synthesis (Montagud et al., 2010) and a plural objective scheme of biomass and metabolite synthesis (Burgard et al., 2003; Pharkya et al, 2004). In constrast, the minimization objective functions are: redox power, (Knorr et al., 2007), ATP formulation (Knorr et al., 2007; Vo et al., 2004), and nutrient uptake (Segrè et al., 2002).

There are numerous of software tools that carry out FBA, such as the COBRA toolbox (Becker et al., 2007) that is coded in Matlab. Others are Pathway tools (Paley et al., 2012), BioMet toolbox (online usage) (Cvijovic et al., 2010) and OptGene (offline usage) (Patil et al., 2005; Rocha et al., 2008)

1.2.3 Genome-scale metabolic models (GSMMs)

Genome-scale metabolic models (GSMMs) provide a relationship between the genotype and phenotype; they provide a holistic view of the cellular metabolism. Once validated, GSMMs provide a platform to effectively interrogate cellular metabolism, such as characterizing metabolic resource allocation, predicting phenotype, and designing experiments to verify model predictions, as well as designing mutant strains with desired properties (Liu et al., 2010; Oberhardt et al., 2009). More importantly, GSMMs allow systematic assessment of how a genetic or environmental perturbation would affect the organism as a whole (Becker et al., 2007).

GSMMs were developed in the 1990's due to the emergence of sequencing whole genomes (Schilling et al., 1999). The first GSMMs were achieved in the organism of bacteria for *H. influenza* (Schilling and Palsson, 2000) and *E. coli* (Edwards and Palsson, 2000). However, there were metabolic models before this, starting with Fell and Small (1986), Mavrovouniotis

and Stephanopoulos (1992), and Savinell and Palsson (1992), however these models did not contain all the reactions in the genome due to the lack of sequencing technology. The price of sequencing entire genomes has been reduced in recent years, and this has opened the door for metabolic reconstructions (Henry et al., 2010).

Developing a reliable GSMM is comprised in four steps: (1) network reconstruction, (2) manual curation and building mathematical model, (3) model validation using experimental data, and (4) refinement of the model by iterations between computational and experimental parts. An annotated genome must be supplied to reconstruct a GSMM. Genes account for metabolic functions and draft reconstructions are constructed, which tell us the relationship between genes, reactions, and metabolites.

Figure 1.8 depicts the biochemistry hierarchy staring from genomics to metabolomics. The GSMMs that are used in this work only gather information from the genome, and does not take into account data from transcriptome, proteome, and metabolome. The study of the transcriptome allows researchers to draw information about the gene expression patterns (Marioni et al., 2008; Mockler and Ecker, 2005; Wang et al., 2009). Proteomics looks at the quantification of protein concentrations, where this is commonly measured through mass spectrometry (Gstaiger and Aebersold, 2009; Sabido et al., 2012). Information from metabolome and fluxome provides information that is closest in depicting what is happening in the cellular state. The metabolome measures all the intracellular and extracellular metabolites, such as lipids and amino acids either over time or under a given condition (Scalbert et al., 2009).

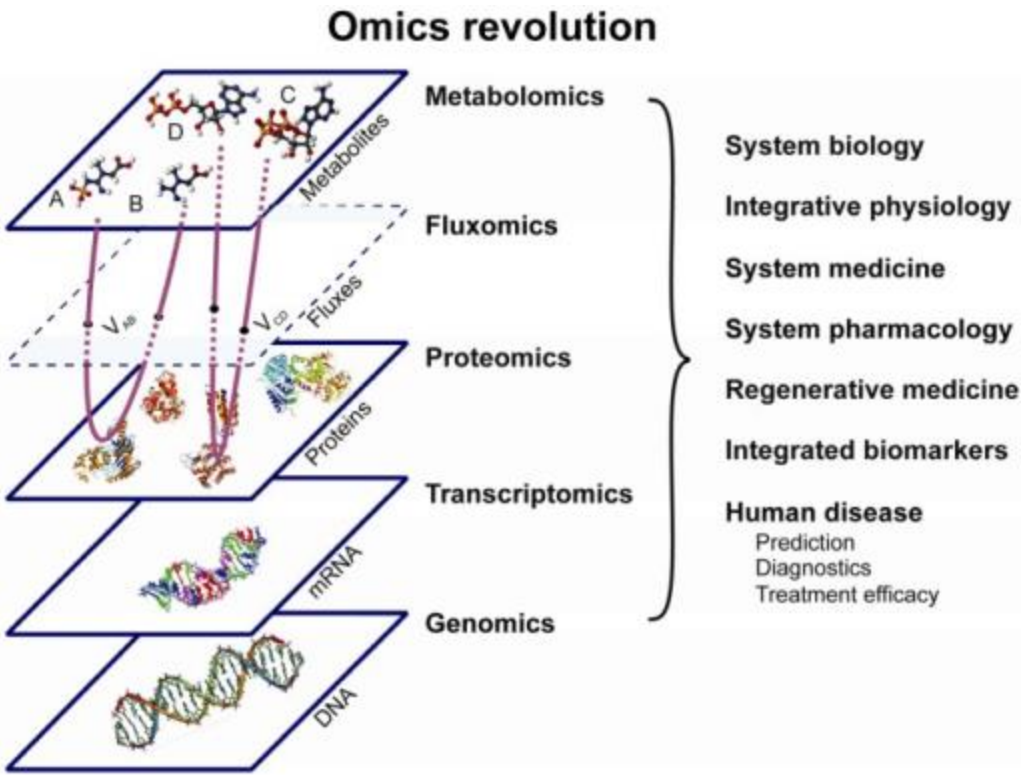

Figure 1.8**:** Plurality of levels for reconstruction of GSMM (Nemutlu et al., 2012)

Fluxomics provides the rate of metabolic reactions at the scale of the network. Again mass spectrometry provides a steadfast way to detect these metabolites. Fluxomics is done through isotope labeling, where then metabolic flux analysis is applied to determine the rate of metabolite conversion (Krömer et al., 2009; Sanford et al., 2002). There have recently been the developments of "next-generation" models that include these omics measurements with other advances, such as protein translocation in the cell membrane, protein structures in enzymes, and enzyme production costs (King et al., 2015).

Metabolic databases provide a plethora of ways to map a gene to a reaction. BRENDA (Schomburg et al., 2002), MetaCyc (Karp et al., 2002) and KEGG (Kanehisa and Goto, 2000) are commonly used ones. It is important to have a vast amount of diverse sources in order to avoid the presence of false negatives and false positives. A standard procedure for the

reconstruction process has been published (Feist et al., 2009: Thiele and Palsson, 2010). Literature papers and textbooks also provide a valuable source of knowledge about reactions and enzymes, such as EC numbers, reaction localization, reaction reversibility, and gene association. It is important to have strain specific information.

Next, gap filling is needed to balance out the metabolites, where they can balance out stoichiometries or cofactor usage. The stoichiometric matrix is then formulated, and constraints are defined. The biomass reaction equation is found by knowing the relative amounts of lipids, amino acids, carbohydrates, and nucleic acids. Computational analysis is then carried through FBA and these simulation results are compared with validation experiments. There are various validation experiments: comparing production rates, lethal reactions, and omics experiments, such measuring fluxes. Gaining information on the exchange reactions are boundary parameters, and this constrains the model to be operating in experimental regions. Our recent work provides another validation approach that looks at how metabolic pathways response as the system is perturbed. Here qualitative information is extracted and this can be compared with established claims (Damiani et al., 2015).

Overall the reconstruction process can be thought as assembling a jigsaw puzzle, where the pieces of the puzzle are supplied, but the problem lies in fitting everything together. This results in this being an iterative process, where there are many repetitive steps for model refinement. The pieces of the puzzle can be viewed as the genomics, physiological and biochemical data and putting the pieces together using gap filling strategies of experimental data and computational analysis. Figure 1.9 exhibits the workflow for constructing a high quality GSMM.

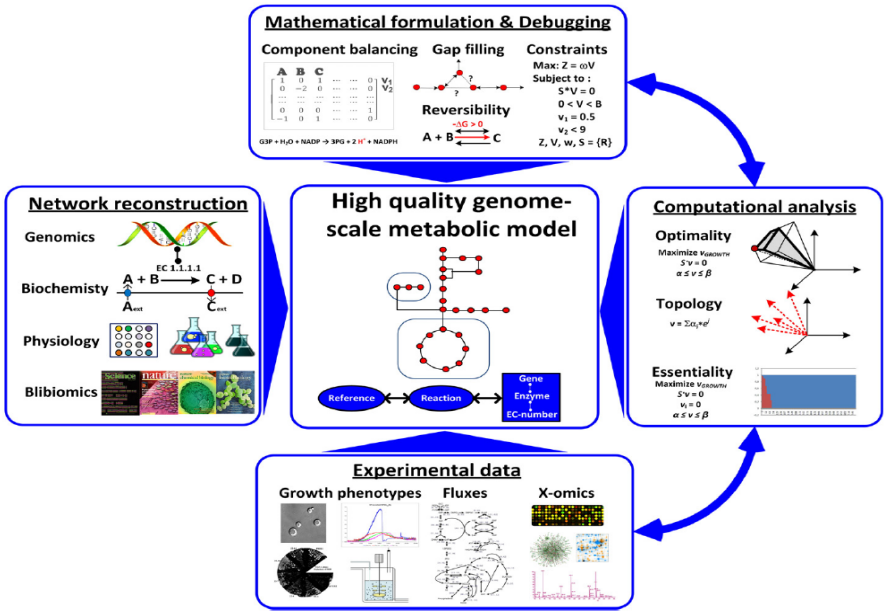

Figure 1.9: Process for formulating high quality genome-scale models (Thiele and Palsson, 2010)

Once a GSMM has been validated and there are a plethora of applications: investigating hypothesis-driven discovery, study of multi species interactions, contextualization of high-throughput data, and guidance of metabolic engineering (Kim et al., 2012; Oberhardt et al., 2009; Österlund et al., 2012).

Table 1.1. Success of GSMMs for production of biofuels. Ethanol: *E. coli* (Anesiadis et al., 2008), *S. cerevisiae* (Bro et al., 2006; Mahadevan and Henson, 2007) and *Z. mobilis* (Lee et al., 2010). Butanol: *E. coli* (Ranganathan et al., 2010; Lee et al., 2011), C. acetobutylicum (Borden et al., 2010; Lütke-Eversloh and Bahl, 2011), and *L. brevis* (Berezina et al., 2010).

Biofuels	Organism	Application
Ethanol	E. coli	Ethanol and higher alcohol production
	S. cerevisiae	Improving ethanol production
	Z. mobilis	Ethanol and succinic acid production
Butanol	E. coli	1-butanol production and tolerance
	C. acetobutylicum	Improving butanol tolerance and production
	L. brevis	Reconstruction of metabolic pathways for n-butanol production

GSMNM has shown to be an avenue for success in recent years in term of metabolism engineering, where Table 1.1 displays how GSMNM were used to improve production of a biofuel of interest.

Most of our work will focus on assessing (Chapter 3), refining GsMNM (Chapter 4), and providing metabolic engineering strategies (Chapter 5). Figure 1.10 demonstrates the iterative process of GSMM, and how they can be used to overproduce a desired compound. Biologists today are more focused on how they can use GSMM for hypothesis driven experiments. In order to driven carbon fluxes for overproduction of a specific metabolite, there has to be a rewiring of the metabolic network. In the last 15 years, there have been tools that have developed for this purpose, such as Optknock (Burgard et al., 2003), OptGene (Rocha et al., 2008), and OptStrain (Pharkya et al., 2004). These tools allow for bi-level optimization, which allows for optimization of the desired product that is subject to optimization of the biomass formation. Optknock finds genes to delete, while OptGene utilizes evolutionary principles to find mutations. OptStrain not only finds gene deletions, but genes can be added to the network. OptForce (Ranganathan et al., 2010) provides either amplification or reduction of reaction fluxes for overproduction of a desired production.

Even through this work there is still a challenge involved for rational strain design, since there can be multiple solutions, thus it does not imply that a unique solution exists. A tool known as flux variability analysis (FVA) calculates the maximum and minimum allowable fluxes through each reaction; this provides researchers with the robustness of each reaction (Gudmundsson and Thiele, 2010). Another aspect to consider is the genes expression and fluxes are not always linear to each other (Ranganathan et al., 2010). Looking at the regulatory mechanisms will definitely extract this non-linear relationship (Daran-Lapujade et al., 2007).

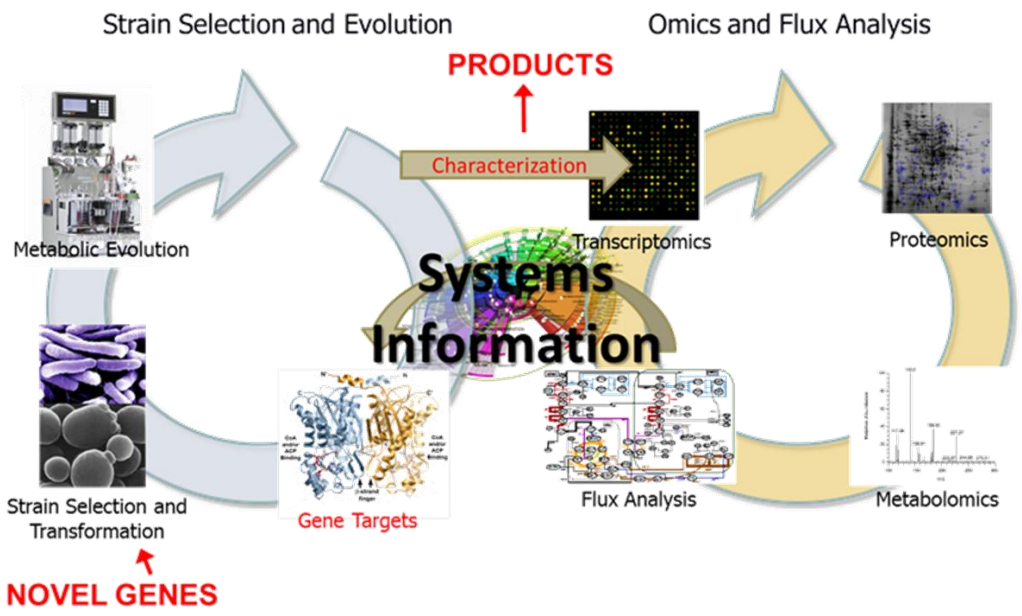

Figure 1.10: Flow path of work of GsMNM for metabolic improvement of a desired compound. (Iowa State University)

Chapter 2: System identification based framework

2.1 Introduction

In microbial metabolism, hundreds and even thousands of network reactions are involved. Existing approaches, such as elementary mode analysis (EMA) and flux balance analysis (FBA), can provide detailed flux distributions under different conditions and therefore provide descriptions of different phenotypes (Lewis et al., 2012). However, due to the model complexity, simply comparing different quantitative flux distributions is very difficult to pinpoint the potential errors contained in the network model. In addition, it is challenging to extract underlying mechanistic insight, such as the key reactions that govern a phenotype, interdependency of the key reactions that govern a phenotype, and key metabolic differences between two phenotypes from the numerical results. It is worth noting that these qualitative interpretations are most desirable and valuable for biologists, as they are straightforward to understand, and can be easily integrated into existing knowledge for different applications, such as mutant design. To address these challenges, a system identification (SID) based framework is proposed to extract biological knowledge embedded in a GSMM by performing designed *in silico* experiments. The extracted knowledge is then compared with existing knowledge for model validation and refinement.

2.2 Procedure

System identification (SID) is the science of building (or reverse engineering) mathematical models of dynamic systems from observed input-output data. In the proposed framework, we extended the concept of "model" to "knowledge" embedded in a system. Our aim

is to extract biological knowledge from a cellular metabolism (i.e., the system), where a GSMM serves as the simulator of the system to provide input-output data. The flow diagram of the proposed SID framework is shown in Figure 2.1, which involves the following three major steps.

1) *In silico* experiments are designed to perturb the GSMM;
2) Multivariate statistical tools are applied to extract knowledge such as how perturbation propagates & affects different pathways/subsystems;
3) The extracted knowledge is then visualized and compared with existing knowledge for model assessment.

Many multivariate statistical analysis tools (*e.g.*, principal component analysis (PCA) (Wold et al., 1987), partial least squares (PLS) (Wold, 1985), fisher discriminant analysis (FDA) (Scholkopft and Mullert, 1999), support vector machines (SVM) (Hearst et al., 1998) etc.) can be used to extract knowledge from the high dimensional data generated from the designed *in silico* experiments. In this work, PCA is chosen because it serves the purpose of finding how a perturbation propagates through a linear network and extracting the correlations among different fluxes. The biological knowledge embedded in the network model is extracted through the PCA loadings, which will be illustrated in more detail later. It is worth noting that because the metabolic network is linear, if only one degree of perturbation is introduced within a series of *in silico* experiments, one principal component (PC) is sufficient to capture 100% of the variation, provided that all *in silico* experiments are in the same phenotype. Here, the same phenotype means that the series of experiments does not result in saturation (*i.e.*, flux reaching its upper/lower limit) nor network structure changes (*i.e.*, activation/deactivation of reactions). Under this condition, the variations among different reactions can be completely captured by the loading of a single PC. Therefore, by examining the loading, we can identify how the introduced

perturbation propagates through the whole network and what reactions or subsystems are affected the most by the perturbation.

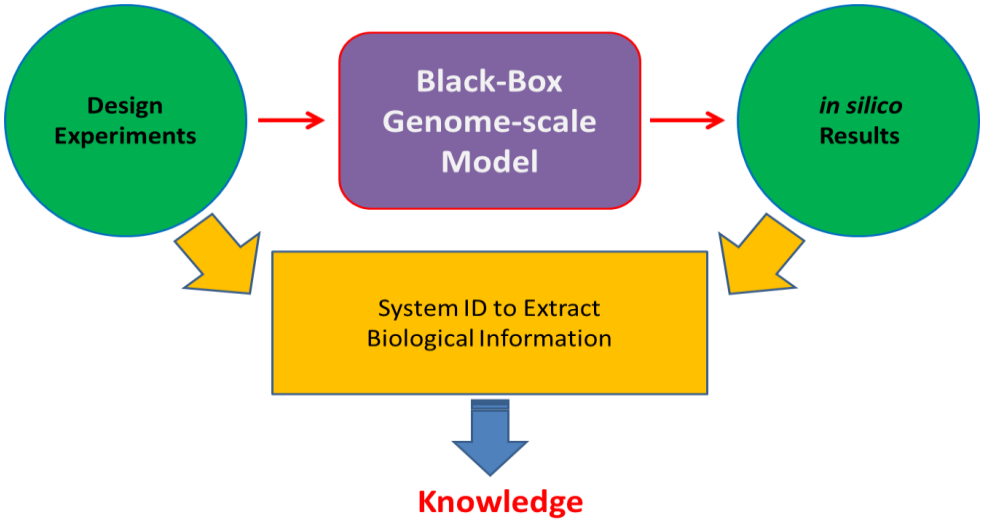

Figure 2.1: System identification based framework

2.3 Illustrative example

A simple network is constructed as shown in Figure 2.2. The network consists of 5 metabolites and 9 reactions, which are listed in Table 2.1. Among all reactions, 3 are external reactions and 6 are internal reactions. The corresponding stoichiometric matrix S is shown in Equation 2.1, in which rows correspond to the metabolites, while columns represent the reactions. The constraints we consider are: $0 \leq re1 \ldots . re9 \leq Inf$.

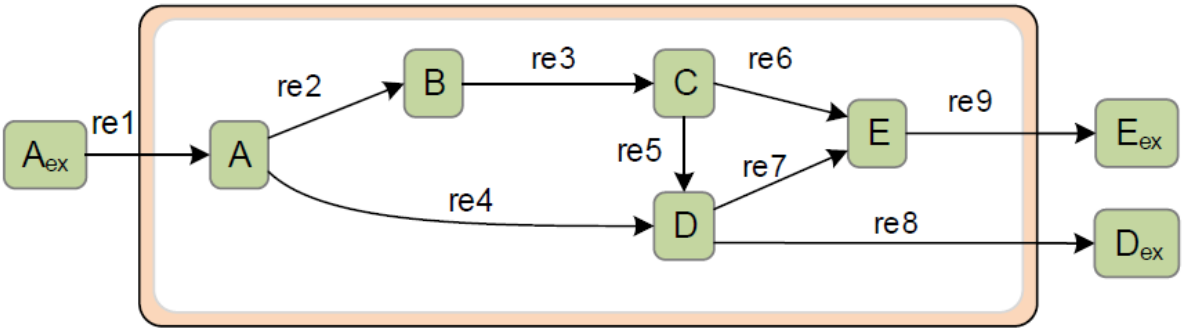

Figure 2.2: Reaction network scheme

Table 2.1: Internal and exchange reactions

Internal reactions		Exchange reactions
re2: A $\rightarrow$ B	re5: C $\rightarrow$ D	re1: $A_ex \rightarrow$ A
re3: B $\rightarrow$ 0.5 C	re6: C $\rightarrow$ 2 E	re8: D $\rightarrow D_{ex}$
re4: A $\rightarrow$ 2 D	re7: 0.5 D $\rightarrow$ E	re9: E $\rightarrow E_{ex}$

$$S = \begin{bmatrix} 1 & -1 & 0 & -1 & 0 & 0 & 0 & 0 & 0 \\ 0 & 1 & -1 & 0 & 0 & 0 & 0 & 0 & 0 \\ 0 & 0 & 0.5 & 0 & -1 & -1 & 0 & 0 & 0 \\ 0 & 0 & 0 & 2 & 1 & 0 & -0.5 & -1 & 0 \\ 0 & 0 & 0 & 0 & 0 & 2 & 1 & 0 & -1 \end{bmatrix} \quad (2.1)$$

Two case studies have been used here. The first one is to maximize production of metabolite D as the objective function of FBA, the second one picks maximal production of metabolite E as the objective function. For both cases, we investigate how the flux distribution would be acted if we increase the pickup rate of substrate A. In particular, we would like to identify what reactions are acted most significantly if pickup rate of A increases.

2.3.1 Case study 1: Objective function: maximal flux of re8 (production of D)

In this case study, we first conduct a series of 100 *in silico* experiments by varying the flux of re1 (pick up rate of A) from 2 to 4 mmol/gDCW/hr with a step size of 0.02. This set of experiments results in a 9 x 101 data matrix, with each column represents the 9 reaction fluxes for a given substrate pick up rate. We then perform PCA on the data matrix, which confirms that one principal component (PC) captures 100% of the variance contained in the data matrix. The scaled loading of the PC is plotted in Figure 2.3. With increased substrate pickup rate (which is scaled to be 1 as the basis), only re4 and re8 are affected with a scale of 1 and 4, which indicates that flux of re4 increases with the same amount as that of re1while flux of re8 increase 4 times the amount of increase in flux of re1. It is worth noting that a negative loading in this case would indicate a decreased ux. Figure 2.4 visualizes the analysis result by highlighting the fluxes that are affected by increasing flux of re1.

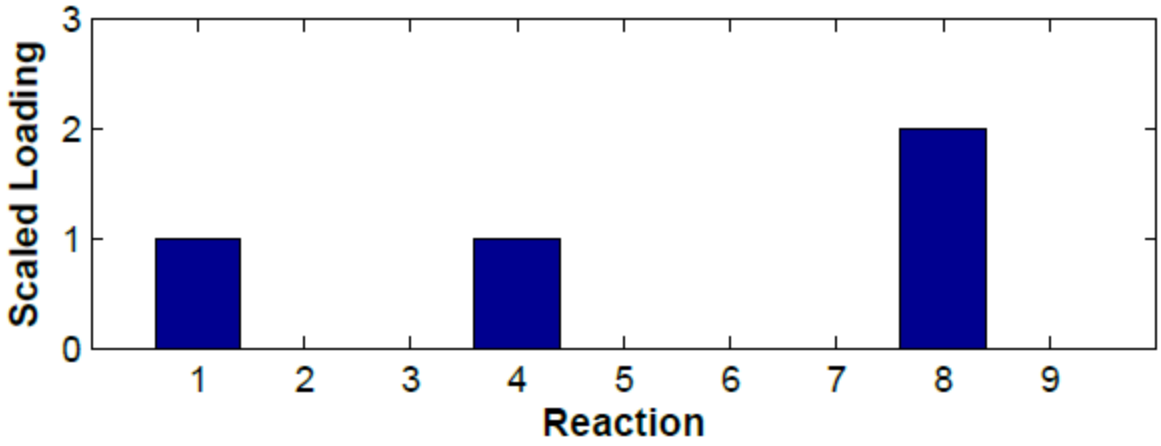

Figure 2.3: Scaled PCA loading for case study 1

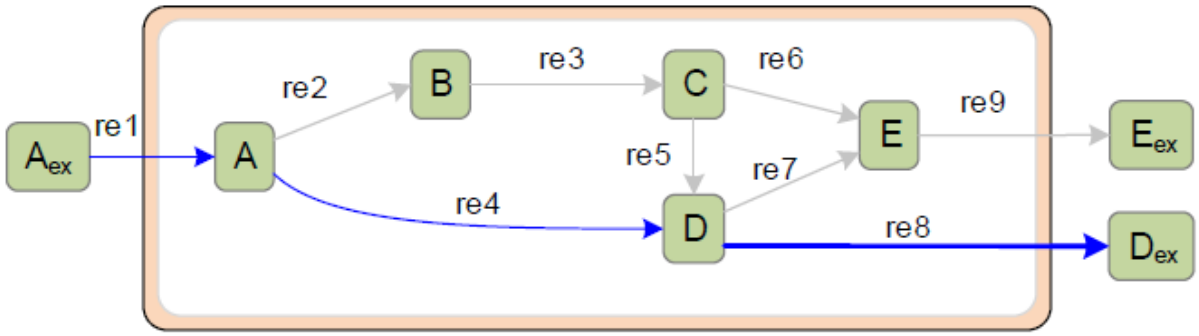

Figure 2.4: Visualization of the analysis results for case study 1. The reactions that are affected by increasing flux of re1 are highlighted in blue. The line thickness is proportional to its loading.

2.3.2 Case study 2: Objective function: maximal flux of re9 (production of E)

In this case study, similar steps as in case study 1 were carried out, with the only difference being in the objective function of FBA. In this case study, the objective function is to maximize the production of E. The PC loading and network visualization are plotted in Figure 2.5 and Figure 2.6.

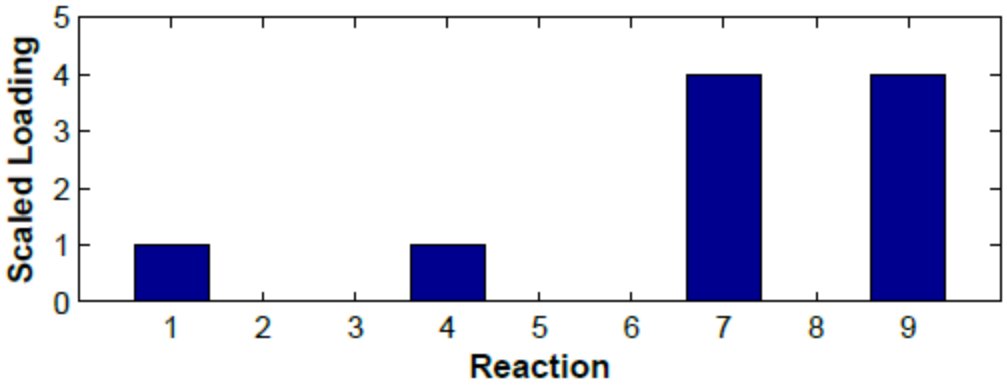

Figure 2.5: Scaled PCA loading for case study 2

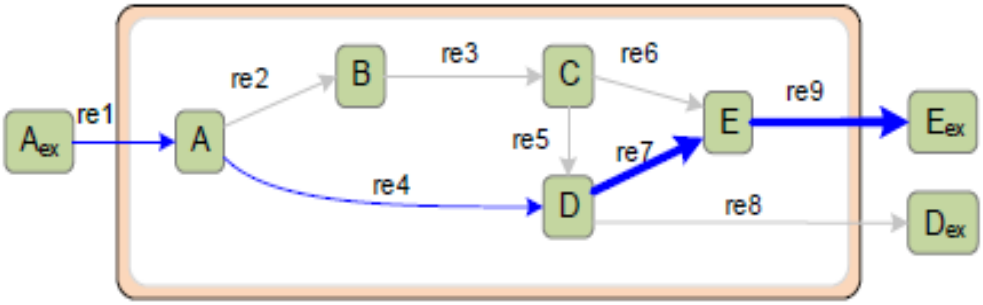

Figure 2.6: Visualization of the analysis results for case study 2. The reactions that are affected by increasing flux of re1 are highlighted in blue. The line thickness is proportional to its loading.

Both case studies show that even though the "hypothetical cell" has an alternative route to produce D and E, i.e., the one with intermediate metabolite C, it does not choose the alternative route because the route does not maximize the objective function. This is due to the difference in stoichiometric coefficients (A → 0.5 C → 0.5 D while A → 2 D for the chosen route). If the alternative route were chosen, less product would be produced. This illustrative example shows that the proposed method can systematically identify the reactions that would be affected by the introduced perturbation (e.g., increased substrate pickup rate in this case) without going through the detailed examination of the network stoichiometry. Such examination is nontrivial even for relatively small network models, such as central carbon metabolic networks,

and quickly becomes infeasible when the size of the network increases. But with the proposed method, we can easily examine how a perturbation would affect the whole network and identify the key reactions that are affected the most by the perturbation.

Chapter 3: Comprehensive Evaluation of Two GSMMs for *S. stipitis*

3.1 Introduction

The complete genome of *S. stipitis* has been sequenced (Jeffries et al., 2007), which provides the foundation for genome-scale metabolic network reconstruction. Based on the sequenced genome, several metabolic network models have been published recently (Caspeta et al., 2012; Balagurunathan et al., 2012; Liu et al., 2012; Liang et al., 2013). Among them, two genome-scale models: iSS884 (Caspeta et al., 2012) and iBB814 (Balagurunathan et al., 2012) represent significant steps forward in gaining a systematic understanding of cellular metabolism of *S. stipitis*. For metabolic network models, it is clear that the quality of the model determines the outcome of the application. Therefore, it is critically important to determine how accurate a metabolic network model is, particularly for a genome-scale model, in describing the microorganism's cellular metabolism. Currently model validation is done primarily through wet lab experiments, i.e., comparing model predictions with experimental measurements. Due to the cost and technical difficulties associated with getting intracellular measurements, most experimental measurements are limited to cross membrane fluxes such as substrate uptake rates, production secretion rates, and cell growth rates. However, due to the scale and complexity involved in GSMMs, a good agreement between measured and computed cross-membrane fluxes does not necessarily indicate that the model quality is high. Therefore, new methods are needed to effectively evaluate the quality of GSMMs. In this work, we propose system identification (SID) based framework to examine metabolic network models in a systematic way. First, the SID framework is applied to extract qualitative biological knowledge embedded in GSMMs, which is difficult, if not impossible, to be obtained through existing methods. Then the extracted knowledge is compared with the existing knowledge for model quality assessment or validation.

3.2 Materials and Methods

The materials that were used were two genome-scale model, iSS884 and iBB814. The genome-scale metabolic models were evaluated by flux balance analysis (FBA), in which the COBRA toolbox (Schellenberger et al., 2011) was used. SID framework was used for model validation. Manual examination of the two genome-scale models was carried out by comparison of the reaction subsystems.

3.2.1 Two published genome-scale models: iSS884 and iBB814

iSS884 (Caspeta et al., 2012) was constructed semi-automatically by integrating automatic reconstruction with *S. cerevisiae* as a reference framework and manual curation and modification. iBB814 (Balagurunathan et al., 2012) was constructed manually by following a published protocol (Thiele and Palsson, 2010) for generating a high-quality genome-scale metabolic reconstruction. iSS884 includes 1332 reactions, 922 metabolites and 4 compartments; iBB814 includes 1371 reactions, 644 metabolites and 3 compartments. More detailed comparison can be found in Appendix A1. Both models have significant experimental validations and both performed well in matching the model predictions with some experimental measurements.

3.2.2 *In silico* experiments

The genome-scale metabolic models were evaluated by flux balance analysis (FBA), in which the COBRA toolbox (Schellenberger et al., 2011) was used. For all the simulations, the objective function was biomass growth. The upper limits of xylose and oxygen uptakes were varied based on the preselected conditions, while the other exchange compounds (NH^{4+}, H^{+}, $SO4^{2-}$, Pi^{2-}, H_2O, Fe^{2+}) were given the option to enter and exit the network freely, with upper and lower bounds of -1000 to 1000 mmol/gDW·hr. The final metabolic products (CO_2, ethanol, acetic acid, etc.) were allowed to exit the system freely, where the reaction flux was constrained

to 0 – 1000 mmol/gDW·hr, which prevents product uptake. The growth associated maintenance energy was set to 2.6 mmol/gDW·hr (Balagurunathan et al., 2012). This setup was applied to all *in silico* simulations for both models.

3.2.3 Phenotype phase plane (PhPP) analysis

Phenotype phase plane (PhPP) analysis (Edwards et al., 2002; Bell and Palsson, 2005) is an extension of FBA that allows the study of metabolic genotype-phenotype relation. Two substrate parameters are varied independently, such as oxygen and carbon substrate, where the optimal flux distributions are calculated for all points in the selected plane. There are a finite number of optimal metabolic flux maps in the plane, which is known as a phenotype phase. Phenotype phases are each fundamentally distinct based on how model optimally chooses to use certain pathways. Each phenotype is generated by calculating shadow prices of the metabolites throughout the plane. Shadow price is a linear programming term used to define the sensitivity of a parameter on the objective function, and can be calculated from the dual solution in a linear programming problem. In this case, the parameter is the metabolite, and the objective function is the growth rate. Therefore in each phenotype, each metabolite will have a constant value, and are different in other phenotypes. Phenotype phase plane (PhPP) analysis was performed on iSS884 and iBB814 in order to gain a global view on the growth and the production of ethanol and CO_2, with xylose and oxygen as the two independent variables. The phenotypes were specified by color.

3.2.4 Conventional point-matching using experimental data

We also carried out experimental validations in a traditional way, which consists of both quantitative and qualitative validations. For quantitative validation, the substrate (xylose, glucose, and oxygen) uptake rates were set to be the same as the experimentally operated value,

then the model predictions of the production secretion rates (CO_2, ethanol, cell growth) were compared with the experimental reported values to assess the model accuracy. For qualitative validation, the validation experiments for inhibition and mutants were implemented by removing relevant reactions from the network models, and then the predictions of the modified models were compared with reported experimental outcomes, where the results were evaluated by checking if there was cell growth or product secretion.

3.2.5 System identification (SID) framework

As already discussed, SID framework was used to take heavily computation quantitative results that come from prepared *in silico* experiments, and extracted embedded biological knowledge through PCA. The results are then visualized through metabolic colored maps. Being qualitative in nature, this allows for biologist to easily interpret this information and make system guided decisions.

3.2.6 Manual Examination

The published models were written in different metabolites labeling schemes, so the first step was to convert iSS884 metabolites to the naming formulation of iBB814. Different reactions were categorized by subsystems and pathways, where the reactions of the two models were compared by subsystems/pathways to assess their similarities and differences. The KEGG database was used to obtain strain specific information on different reactions. Finally, the components and stoichiometry of the biomass growth equation were compared.

3.3 Results and Discussion

As discussed earlier, the two published models represent significant steps forward towards a better systems level understanding of *S. stipitis'* metabolism. At the same time, despite

the fact that both models have significant experimental validations and both performed well in matching the model predictions with some experimental measurements, they have limitations. This is expected since they were the first genome-scale models on *S. stipitis.* For example, neither model predicts the production of xylitol under any condition – aerobic, oxygen-limited or anaerobic. It is well-known that xylitol is a key byproduct produced by *S. stipitis* under oxygen-limited condition due the redox imbalance caused by xylose fermentation step (XR and XDH) (Slininger et al., 1985; Slininger et al., 1991). Therefore, being able to predict xylitol production under oxygen limitation is very important – especially if the model to help identify candidates for balancing cellular redox potential, as well as for mutant development.

In this work, comprehensive evaluations of the two genome-scale models (iSS884 and iBB814) were conducted with the aim to detect potential errors and to identify a model that agrees better with existing biological knowledge to serve as the basis for further model improvement. To achieve this goal, we first conducted various *in silico* experiments to examine each model's global behavior through phenotype phase plane (PhPP) analysis, and to compare the model predictions with additional experimental results reported in literature. However, the obtained results from this step led to conflicting conclusions. Next, we designed *in silico* experiments and applied the proposed system identification framework to extract biological knowledge from the *in silico* experimental data. We then examined whether the extracted knowledge agrees with existing understandings. The system identification approach identified several key abnormal behaviors in both models, and detailed analyses show that in general iBB814 agrees with existing understanding better. Finally, to pinpoint the fundamental reasons (*i.e.*, which reactions in the network) for the abnormal behaviors, we conducted thorough manual examination of the models. Guided by the results obtained from the system identification

approach, the major artifacts of both models were identified, which provides some explanations for the abnormal behaviors of both models.

3.3.1 Model comparison using the existing methods

In this section, the following existing methods were carried out to compare the two models: PhPP analysis and conventional point-matching using experimental data. Simulations were conducted in MATLAB using COBRA toolbox (Schellenberger et al., 2011) to carry out FBA in calculating the fluxes of different reactions, which in the literature is known as in silico experiments.

3.3.1.1 Phenotype phase plane (PhPP) analysis

In this analysis, xylose and oxygen uptake rates were chosen as the independent variables, with each of them varying from 0 – 10 mmol/gDW·hr. Figure 3.1 (a) and (b) show how cell growth rate is affected by different substrate uptake rates, where the differently colored regions represent different growth behaviors. Overall, cell growth profiles predicted by iSS884 and iBB814 are similar to each other, except that the growth rate predicted by iBB814 is significantly lower than iSS884. The ethanol and CO_2 production profiles predicted by the two models are shown in Figure 3.1 (c) and (e) for iSS884, (d) and (f) for iBB814. The ethanol profiles are similar between the models, except that iSS884 predicts a larger area of zero ethanol production, which is shown as the green phenotype. The CO_2 profiles are similar between the two models as well. Overall, Figure 3.1 indicates that both models have their share of similarities

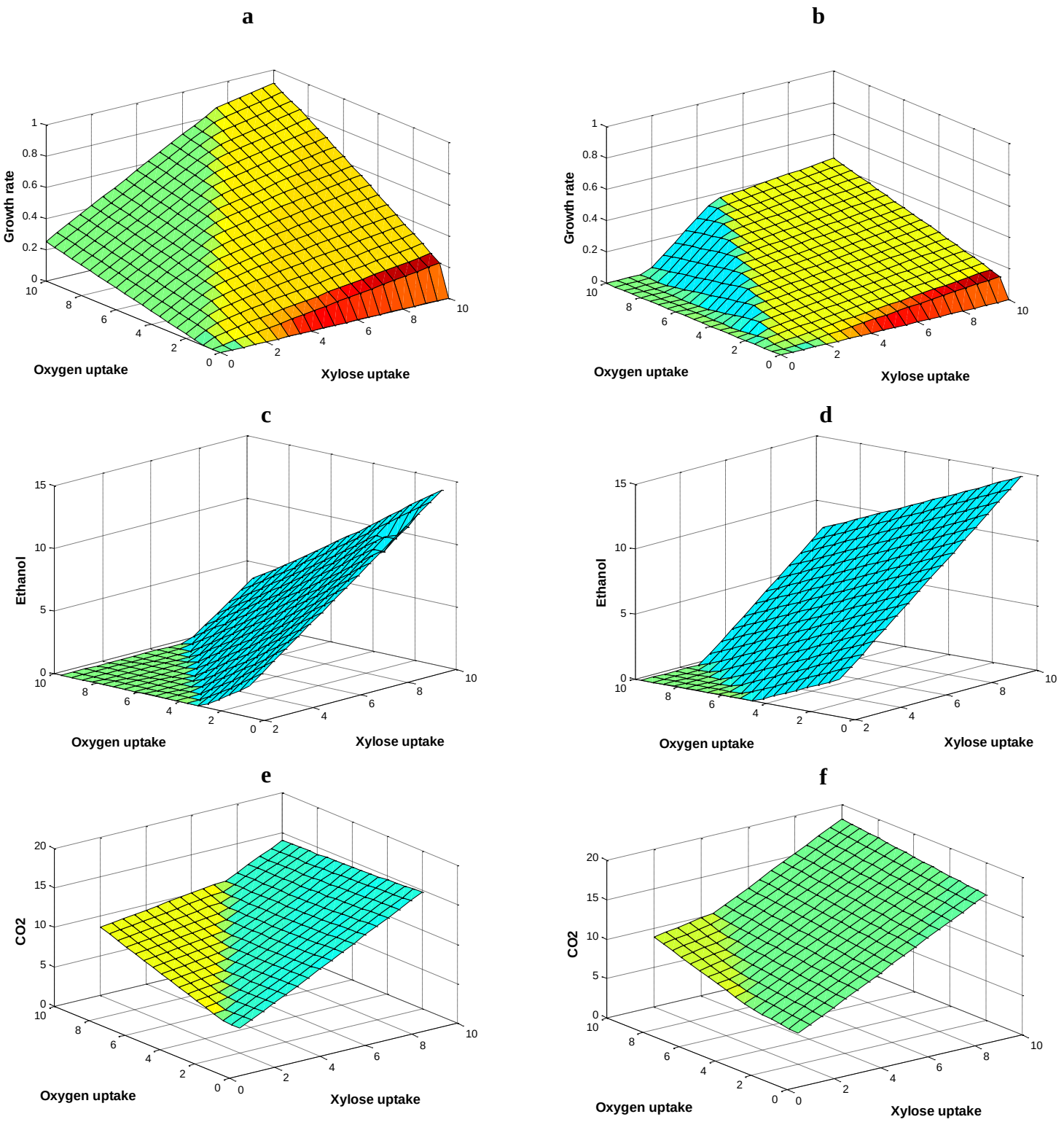

Figure 3.1: Phenotype phase plane analysis. (a) growth rate of iSS884, (b) growth rate of iBB814, (c) ethanol production of iSS884, (d) ethanol production of iBB814, (e) CO_2 production of iSS884, (f) CO_2 production of iBB814

and differences. It is difficult to conclude which model is better, as the differences are subtle and no complete set of experimental data is available that covers the ranges of oxygen and xylose uptake rates for model validation and comparison.

3.3.1.2 Conventional point-matching using experimental data

To further compare the models, we use several experimental data sets reported in the literature to carry out model validation in a traditional way. To provide a fair comparison, model validation consists of two quantitative and two qualitative case studies. One quantitative data set was from (Caspeta et al., 2012), in which iSS884 model was published; the other was from an independent source (Li, 2012). In addition, one qualitative data set was from (Balagurunathan *et al.*, 2012), in which iBB814 model was published, the other was from an independent source (Jin *et al.*, 2005).

For quantitative validation, Figure 3.2 shows the comparison results using the experimental data reported in (Caspeta et al., 2012). The model inputs (*i.e.*, xylose and oxygen) were set to the experimental values, and model predictions (*i.e.*, biomass, ethanol and CO_2 fluxes) were compared with the experimental values at three different oxygen utilization rates (OUR). From Figure 3.2, it appears that iSS884 performs better than iBB814, particularly for the biomass growth.

Figure 3.3 shows the comparison results using the independent data set reported in (Li, 2012). This case study consists of four experimental conditions: two carbon sources (glucose and xylose) combined with two oxygenation conditions (aerobic and oxygen-limited). Similar to the previous case study, the model inputs (*i.e.*, xylose or glucose, and oxygen) were set to the experimental values, and model predictions (*i.e.*, ethanol, CO_2, and biomass) were compared with experimental values.

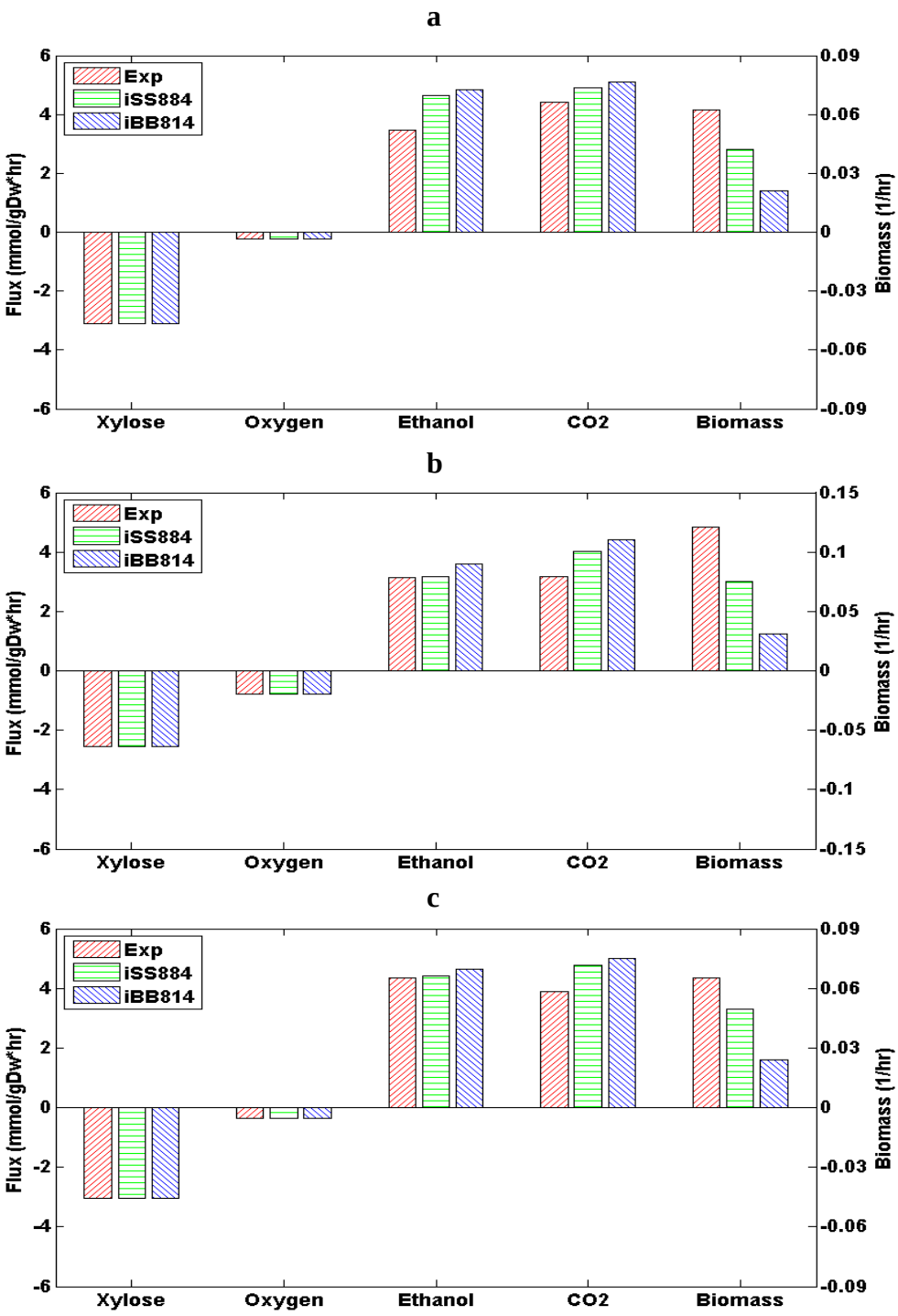

Figure 3.2: Model validation using experimental data (Caspeta et al., 2012) in which iSS884 was published. The model inputs (i.e., xylose and oxygen) were set to the experimental values, and model predictions (i.e., ethanol, CO2, and biomass) were compared with experimental values at different OUR levels. (a) OUR = 0.24, (b) OUR = 0.35, (c) OUR= 0.75. Bars filled with solid blue are experimental values; bars filled with horizontal red lines are model iSS884 predictions; bars filled with vertical green lines are model iBB814 predictions. The left y-axis is for ethanol and CO2 fluxes; while the right y-axis is for biomass. Overall, the predictions of iSS884 are better than iBB814, especially the biomass predictions

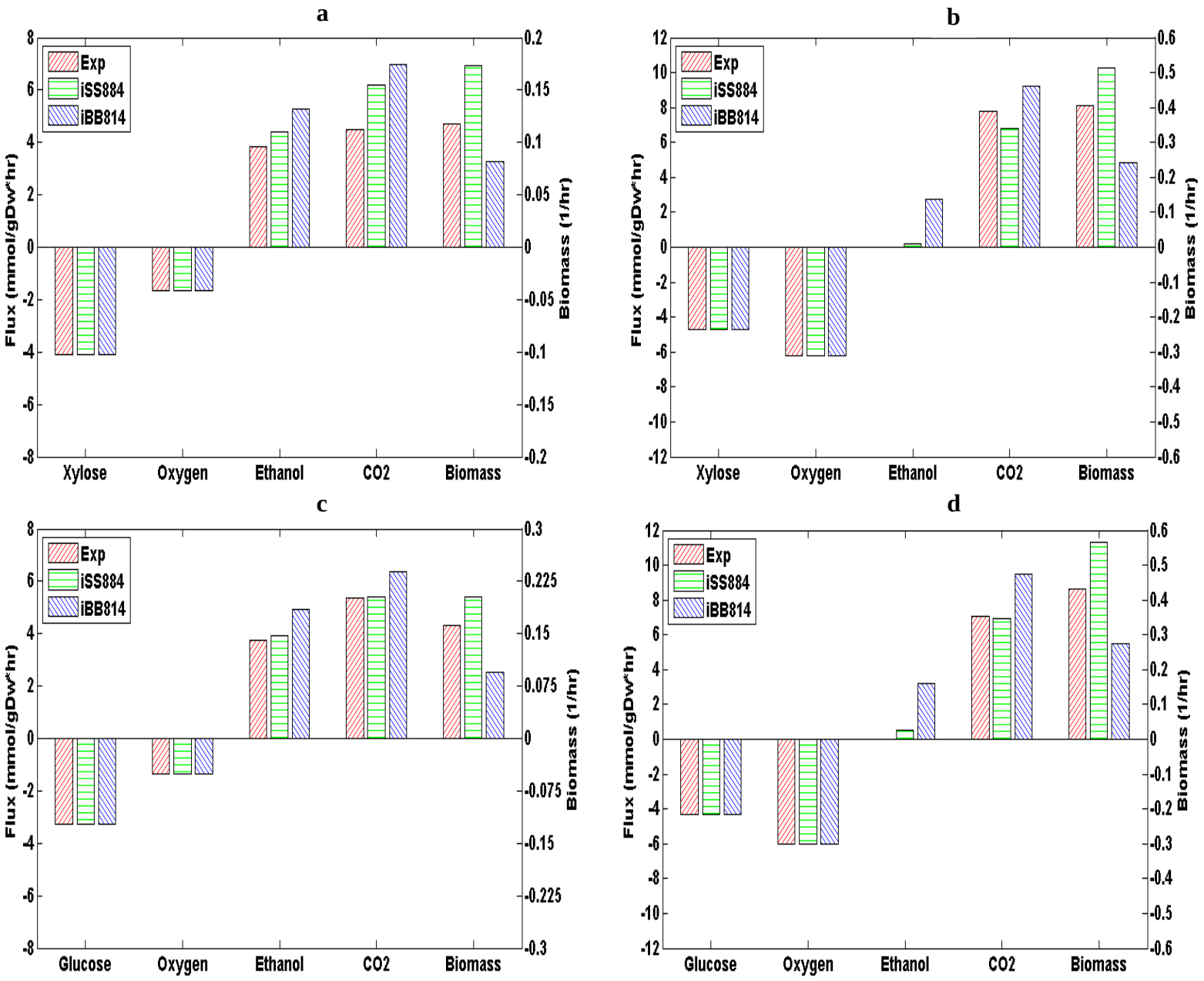

Figure 3.3: Model validation using experimental data from an independent source (Li, 2012). (a) Xylose as carbon source under micro-aerobic condition**,** (b) Xylose as carbon source under aerobic condition, (c) Glucose as carbon source under micro-aerobic condition, (d) Glucose as carbon source under aerobic condition. The model inputs (*i.e.*, xylose or glucose, and oxygen) were set to the experimental values, and model predictions (*i.e.*, ethanol, CO_2, and biomass) were compared with experimental values. The left y-axis is for ethanol and CO_2 fluxes; while the right y-axis is for biomass. Overall, the predictions of iSS884 are better than iBB814, particularly the ethanol and biomass predictions

This case study also shows that the predictions from iSS884 agree with the reported experimental values better than those from iBB814, particularly for ethanol.

This experiment examine how inhibition of electron transport chain (ETC) complexes would affect cell growth and formation of alternative oxidase (AOX), complex I, III, and IV, when grown on glucose and xylose. In wet lab experiments, inhibition was performed by adding different inhibitors to the substrate; while for *in silico* experiments, inhibition was implemented by removing the corresponding reaction catalyzed by the inhibited enzyme. Tables 3.1 shows the comparison results where the model predictions that agree with the reported experimental results are shaded. Table 3.1 indicates that overall iBB814 is more consistent with the experimental data compared to iSS884. Specifically, out of 26 cases examined, only 4 were predicted correctly by iSS884, while 19 were predicted correctly by iBB814.

Table 3.1: The effects of inhibiting electron transport chain complexes on cell growth and formation of AOX and Complex III or IV for glucose and xylose: comparison of iSS884 (884) and iBB814 (814) to experimental (Exp) results. Symbols: complete inhibition (- -), partial inhibition (-), negligible (0), enhanced (+), information not available (NA). The model predictions that match the experimental results are shaded. It can be seen that iBB814 predictions are significantly better than iSS884

Complex	Effect on Growth						Effect on Formation of AOX and Complex III or IV					
	Glucose			Xylose			Glucose			Xylose		
	Exp	**884**	**814**	**Exp**	**884**	**814**	**Exp**	**884**	**814**	**Exp**	**884**	**814**
I	- -	0	0	-	0	0	- -	0	- -	-	0	-
III	NA	0	-	-	0	-	NA	0	-	-	0	-
AOX	0	-	0	+	-	0	0	+	0	+	+	+
IV	-	0	-	-	0	-	0	0	0	+	0	+
IV and AOX	- -	-	- -	- -	-	- -	- -	- -	- -	- -	- -	- -
I + del AOX	- -	-	0	- -	-	0	- -	0	- -	- -	+	- -
I + del IV	- -	0	-	- -	0	-	- -	0	- -	- -	0	- -

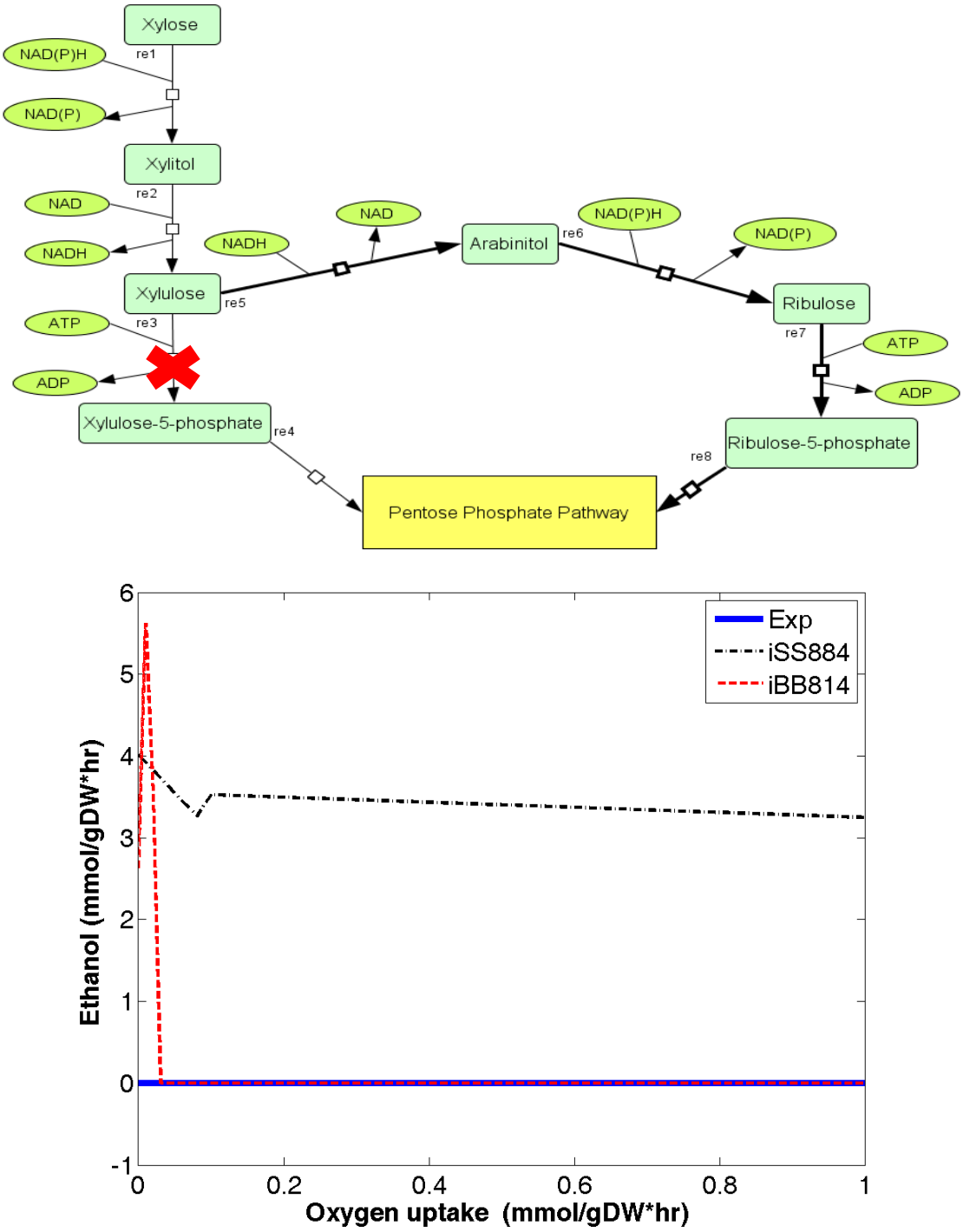

Figure 3.4: Model comparison of the wild type vs. the mutant with the alternative route into the pentose phosphate pathway for metabolizing xylose by deletion of xylulokinase reaction. (a) Schematic diagram of the wild type xylose metabolism (thin arrows with active xylulokinase reaction (re3)) and mutant with the alternative route (bold arrows with the deletion of re3). (b) Comparison of ethanol production: wild type iSS884 model (solid green line) vs. iSS884 mutant (dashed blue line); wild type iBB814 model (solid green line) vs. iBB814 mutant (dashed blue line). iBB814 correctly predicts the experimental result, while iSS884 does not.

Figure 3.4 shows the comparison results using the independent qualitative data reported in (Jin et al., 2005). This case study examines the impact of knocking out Xylulokinase (re3), resulting in an alternative route to pentose phosphate pathway (PPP), as shown in Figure 3.4(a). The experiments show that the resulted mutant did not produce ethanol under various oxygen uptake rates. This knock-out strain was simulated by removing the Xylulokinase (re3) from both models. Then the predicted ethanol production from the mutant strains were compared with those of the wild strains, as shown in Figure 3.4 (b) for iSS884 and iBB814. Figure 3.4 (b) show that iBB814 correctly predicts the experimental result, while iSS884 does not.

3.3.1.3 Model comparison through the SID framework

In the proposed SID framework, designing appropriate *in silico* experiments plays a key role in facilitating the extracting of mechanistic insights from the metabolic models. The basic idea that guides the design of *in silico* experiments performed in this section is the following: the effect of increased oxygen uptake rate is well known: increased fluxes through TCA cycle, ETC, and maybe increased substrate uptake rate, as well as increased fluxes through glycolysis and PPP (Passoth et al., 1996; Joseph-Horne et al., 2001). Based on this knowledge, the following *in silico* experiments were designed to examine the effect of increased oxygen uptake rate. The oxygen uptake rate is varied between 0.10 – 0.15 mmol/gDW·hr for oxygen-limited condition and between 6.0 – 6.3 mmol/gDW·hr for aerobic condition, with a step size of 0.0001 and 0.0002 mmol/gDW·hr, respectively. The xylose uptake rate has an upper limit of 5 mmol/gDW·hr. FBA is carried out to perform *in silico* experiments for the specified conditions, which results in flux matrices of 1500×1332 for iSS884 (*i.e.*, 1500 samples/conditions for 1332 reactions), and 1500×1371 for iBB814, under either oxygen-limited or aerobic condition. Principal component analysis (PCA) is applied to analyze the resulted flux matrices. Since only

one degree of change (*i.e.*, increasing oxygen uptake rate) is introduced to the metabolic network, one principal component (PC) is expected to capture all variations within the flux matrix, which was confirmed by our computation results.

The loadings of the PC provide information on how different reactions are affected by the introduced change (*i.e.*, the increased oxygen uptake rate in this case). The reactions that are affected the most can be easily identified as they would have high values in the loading. Because of the size and complexity associated with GSMMs, it is desirable to visualize the knowledge extracted by the SID framework. Figure 3.5 visualizes how the modeled metabolism responds to increased oxygen uptake rate, which was generated in the following way: first, reactions affected significantly by the increased oxygen uptake rate are identified by sorting based on their loadings; next, the identified reactions are registered to different subsystems; finally, color-coded plots were generated based on the results obtained in the previous steps. The two models were compared under oxygen-limited condition (Figure 3.5 (a): iSS884; and (b): iBB814) and under aerobic condition. Figure 3.5 shows how different reactions are affected by the introduced perturbation (*i.e.*, the increased oxygen uptake rate under oxygen-limited and aerobic condition). In Figure 3.5, green indicates up regulation or flux increase with increased oxygen uptake rate; red indicates down regulation or flux decrease with increased oxygen uptake rate; grey indicates no effect with increased oxygen uptake rate. In addition, the line width indicates the level or magnitude of the flux change. Figure 3.5 shows that both models contain some errors as the model predicted responses do not fully agree with existing knowledge. Table 3.2 and Table 3.5 show whether the major pathways in the central carbon metabolism were in the correct or incorrect direction under oxygen-limited and aerobic conditions respectively. In Table 3.2, xylose metabolism is predicted wrong for the both the models, since the models do not

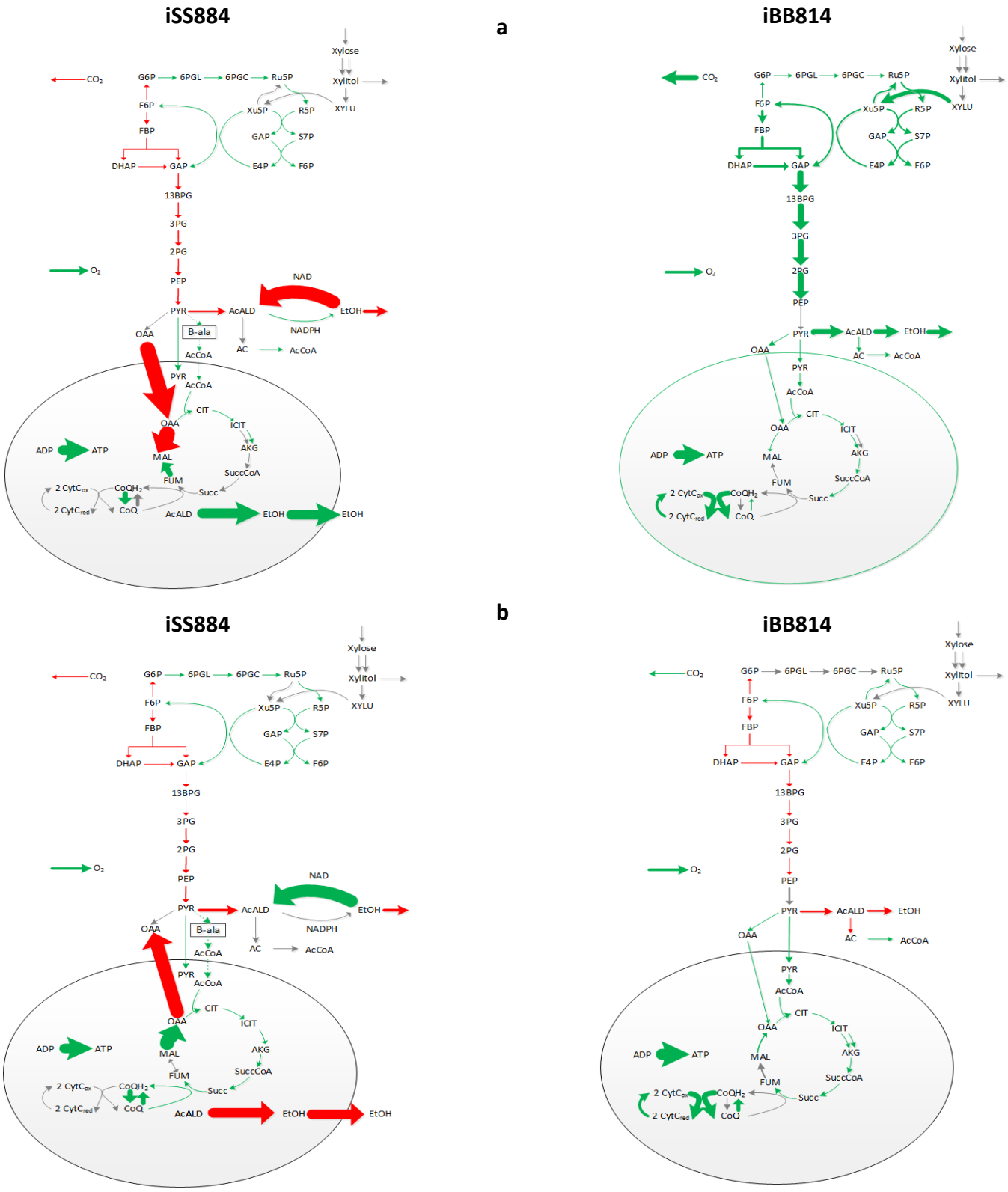

Figure 3.5: The SID framework identifies how fluxes are affected by the increased oxygen uptake rate. (a) oxygen-limited and (b) aerobic condition in model iSS884 and iBB814. Color code: red – flux decrease, green – flux increase, gray – not affected. Line width indicates effect level

predict xylitol production. Both branches of the PPP are correct in iSS884, while iBB814 behave in the opposite response. Glycolysis is the only pathway that was correct for both models. The TCA cycle was expected to be branched for oxygen-limited condition, which was the case for iSS884, and the ETC was in the correct direction for iBB814. The errors from the branches of PPP in iBB814 could be contributed to the lack of xylitol production. Looking at the TCA cycle, we see that the advent of acetyl-CoA into the mitochondria occurs by different routes, which seems unusual since the pathways of the central carbon metabolism have been firmly established. In iSS884, pyruvate does not enter TCA cycle directly under either oxygen-limited or aerobic condition, while in iBB814 it does..

Table 3.2: SID results of iSS884 and iBB814 under oxygen-limited condition. The symbol ✓ represents the correct direction from the model and ⊘ represents the incorrect direction from the model.

Pathways	iSS884	iBB814
Xylose metabolism	⊘	⊘
Oxidative - PPP	✓	⊘
Non-oxidative – PPP	✓	⊘
Glycolysis	✓	✓
TCA cycle	✓	⊘
ETC	⊘	✓

In iSS884, pyruvate enters amino acid metabolism, as well as being used for ethanol production, without being converted into acetyl-CoA. Further investigation was done using the SID

framework to reveal the fine details of the models. Here we use ETC and ethanol production as two case studies and apply SID framework to reveal more details of the two subsystems. Figure 3.6 (a) and (c) plot the loadings of different reactions carried out by different ETC complexes for iSS884 and iBB814 respectively, and Figure 3.6 (b) and (d) visualize the loadings with a schematic plot of ETC for iSS884 and iBB814 respectively. Note that the line width of the arrow corresponds to the magnitude of the relative loading (*i.e.*, how much the flux is affected by the increased oxygen uptake rate), instated of the magnitude of the flux. Table 3.3 lists the fluxes carried by different reactions in ETC under two specific OUR conditions (0.25 and 0.40 mmol/gDW·hr). Figure 3.6 and Table 3.3 show that in iSS884, only complex I and alternative oxidase (AOX) are affected, while complex II, III, and IV are not. Further examination of the fluxes shows that complex II, III, IV does not carry a flux (as shown in Table 3.3), which does not agree with the existing knowledge. In contrast, in iBB814, complexes I, III, IV and non-proton translocase are affected, and the fluxes through them all increase with oxygen uptake rate, which agrees with common knowledge. Next, we further examined the production of ethanol.

Table 3.3: Comparison of detailed fluxes through ETC in iSS884 and iBB814 under two different OUR conditions (OUR I = 0.25 mmol/gDW·hr and OUR II = 0.40 mmol/gDW·hr).

RXN Complex		iSS884		iBB814	
		OUR I	OUR II	OUR I	OUR II
re1	I	0.37	0.66	0.20	0.37
re2	II	0	0	0	0
re3	III	0	0	0.42	0.71
re4	IV	0	0	0.21	0.36
re5	AOX	0.38	0.66	0	0
re6	Non P.	N/A	N/A	0.20	0.27

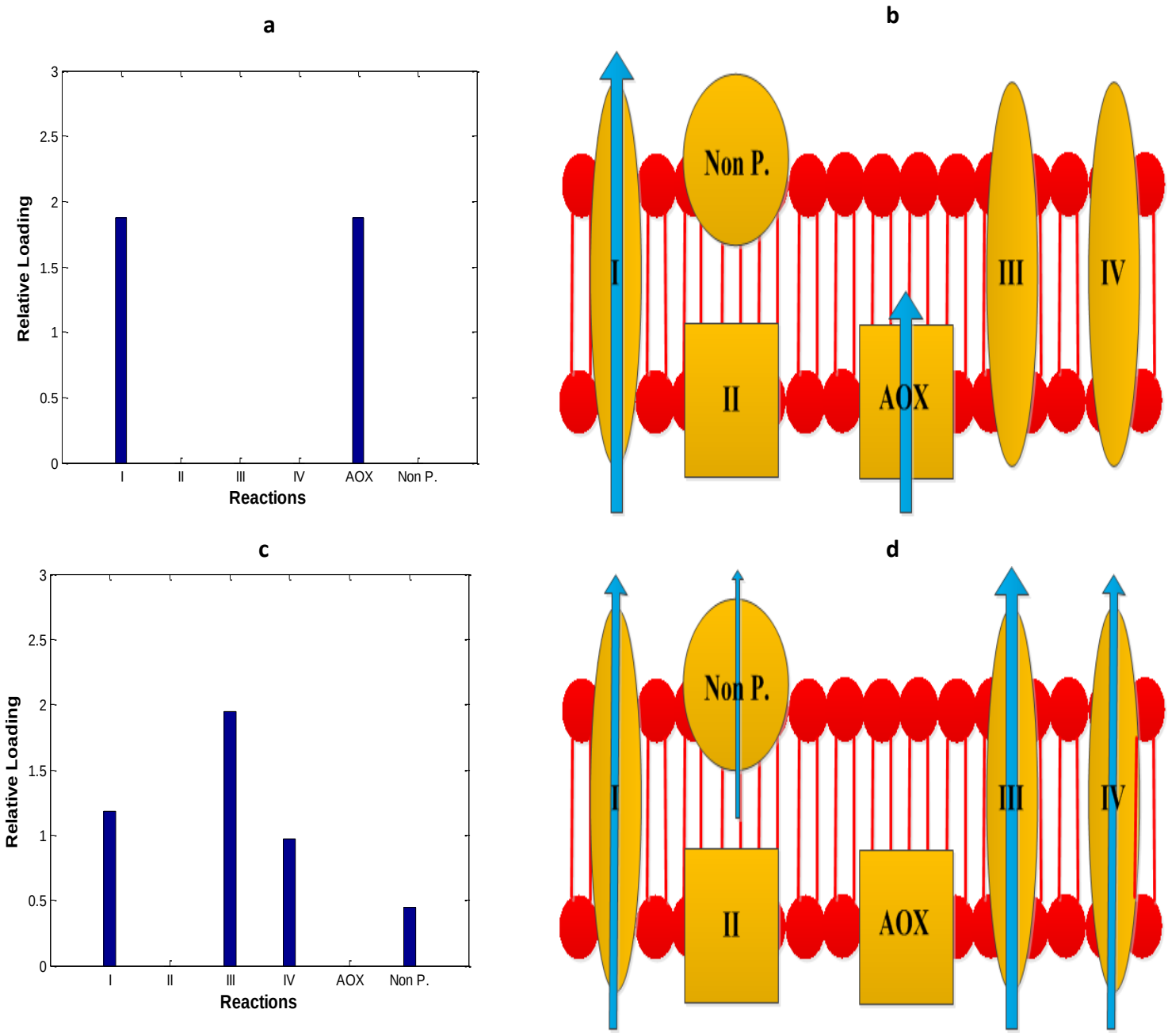

Figure 3.6: Comparison of electron transport chain (ETC) through the SID framework for iSS884 and iBB814 under oxygen-limited condition: (a) Relative loading plots for iSS884 and (c) iBB814. (b) Schematic diagram of the machinery in the ETC for iSS884 and (d) iBB814, where the line weight corresponds to the magnitude of the relative loading for the different machinery shown in (a) and (c).

Table 3.4 shows the fluxes carried by different reactions in iSS884 and iBB814 under OUR = 0.10. From Table 3.4, we see that in iSS884 the major production of ethanol occurs in the mitochondria, while the cytosol reaction converts NADH to NADPH, with both fluxes

almost hitting the upper limit (1000), which is not likely to happen. While in iBB814, ethanol is only produced in cytosol, which is more reasonable.

Table 3.4: Comparison of ethanol production routes in iSS884 and iBB814. Both models have NADH and NADPH dependent reactions in the cytosol, while iSS884 contains an additional reaction in the mitochondria. The numbers represent the fluxes of the reactions. It shows iSS884 utilize the cytosol reaction to convert NADH into NADPH, while the major ethanol production occurs in mitochondria

Compartment	**iSS884**	**iBB814**
Cytosol	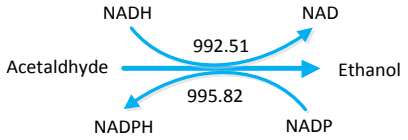	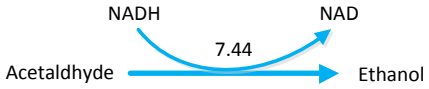
Mitochondria	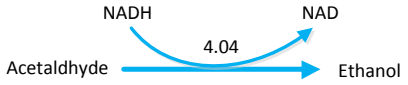	Not Exist

Moving to aerobic conditions, we now see great improvements in iBB814. Note that xylose metabolism row was removed, since xylitol is not produced under aerobic condition. Once again the oxidative branch of PPP is in the incorrect for iBB814, which now tells us that it has to do with the production NADPH. Table 3.6 shows fluxes of the NADPH producing pathways of iBB814 under oxygen-limited and aerobic condition. For oxygen-limited condition, R_x2 from Table 3.6 is about three times of the amount of R_x1 (oxidative branch of PPP) and R_x3. For aerobic, R_x3 is significantly higher than the other non-zero flux reaction, R_x2, and now the oxidative branch of PPP flux is zero. It is important to point out that R_x2 and R_x3 are not in iSS884, which provides a stand-alone NADPH producing reaction.

Table 3.5: SID results of iSS884 and iBB814 aerobic condition. The symbol ✓ represents the correct direction from the model and ⊘ represents the incorrect direction from the model

Pathways	iSS884	iBB814
Oxidative - PPP	✓	⊘
Non-oxidative – PPP	✓	✓
Glycolysis	✓	✓
TCA cycle	✓	✓
ETC	⊘	✓

Table 3.6: NADPH production pathways for iBB814. Oxygen-limited condition: OUR I = 0.20 mmol/gDW·hr and OUR II = 0.35 mmol/gDW·hr. Aerobic condition: OUR I = 6.0 mmol/gDW·hr and OUR II = 6.3 mmol/gDW·hr. 6pgc: 6-phosphogluconate, ru5p-D: ribulose 5-phosphate, acald: acetaldehyde, ac: acetic acid, icit: isocitrate, akg: alpha-ketoglutarate

R_x	Reaction	Oxygen-limited		Aerobic	
		OUR I	OUR II	OUR I	OUR II
1	nadp[c]+ 6pgc[c] -> nadph[c] + co_2[c] + ru5p-D[c]	0.026	0.023	0	0
2	h2o[c] + nadp[c] + acald[c] -> 2 h[c] + nadph[c] + ac[c]	0.092	0.085	0.038	0.031
3	nadp[c] + icit[c] -> akg[c] + nadph[c] + co2[c]	0.030	0.034	0.59	0.62

3.3.1.4 Manual examination guided by the SID framework

In Section 3.3.1.3, several system level differences between the two models have been revealed by the SID framework. To confirm these findings and to identify the root causes (e.g., specific reactions) that result in the different model behaviors, manual examination was carried out to compare the reactions, metabolites, genes and compartments. Figure 3.7 (a) shows the number of reactions in different subsystems that are unique to or overlap between iSS884 and iBB814. Overall, the two models often share less than one-half to one-third of the reactions, with the least overlap in the lipid subsystem. Specifically, one major difference in the lipid subsystem is the formulation procedure of saturated fatty acid: iSS884 uses a stepwise procedure, which has more intermediate steps, while iBB814 is simplified. The details on saturated fatty acid biosynthesis can be found in Appendix A2. In summary, iBB814 provides more flexibility, since a fatty acid of any even length between 2 and 26 can be formed. In contrast, iSS884 employs a linear stepwise reaction which only produces the fatty acid with 12, 14, 16 and 18 carbons, while the shorter chain fatty acids are only used as the intermediates because they are all ACP bonded.

The amount of amino reactions in both models is about the same and between the models they more than half of the reactions. The amino acid subsystems are crucial to the metabolism, since they represent a majority of the metabolites in the biomass reaction. Analysis was done on the amino acid subsystems to see what routes the models took for amino acid production. Table 3.7 shows the results of the amino acids for the models, where 11 out of the 19 amino acid reactions were the same. For the ones that were different, 3 dealt with different cofactors usage (L-glutamate, L-histidine, and L-proline). In L-alanine the reaction was the same, but iSS884 occurred in the cytosol and iBB814 in the mitochondria. The other 4 amino acids (L-cysteine, glycine, L-serine, and L-valine) were from different precursors.

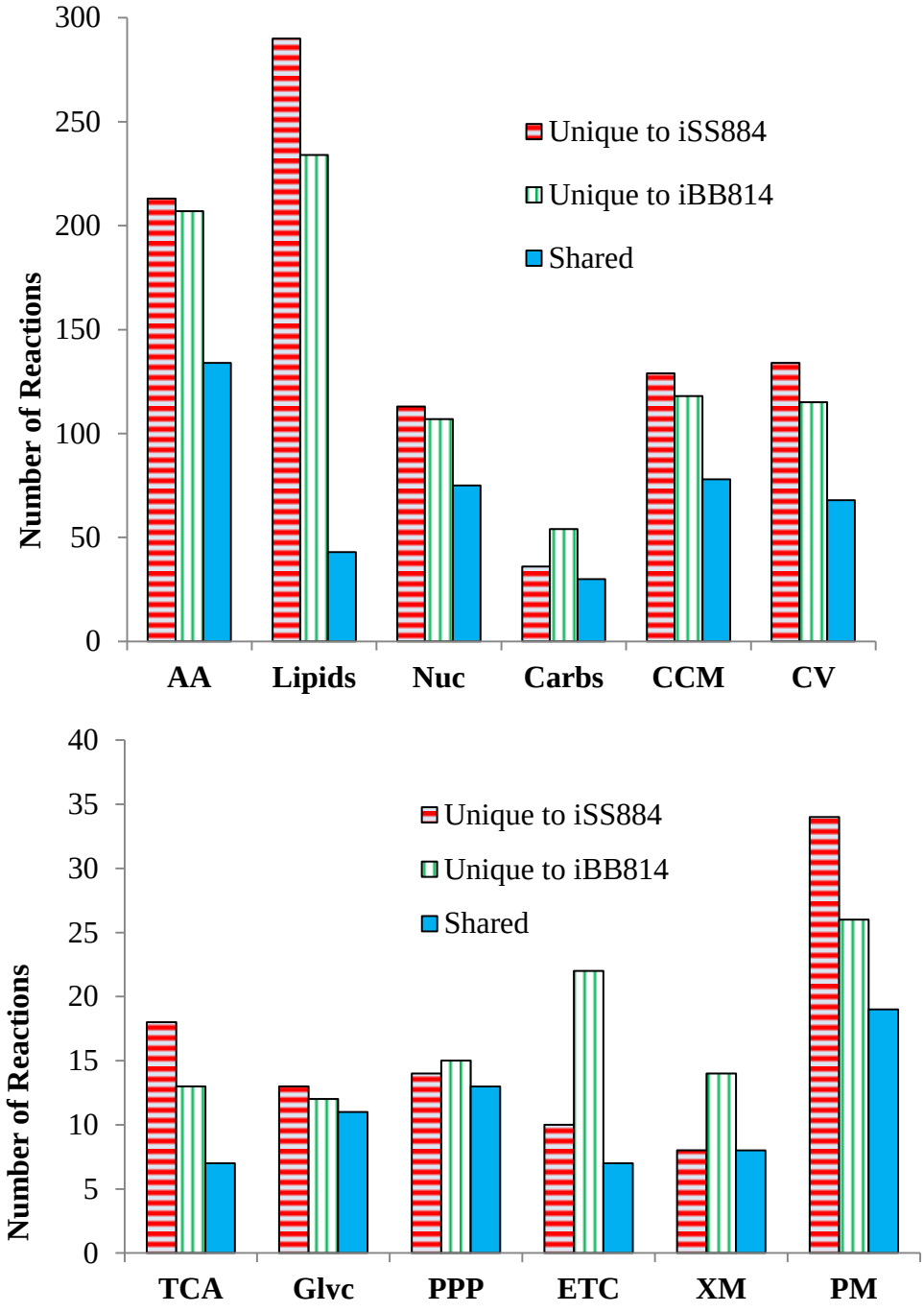

Figure 3.7: Comparison of constituent reactions in iSS884 and iBB814: (a) subsystem breakdown, (b) central carbon metabolism breakdown. AA – amino acids, Nuc – nucleotides, Carbs – carbohydrates, CCM- central carbon metabolism, CV- cofactors and vitamins, TCA – tricarboxylic acid cycle, Glyc – Glycolysis, PPP – pentose phosphate pathway, ETC – electron transport chain, XM- xylose metabolism, PM – pyruvate metabolism. Legend: Bars filled with horizontal red lines – number of reactions unique to iSS884; Bars filled with vertical green lines are number of reactions unique to iBB814; Bars filled with solid blue are number of reactions shared between iSS884 and iBB814

Table 3.7: Amino acid production routes under oxygen-limited condition

Amino Acids	iSS884	iBB814	Description
L-Alanine	[c]	[m]	Same reaction
L-Arginine			Same reaction
L-Asparagine			same reaction
L-Aspartate			Same reaction
L-Cysteine	serine	acetyl-serine	Both use hydrogen sulfide
L-Glutamine			Same reaction
L-Glutamate	nadph	nadh	Same reaction different redox
Glycine		2 rxns used	Different reaction
L-Histidine	nad	2 nad	Same reaction - different redox amounts
L-Isoleucine			Same reaction
L-Leucine			Same reaction
L-Lysine			Same reaction
L-Phenylalanine			Same reaction
L-Proline	nadh	nadph	Same reaction - different redox
L-Serine	[m] gly	[c] rxn fpser	Different reaction
L-Threonine			Same reaction
L-Tryptophan			Same reaction
L-Tyrosine			Same reaction
L-Valine[c]	from ala-L	from glu-L	Different reaction

Despite the models have a lot of different amino acid reactions, when looking at the reactions that are activated they are quite similar. It was surprising to see the central carbon metabolism (CCM) show a lot of differences, because these pathways have been well studied.

Figure 3.7 (b) shows the number of reactions of different pathways in the CCM that is unique or overlaps between iSS884 and iBB814. Again the two models share less than one-half of the reactions in any of the pathways. For the TCA cycle, the main finding is that iSS884 contains more detailed reactions, i.e. more intermediates are included. These metabolites were linked with the pyruvate metabolism, which is another subsystem that shows a lot of

discrepancies. Figure 3.8 shows how the intermediate reaction of the TCA cycle is linked to the pyruvate metabolism.

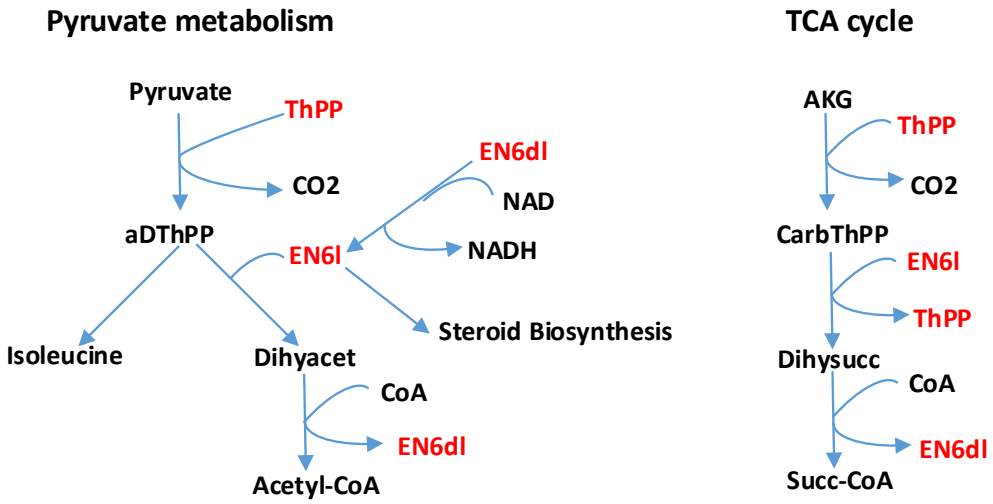

Figure 3.8: Reactions of the pyruvate metabolism linkage to TCA cycle. Metabolites highlighted in red are intermediate metabolites. ThPP: Thiamin diphosphate, aDThPP: 2-(alpha-Hydroxyethyl)thiamine diphosphate, EN6dl: Enzyme N6-(dihydrolipoyl)lysine, EN6l: Enzyme N6-(lipoyl)lysine, Dihyacet: [Dihydrolipoyllysine-residue acetyltransferase] S-acetyldihydrolipoyllysine, AKG: alpha ketoglutarate, 3-CarbThPP: 3-Carboxy-1-hydroxypropyl-ThPP, Dihysucc: [Dihydrolipoyllysine-residue succinyltransferase] S-succinyldihydrolipoyllysine, Succ-CoA: succinyl-CoA

The pyruvate metabolism of iSS884 contains 8 more reactions than iBB814, and Figure 3.8 shows reactions that are unique in iSS884. One of the main tasks of the pyruvate metabolism is the conversion of pyruvate to acetyl-CoA, which is done through the reaction of pyruvate dehydrogenase. iSS884 uses a really complex form of this, which actually causes discontinuity in the reaction, such that under both oxygen-limited and aerobic condition NADH is produced from the conversion of EN6dl to EN6l, but acetyl-CoA is not produced. iBB814 uses the simplified form of pyruvate dehydrogenase by just using a single reaction, which is shown in Table 3.8. iSS884 has two other ways in producing acetyl-CoA, the first is done in the beta-alanine

pathway, which begins at the precursor, L-aspartate, and three reactions follow for production of acetyl-CoA. The acetyl-CoA that is produced from the beta-alanine pathway occurs in the cytosol, where it is then converted into another metabolite which is then transported into the mitochondria and later reconverted to acetyl-CoA. Based on fundamental biochemistry knowledge and thermodynamics, this passage seems quite unrealistic. A final point to talk about on the pyruvate metabolism of iSS884 is the absence of aldehyde dehydgronase, which is an essential reaction for the production of NADPH, we have seen in the last section in Table 3.6 that it carries the highest flux for the production of NADPH for iBB814.

Moving to the TCA cycle, in the mitochondria, iBB8814 can utilize both NAD+ and NADP+ for isocitrate dehydrogenase, while iSS884 only utilizes NAD+. In cytosol, iBB814 uses NADP+ while iSS884 uses NAD+, where these reactions can be seen in Table 3.8. Under both oxygen-limited and aerobic condition, iBB814 utilizes all isocitrate dehydrogenase reactions.

Other major metabolic differences between the two models are summarized in Table 3.8, where the key metabolic artifacts are listed. It is somewhat surprising to see that iSS884 does not include NADH-coupled xylose reductase activity, which should be considered greatly important when considering the redox balance during xylose assimilation. iBB814 uses solely the NADH-coupled xylose reductase reaction. By combining with the findings obtained from Section 3.3.1.3, we believe that the differences in the cofactor utilization in the central carbon metabolism as cited above are some of the fundamental reasons for the different behaviors of the two models, due to the role that redox balancing plays in xylose fermentation.

For ETC, the number of protons being transported from the mitochondrial to the cytosol in Complex I, III, and IV are different between the two models. Generally speaking, more

protons are transported across mitochondrial membrane in iBB814 than in iSS884. In addition, iSS884 does not contain non-proton translocase, and alternative oxidase (AOX) is not balanced as shown in Table 3.8. These fundamental differences in ETC are the root cause for the failed validation result shown in Table 1 for iSS884. They are also the reason for the abnormal behavior of iSS884 shown in Figure 3.8 where complexes II, III, IV do not carry a flux. Looking at the active reactions, only one of the non-proton translocases carries a flux, which the consumption of NADH in the cytosol.

Finally, one important aspect of GSMMs is the biomass composition (i.e., growth equation), which was used as the objective for all the in silico simulations. Biomass composition in iSS884 was developed from *S. cerevisiae* amino acid data and related strains that are classified in the same family, while that of iBB814 was based on the experimentally measured metabolites. The complete biomass composition of both models can be found in Appendix A3. Variations in the amino acid metabolites amounts are significant, where 9 amino acids differ in over 50%. The major differences arise in the fatty acid metabolites, where ISS884 and iBB814 contain 17 and 5 respectively. The carbohydrate represents the smallest subsystem. Although it is difficult to say which metabolite composition should be included, iBB814 seems more trustworthy since the composition was measured experimentally.

In summary, it appears that iSS884 contains more errors than iBB814. However, it is worth noting that iSS884 was constructed through a semi-automatic approach, which could save significant time and manpower. Because a reference framework is required in the semi-automatic approach, it is understandable that the selection of the reference framework could have a big impact on the reconstructed model. Because *S. cerevisiae* is a Crabtree positive strain while *S. stipitis* is Crabtree negative, *S. cerevisiae* may not be an ideal reference to use in this case.

Table 3.8: Metabolic artifacts that differ between iSS884 and iBB814

Reaction		**iSS884**	**iBB814**
Xylose reductase: NADH		Absent	H[c] + NADH[c] + XYL-D[c] → NAD[c] + XYLT[c]
Pyruvate Dehydrogense		Complex Form Fig. 3.8	CoA[m] + NAD[m] + PYR[m] → ACCoA[m] + CO_2[m] + NADH[m]
Isocitrate Dehydrogenase		ICIT[m] + NAD[m] → AKG[m] + CO_2[m] + NADH[m]	ICIT[m] + NAD[m] → AKG[m] + CO_2[m] + NADH[m] ICIT[m] + NADP[m] → AKG[m] + CO_2[m] + NADPH[m]
		ICIT[c] + NAD[c] → AKG[c] + CO_2[c] + NADH[c]	ICIT[c] + NADP[c] → AKG[c] + CO_2[c] + NADPH[c]
Aldehyde Dehydgronase NADP dependent		Absent	ACALD[c] + NADP[c] + H_2O[c] → NADPH[c] + AC[c] + 2 H[c]
ETC	I	2 H[m] + NADH[m] + Q[m] → H[c] + NAD[m] + QH_2[m]	4 H[m] + NADH[m] + Q[m] → 4 H[c] + NAD[m] + QH_2[m]
	II	FADH2[m] + Q[m] → FAD[m] + QH2[m]	FADH2[m] + Q[m] → FAD[m] + QH2[m]
	III	H[m] + QH_2[m] + 2 FICYTC[m] → 2 H[c] + Q[m] + 2 FOCYTC[m]	4 H[m] + QH_2[m] + 2 FICYTC[m] → 4 H[c] + Q[m] + 2 FOCYTC[m]
	IV	8 H[m] + O_2[m] + 4 FOCYTC[m] → 4 H[c] + 4 FICYTC[m] + 2 H_2O[m]	8 H[m] + O_2[m] + 4 FOCYTC[m] → 8 H[c] + 4 FICYTC[m] + 2 H_2O [m]
	AOX	2 H[m] + QH_2[m] + 0.5 O_2[m] → Q[m] + H_2O[m]	QH_2[m] + 0.5 O_2[m] → Q[m] + H_2O[m]
	Non-proton translocases	Absent	Present

3.4 Conclusion

Currently standardized protocols have been published on how to reconstruct a genome-scale model from a sequenced genome. However, how to assess the quality and accuracy of a genome-scale metabolic network model remains challenging. Due to the scale and complexity

involved in genome-scale models, simply comparing measured and computed cross-membrane fluxes is not sufficient to guarantee model accuracy and model predictive capability. In this work, we developed a system identification based framework to analyze metabolic network models. By performing system identification using designed *in silico* experiments, the proposed approach enables the extraction of qualitative biological knowledge embedded in the network model, which in turn can be used to assess model quality as well as to troubleshoot the hidden errors. The developed framework is applied to assess two recently published genome-scale models of *S. stipitis*: iSS884 and iBB814. The traditional model validations performed in this work led to conflict conclusions: iSS884 performs better in the two quantitative validations while iBB814 performs better in the two qualitative validations. When the SID framework was applied, it was found that iBB814 agrees better with existing knowledge on *S. stipitis* and some significant errors were identified for iSS884. Finally, through SID guided manual examination, the root cause for the errors contained in both models was identified, which explained (at least partially) the findings through the SID framework. The SID framework also provided insight on where to make improvements to iBB8814. Both branches of the PPP need to be corrected under oxygen-limited and aerobic condition. Also the TCA cycle under oxygen-limited condition needs to be branched. Finally, the major change that needs to take place is xylitol production. In summary, it was shown that the proposed SID framework is an effective tool for metabolic network analysis, particular for complex genome-scale models.

Chapter 4: An improved GSMM for *S. stipitis*

4.1 Introduction

Recently, two genome-scale models of *Scheffersomyces stipitis* have been published, iSS844 and iBB814, where these provide significant step forward in gaining systems understanding of the cellular metabolism. The previous section displayed how iBB814 had more favorable results than iSS884 in terms of tracking the metabolic flow using our system identification method. However, iBB814 still has errors in fundamental metabolic flow and validation experiments:

1. Absence of xylitol production (xylose metabolism)

2. Oxidative branch and non-oxidative of PPP incorrect direction (oxygen-limited)

3. Oxidative branch not activated and non-oxidative of PPP incorrect direction (aerobic)

4. Glycolysis (oxygen-limited)

5. Improvement in qualitative and quantitative validation experiments

Therefore, a modified model was formulated, iAD828, which is based on iBB814. Our SID framework guided the construction of the modified model by uncovering the key reactions. iAD828 shows improved results of the validation experiments compared with iSS884 and iBB814, and now there is xylitol production present, which is in agreement with published xylitol experimental data. Now, the phenotypes under oxygen-limited condition are more reliable since xylitol is present. The oxygen uptake was perturbed under specific oxygen-limited phenotypes and for an aerobic condition, and response of the metabolic flux through the crucial

central carbon metabolism (xylose metabolism, glycolysis, pentose phosphate pathway, citric acid cycle, and oxidative phosphorylation) shows improvement with biological information. With these findings, iAD828 is a substantial progression of a wealth of knowledge for elucidating the cellular metabolism of *S. stipitis*.

Refinement of GSMMs is a lengthy process that requires years of computational and experimental research. S. *cerevisiae* can be considered a "brother" strain to *S. stipitis*, and there has been adjustments made, since 2003, which was the year of the first GSMM for S. *cerevisiae*. Over the span of years, modifications were made for improvement, such as adding compartments, pathways, and apply omics data. Figure 4.1 shows the progression of the GSMM of S. *cerevisiae* through the years. The main point here to digest is that model refinement is a laborious process, and many significant advances were made in this work for S. *stipitis*.

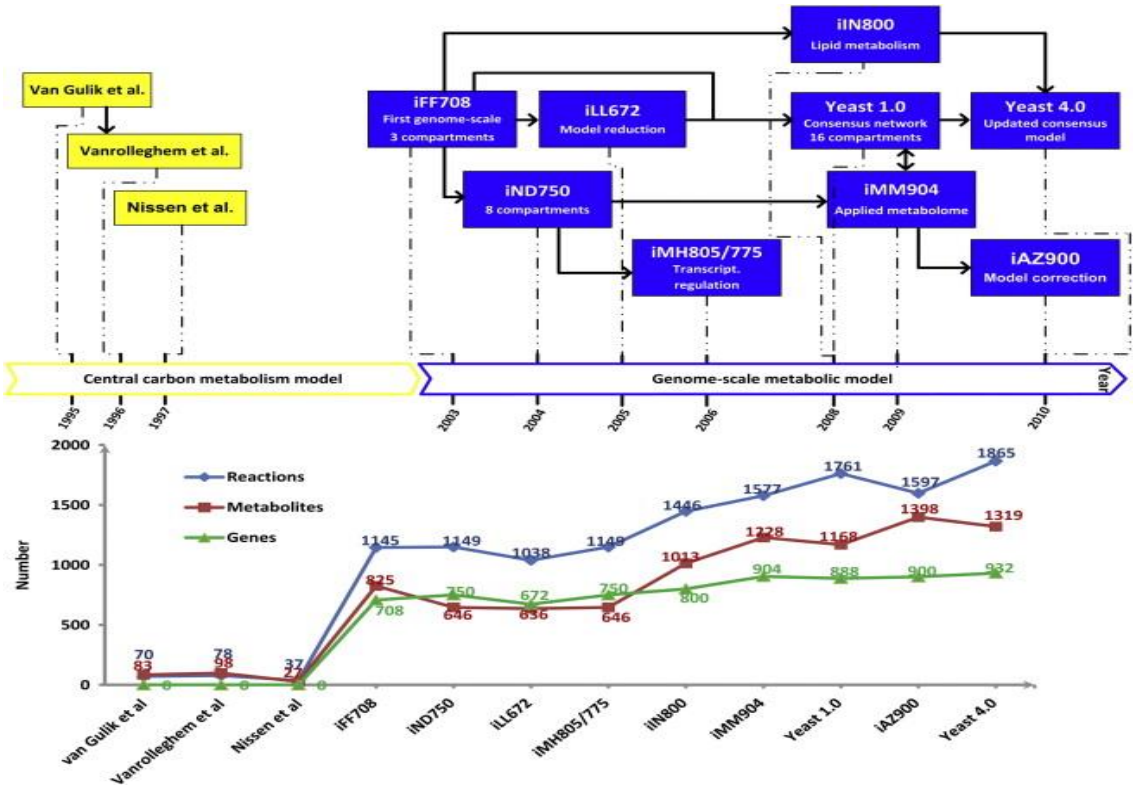

Figure 4.1: Development of GSMMs for *S. cerevisiae* through the years

4.2 Material and Methods

4.2.1 Overview of GSMMSs of *S. stipitis*

The genome-scale model of iBB814 was used as the baseline model, and this invoked creating a new genome-scale model, iAD828. Databases, such as KEGG and MetaCyc, were used to find metabolic reactions, as well as iSS84 and unpublished genome-scale model of *S. stipitis*. The same tools were, FBA and SID framework, where SID framework was used to guide the reaction modifications. Table 4.1 shows the breakdown of the number reactions, metabolites, genes, and compartments for GSMMS of *S. stipitis*. Appendix A4 and A5 show the reaction and metabolite list respectively.

Table 4.1: Breakdown GSMMs of *S. stipitis*

Specification	**iSS884**	**iBB814**	**iAD828**
Approach	Semi-Automatic	Manual	Manual/SID framework
Reactions	1332	1371	1381
Cytosol	824	757	762
Mitochondria	207	125	130
Peroxisome	60	N/A	N/A
Transport	239	489	489
Metabolites	922	644	971
Genes	884	814	828
Percent of Genome (%)	15.1	14.4	14.7
Compartment	Cytosol, Exchange, Mitochondria, Peroxisome	Cytosol, Exchange Mitochondria	Cytosol, Exchange Mitochondria

4.2.2 SID framework

In the previous chapter, SID framework was used to pinpoint the metabolic response of the genome-scale model as the oxygen uptake rate increased. The SID framework was used to

guide the modifications. For this example, the objective was to cause the oxidative branch of pentose phosphate pathway (PPP) to be in the correct direction, where Figure 4.2 shows the oxidative branch of PPP being inactive for aerobic conditions. The oxidative branch of PPP was non-active in aerobic growth, and the goal was to cause it to increase with increasing oxygen uptake.

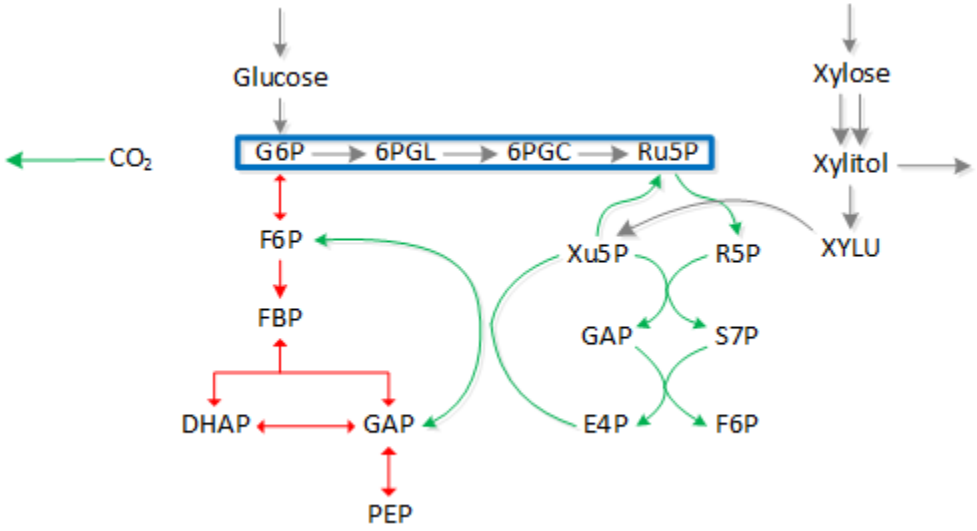

Figure 4.2: Early rendition of iAD828 showing oxidative branch of PPP being not active. The blue box encapsulates the oxidative branch of PPP. The gray arrows represent that the pathway is inactive

Figure 4.3 demonstrates how SID framework was used to correct the direction of the oxidative branch of PPP. Figure 4.3 (a) provides a flow diagram of the various steps used. This is done by forcing the flux through oxidative branch of PPP, while being in the same phenotype (aerobic conditions). The xylose pickup rate was 5 mmol/gDW·hr and the oxygen pickup rate was varied from 4 - 6.5 mmol/gDW·hr. The oxidative branch of PPP was varied between 1 – 2 mmol/gDW·hr, which was based on data from iSS884.

a

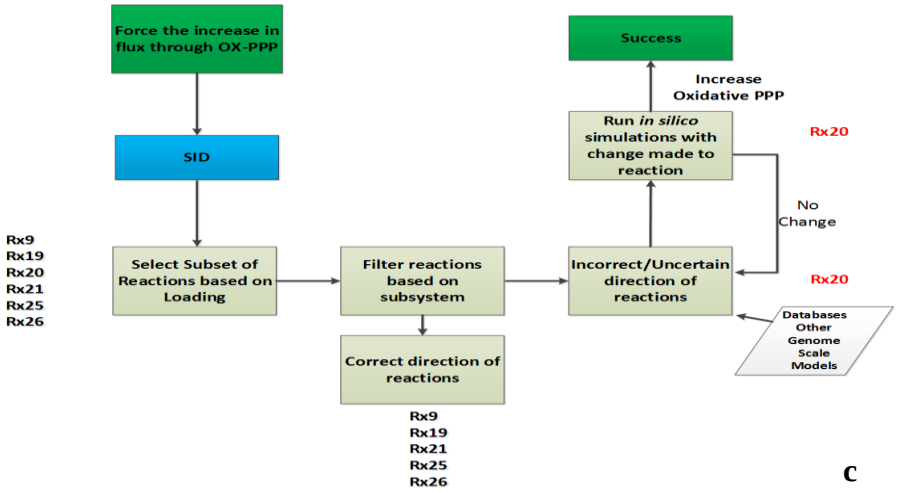

b

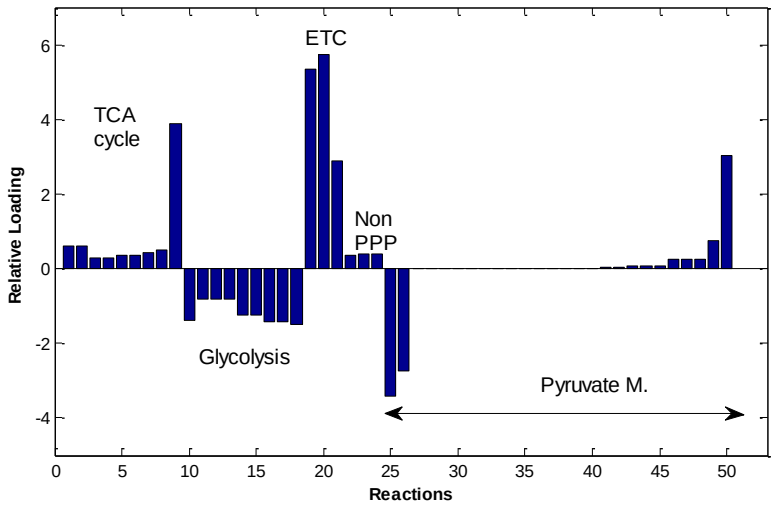

c

Reaction	Reaction equation
Rx9	nad[m] + mal-L[m] ⇔ h[m] + nadh[m] + oaa[m]
Rx19	5 h[m] + nadh[m] + q6[m] → 4 h[c] + nad[m] + q6h2[m]
Rx20	2 h[m] + q6h2[m] + 2 ficytc[m] → 4 h[c] + q6[m] + 2 focytc[m]
Rx21	8 h[m] + o2[m] + 4 focytc[m] → 4 h[c] + 2 h2o[m] + 4 ficytc[m]
Rx25	nad[c] + mal-L[c] <=> h[c] + nadh[c] + oaa[c]
Rx26	h[c] + pyr[c] → acald[c] + co2[c]

Figure 4.3: Guided modification of SID framework. The direction of the oxidative branch of PPP was corrected by SID framework. (a) Flow chart displaying how SID framework was used to uncover the reaction responsible for incorrect direction of the oxidative branch of PPP. (b) Loading plot showing important reactions identified from SID framework. (c) Reaction equations of the reactions selected by SID framework. Appendix A5 has the metabolite names for the metabolites.

Next, the reactions were filtered out based on whether they were moving in the correct or incorrect direction. Figure 4.3 (b) displays the reaction loadings for the main subsystems, where Figure 4.3 (c) shows the reactions that have the highest loading value. Reactions in the correct direction involved the glycolysis pathway, electron transport chain, exchange, and pyruvate metabolism. One reaction (Rx20) was selected for the incorrect direction, which is cytosolic malate dehydrogenase, where the literature shows it is favored in the forward direction. When the direction of this reaction is blocked, and simulations are run under aerobic conditions, this results in the oxidative branch of PPP now being activated and in the correct direction. Reactions can be added to the metabolic model by metabolic databases and genome-scale models of analogous strains. For example, a main focus of iAD828 was the production of xylitol. It was decided to use sensitivity analysis on the model to detect, which metabolite played a role in xylitol production by changing the amount in the objective function. GMP was identified to be an essential metabolite for xylitol production. Next, the specific reactions were selected from the subsystems that contained GMP, such as the purine metabolism, and subsystems that were impacted from the GMP containing subsystems, like PPP. Therefore reactions from metabolic databases (KEGG), and other genome-scale models (iSS884, unpublished *S. stipitis* model, and *S. cerevisiae*, etc) were selected and implemented into the model. If the modification of the reaction causes no affect then the steps are looped back.

Tables 4.2-4.4 shows the reactions that were modified, deleted, and added, respectively in iAD828. There were 13 reactions that were modified. RX_m 1 -3 changes occurred in complex I, III and IV of the electron transport change, where the protons were balanced. RX_m 4 - 6 reversible reaction was blocked to ensure the TCA cycle was moving in the proper direction. As mentioned early, malate dehydrogenase, RX_m 7, when blocked resulted in the oxidative branch

of the PPP to be in the correct direction for aerobic conditions. Also RX_m 7 plays a role in byproduct production, such as ethanol (a) and acetic acid (b), which is shown in Figure 4.4.

Table 4.2: Reactions that were modified in iAD828

RX_m	Reactions	Change
1	5 h[m] + nadh[m] + q6[m] -> 4 h[c] + nad[m] + q6h2[m]	Proton Change
2	2 h[m] + q6h2[m] + 2 ficytc[m] -> 4 h[c] + q6[m] + 2 focytc[m]	
3	8 h[m] + o2[m] + 4 focytc[m] -> 4 h[c] + 2 h2o[m] + 4 ficytc[m]	
4	adp[m] + pi[m] + succoa[m] ⇔ succ[m] + atp[m] + coa[m]	Reverse direction blocked
5	gdp[m] + pi[m] + succoa[m] ⇔ succ[m] + gtp[m] + coa[m]	Reverse direction blocked
6	nad[m] + mal-L[m] ⇔ oaa[m] + h[m] + nadh[m]	Reverse direction blocked
7	nad[c] + mal-L[c] ⇔ oaa[c] + h[c] + nadh[c]	Reverse direction blocked
8	atp[c] + r5p[c] ⇔ h[c] + amp[c] + prpp[c]	Reverse direction blocked
9	atp[c] + gdp[c] ⇔ adp[c] + gtp[c]	Reverse direction blocked
10	atp[c] + dgdp[c] ⇔ adp[c] + dgtp[c]	Reverse direction blocked
11	atp[c] + dadp[c] ⇔ adp[c] + datp[c]	Reverse direction blocked
12	akg[m] + ile-L[m] ⇔ glu-L[m] + 3mop[m]	Reverse direction blocked
13	akg[m] + leu-L[m] ⇔ glu-L[m] + 4mop[m]	Reverse direction blocked

Ethanol production is extended when RX_m 7 was present, and this was negative implications when compared with aerobic validation experiments, talked about later. Acetic acid production was present when RX_m 7 was present. When RX_m 8 was operating in the reversible direction this resulted in a flux value around -999 mmol/gDW·hr when the oxygen uptake rate was above 0.78 mmol/gDW·hr. RX_m 9 – 11 reverse direction was blocked in order to prevent the fluxes from hitting the lower bound (-1000), which would cause high production rates of ATP through this reaction. This is not realistic, because we know that ATP synthesis should be dominant in the electron transport chain. Similar to RX_m 9 – 11, RX_m 12 -13 results in fluxes that are close to hitting the lower bound and these are also coupled to each other.

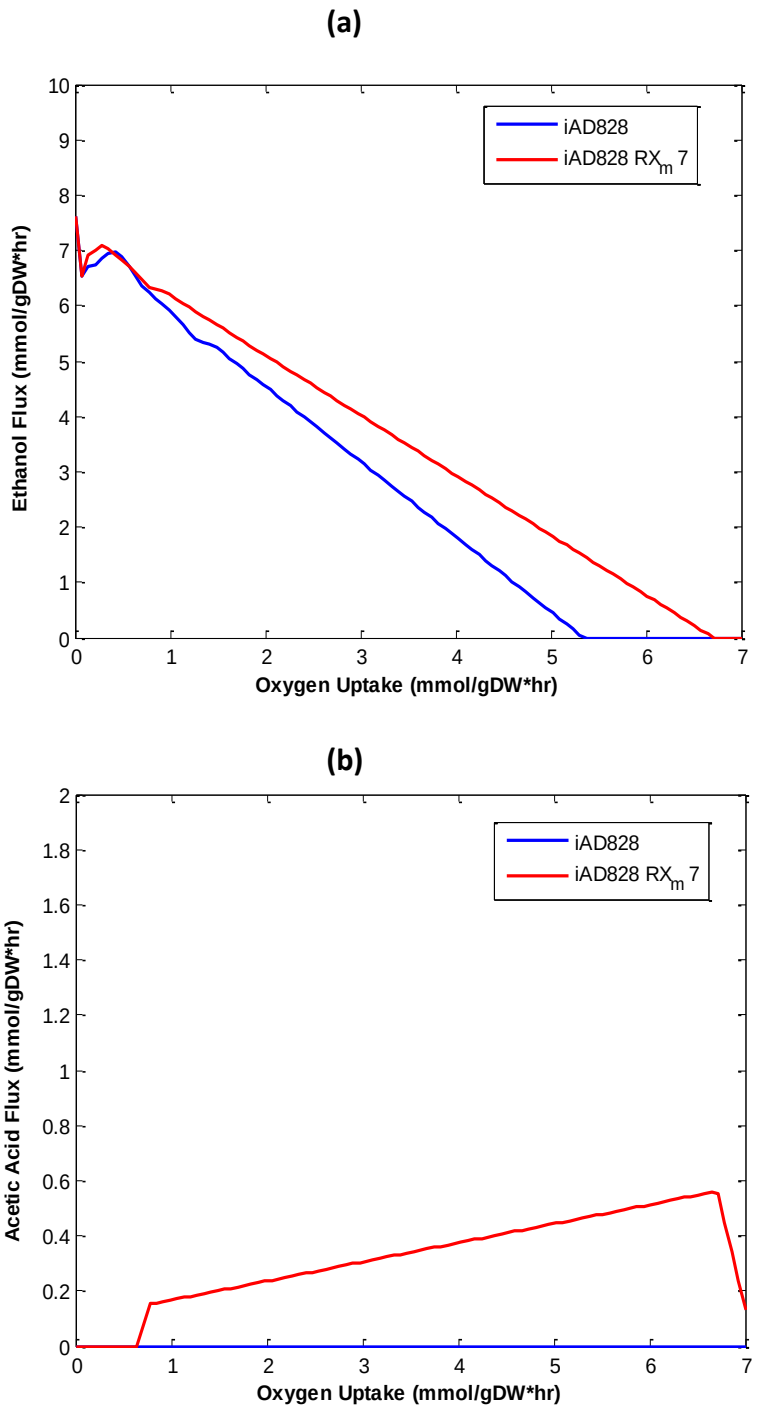

Figure 4.4: Effect of RX_m 7 on ethanol and acetic acid production for iAD828

Table 4.3 shows the deleted reactions, by not deleting RX_d 1and 2 results in no xylitol production. This information was found from unpublished genome-scale model of *S. stipitis* (Li, 2012). Rx_d 3 was deleted, because this reaction would cause a loop with complex II. Rx_d 4 and 5 was deleted, because this caused irregular behavior in the TCA cycle, by this reaction in the TCA

cycle (mitochondria) by blocked. Deleting RX_d 6 enhanced the strength of iAD828, because validation experiments that were taken from iBB814 were changed from incorrect to correct, these results will be presented later.

Table 4.3: Reactions deleted from iAD828

RX_d	Reactions	Reason
1	abt-D[e] ->	Impact on xylitol
2	abt-L[e] ->	
3	fum[c] + fadh2[m] -> succ[c] + fad[m]	Causes loop
4	fum[c] + h_2o[c] -> mal-L[c]	Branch TCA cycle
5	nadp[c] + icit[c] -> nadph[c] + co2[c] + akg[c]	TCA cycle
6	glu5sa[m] + h2o[m] + nadp[m] -> glu-L[m] + 2 h[m] + nadph[m]	Improved model prediction
7	h[c] + nadph[c] + akg[c] + nh4[c] -> nadp[c] + h2o[c] + glu-L[c]	Improved model prediction

Table 4.4 displays the reactions that were added to the model, where the RX_A 1 and 2 were shown to have an impact on xylitol, where RX_A 1 was taken from iSS884 and RX_A 2 was identified in metabolic database for *S. stipitis*, both were taken from the purine metabolism. RX_A 3 also had an effect on xylitol production, where this reaction was located in the mitochondria in iBB814. One of the problems that were encountered was matching the model results to the experimental validation results, under aerobic conditions, when both glucose and xylose was used as the substrate. The validation experiment showed no ethanol production, where iAD828 was producing ethanol. This was due to having not enough NADH being oxidized in the cytosol. An oxidation reaction that alleviates the amount of NADH in the cytosol was glutamate dehydrogenase, which uses akg[c]. RX_A 4, 8, and 11 were reactions that played as a source for akg[c] production. RX_A 4 operates in the reverse direction, RX_A 8 is a mitochondria transport reaction that proceeds in the forward direction, and RX_A 11 is a mitochondria transport reaction that operates in the reverse direction.

Table 4.4: Reactions added to iAD828

RX_A	Reactions	Reason
1	prpp[c] + gua[c] <=> ppi[c] + gmp[c]	Impact on xylitol
2	h2o[c] + gsn[c] <=> nh4[c] + xtsn[c]	
3	ser-L[c] + 0.01 cdpdag[c] <=> 0.01 ps[c] + cmp[c]	
4	ala-L[c] + akg[c] <=> pyr[c] + glu-L[c]	Impact on ethanol – minimal
5	glu-L[m] + h[m] -> co2[m] + 4abut[m]	Succinate bypass
6	akg[m] + 4abut[m] <=> glu-L[m] + succsal[m]	
7	h2o[m] + nadp[m] + succsal[m] -> succ[m] + 2 h[m] + nadph[m]	
8	akg[m] + mal-L[c] <=> akg[c] + mal-L[m]	Impact on ethanol and xylitol
9	h[c] + nadh[c] + glu-L[c] <=> 2 h_2o[c] + nad[c] + 1pyr5c[c]	
10	glu-L[m] + h[m] + nadh[m] <=> 2 h_2o[m] + nad[m] + 1pyr5c[m]	
11	akg[c] + 2oxoadp[m] <=> akg[m] + 2oxoadp[c]	Impact on ethanol
12	h_2o[c] + ptd1ino[c] <=> 12dgr[c] + mi1p-D[c]	

These reactions cause an excess of akg[c] in the model that needs to be consumed, and the model choses to use glutamate dehydrogenase. Therefore, there is now the validation experiments match the model results under aerobic condition for both glucose and xylose. The succinate bypass RX_A 5 - 7 was implemented in the model, as an alternative route to produce succinate in the mitochondria as imposed from the TCA cycle. Another part that added to having successful matching of the model to the validation experiments were RX_A 9 and 10, these reactions were found in the *S. cerevisiae* model. RX_A 12 played a role in ethanol and xylitol production.

4.2.3 *In silico* examination and traditional experimental validation

The genome-scale metabolic models were evaluated by flux balance analysis (FBA), in which the COBRA toolbox (Schellenberger et al., 2011) was used. For all the simulations, the objective function was biomass growth. The upper limits of xylose and oxygen uptakes were varied based on the preselected conditions, while the other exchange compounds (NH^{4+}, H^+, $SO4^{2-}$, Pi^{2-}, H_2O, Fe^{2+}) were given the option to enter and exit the network freely, with upper and

lower bounds of -1000 to 1000 mmol/gDW·hr. The final metabolic products (CO_2, ethanol, acetic acid, etc.) were allowed to exit the system freely, where the reaction flux was constrained to 0 – 1000 mmol/gDW·hr, which prevents product uptake. The growth associated maintenance energy was set to 2.6 mmol/gDW·hr (Balagurunathan et al., 2012). This setup was applied to all *in silico* simulations for both models.

4.3 Results and Discussion

3D plots that varied xylose and oxygen were made for iAD828 for growth, ethanol, and CO_2, which were compared with the published genome-scale metabolic network models of iSS884 and iBB814. Note that xylitol was only done for iAD828, since iSS884 and iBB814 does not produce xylitol. SID framework was used to compare iSS84 and iBB814 with the newly developed model of iAD828, under oxygen-limited and aerobic conditions. The central carbon metabolism was the focus since it encompasses the significant metabolic behavior and literature was available. iAD828 had a major improvement compared to the previous models, since xylose metabolism, glycolysis, oxidative and non-oxidative PPP, TCA cycle, and ETC are now operating correctly. The same validation experiments that were used in comparing iSS884 and iBB814 were used to show how iAD828 outperforms the former models. A recently published paper was used to validate the production of xylitol for iAD828.

4.3.1 Phenotype phase plane analysis

In this analysis, xylose and oxygen uptake rates were chosen as the independent variables, with each of them varying from 0 – 10 mmol/gDW·hr for the analysis of growth rate, ethanol and CO_2. Since xylitol is only produced under oxygen-limited condition, iAD828 results were compared with the published models of iSS884 and iBB814.

(a)

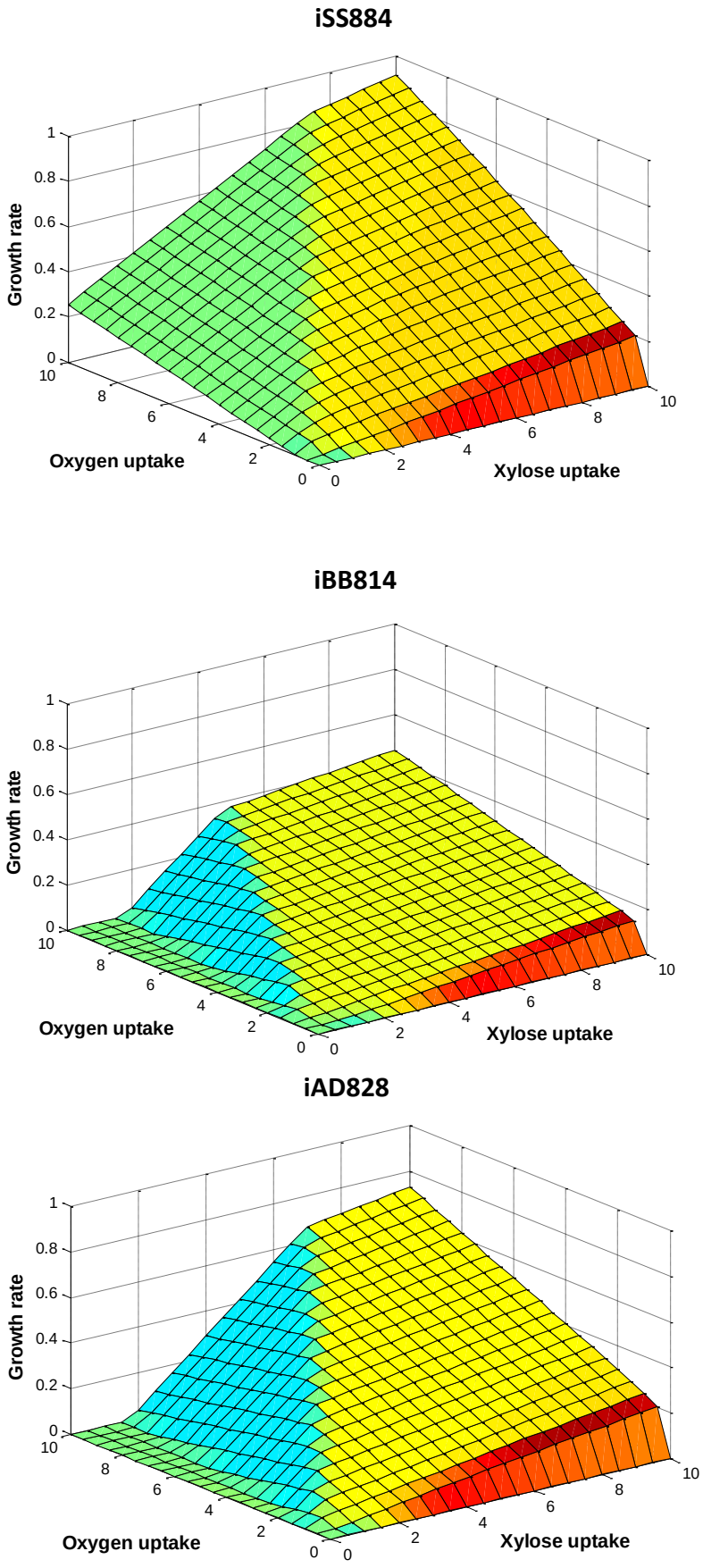
iSS884
Growth rate
Oxygen uptake
Xylose uptake
iBB814
Growth rate
Oxygen uptake
Xylose uptake
iAD828
Growth rate
Oxygen uptake
Xylose uptake

(b)

iSS884

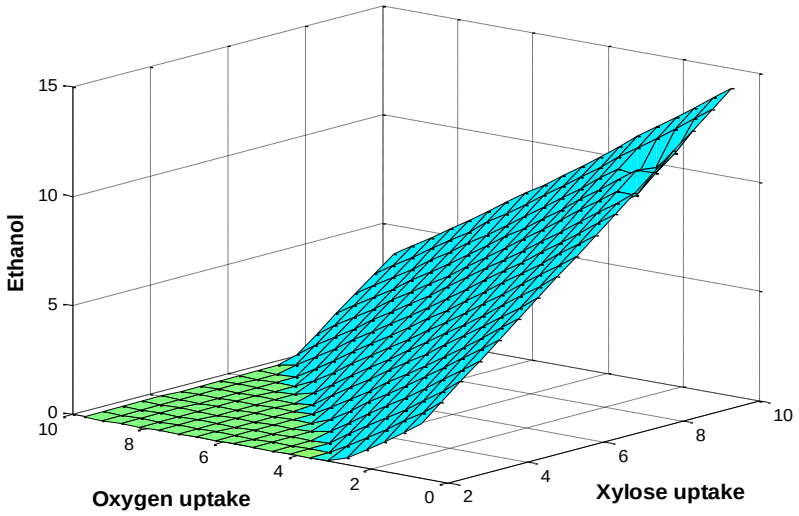

iBB814

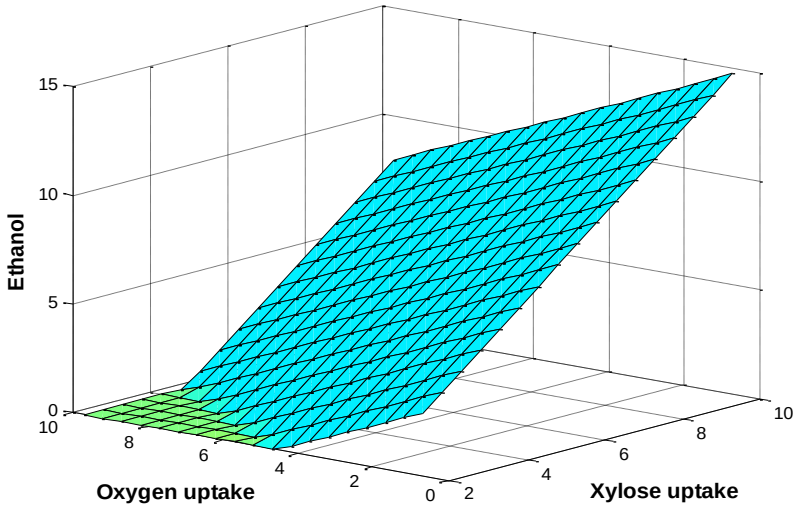

iAD828

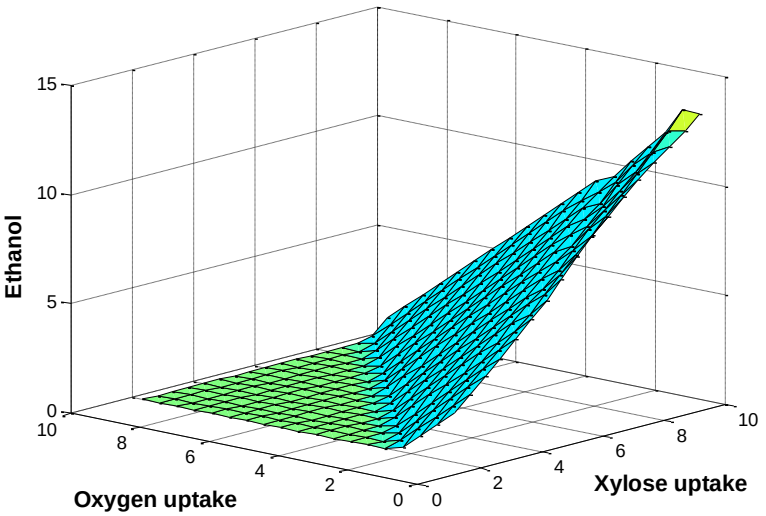

(c)

iSS884

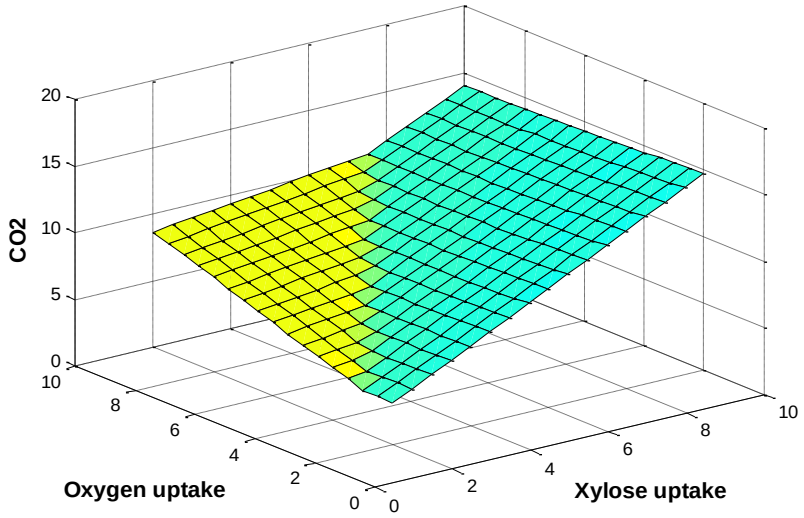

iBB814

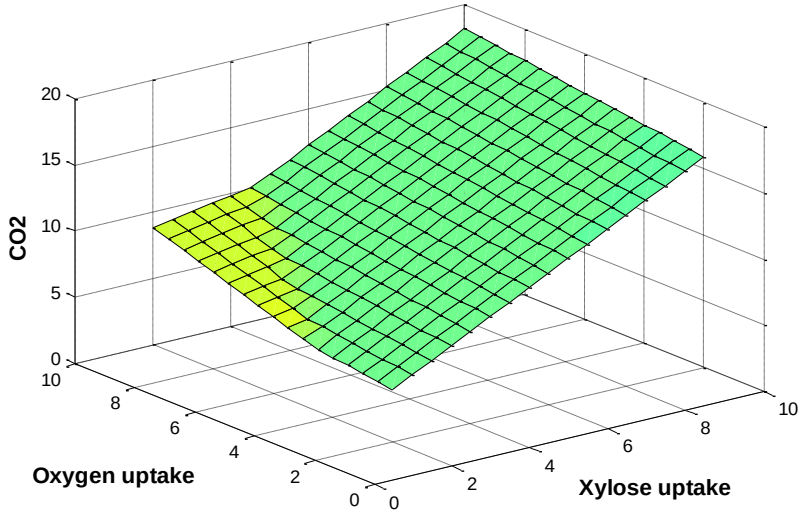

iAD828

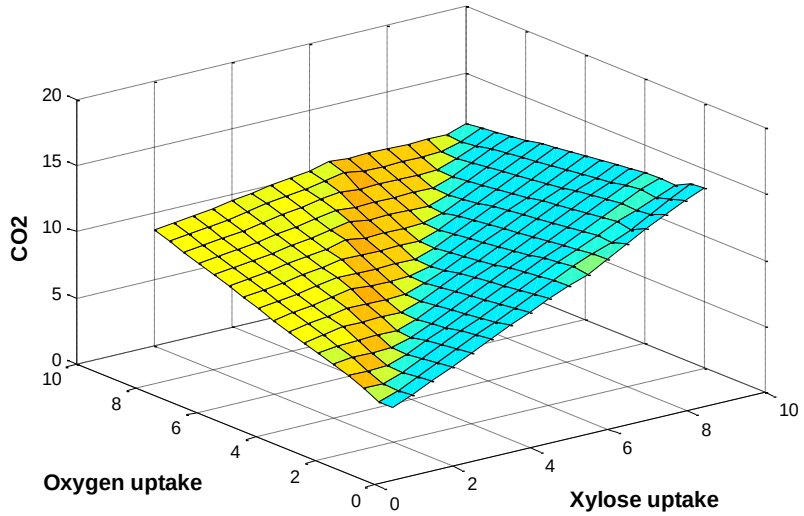

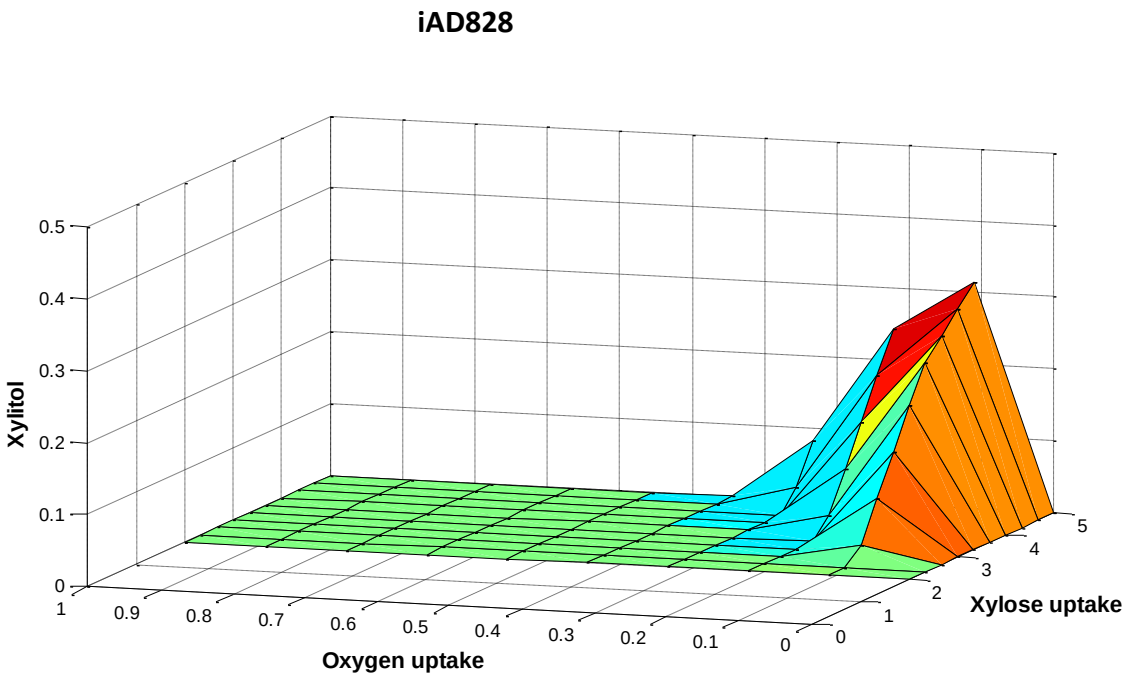

Figure 4.5: 3D product profiles: (a) Growth rate, (b) Ethanol, (c) CO_2, (d) Xylitol

Figure 4.5 (a) show how cell growth rate is affected by different substrate uptake rates, where the differently colored regions represent different growth behaviors. Overall, cell growth profiles predicted by iSS884 and iBB814 are similar to each other, except that the growth rate predicted by iBB814 is significantly lower than iSS884 and iAD828. Figure 4.5 (b) shows the ethanol profiles for the models, where both iSS884 and iAD828 predicts a larger area of zero ethanol production, which is shown as the green phenotype. Figure 4.5 (c) shows the CO_2 production profiles for the models, where iSS884 and iAD828 have great similarity. Figure 4.5 (d) shows the xylitol production profile for iAD828, where the xylitol production rate only occurs under oxygen-limited conditions.

4.3.2 Model comparison through the SID framework

SID framework was carried out on iSS884, iBB814, and iAD828, where 2D phenotype phase plots were generated to compare the distribution of the phenotypes, which is shown in

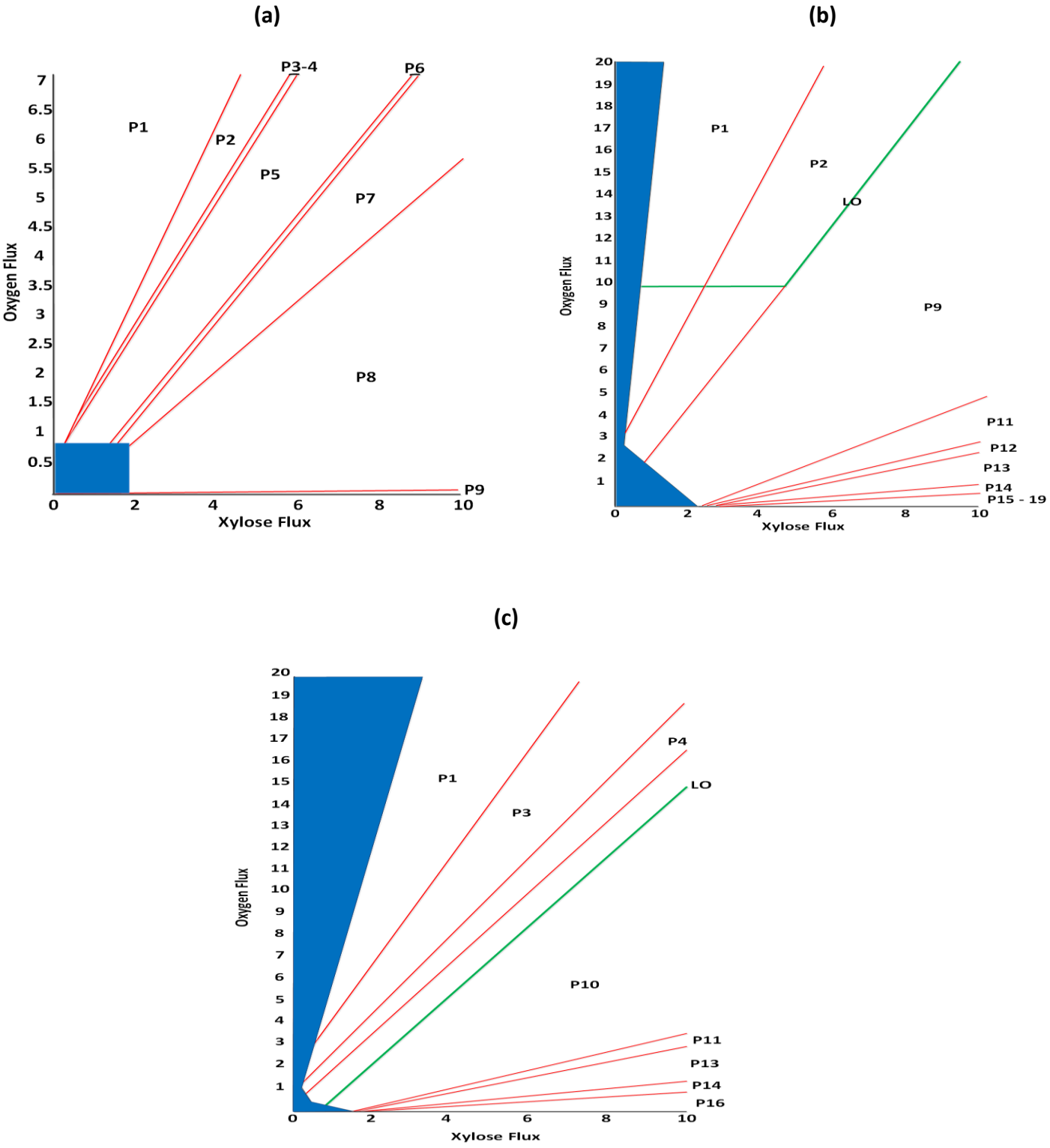

Figure 4.6: 2D phenotype phase plots. (a) iSS884, (b) iBB814, and (c) iAD828

Figure 4.6 (a) – (c) respectively. The phenotypes are labeled as P and are ordered by the most oxygen plentiful to least (aerobic to oxygen-limited). The blue regions represent infeasible regions. iSS884 has the fewest phenotypes, where P1 and P8 encompass the majority of the metabolic behavior. Certain phenotypes change only minimally, which is why they are combined, for example, P3 and P4 in iSS884. Moving to iBB814, P9 is the most dominant phenotype in terms of representing the phenotypic space, where P1 and P2 ahave large phenotypic regions. As the oxygen pickup rate decreases from P2, there are a lot of phenotypes that occupy very minimal metabolic behavior, which are omitted from the plot, such P3 – P8. The infeasible region of iBB814 is larger and infeasible regions exist in the aerobic region. iAD828 has similar amount of phenotypes compared to iBB814, where it has similar features as iBB814 in terms of the infeasible region and lower oxygen region phenotypes. The LO for iSS884 always hits the lower bound for the oxygen uptake (-1000 mmol/gDW·hr: maximum uptake) and that is why it is not shown in the plot, thus iSS884 has a serious error in the phenotypic makeup. The LO for iBB814, hits an oxygen pickup rate of 10 mmol/gDW·hr for a xylose pickup range of 1.8 to 4.69 mmol/gDW·hr, then the oxygen pickup rate increases for xylose pickup rates above 4.69 mmol/gDW·hr, which is designated by the green line and labeled LO. The LO for iAD828 has the correct response, since it the LO should been a diagonal line. LO is defined as the optimal relationship between the xylose and oxygen uptake rates.

The first condition that was investigated was under oxygen-limited condition, where the results are shown in Figure 4.7. The oxygen pick up rate varied from 0.11 – 0.15 mmol/gDW·hr. This correlated with the following phenotypes: P8 for iSS884, P17 for iBB814, and P17 for iAD828. Both branches of the PPP, oxidative and non-oxidative for all the models are correctly regulated. iSS884 and iAD828 have the glycolysis pathway downregulated, while iBB814 is

upregulated, where the literature is in accordance with iSS884 and iAD828 (Skoog and Hahn-Hägerdal, 1990). The xylose metabolism is affected differently in iAD828, due to the production of xylitol, which is shown to be a key byproduct under oxygen-limited condition. iSS884 has irregular behavior in ethanol production, because it not only occurs in two compartments, but there is also a reaction that proceeds in the wrong direction, which consumes ethanol. That is shown in Figure 4.7 by the thick red line with NAD above it, signifying that it utilizes this type of cofactor. The reaction that produces ethanol in the cytosol uses NADPH, but there is not much change. The major variation of ethanol production occurs in the mitochondria, where this reaction is upregulated. As noted in the previous chapter that both reactions in the cytosol are close to hitting the upper bound, above 990 mmol/gDW·hr.

One place this unusual behavior is traced to is that malate dehydrogenase is operating in reverse direction in the TCA cycle, and is very heavily downregulated, which is directly connected to the high amount of oxaloacetate (oaa) that is being transported from the cytosol. The irregular behavior of ethanol production and reactions connected to malate dehydrogenase in the mitochondria show iSS884 inability to have a biologically sound redox balance. iAD828 follows iSS884 in that ethanol production is declining, while iBB814 has increasing ethanol production. All models have a branched TCA cycle; however there are distinctions between the models. iSS884 and iAD828 branch at the same point, however there is irregular behavior in iSS884 and iBB814, where malate dehydrogenase is operating in the reverse direction. Lastly, the electron transport chain of iBB814 and iAD828 share similar characteristics, though iBB814 has a low upregulation of complex I compared to iAD828. As previous described, iSS884 has biologically irregular behavior in the electron transport chain.

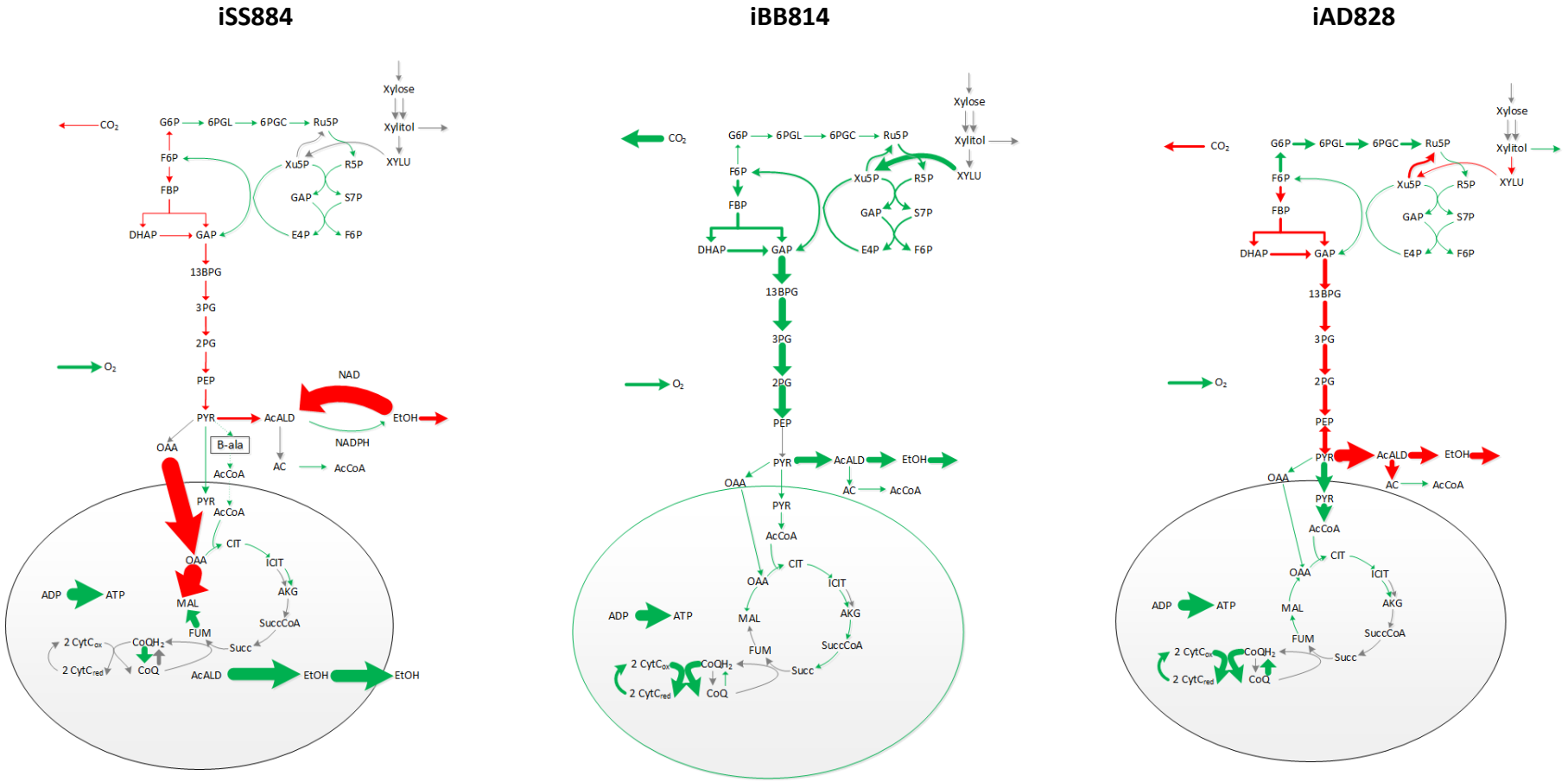

Figure 4.7: Comparison of SID framework results for iSS884, iBB814, and iAD828 under oxygen-limited condition

The next phenotype that was examined, P16, dealt with a decrease in xylitol production rate, where the oxygen uptake rate was varied 0.161 – 0.385 mmol/gDW·hr, where the results are shown in Figure 4.8 This phenotype results in a major shift in the direction of regulation glycolysis, and the regulation direction of the byproducts of ethanol and carbon dioxide. All the remaining central carbon metabolism pathways stay in the same regulation direction as P17. The upregulation oxidative branch of the pentose phosphate pathway for P16 has diminished in comparison to P17.

The next phenotype P14 that was investigated was still under oxygen-limited condition, but now the xylitol production is eliminated, which is shown in Figure 4.9. The oxygen uptake rate was varied between 0.67 – 0.90 mmol/gDW·hr.

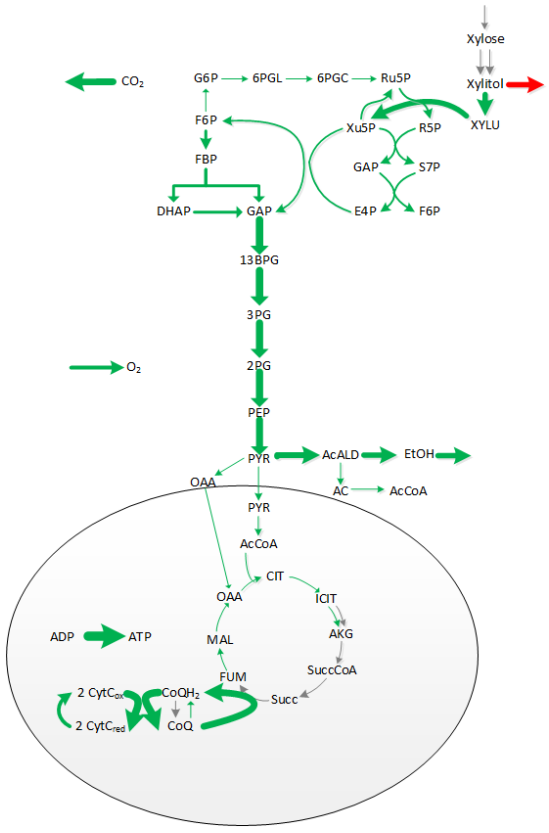

Figure 4.8: SID framework results of P16 for iAD828

The glycolysis pathway reverts back to the correct regulation direction as in P17, but now is downregulated in a less magnitude. Also the products of CO_2 and ethanol follow the similar trend in P17. Like the previous phenotypes of P17 and P16, the TCA cycle is branched, however the branching is different in that now succinate dehydrogenase is the reaction occurring after the branching.

Curiosity was raised about what reaction pathways affected the incorrect regulation direction of glycolysis in P16. There was a change in the regulation direction of the production profile of xylitol from increasing to decreasing. It was decide to see whether eliminating xylitol production would result in shifting the glycolysis pathway fluxes to the correct regulation direction. This was done by blocking the exchange reaction of xylitol.

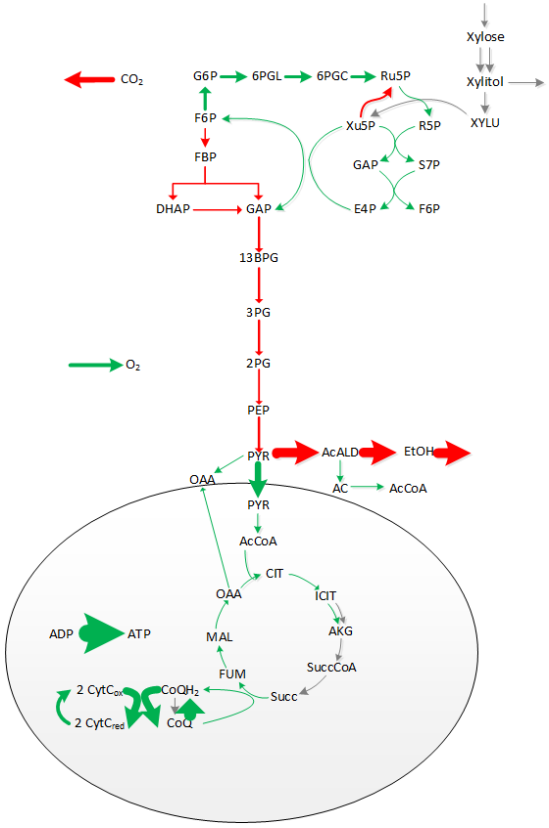

Figure 4.9: SID framework results of P14 for iAD828

Removing xylitol production does not cause the glycolysis pathway to change to the correct response. One interesting change that was found when blocking the xylitol production was that now the oxidative branch of PPP was downregulated. This brought about possible explanation, that in P16 the oxidative branch of the PPP was reduced in activation. This propagated *in silico* experiments that forced the upregulation of the oxidative branch to be above the optimized solution. This in turn caused the xylitol production to be decreased to zero. The region where xylitol production was zero resulted in glycolysis now being in the correct regulation direction. Looking at the loading values for the oxidative branch and non-oxidative branch of PPP, we find that the loading value is always higher for the oxidative branch when the glycolysis pathway is in the correct direction. A final study was conducted on P16 that lowers the upregulation of the non-oxidative branch of PPP to be less than the oxidative branch of PPP. The results are agreement with what was observed before, which brought about glycolysis in the correct regulation direction. It is evident from this analysis that glycolysis, oxidative branch of PPP, and non-oxidative branch of PPP are correlated.

The next phenotype P10 in iAD828 that was examined was in the aerobic regime, and this was compared with iSS884 (P5) and iBB814 (P9), which is seen in Figure 4.10. First looking at the oxidative branch of PPP, iSS884 and iAD828 have it in the correct regulation direction, while iBB814 does not have the reactions affected. The next subsystems that were investigated were glycolysis and the non-oxidative branch, and all models have correct responses. Turning to the TCA cycle, we see that iAD828 is the only model where the TCA cycle is fully activated; both iSS884 and iBB814 have fumarase reaction inactivated, thus causing a branch. Also in iSS884, malate dehydrogenase is heavily upregulated compared to the other TCA cycle reactions that are all on the same magnitude. As stated before, the electron

transport chain in iSS884 is partially activated, which is against literature, which adheres to full activation. Again irregular behavior is involved in ethanol production for aerobic condition, where the upper bound is hit for the cofactor NADPH throughout this phenotype, which why it is given a gray lines since there is no variation. Ethanol is used as a reactant for acetaldehyde production in the cytosol by using the cofactor NAD, which heavily upregulated. In the mitochondria, we see that ethanol production is significantly downregulated. As in oxygen-limited condition, oxaloacetate transportation between the cytosol and mitochondria is heavily varied, but now for aerobic condition it is transported to the mitochondria. iBB814 and iAD828 show biologically regular behavior for ethanol, where both of them are downregulated.

The final phenotype that was investigated was the line of optimality, which is defined as the optimal relationship between the xylose and oxygen uptake rates. In other words, this provides the model with optimal utilization of both substrates, neither one is limited. The line of optimality was determined by setting the oxygen uptake to the upper bound and varying the xylose uptake. This allows for the model to select the optimal oxygen pickup for each xylose uptake. SID framework was carried out on iSS884, iBB814, and iAD828, where the results are displayed in Figure 4.11. Unfortunately for iSS884, the oxygen uptake was always hitting the lower bound of -1000 mmol/gDW•hr, meaning that this model failed in determining the optimal substrate uptakes. For iBB814, we see that mostly all the subsystems are upregulated; however the oxidative branch of PPP was being downregulated, meaning this too fails the tests for the line of optimality. iAD828 was the only model that responded correctly, where all the appropriated subsystems were in the correct direction of regulation, with no byproducts being produced.

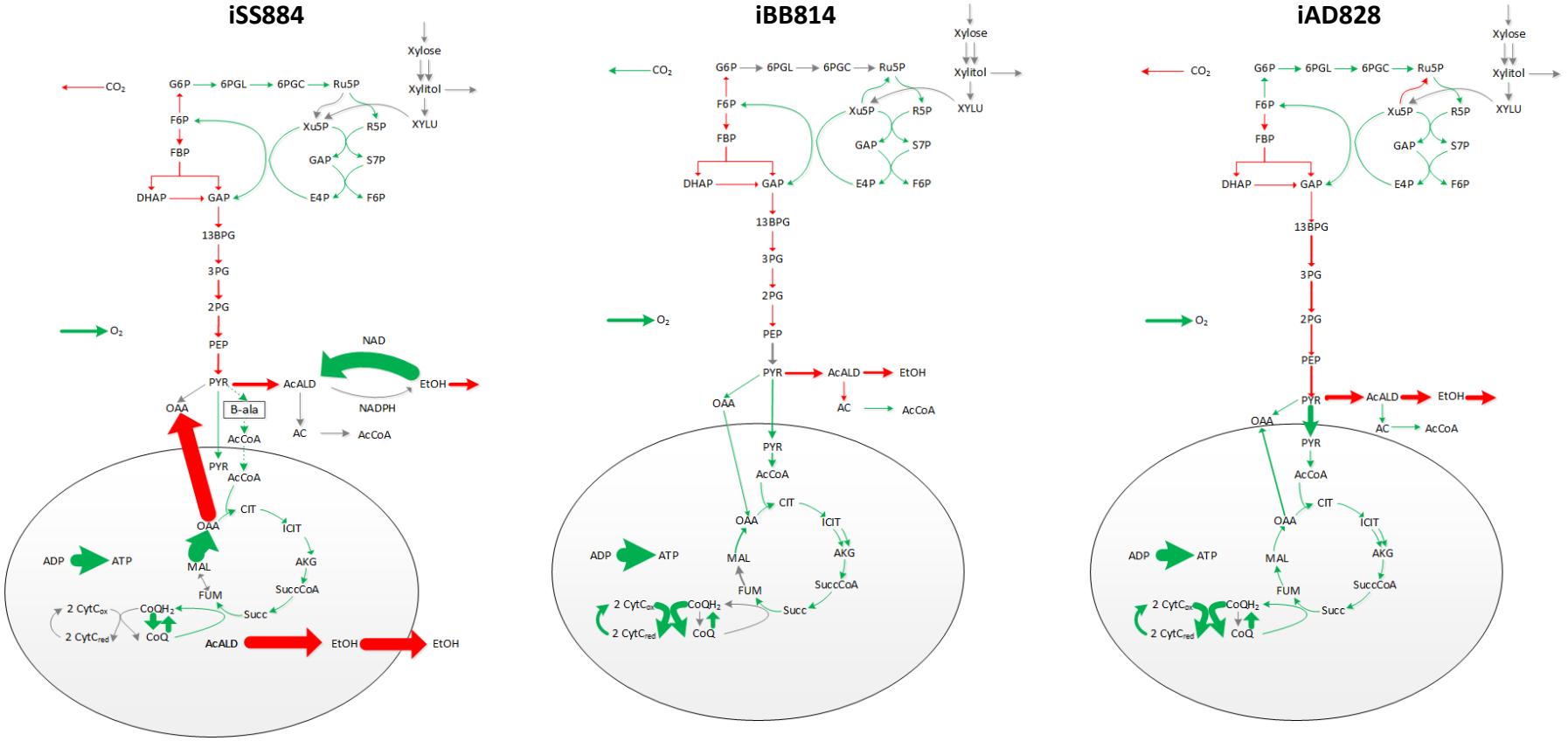

Figure 4.10: Comparison of SID framework results under aerobic condition for iSS884, iBB814, and iAD828

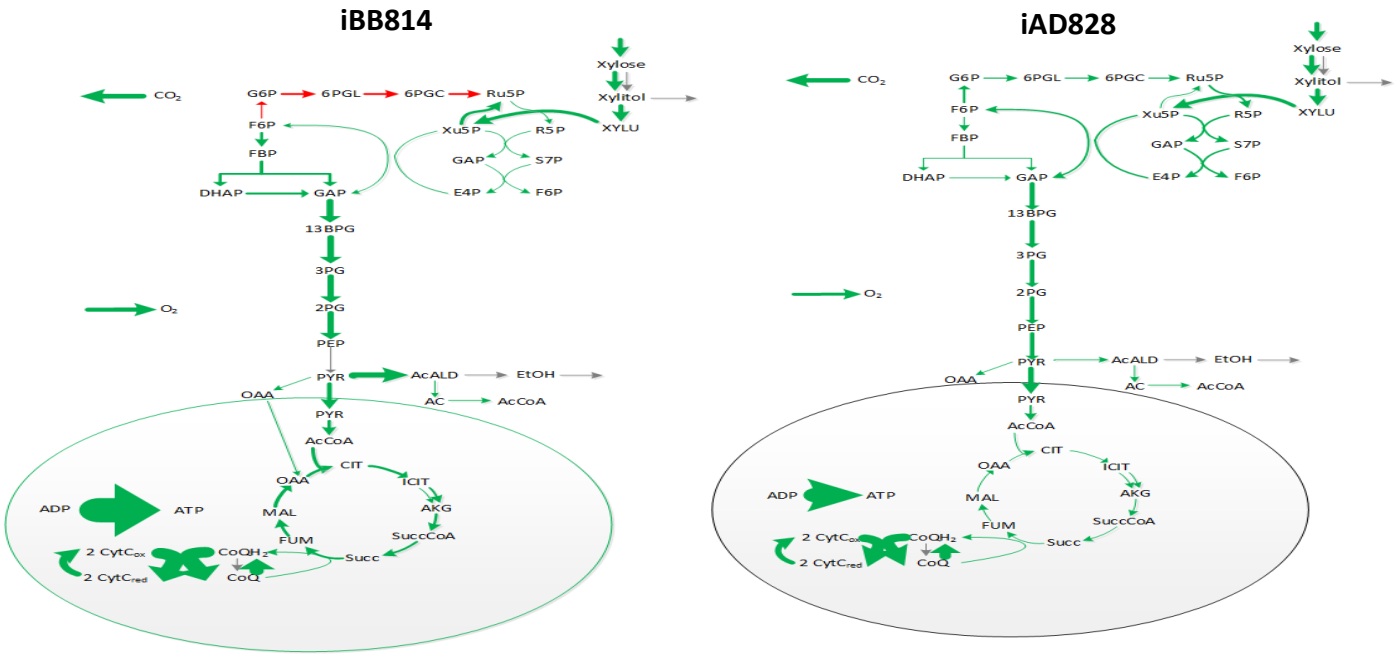

Figure 4.11: Line of optimality SID framework results of iBB814 and iAD828

Lastly, iAD828 is in agreement with the literature in comparing the metabolic behavior under oxygen-limited condition and aerobic condition (Li, 2012), which is seen in Table 4.5. For Case 1, glycolysis is more affected under oxygen-limited condition, because the energy metabolism is less efficient under oxygen-limited condition. Supporting evidence for this is demonstrated by expression data of the upregulation of genes that translate into glycolytic enzymes, such as Fba1, Pfk1, Pfk2, Gpm1.1, Gpm1.2, Pgk1, and Tpi1 (Jeffries et al., 2007).

Table 4.5: Metabolic artifacts to further validate iAD828. Case 1 shows glycolytic genes: Gpm - Phosphoglycerate mutase, Pfk - Phosphofructokinase, Pgk - Phosphoglycerate kinase, Fba - Fructose-1,6-bisphosphate aldolase, Tpi - Triose Phosphate Isomerase.

Case 1	Genes	Oxygen -L	Aerobic
	Gpm1.1,2	7.32	6.79
	Pfk1,2	2.92	2.55
	Pgk1	7.40	6.95
	Fba1	2.92	2.55
	Tpi1	2.92	2.54
Case 2	Reactions	Oxygen-L	Aerobic
	Fatty acid synthase (n-C10:0)	2.94×10^{-3}	0
	Fatty acid synthase (n-C12:0)	2.85×10^{-3}	0
	Fatty acid synthase (n-C14:0)	2.31×10^{-3}	0
	Fatty-acyl-CoA synthase (n-C16:0CoA)	2.03×10^{-3}	0
	Fatty acid synthase (n-C18:0)	8.10 x 10-4	0
Case 3	Reactions	Oxygen-L	Aerobic
	Citrate -> α-Ketoglutarate	0.08	0.61
	α-Ketoglutarate -> Succinate	0.00	0.26
	Succinate -> Fumarate	0.00	0.37
	Fumarate -> Oxaloacetate	0.03	0.47

This was simulated by collecting the fluxes under oxygen-limited and aerobic for the glycolytic reactions that were impacted. As shown in Table 4.5, the flux values are higher under oxygen-limited condition, which agrees with the literature. For Case 2, the literature shows that fatty acid synthesis transcripts are higher under oxygen-limited condition. *In silico* simulations were run in iAD828 that demonstrated this by only having fatty acid synthesis reactions active under oxygen-limited condition (Jeffries, 2006). Moving to Case 3, the TCA cycle should be utilized more under aerobic condition, due to being the most efficient pathway for ATP production. iAD828 validates this result by having a higheer flux under aerobic condition (Li, 2012).

4.3.3 Validation experiments

To further confirm iAD828, the same validation experiments that were carried out in Chapter 3 are shown here. Validation experiments that were taking from the independent data

set are shown in Figure 4.12. The *in silico* results were compared with the validation experiments by equating the xylose and oxygen uptake rates of the experiment (Exp) to the models (iSS884, iBB814, and iAD828), and comparing the outputs, ethanol, CO_2, and biomass. Under xylose oxygen-limited condition, seen in Figure 4.12 (a), the experimental ethanol production is very close to the ethanol of iAD828. For carbon dioxide, iSS884 and iBB814 are a lot higher than the experimental value, while iAD828 is relatively high; however it is the closest to the experimental value. For the biomass growth, no model pinpoints the experimental results, but iBB814 and iAD828 show considerable accurate results, while iSS884 has the highest offset. Moving to xylose aerobic condition, shown in Figure 4.12 (b), iAD828 is the only model that is in conjunction with the experiment of having no ethanol production. iSS884 is really close to zero, while iBB814 fairs poorly. The models overall have a better prediction performance for CO_2 in this case, where iAD828 has the best results and iSS884 is very close behind. For biomass production, iAD828 is extremely close to the experimental value, and taking note that iBB814 is relatively very low to the experimental value. Changing to glucose oxygen-limited condition, shown in Figure 4.12 (c), ethanol and carbon dioxide for iSS884 and iAD828 prediction is really well compared to the experimental values, while iBB814 has the worst prediction. For biomass production, iAD828 fairs slightly better than iSS884 followed by iBB814. Moving to the final case of glucose aerobic, shown in Figure 4.12 (d), again similar behavior of xylose aerobic condition is illustrated here. For carbon dioxide, iSS884 and iAD828 are on target with the experimental, while iBB814 is lagging behind. For biomass, iAD828 is the only model that has great prediction performance.

The other quantitative experiment was from iSS884 paper, which is displayed in Figure 4.13, where the same comparison procedure is used. These validation experiments deal with very low oxygen conditions at less than 1 mmol/gDW·hr, compared to the independent set where the levels were much higher. Beginning with the lowest oxygen uptake rate, which is displayed in Figure 4.13 (a), overall the models perform very similar for ethanol and CO_2, but there is a distinction of iBB814 from iSS884 and iAD828 in terms of growth rate, were iSS884 and iAD828 are more accurate. The similar trend is observed in Figure 4.13 (b) and (c).

Switching to qualitative validation experiments, where deleting the original entry reaction into the PPP and configuring an alternative route to PPP by genetically engineering the pathway brought about zero ethanol production. The schematic diagram is shown in Figure 4.14 (a). The results of the experimental and comparison of the GSMMS of iSS884, iBB814, and iAD828 are shown in Figure 4.14 (b). iAD828 has complete agreement with the experimental results. The ethanol production for iBB814 can be misleading; it is only nonzero at the initial point of a zero oxygen uptake rate, and not under very low oxygen conditions. iSS884 has the worst performance, where has nonzero production rates of ethanol. The similarities between iAD828 and iBB814 are due to iAD828 being derived from iBB814.

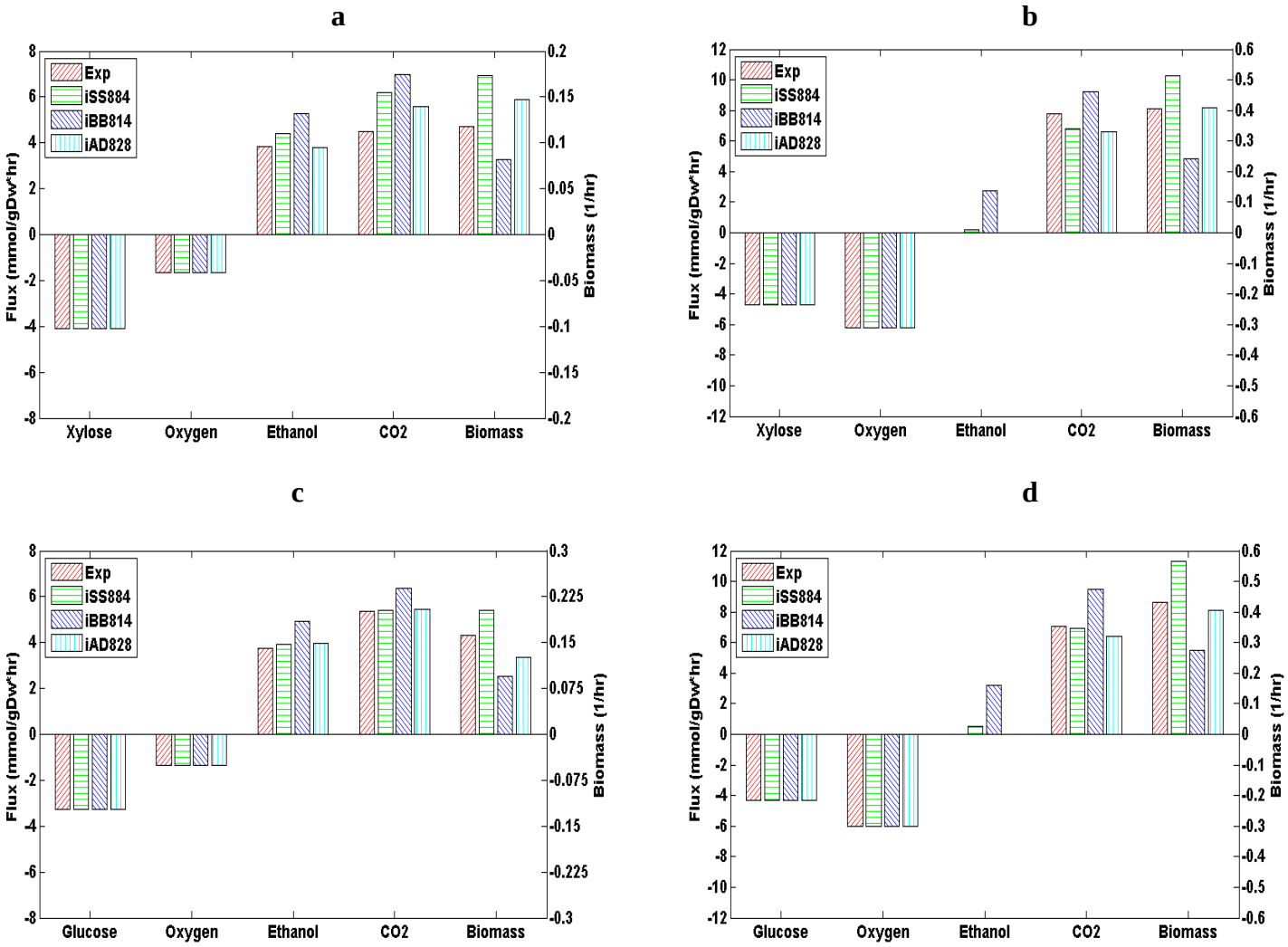

Figure 4.12: Model validation using experimental data from an independent source (Li, 2012). (a) Xylose as carbon source under micro-aerobic condition**,** (b) Xylose as carbon source under aerobic condition, (c) Glucose as carbon source under micro-aerobic condition, (d) Glucose as carbon source under aerobic condition. The model inputs (*i.e.*, xylose or glucose, and oxygen) were set to the experimental values, and model predictions (*i.e.*, ethanol, CO_2, and biomass) were compared with experimental values. The left y-axis is for ethanol and CO_2 fluxes; while the right y-axis is for biomass. Red- Experiement, Green - iSS884, Blue - iBB814, and Light blue - iAD828 Overall, the predictions of iAD828 shows improvement compared to iSS884 and iBB814.

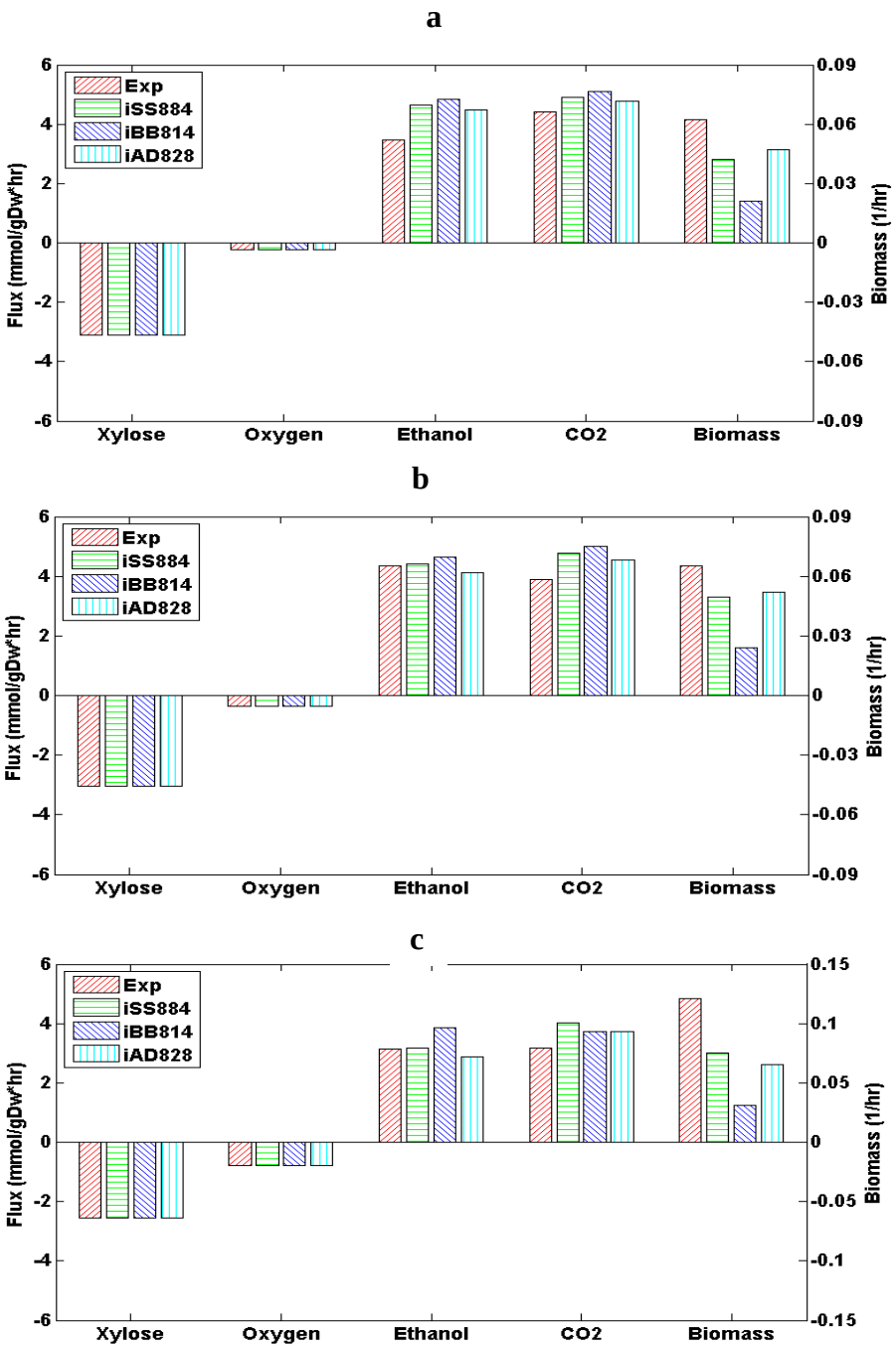

Figure 4.13: Model validation using experimental data from Caspeta et al. (2012) in which iSS884 was published. The model inputs (i.e., xylose and oxygen) were set to the experimental values, and model predictions (i.e., ethanol, CO2, and biomass) were compared with experimental values at different OUR levels: (a) OUR = 0.24, (b) OUR = 0.35, (c) OUR= 0.75. Bars filled with red lines are experimental values; bars filled with green lines are model iSS884 predictions; bars filled with blue lines are model iBB814 predictions; bars filled with light blue lines are model iAD828. The left y-axis is for ethanol and CO2 fluxes; while the right y-axis is for biomass.

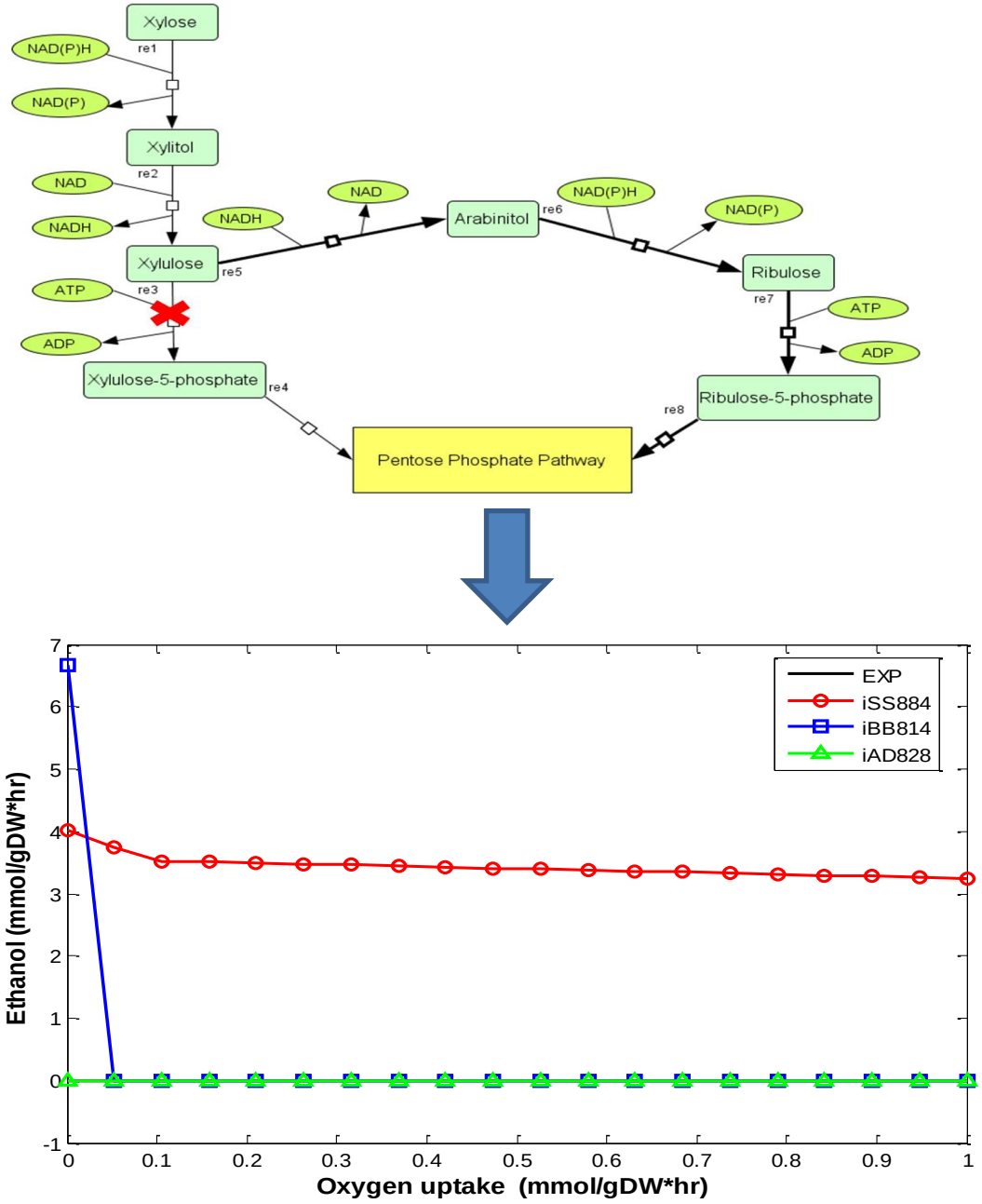

Figure 4.14: Model comparison of the mutant strains of iSS884, iBB814, and iAD828. The mutant with the alternative route into the pentose phosphate pathway for metabolizing xylose by deletion of xylulokinase reaction. (a) Schematic diagram of the wild type xylose metabolism (thin arrows with active xylulokinase reaction (re3)) and mutant with the alternative route (bold arrows with the deletion of re3); (b) Comparison of ethanol production: EXP is the experimental results (solid black line), iSS884 (red circle), iBB814 (blue square), and iAD828 (green triangle).

The other qualitative validation experiment was deleting electron transport chain complexes and classifying the response in different categories of cell growth, the results are shown in Table 4.6. The symbol - - is complete inhibition, for partial inhibition the symbol is -, the symbol for negligible is 0, and the symbol for increase is +. Complete inhibition occurred when the growth rate of the deleted complex(s) was zero. For partial inhibition, this percent decrease of growth rate was based on the oxygen uptake rate, since at a lower oxygen uptake the percent decrease diminishes. The paper that was used did not cite an oxygen uptake rate, so different oxygen uptake rates were run to see if this would result in unusual behavior. The oxygen uptake rate was set at 2 mmol/gDW·hr and for all the partial inhibition cases the percent decrease in growth was over 15 %. For the last case, I + del IV, the percent decrease of growth was 45% and 51 %, for glucose and xylose respectively, which was the highest percent decrease for all the cases, so even though iAD828 did not reach complete inhibition it is still on the right track. Overall, iAD828 results supersede the previous models.

Table 4.6: The effects of inhibiting electron transport chain complexes on cell growth for glucose and xylose: comparison of iSS884 (884) and iBB814 (814) to experimental (Exp) results. Symbols: complete inhibition (- -), partial inhibition (-), negligible (0), enhanced (+), information not available (NA). The model predictions that match the experimental results are shaded. Improvement is made for iAD828 compared to the other models.

Complex	Effect on Growth							
	Glucose				Xylose			
	Exp	**iAD828**	**iSS884**	**iBB814**	**Exp**	**iAD828**	**iSS884**	**iBB814**
I	- -	-	0	0	-	-	0	0
III	NA	-	0	-	-	-	0	-
AOX	0	0	-	0	+	0	-	0
IV	-	-	0	-	-	-	0	-
IV and AOX	- -	- -	-	- -	- -	- -	-	- -
I + del AOX	- -	- -	-	0	- -	- -	-	0
I + del IV	- -	-	0	-	- -	- -	0	-

The iAD828 was used to reproduce the experimental data for xylitol production. Since oxygen uptake rate was not provided for in the experiments, thus ethanol yield was matched between the experiment and model, whereby this was done by changing the oxygen uptake rate and the xylose reductase (XR) redox ratio. The output that was calculated was xylitol production, and this was compared with the experimental values, which are shown in Table 4.7. For all the cases, iAD828 prediction performance of xylitol is very impressive. The results tell us that *S. stipitis* adapts to the environment by adjusting the XR redox ratio. Xylose reductase reaction has two pathways, one uses NADH and the other NADPH. There is not a determined ratio in the literature between the reactions, however the enzyme activity has been recorded, where the XR activity ratio was determined to be 2.20.

Table 4.7: Comparison of iAD828 xylitol results to experimental data. $Y_{E/S}$ is the ethanol yield, where xylose is the substrate (S). Xylose reductase (XR) redox ratio and oxygen uptake rate (OUR) was varied. Minimized the error between ethanol yield of experiment and prediction from iAD828, then examined the xylitol production of both experimental and prediction.

Case #	$Y_{E/S}$ Experiment	$Y_{E/S}$ Prediction	Xylitol Experimental	Xylitol Prediction	Ratio of XR NADPH/NADH	OUR
1	0.3277	0.3296	0.143	0.142	3.26/1.74	2.00
2	0.3582	0.3540	0.0947	0.1078	2.17/2.73	1.93
3	0.3759	0.3769	0.0116	0.0121	2.14/2.86	1.61
4	0.4369	0.4295	0.0174	0.0178	0.01/4.99	0.380

Other papers have suggested that the NADPH route is more active in terms of enzyme activity. Nonetheless, it is not clear whether enzyme activity is directly proportional to flux value; therefore it is not a fair assessment to rely on enzyme activity. The general trend was that the XR redox ratio increased for increasing ethanol yields. Based on intuition, this trend is reasonable, since the reaction (xylose dehydrogenase) following utilizes NAD, which if more of

the NADH reaction of xylose reductase is taken this means greater amounts of available NAD for xylose dehydrogenase is present. As a result, abundant NADH is produced from xylose dehydrogenase and this is provides NADH available for ethanol production. As more carbon flux is pushed through the NADPH xylose reductase reaction then less NADH is available for ethanol production, thus less ethanol is produced.

4.3.4 Redox analysis of iAD828

The elucidation of redox balance of *S. sitpitis* is an important analysis, since it has yet been established what reactions govern the redox, and currently the understanding is poor. If understanding of the redox balance is brought to maturity then this will bring about great potential for successful recombinant strains. iAD828 shows improvement compared to the previous published model, thus it was used to investigate the redox mechanism for *S. sitpitis*.

The key redox reactions were determined by examining the loadings from the SID framework results, where Figure 4.15 displays the relative loading for main redox reaction for P17. Loadings in the positive direction represent a positive correlation between oxygen uptake rate, and for the negative direction there is a negative correlation. Table 4.8 shows the description of the reactions in Figure 4.15, and the starting, ending, and difference of flux values. There are 3 NADH cytosolic consumption reactions (Rx1, Rx4 and Rx9), where Rx9 is the ethanol producing reaction. Excluding Rx9, Rx1 is the main NADH consumption reaction, which is upregulated approximately 4.7X less than Rx9. The other NADH consumption reaction, Rx4, is very insignificant. There are two NADH cytosolic production reactions that were selected, Rx5 and Rx6, where we see that Rx5 is hardly affected and Rx6 is heavily affected negatively. Rx6 is located in the glycolysis pathway, and that is reason why there is such a large flux value. The last cytosolic reactions to discuss are NADPH producing reactions, Rx8 and

Rx10, whereby they are responding in opposing directions. Rx8 is the oxidative branch of PPP, and this is the essential reaction for NADPH production for this phenotype.

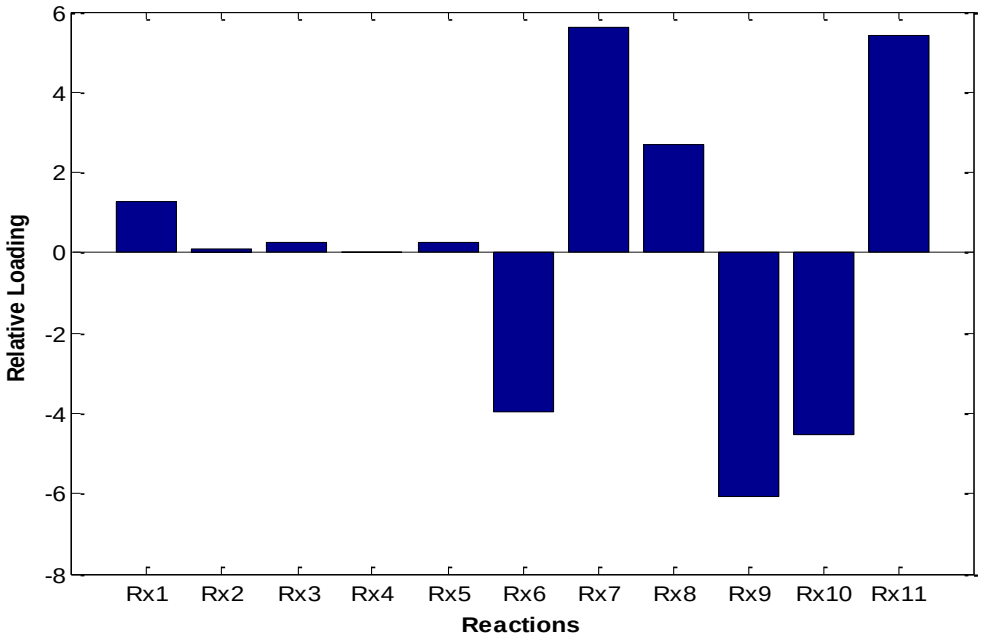

Figure 4.15: Key redox reactions that were identified in P17. Relative loading scales each reaction loading to the oxygen uptake loading.

Switching gears to the mitochondria, the two reactions in the TCA cycle, Rx2 and Rx3, are minimally changed. The reactions Rx7 and Rx11 are greatly upregulated, which are complex I and pyruvate dehydrogenase respectively. It would be wise to conclude that Rx7 and Rx11 are somewhat correlated. Since pyruvate dehydrogenase produces mitochondria NADH, which is then utilized by complex I. One other point to make for P17 is the magnitude of the flux values, Rx6 and Rx9 have high flux values compared to the other reactions The other reactions that have semi-high flux values (Rx1, Rx5, Rx6, and Rx10) are important, because in metabolic engineering we are interested in taking these reactions and utilizing them for the production of chemical valuable products. These are actually the reactions that matter to use, since these are the reactions that can be manipulated, other reactions, like Rx6 in the glycolysis will be difficult

to perturb since this would mean that the glycolysis pathway would have to be affected, which has many regulation schemes.

Table 4.8 Key redox reactions identified by SID framework for P17. $Flux_s$ is the starting flux value. $Flux_e$ is the ending flux value. Flux Δ is the difference between the $Flux_s$ and $Flux_e$. The units for the flux is mmol/gDW·hr. The Reaction # is the same reaction shown in Figure 4.15.

Reaction #	Reaction	$Flux_s$	$Flux_e$	Flux Δ
Rx1	h[c] + nadh[c] + akg[c] + nh4[c] <=> h2o[c] + nad[c] + glu-L[c]	0.39	0.40	0.01
Rx2	nad[m] + mal-L[m] <=> oaa[m] + h[m] + nadh[m]	0.033	0.035	0.002
Rx3	adp[m] + icit[m] -> akg[m] + nadph[m] + co2[m]	0.083	0.087	0.004
Rx4	h[c] + nadh[c] + dhap[c] -> nad[c] + glyc3p[c]	0.0023	0.0025	0.0002
Rx5	nad[c] + 3pg[c] -> h[c] + nadh[c] + 3php[c]	0.074	0.078	0.004
Rx6	nad[c] + pi[c] + g3p[c] <=> h[c] + nadh[c] + 13dpg[c]	7.4	7.3	-0.1
Rx7	5 h[m] + nadh[m] + q6[m] -> 4 h[c] + nad[m] + q6h2[m]	0.10	0.18	0.08
Rx8	nadp[c] + 6pgc[c] -> nadph[c] + co2[c] + ru5p-D[c]	0.02	0.06	0.04
Rx9	h[c] + acald[c] + nadh[c] <=> etoh[c] + nad[c]	6.80	6.70	-0.1
Rx10	nadp[c] + acald[c] + h2o[c] -> 2 h[c] + nadph[c] + ac[c]	0.22	0.15	-0.07
Rx11	coa[m] + pyr[m] + nad[m] -> accoa[m] + nadh[m] + co2[m]	0.048	0.13	0.082

For P16, surprisingly all the redox reactions are upregulated. Like P17, Rx6 and Rx9 are heavily affected, but now they have reversed their direction. Rx4 had a very insignificant response in P17, but in P16 it is highly upregulated. Rx1 remains quite similar as in P17. The disturbance on the NADPH producing reactions are reduced, and so are complex I and pyruvate dehydrogenase. It is important to point out that this phenotype is where ethanol production is being increased. Could we use the behavior of this phenotype to discover ways to increase the production of ethanol? It is difficult to give a clear answer to this question, but we do know what is happening metabolically when ethanol production is increased. The results for P16 are shown in Figure 4.16 for the loadings, and metabolic fluxes in Table 4.9.

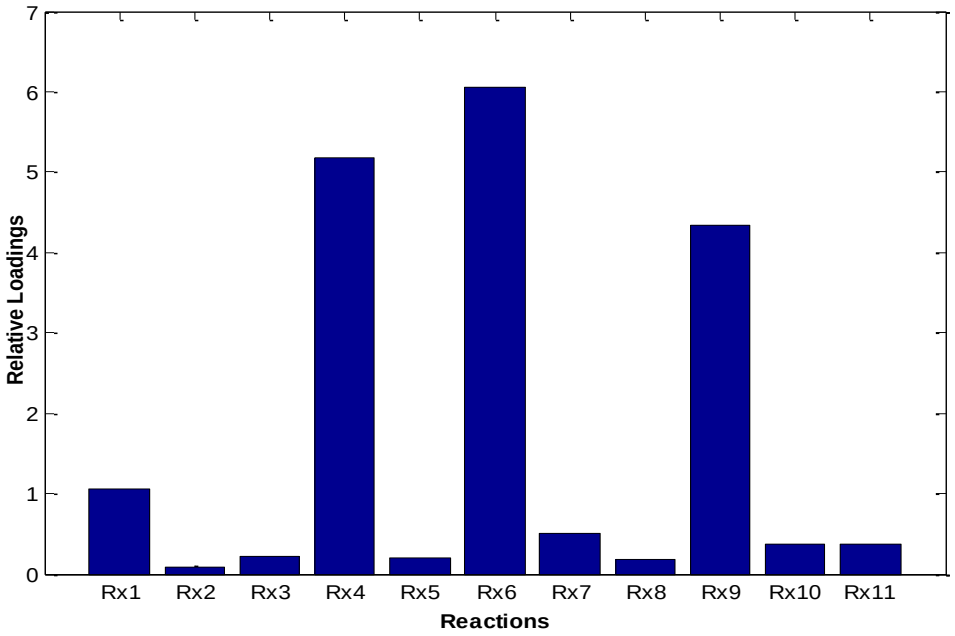

Figure 4.16: Key redox reactions that were identified in P16. Relative loading scales each reaction loading to the oxygen uptake loading.

Table 4.9: Key redox reactions identified by SID framework for P16. $Flux_s$ is the starting flux value. $Flux_e$ is the ending flux value. Flux Δ is the difference between the $Flux_s$ and $Flux_e$. The units for the flux is mmol/gDW·hr. The Reaction # is the same reaction shown in Figure 4.16.

Reaction #	Reaction	$Flux_s$	$Flux_e$	Flux Δ
Rx1	h[c] + nadh[c] + akg[c] + nh4[c] <=> h2o[c] + nad[c] + glu-L[c]	0.41	0.49	0.08
Rx2	nad[m] + mal-L[m] <=> oaa[m] + h[m] + nadh[m]	0.035	0.041	0.006
Rx3	adp[m] + icit[m] -> akg[m] + nadph[m] + co2[m]	0.088	0.10	0.0012
Rx4	h[c] + nadh[c] + dhap[c] -> nad[c] + glyc3p[c]	0.0032	0.39	0.39
Rx5	nad[c] + 3pg[c] -> h[c] + nadh[c] + 3php[c]	0.079	0.094	0.0015
Rx6	nad[c] + pi[c] + g3p[c] <=> h[c] + nadh[c] + 13dpg[c]	7.3	7.8	0.5
Rx7	5 h[m] + nadh[m] + q6[m] -> 4 h[c] + nad[m] + q6h2[m]	0.20	0.24	0.04
Rx8	nadp[c] + 6pgc[c] -> nadph[c] + co2[c] + ru5p-D[c]	0.069	0.083	0.014
Rx9	h[c] + acald[c] + nadh[c] <=> etoh[c] + nad[c]	6.7	7.0	0.3
Rx10	nadp[c] + acald[c] + h2o[c] -> 2 h[c] + nadph[c] + ac[c]	0.14	0.17	0.03
Rx11	coa[m] + pyr[m] + nad[m] -> accoa[m] + nadh[m] + co2[m]	0.14	0.17	0.03

For P14, there are a lot of changes going on compared with the previous phenotypes, where the loadings are shown in Figure 4.17 with the fluxes in Table 4.10. Rx6 is

downregulated, but now in the same magnitude as P17 and P16, which was previously explained that glycolysis has less of than affected as oxygen uptake rates are elevated.

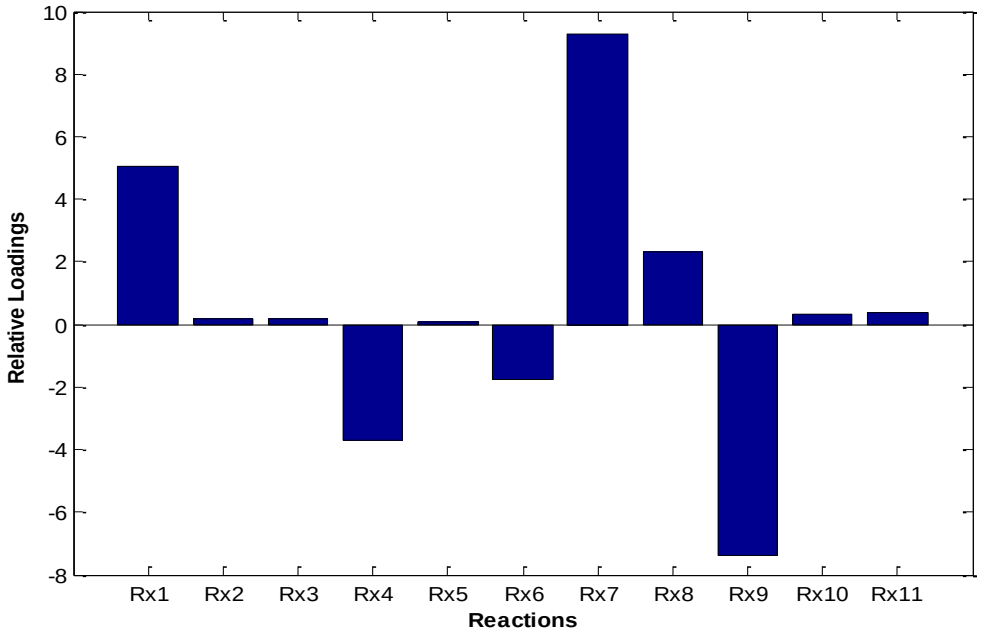

Figure 4.17: Key redox reactions that were identified in P14. Relative loading scales each reaction loading to the oxygen uptake loading.

Table 4.10: Key redox reactions identified by SID framework for P14. $Flux_s$ is the starting flux value. $Flux_e$ is the ending flux value. Flux Δ is the difference between the $Flux_s$ and $Flux_e$. The units for the flux is mmol/gDW·hr. The Reaction # is the same reaction shown in Figure 4.17.

Reaction #	Reaction	$Flux_s$	$Flux_e$	Flux Δ
Rx1	h[c] + nadh[c] + akg[c] + nh4[c] <=> h2o[c] + nad[c] + glu-L[c]	0.84	1.04	0.20
Rx2	nad[m] + mal-L[m] <=> oaa[m] + h[m] + nadh[m]	0.067	0.11	0.043
Rx3	adp[m] + icit[m] -> akg[m] + nadph[m] + co2[m]	0.12	0.14	0.02
Rx4	h[c] + nadh[c] + dhap[c] -> nad[c] + glyc3p[c]	0.069	0.004	0.065
Rx5	nad[c] + 3pg[c] -> h[c] + nadh[c] + 3php[c]	0.089	0.10	0.011
Rx6	nad[c] + pi[c] + g3p[c] <=> h[c] + nadh[c] + 13dpg[c]	7.6	7.5	-0.1
Rx7	5 h[m] + nadh[m] + q6[m] -> 4 h[c] + nad[m] + q6h2[m]	1.1	1.5	0.4
Rx8	nadp[c] + 6pgc[c] -> nadph[c] + co2[c] + ru5p-D[c]	0.28	0.37	0.09
Rx9	h[c] + acald[c] + nadh[c] <=> etoh[c] + nad[c]	6.4	6.1	0.3
Rx10	nadp[c] + acald[c] + h2o[c] -> 2 h[c] + nadph[c] + ac[c]	0.20	0.23	0.03
Rx11	coa[m] + pyr[m] + nad[m] -> accoa[m] + nadh[m] + co2[m]	0.22	0.28	0.06

Complex I (Rx7) is heavily upregulated, meaning that more ATP generation is required.Rx1 is now upregulated a lot, and this seems to be counteracted by the NADH consuming reaction that is negatively affected. The redox reactions in the TCA cycle are again minimally affected.

Even though redox balance under oxygen-limited conditions is more significant, because this is the oxygen range where valuable products occur. However, it is important to draw a contrast on how the metabolism responses under aerobic condition, which is where the microorganism would operate to maximize cell growth. Figure 4.18 displays the reaction loadings of P4, whereby only a few redox reactions govern the metabolism as compared to the oxygen-limited phenotypes. Again, Complex I is a dominate redox reaction (Rx7), which is in conjunction with the literature, since energy production of ATP is heavily elevated under aerobic condition. Ethanol production (Rx9) is severely downregulated, which is in agreement with the literature, due to the nature of *S. stipitis* being a Crabtree negative strain.

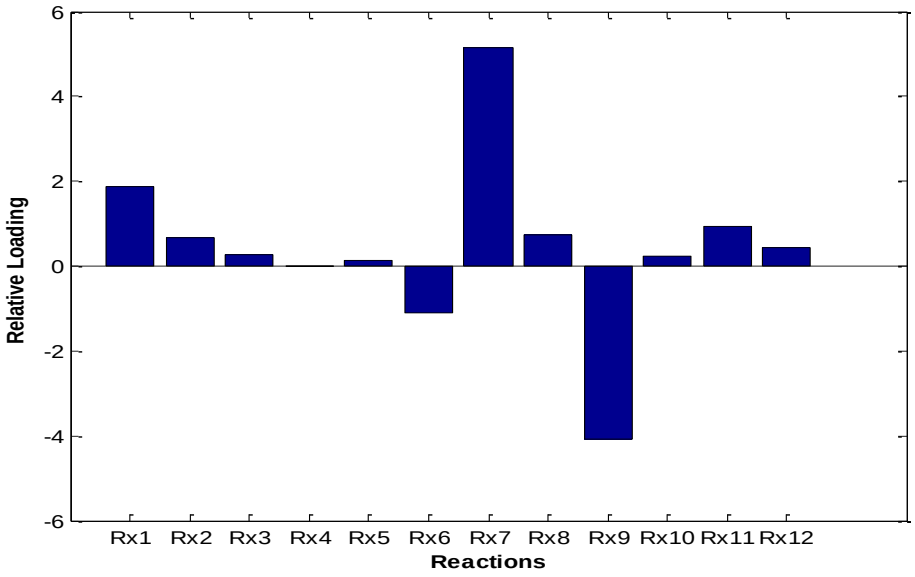

Figure 4.18: Key redox reactions that were identified in P10. Relative loading scales each reaction loading to the oxygen uptake loading.

Rx1 continues to show up in all the phenotypes as the main NADH cytosolic consumption reaction. The role of Rx5 on the metabolism was diminished greatly. The reaction loadings in the TCA cycle increased, but it is still very small in comparison to Rx7 and Rx9. Table 4.11 shows the flux values of the redox reactions. An extra reaction was added, which is in the TCA cycle, this is the reaction that causes the TCA cycle to be unbranched.

Table 4.11: Key redox reactions identified by SID framework for P10. $Flux_s$ is the starting flux value. $Flux_e$ is the ending flux value. Flux Δ is the difference between the $Flux_s$ and $Flux_e$. The units for the flux is mmol/gDW·hr. The Reaction # is the same reaction shown in Figure 4.16.

Reaction #	Reaction	$Flux_s$	$Flux_e$	Flux Δ
Rx1	h[c] + nadh[c] + akg[c] + nh4[c] <=> h2o[c] + nad[c] + glu-L[c]	1.4	2.3	0.9
Rx2	nad[m] + mal-L[m] <=> oaa[m] + h[m] + nadh[m]	0.18	0.54	0.36
Rx3	adp[m] + icit[m] -> akg[m] + nadph[m] + co2[m]	0.25	0.38	0.13
Rx4	h[c] + nadh[c] + dhap[c] -> nad[c] + glyc3p[c]	0.0047	0.0072	0.0025
Rx5	nad[c] + 3pg[c] -> h[c] + nadh[c] + 3php[c]	0.12	0.18	0.06
Rx6	nad[c] + pi[c] + g3p[c] <=> h[c] + nadh[c] + 13dpg[c]	7.4	6.8	-0.6
Rx7	5 h[m] + nadh[m] + q6[m] -> 4 h[c] + nad[m] + q6h2[m]	2.3	4.9	2.6
Rx8	nadp[c] + 6pgc[c] -> nadph[c] + co2[c] + ru5p-D[c]	0.47	0.82	0.35
Rx9	h[c] + acald[c] + nadh[c] <=> etoh[c] + nad[c]	5.4	3.4	-2.0
Rx10	nadp[c] + acald[c] + h2o[c] -> 2 h[c] + nadph[c] + ac[c]	0.23	0.35	0.12
Rx11	coa[m] + pyr[m] + nad[m] -> accoa[m] + nadh[m] + co2[m]	0.48	0.93	0.45

The finally phenotype that was examined was the line of optimality (LO), where Figure 4.19 convenes the redox reaction loadings, where the fluxes are accompanied in Table 4.12. The most dominant redox reaction is Rx7, which tells us that the model favors this reaction pathway for energy production. The next redox reaction that is responsible for governing the redox balance is Rx6. It is not surprising that the electron transport chain and glycolysis pathway provides the majority of variation of redox. Both of these are fundament pathways for carbon and energy conversion. Other redox reactions that supply the redox variation is Rx1, Rx8, and Rx11.

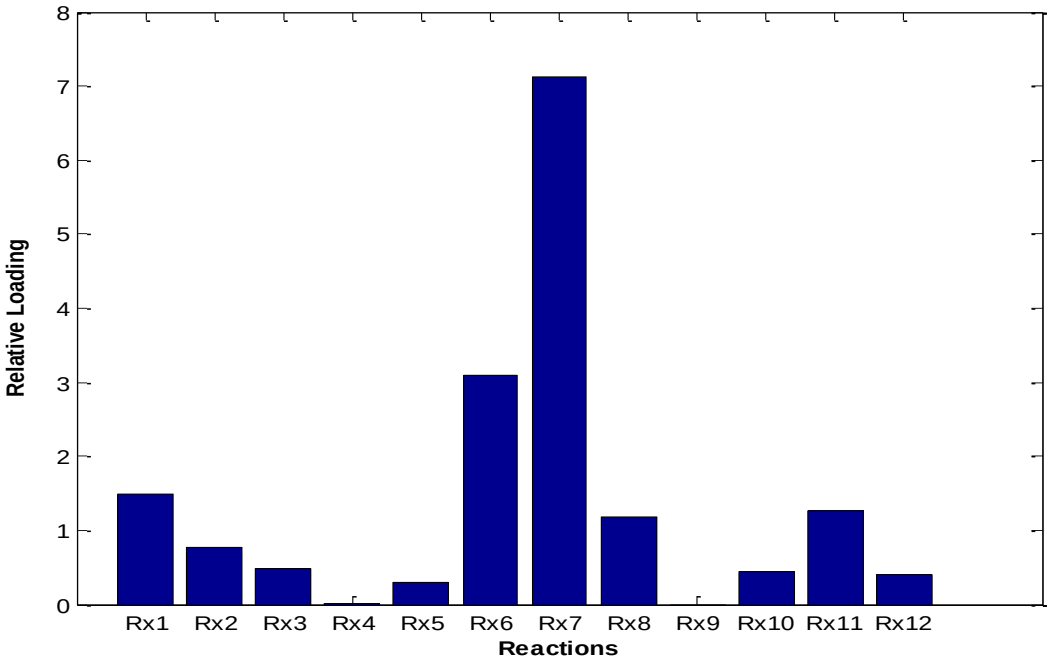

Figure 4.19: Key redox reactions that were identified in LO. Relative loading scales each reaction loading to the oxygen uptake loading.

Table 4.12: Key redox reactions identified by SID framework for LO. $Flux_s$ is the starting flux value. $Flux_e$ is the ending flux value. Flux Δ is the difference between the $Flux_s$ and $Flux_e$. The units for the flux is mmol/gDW·hr. The Reaction # is the same reaction shown in Figure 4.19.

Reaction #	Reaction	$Flux_s$	$Flux_e$	Flux Δ
Rx1	h[c] + nadh[c] + akg[c] + nh4[c] <=> h2o[c] + nad[c] + glu-L[c]	0.33	2.0	1.67
Rx2	nad[m] + mal-L[m] <=> oaa[m] + h[m] + nadh[m]	0.40	2.7	2.3
Rx3	adp[m] + icit[m] -> akg[m] + nadph[m] + co2[m]	0.14	1.6	1.46
Rx4	h[c] + nadh[c] + dhap[c] -> nad[c] + glyc3p[c]	0.0026	0.0030	0.0004
Rx5	nad[c] + 3pg[c] -> h[c] + nadh[c] + 3php[c]	0.089	1.00	0.011
Rx6	nad[c] + pi[c] + g3p[c] <=> h[c] + nadh[c] + 13dpg[c]	1.1	10	8.9
Rx7	5 h[m] + nadh[m] + q6[m] -> 4 h[c] + nad[m] + q6h2[m]	3.1	25	21.9
Rx8	nadp[c] + 6pgc[c] -> nadph[c] + co2[c] + ru5p-D[c]	0.43	4.00	3.57
Rx9	h[c] + acald[c] + nadh[c] <=> etoh[c] + nad[c]	0	0	0
Rx10	nadp[c] + acald[c] + h2o[c] -> 2 h[c] + nadph[c] + ac[c]	0.13	1.4	1.27
Rx11	coa[m] + pyr[m] + nad[m] -> accoa[m] + nadh[m] + co2[m]	0.54	4.3	3.76

4.3.5 Limitations of iAD828

It is evident that iAD828 has made great strides in model performance, when examining the SID framework and experimental validation results. Nonetheless, there are still limitations that iAD828 imposes that if corrected would greatly strengthen the model prediction. Wet lab experiments show that acetic acid is produced simultaneously with xylitol under oxygen-limited conditions, where iAD828 lacks this capability (Kim, 2015). By using SID framework, the phenotypes were analyzed and discovered that there were 20 phenotypes. The robustness under low oxygen conditions is very poor; many phenotypes were generated with very small changes in oxygen pickup rate. This error could be contributed to the lack of activation of alternative oxidase, which is another route to reduce oxygen. Alternative oxidase has shown to be active under very low oxygen levels (Shi et al., 2002), which could bring stability to the model. iAD828 chooses not activated alternative oxidase. Also under high oxygen conditions, there are phenotypes appearing that have small differences in oxygen pickup rate.

4.4 Conclusion

A newly genome-scale metabolic model iAD828 of *S. stipitis* was developed through SID framework, which supersedes the published models of iSS884 and iBB814. Validation done through SID framework clearly demonstrates that key metabolic advances were accomplished in iAD828: the xylose metabolism produced xylitol under oxygen-limited condition, both branches of PPP are operating in the correct response for both oxygen-limited and aerobic condition, and glycolysis is in the correct direction under oxygen-limited condition. Also the line of optimality now exists for iAD828, which was incorrect for the previous models. The line of optimality can provide great insight on what are the optimal metabolic conditions, and it has been shown to quantitatively link the genotype with the phenotype through experiments (Edwards et al., 2002).

Other improvements were the correct metabolic behavior between the states of oxygen-limited and aerobic condition, such as glycolysis fluxes higher under oxygen-limited condition, TCA cycle fluxes higher under aerobic condition, and fatty acid biosynthesis higher under oxygen-limited condition. The quantitative validation experiments favored iAD828 for two separate data sets, and more importantly the qualitative validation experiment showed significant improvement Also an additional experiment was compared with iAD828 in order to evaluated the *in silico* predictions of xylitol production. These model improvements are essential to having a more accurate depiction of the relationship between the genotype and phenotype. Here metabolic information was extracted that expands our understanding of *S. stipitis*. This can provide systematic assistance of the development of recombinant strains for the production of a metabolite of interest.

Chapter 5: Cofactor engineering strategies for *S. stipitis*

5.1 Introduction

The regulation of catabolic and anabolic activity in microorganisms is essential for determining the optimal phenotype for growth and producing biochemical valuable products (Verho et al., 2003). The cofactors NAD(H) and NADP(H) play unique roles in the metabolism, whereby NADH is primarily used in the catabolism, while NADPH prefers usage in the anabolism. The respiratory cofactor NADH is principally utilized for ATP production through transferring electrons to oxygen through electron transport chain. Cytosolic NADH is generated from the sugar dissimilation subsystem of glycolysis, while the TCA cycle provides mitochondria NADH. Concurrently, NADPH provides electrons for biosynthetic reactions, such as amino acid synthesis. Production of cytosolic NADPH is accomplished in the oxidative branch of PPP and pyruvate metabolism by the aldehyde dehydrogenase reaction. Despite the different functions of NADH and NADPH, they are interconnected to each other, for example glycolysis provides building blocks for anabolic reactions and central metabolites, while pyruvate and acetyl-CoA are used as precursors for biosynthetic reactions (Heux et al., 2006; Hou et al., 2009; Wandrey, 2004)

Under oxygen-limitations, NADH is in excess, and is re-oxidized for ethanol production. Also the byproduct xylitol is produced, because of a cofactor imbalance of the first two reactions (xylose reductase and xylitol dehydrogenase) of the xylose metabolism (Passoth et al., 1996). Xylose reductase uses both NADH and NADPH, and xylitol dehydrogenase utilizes only NAD; however some literature shows even NADP is used (Jeffries, 2006; Watanabe et al., 2007).

As demonstrated from the previous chapter, iAD828 provides significant performance enhancement, therefore we want to use this model to guide metabolic engineering strategies for

overproduction of ethanol. The cofactor balance is an important element to solve, because there is yet a concrete conclusion and it is a very significant issue for the *S. cerevisiae* recombinant strain

5.2 Materials and methods

5.2.1 *In silico* experiments

The genome-scale metabolic model of iAD828 were evaluated by flux balance analysis (FBA), in which the COBRA toolbox (Schellenberger et al., 2011) was used. The objective function of growth was used for all *in silico* experiments, except for case study that switched the objective function to ethanol production. For optimization of ethanol, growth was set at 80 % of the optimal solution for growth (when the objective function is optimization of growth). The upper limits of xylose and oxygen uptakes were varied based on the preselected conditions, while the other exchange compounds (NH^{4+}, H^{+}, $SO4^{2-}$, Pi^{2-}, H_2O, Fe^{2+}) were given the option to enter and exit the network freely, with upper and lower bounds of -1000 to 1000 mmol/gDW·hr. The final metabolic products (CO_2, ethanol, acetic acid, etc.) were allowed to exit the system freely, where the reaction flux was constrained to 0 – 1000 mmol/gDW·hr, which prevents product uptake. The growth associated maintenance energy was set to 2.6 mmol/gDW·hr (Balagurunathan et al., 2012).

5.2.2 SID framework

As in the Chapter 4 and 5, SID framework was used to identify the essential reactions in each phenotype. Different input variables were used to perturb the system, such as oxygen pickup rate and xylose reductase redox ratio preference (NADPH/NADH). The results are then visualized through metabolic colored maps.

5.3 Results and Discussion

Cofactor engineering of the xylose metabolism and the redox balance was investigated to extract embedded metabolic information for the overproduction of ethanol. Xylose reductase preference for NADPH and NADH was altered and SID framework was used to extract the essential metabolic information. Conclusions from this data allowed for uncovering specific strategies and they were imposed on iAD828 for overproduction of ethanol.

5.3.1 Background of cofactor engineering of xylose reductase

S. stipitis is only a handful of strains that have the native ability to digest xylose for ethanol production; therefore genes from the xylose metabolism have been used to construct recombinant strains, such as *S. cerevisiae*. The incorporation of the xylose metabolism into the recombinant strain has shown to be inefficient due to have a cofactor imbalance for the first two reactions in the xylose metabolism, xylose reductase (XR) and xylitol dehydrogenase (XDH) (Jeppsson et al., 2002). Figure 5.1 displays the first three steps for the xylose metabolism in *S. stitipis*, with the corresponding cofactor preference. Xylose reductase has shown to have a dual preference for NADH and NADPH, while xylitol dehydrogenase has shown to predominantly use NAD alone, however reports have shown NADP route is also feasible. In *S. stitipis*, the xylose metabolism and the cofactor regeneration is poorly understood, thus gaining fundament understanding will equip biologist with strategies to make improved recombinant strains.

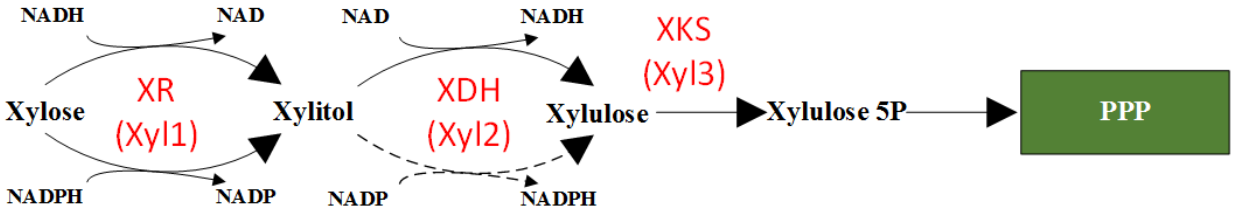

Figure 5.1: Illustration of xylose metabolism in *S. stipitis*. XR: xylose reductase; XDH: xylitol dehydrogenase; XKS: xylulose kinase. The dash line indicates that there is a debate with the existence of the reaction.

5.3.2 Cofactor engineering of xylose reductase on iAD828

The first set of *in silico* experiments looked at a range of oxygen pickup rates from 0 – 4 mmol/gDW·hr, and the XR ratio was changed from 0 to 2. The XR ratio is defined as the NADPH route to the NADH route. XDH used the NAD route only, since iAD828 can only use that route in order to have feasible solutions. Figure 5.2 (a) – (c) shows the results for this set of *in silico* experiments for the growth rate, ethanol production rate, and xylitol production rate respectively. The blue line represents the nominal response, where the model always chooses the NADH route alone. In Figure 5.2 (a), it is evident that that as the XR ratio increases this causes the growth rate to decrease. Figure 5.2 (b) shows that under oxygen-limited condition the ethanol is maximized when XR is zero, however as the oxygen intake rate increases, we find that the ethanol production rate is higher for the upper XR ratios. Figure 5.2 (c) concurs with the literature that more a cofactor imbalance propagates more xylitol production (Jeppsson et al., 2006).

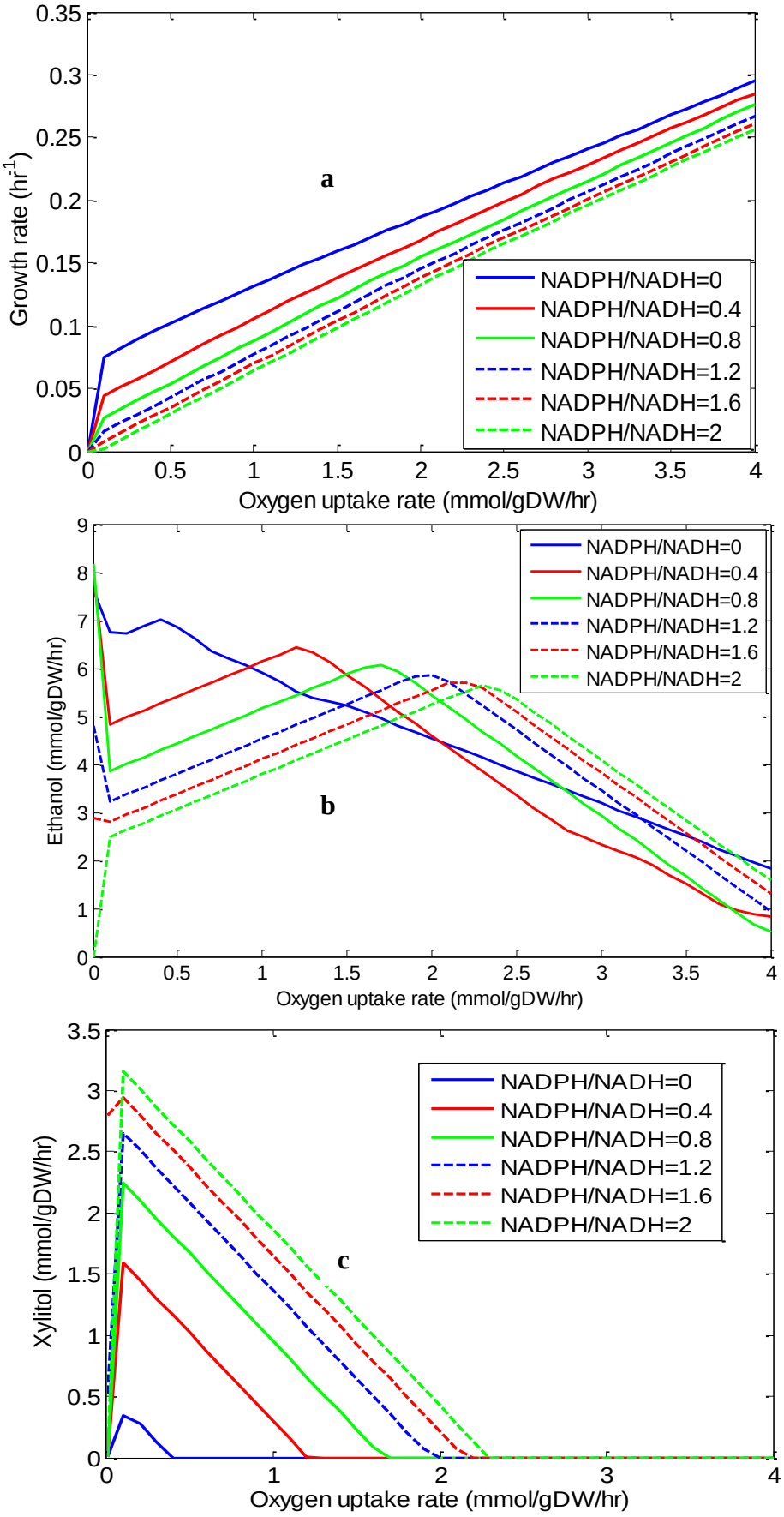

Figure 5.2: Cofactor XR ratio influence on iAD828. (a) growth rate, (b) ethanol production rate, and (c) xylitol production rate

Further investigation was conducted that examined if there was consistency between the phenotypes in the regions of maximum ethanol production under oxygen-limited condition and higher oxygen pickup levels. Except for the XR ratio at zero, all the rest of the XR ratios at the maximum ethanol production rate belonged to the same phenotype. Since the highest ethanol production rate occurs under oxygen-limited condition, *in silico* experiments were then conducted under this condition. The oxygen pickup ranged from 0 to 1 mmol/gDW·hr and the XR ratio was varied now from 0 to 0.4, since this is the ratio that belong to optimal ethanol production. Figure 5.3 exhibits the ethanol production rate for this *in silico* experiment, where there are two ethanol production regions, which represent two different phenotypes, P17 and P16. P17 phenotypic space is represented by a solid black line, which means solutions along this line belong to P17, likewise the same is true for P16 as it is represented as the dash black line.

Recalling back to Chapter 4 to the 2D phenotype phase plane plots in Figure 4.6, P17 only inhabits a very small region, while P16 is much wider. It would be very difficult to keep wet lab experiments in P17, thus P16 is better option to run wet lab experiments. Further examination was performed on P16, where fluxes where collected along the P16 line as XR ratio increased and SID framework was then applied to extract the embedded metabolic information. Table 5.1 shows the results of the flux values of the starting and ending points, and the loadings. For this analysis it is important to taken into consideration both the flux and loading, since just because there is a high loading value does not mean that it has a great impact on the system.

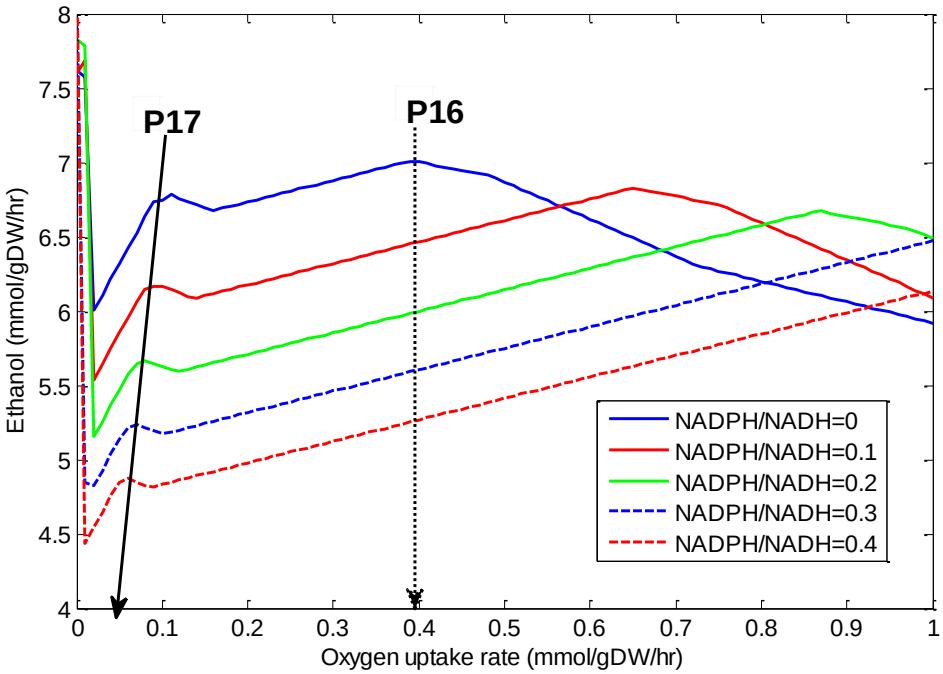

Figure 5.3: Influence of cofactor preference of XR ratio under oxygen-limited condition. P17 is represented by solid black line. P16 is represented by a dash black line.

Table 5.1: Reactions influenced by variation of XR ratio for P16. Fluxs is the starting flux value and Fluxe is the ending flux value. The loading taken from SID framework, which is normalized to the XR ratio

Reaction #	Reaction	$Flux_s$	$Flux_e$	Loading
Rx1	h[c] + nadh[c] + akg[c] + nh4[c] -> h2o[c] + nad[c] + glu-L[c]	0.49	0.33	-0.11
Rx2	h[c] + nadh[c] + dhap[c] -> nad[c] + glyc3p[c]	0.40	0.52	0.088
Rx3	h[c] + acald[c] + nadh[c] -> etoh[c] + nad[c]	7.0	5.3	-1.2
Rx4	nad[c] + pi[c] + g3p[c] -> h[c] + nadh[c] + 13dpg[c]	7.8	5.8	-1.4
Rx5	nad[c] + xylt[c] -> nadh[c] + xylu-D[c] + h[c]	5	3.8	-0.82
Rx6	5 h[m] + nadh[m] + q6[m] -> 4 h[c] + nad[m] + q6h2[m]	0.24	0.16	-0.054
Rx7	coa[m] + pyr[m] + nad[m] -> accoa[m] + nadh[m] + co2[m]	0.17	0.11	-0.04
Rx8	nadp[c] + 6pgc[c] -> nadph[c] + co2[c] + ru5p-D[c]	0.083	0.77	0.48
Rx9	nadp[c] + acald[c] + h2o[c] -> 2 h[c] + nadph[c] + ac[c]	0.17	0.12	-0.04
Rx10	nadp[m] + icit[m] -> akg[m] + nadph[m] + co2[m]	0.11	0.071	-0.024
Rx11	8 h[m] + o2[m] + 4 focytc[m] -> 4 h[c] + 2 h2o[m] + 4 ficytc[m]	0.32	0.34	0.017
Rx12	xu5p-D[c] -> ru5p-D[c]	1.6	0.78	- 0.60
Rx13	r5p[c] + xu5p-D[c] <=> g3p[c] + s7p[c]	1.7	1.5	-0.11
Rx14	h[c] + pyr[c] -> acald[c] + co2[c]	7.2	5.4	-1.3
Rx15	atp[c] + xylu-D[c] --> h[c] + adp[c] + xu5p-D[c]	5.0	3.8	-0.82

5.3.3 Potential metabolic engineering strategies

Oxidative branch of PPP is the leading producer of NADPH, and is heavily affected in the opposite direction of ethanol production, thus more NADPH production from the oxidative PPP results in decrease ethanol production. Some metabolic engineering strategies to consider are having another NADPH producing reaction to be the principal reaction for NADPH generation (Bro et al., 2006). This could be done by redirection of the flux away from the oxidative branch of PPP to the pyruvate metabolism via aldehyde dehydrogenase, Rx9. The indication of redirection of the flux away from the oxidative branch of PPP can also be supported by Rx12 and Rx13, where upregulation of these reactions is would propagate away from a decrease in ethanol production. A strategy that has been implored in *S. cerevisiae* is inserting NADP+-dependent D-glyceraldehyde-3-phosphate dehydrogenase and blocking the oxidative branch of PPP. The reaction that is being added is part of the glycolysis pathway, where there exists a NAD+-dependent D-glyceraldehyde-3-phosphate dehydrogenase reaction, Rx4 (Matsushika et al., 2009a). Based on the results, Rx4 has a negative correlation to ethanol decrease; therefore having more flux through this reaction would improve ethanol production. Another thought is that the oxidative branch of PPP is considered an anabolic pathway, because of the involvement of NADPH production that is used for generation of building blocks for biomass formation, thus pushing fluxes toward catabolic pathways would be more profitable for ethanol production. For NADH consumption reactions, which are Rx1 and Rx2, more benefit for maximizing ethanol production would be to upregulate Rx1 and downregulate Rx2. Moving to the electron transport chain, complex IV downregulation shows that it would increase ethanol production, and the opposite is true for complex I that upregulation would increase ethanol production. However, for complex I and complex IV the loading value is not significantly

affected. Rx15, known as xylulokinase (XKS), upregulating this would provide for ethanol production rate incresase.

5.3.4 Switching the objective function to ethanol production rate

Another consideration is changing the objective function from biomass formation to ethanol production. In order to prevent zero biomass growth, the biomass was held at 80 % of the nominal value for this condition. The intent of this was to see if any clear occurrence of upregulation or deregulation of reaction pathways existed. This could provide additional information that could be used for metabolic engineering strategies. As the previous analysis, the oxidative branch of PPP was again recognized as an important element for manipulation of ethanol production. Also the glycolysis pathway and Rx1 again showed to by parts of the metabolism deemed to be vital.

5.3.5 Metabolic engineering strategy 1

The first metabolic engineering strategy that was proposed was deletion of glucose 6-phosphate dehydrogenase, which would completely inhibit the oxidative branch of PPP, inserting of NADP+-dependent D-glyceraldehyde-3-phosphate dehydrogenase, and deletion of NAD+-dependent D-glyceraldehyde-3-phosphate dehydrogenase. The justification of this strategy is taken from the fact that upregulation of the oxidative branch of PPP seems to be detrimental for ethanol production. The NADP+-dependent D-glyceraldehyde-3-phosphate dehydrogenase provides for an alternative way to produce NADPH, and more flux would be redirected to the pyruvate metabolism for ethanol production. Figure 5.4 (a) – (c) displays the results of iAD828 and iAD828-ME1 (metabolic engineering strategy 1) and how it influenced growth rate, ethanol, and xylitol respectively.

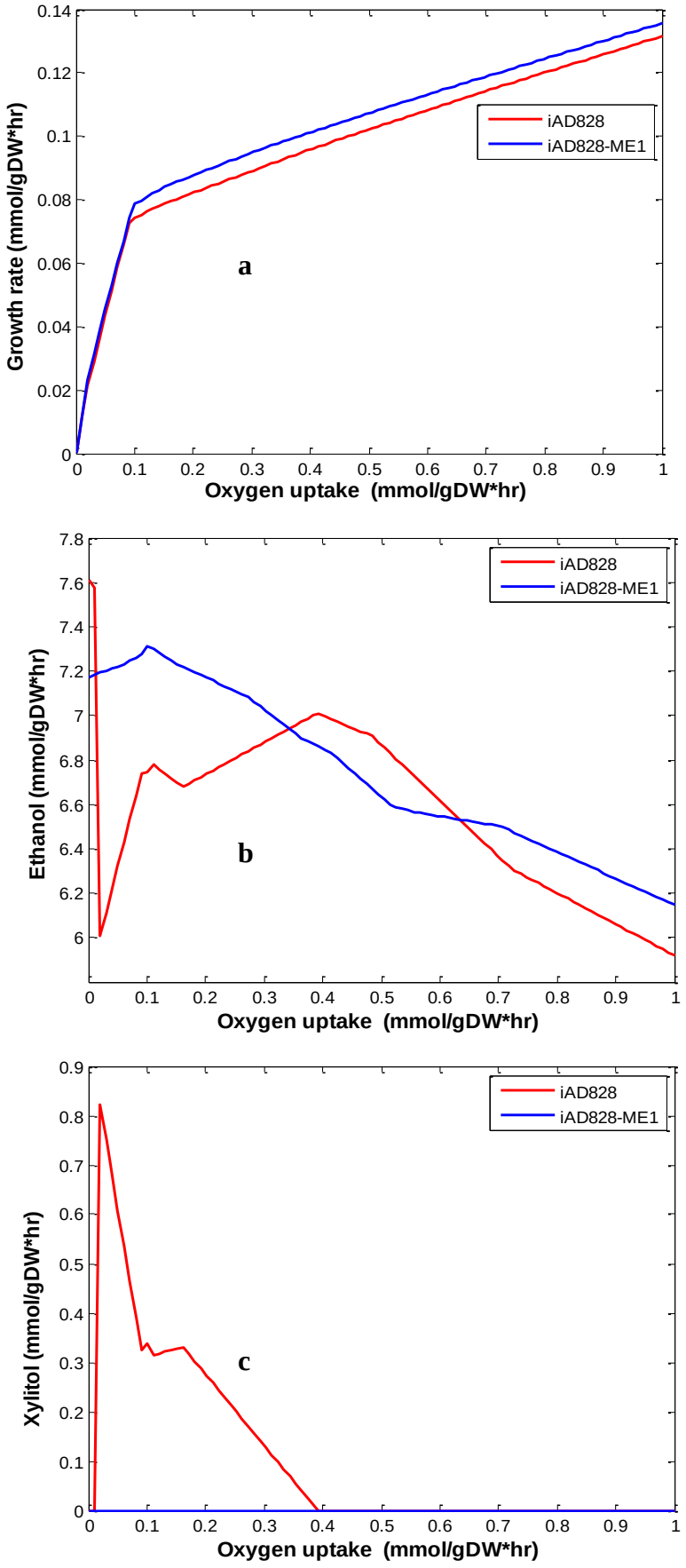

Figure 5.4. Metabolic engineering strategy 1. (a) growth rate, (b) ethanol, (c) xylitol. The red line is iAD828 and the blue line contains the metabolic engineering strategy 1 (iAD828-ME1)

Figure 5.4 (a) shows that the growth rate is higher for iAD828-ME1 than iAD828, which is due having less carbon by converted into CO_2 via the oxidative PPP. Figure 5.4 (b) shows that the ethanol production is higher for iAD828-ME1 (excluding the first point of iAD828) for oxygen pickup rates less than 0.35 mmol/gDW·hr. For the highest ethanol production rate points in both models, iAD828-ME1 has a perecent increase of 7.8 % than iAD828. In the mid region of the Figure 5.4 (b), iAD828 has higher ethanol production. Figure 5.4 (c) shows that iAD828-ME1 was able to eliminate xylitol production. Further analysis was done in the region of optimal ethanol production through SID framework, for the oxygen pickup range of 0.03 – 0.14 mmol/gDW·hr. SID framework revealed that Rx1 was heavily downregulated. Other findings were that the non-oxidative branch of PPP was downregulated. Also glycolysis was split into two regions, the upper part was downregulation (until glyceraldehyde 3 phosphate production) and the lower part was upregulated.

5.3.6 Metabolic engineering strategy 2

From this analysis, another strategy was proposed, iAD828-ME2, which kept the same setup as metabolic engineering 1, except that Rx1 was deleted. The intuition behind this was that Rx1 was a main consumer of NADH, which when deleted would provide more NADH for ethanol production. Figure 5.5 (a) and (b) shows how the growth rate and ethanol production rate was influenced respectively for this strategy compared with iAD828 and iAD828-ME1. The growth rate is the lowest for iAD828-ME2, which is shown by the green line; therefore deletion of Rx1 is directly correlated to growth rate. This is due to Rx1 being a glutamate production reaction, and with deletion of Rx1 this causes the model to select another reaction for glutamate production, which the precursor reaction requires ATP consumption. With the decrease in carbon

flux flowing to cellular growth this allows for carbon to be directed to ethanol production, which results in iAD828-ME2 having the highest ethanol production rate.

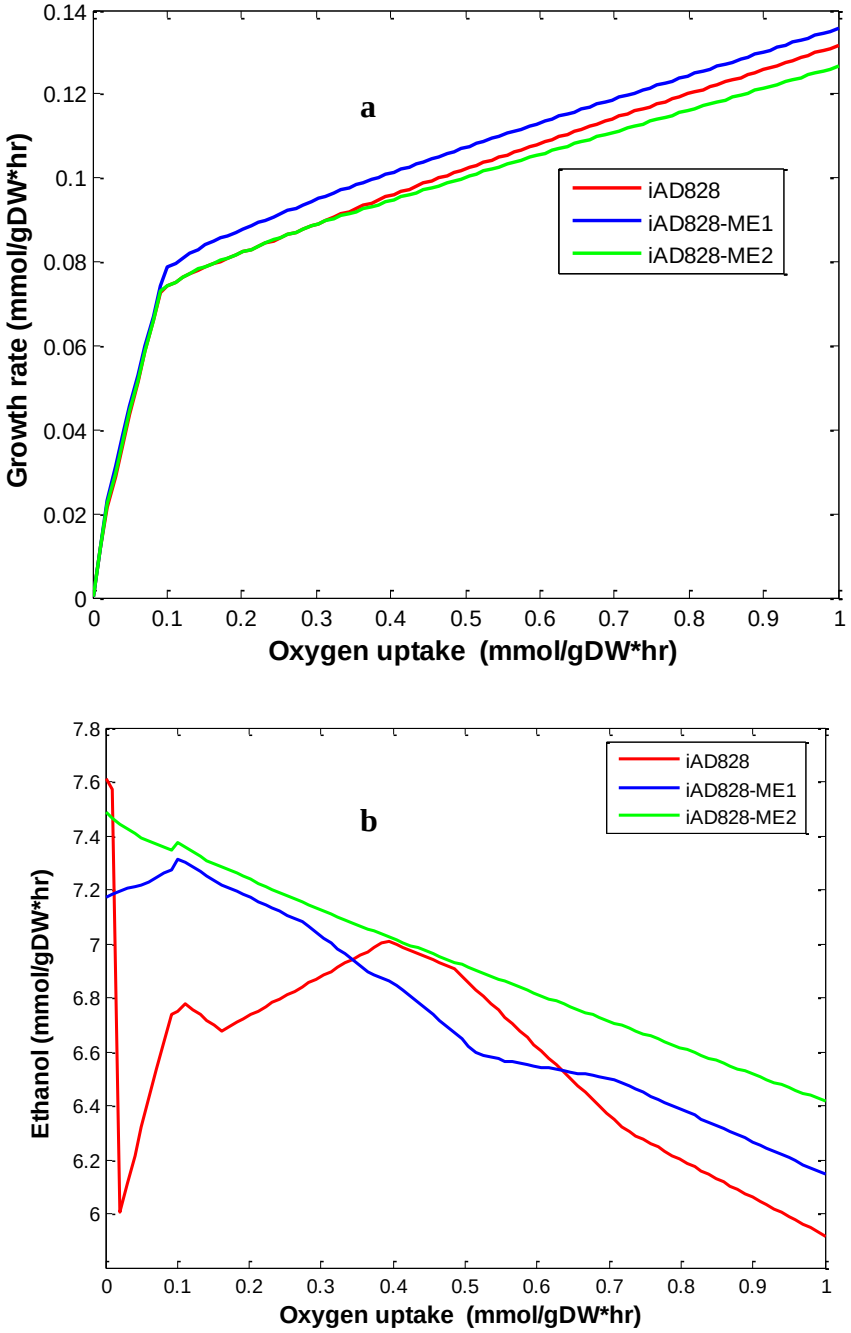

Figure 5.5. Metabolic engineering strategy 2. (a) Growth rate and (b) ethanol.The red line is iAD828, the blue line contains the metabolic engineering strategy 1 (iAD828-ME1), and the green line represents metabolic engineering strategy 2 (iAD828-ME2)

5.4 Conclusion

Due to the metabolic advancements of iAD828, cofactor engineering strategies was applied in order to delegate carbon flux toward ethanol overproduction. Great exposure has been toward the first two steps in the xylose metabolism: xylose reductase and xylitol dehydrogenase, since these enzymes have been inserted into *S. cerevisiae* in order to make a recombinant strain for ethanol overproduction, and have shown to be responsible for the cofactor imbalance. This propagated *in silico* experiments that varied the xylose reductase ratio (NADPH/NADH). iAD828 adheres to the literature, where ethanol production is highest and xylitol production is the lowest when the xylose reductase ratio is the lowest. P16 is the phenotype responsible for optimal ethanol production conditions and SID framework was used to analyze the phenotype. The oxidative branch of PPP was shown to be highly involved in ethanol production, and it would be more favorable if the carbon flux was redirect to the pyruvate metabolism. Based on these results, metabolic engineering strategies were instilled and ethanol overproduction was accomplished.

Chapter 6: A System Identification Based Approach for Phenotype Phase Plane Analysis

6.1 Introduction

The arrival of genome sequencing has brought about the reconstruction of genome-scale models, which provide a systems level understanding of a cellular metabolism through *in silico* methods (Kim et al., 2012). The constraint-based methods have been used on metabolic networks for more than 25 years (Lewis et al., 2012). Metabolic phenotypes of microorganisms are elucidated from these methods that are based on the environmental conditions and the genotype (Karr et al., 2012). One prevalent constraint-based method, phenotype phase plane (PhPP) analysis, provides a global view of each phenotype in genome-scale models by breaking down the metabolic behavior in distinct phases through shadow prices analysis. The shadow price is defined as the effect of the metabolite concentration on the objective function. Two independent variables, typically the carbon and oxygen source, are varied, and the shadow price is calculated for each metabolite. Shadow price analysis has the capability to find if metabolites are limited or in excess, and if metabolites are expelled from the network. The cellular growth is mapped on a two-dimensional plane, which is calculated by varying the two independent variables. The phases describe the metabolic phenotypes, and each phase denotes that the shadow prices of each metabolite are constant (Edwards et al., 2012).

Metabolic phenotypes can be thought of different utilization profiles, in other words each phenotype has a unique flux distribution (Varma et al., 1994). Figure 6.1 demonstrates this idea, where PhPP analysis was performed on the genome-scale model of iAD828. The two independent variables are are xylose and oxygen. Each phenotype is characterized by a different color, for example in Figure 6.1, the yellow region and green region represent separate

phenotypes. Being different phenotypes, this means that the shadow price of a metabolite of interest has different values in the yellow and green regions. For example, glucose 6-phosphate would have different shadow price values in the yellow and green regions. It is important to point out that all the metabolites do not have the same shadow price in each phenotype.

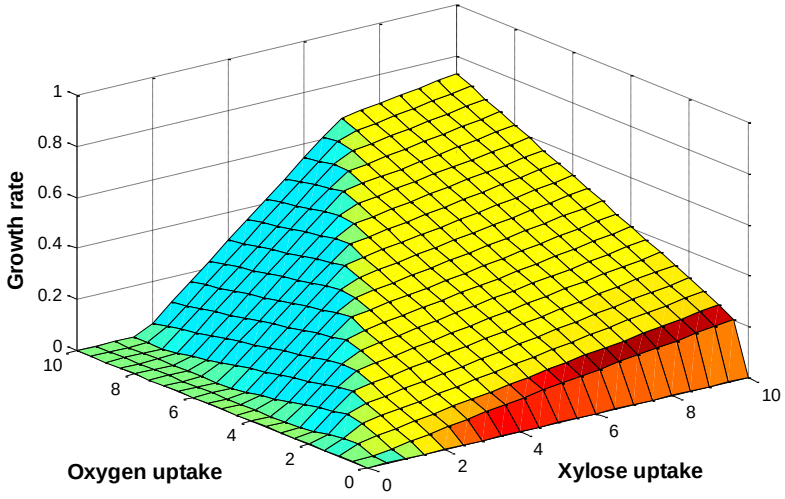

Figure 6.1: Example of PhPP analysis using genome-scale model iAD828.

PhPP analysis does not provide what reactions are responsible for the differences in each phenotype, and furthermore, what reactions are causing the difference between the phenotypes. These shortcomings are very important, and intensify when the scale and complexity of the model increases. In order to overcome these limitations of PhPP analysis, a system identification (SID) based framework was utilized for a novel tool, since it extracts qualitative biological information (such as how different pathways interact with each other) from quantitative numerical results by performing carefully designed *in silico* experiments (Damiani et al., 2015). The basic idea of the developed framework is to treat the genome-scale metabolic network model as a black-box model, and to use designed input sequences (such as a series of substrate pick up rates that keep increasing or decreasing) to perturb the network; then to apply multivariate

statistical analysis tools in order to extract information on how such perturbations propagate through the network.

In this work, a novel tool was developed; SID enhanced PhPP analysis, which overcomes the limitations of PhPP analysis. Several *in silico* experiments have been designed to obtain the same findings provided by shadow price analysis. In addition, SID enhanced PhPP analysis can further provide how different pathways are affected by perturbing the substrates that are in interest, and highlight the metabolic differences among different phenotypes. The same illustrative example provided in the original PhPP analysis paper (Edwards et al., 2002) and the *E. coli* core model were used to demonstrate the effectiveness of SID enhanced PhPP analysis (Orth et al., 2010b).

6.2 Material and Methods

6.2.1 Metabolic models

The illustrative example provided in the original PhPP analysis paper (Edwards et al., 2012) was used, which contains 13 reactions and 8 metabolites. User supplied code was written to carry out the simulations for the illustrative example, that calculated the shadow prices and fluxes. The other model used is the *E. coli* core model, which contains 95 reactions and 72 metabolites. For the *E. coli* core model the COBRA toolbox was used. PLS toolbox in MATLAB was used for principal component analysis.

6.2.2 System identification enhanced PhPP analysis

Phenotype phase plane (PhPP) analysis was carried out using the standard procedure that is seen in the following papers (Duarte et al., 2004; Edwards et al., 2002). System identification framework overview can be found in these following papers (Damiani et al., 2015, Liang et al.,

2013). The SID enhanced PhPP analysis visualized in the block diagram is shown in Figure 6.2. The first block is selection of a particular metabolite to vary; in this case, an input to the system, like carbon or oxygen. By perturbing the system with the input flux, the fluxes of all the reactions are recorded, and then principal component analysis (PCA) is performed. The justification of why PCA is used is that the flux matrix as a multivariable problem, where the variables are the specific reactions and the system is sampled by varying the substrate uptake rate. PCA reduces the dimensionality of the flux matrix to uncorrelated components, known as principal components, which is the linear combination of the original variables. In all our cases one principal component was used to describe all the variation. From PCA, two outputs are given, known as scores and loadings. The scores represent a composite measurement for each sample that is taken; therefore provide a global measurement of what is going on in the model network. Thus the scores provide the number of phenotypes by examining the linear behavior of each score value. When the flux profile changes this causes a different linear segment, which designates a new phenotype. On the other hand, the loadings are weightings for each variable, which tell us how important each reaction is. Whether a reaction is active or non-active, and if being active, whether is it being upregulated or downregulated, and the corresponding weighting.

Comparing SID enhanced PhPP analysis to PhPP analysis, this now allows the different phenotypes to be determined by the scores rather than the shadow prices. This is advantageous, because the whole phenotype plane does not need to be calculated at every carbon and oxygen point, but rather that the boundaries are calculated through the SID enhanced PhPP analysis. Also the accuracy of where each phase exists, it not affected by the grid size, as the PhPP analysis was.

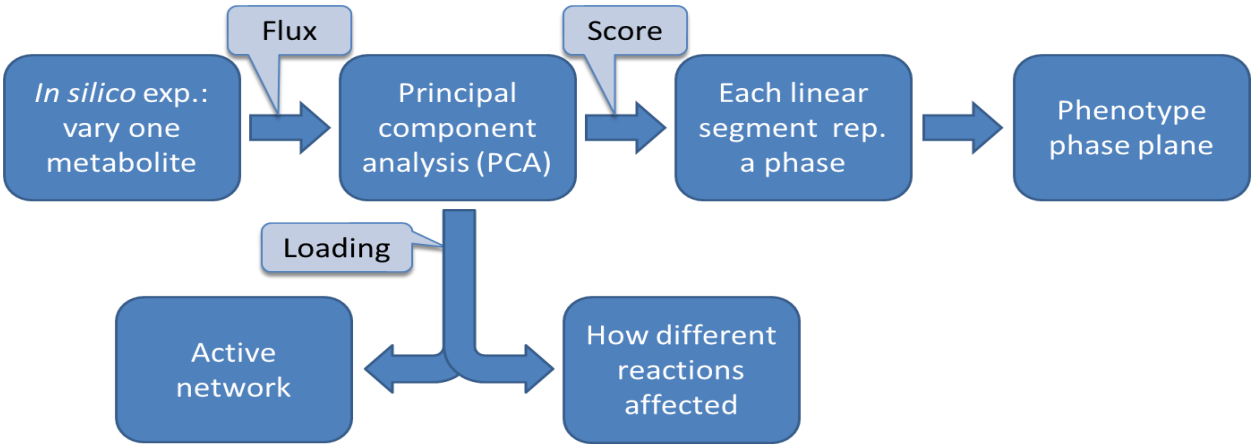

Figure 6.2: Schematic diagram of SID enhanced PhPP analysis

6.3 Results and Discussion

PhPP analysis and SID enhanced PhPP analysis was conducted on a simple metabolic network. Here SID enhanced PhPP analysis demonstrated how scores was used to detect the different phenotypes and how the loadings were used to further characterize the model network. Through PhPP analysis, it was difficult to track the differences in the phenotypes by looking at the shadow prices. The SID enhanced PhPP offered a more complete method, since it provides a better representation of the analyzing of the metabolic network. Next a more detailed metabolic network model, *E. coli* central carbon metabolism model, was utilized to portray the power of the SID enhanced PhPP compared to the traditional method of PhPP analysis. Due to the increasing size of the *E. coli* model, the shadow prices now provided miniscule meaning. Error was shown in the shadow price of the formate exchange flux. Also SID enhanced PhPP analysis was able to detect a "missing" phenotype that PhPP analysis failed to uncover.

6.3.1 Illustrative Example

To demonstrate the new method let us consider the following illustrative example, where the metabolic network and reactions are shown in Figure 6.3. The metabolic network is a very small central carbon model, where there are two compartments the exchange and cytosol that are represented by the symbols [e] and [c], respectively. The carbon uptake is designated by Rx1, where the metabolite used for the carbon is A, and the oxygen uptake reaction is Rx2. The main subsystems of the central carbon metabolism are concise to one reaction. Rx3 is glycolysis, Rx4 is TCA cycle, and Rx8 is the electron transport chain. There are three byproducts, C[e], D[e], and E[c], where are generated through Rx11, Rx6, and Rx7, respectively. There is an ATP dissipation reaction that is denoted by Rx9. The objective function is biomass formulation (Rx10). The table to right in Figure 6.3 shows the stoichiometry of the reactions.

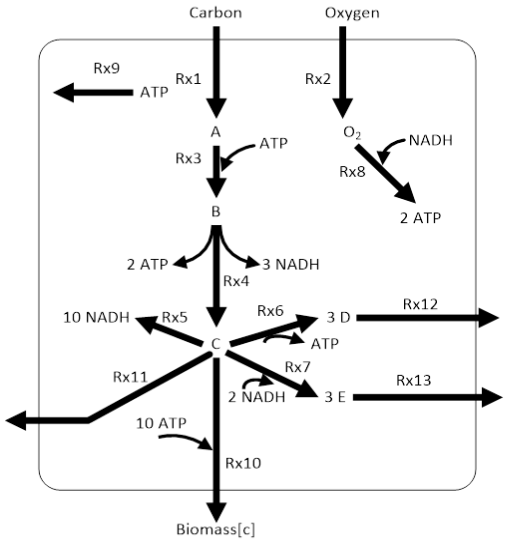

Rx#	Reaction
Rx1	A[e] -> A[c]
Rx2	O2[e] -> O2[c]
Rx3	A[c] + ATP[c] -> B[c]
Rx4	B[c] -> 2 ATP[c] + 3 NADH[c] + C[c]
Rx5	0.2 C[c] -> 2 NADH[c]*
Rx6	C[c] -> 3 D[c] + ATP[c]
Rx7	C[c] + 2 NADH[c] -> 3 E[c]
Rx8	NADH[c] + O2[c] -> 2 ATP[c]
Rx9	ATP[c] -> ATP[e]
Rx10	C[c] + 10 ATP[c] -> Biomass[c]
Rx11	C[c] -> C[e]
Rx12	D[c] -> D[e]
Rx13	E[c] -> E[e]

Figure 6.3: Illustrative example of network and reactions

PhPP analysis was performed on the illustrative example and the results are shown in Figure 6.4. There are four phenotypes, P1, P2, P3, and P4, and this is translated into a 2D plot. The blue lines are the boundary lines between the phenotypes, and the blue line that separate P1

and P2 is known as the line of optimality (LO), which is defined as the optimal ratio of oxygen and carbon uptake. The green regions in the 3D plot represent the infeasible regions, which are shown in the 2D plot by the light blue regions.

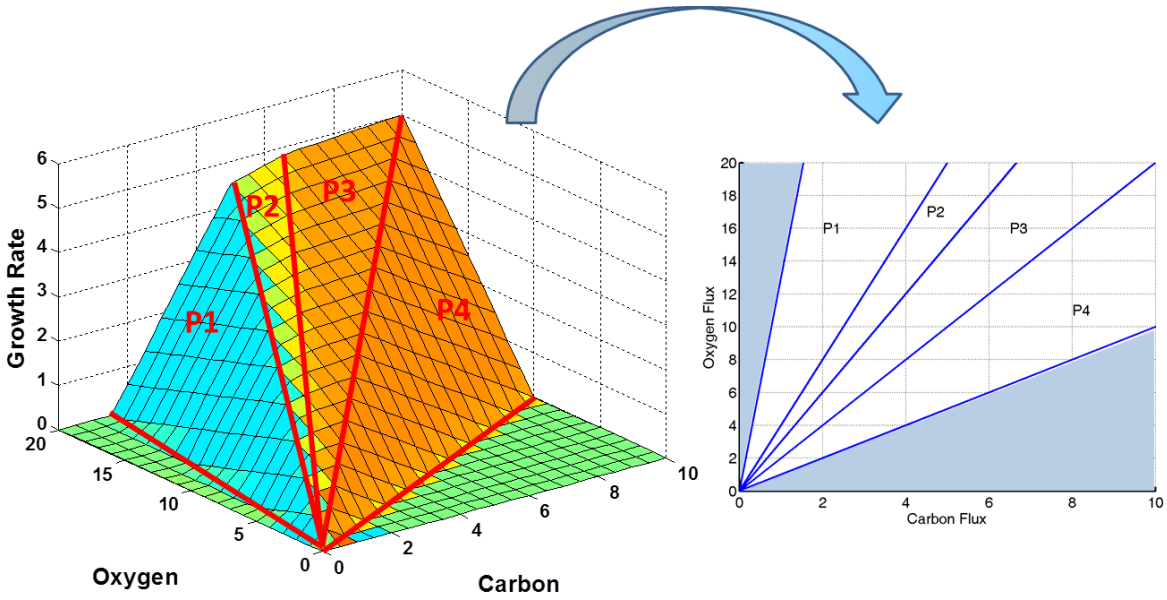

Figure 6.4: PhPP analysis of illustrative example

The SID enhanced PhPP analysis calculates the scores by varying one independent variable at a time, where this can be done for each variable. The results of this analysis are shown in Figure 6.5. The scores calculated when varying the carbon flux are shown by the plot at the bottom left corner. While the plot to the right shows the scores plot for varying oxygen flux. The linearity of each line segment represents a specific phenotype, and the direction of the linear segment changes represents shifting into another phenotype. For example, the boundary line between P2 and P3 shows that the scores plot of oxygen and carbon is determined at different points on the boundary line, thus the two points are connected and the boundary line is found.

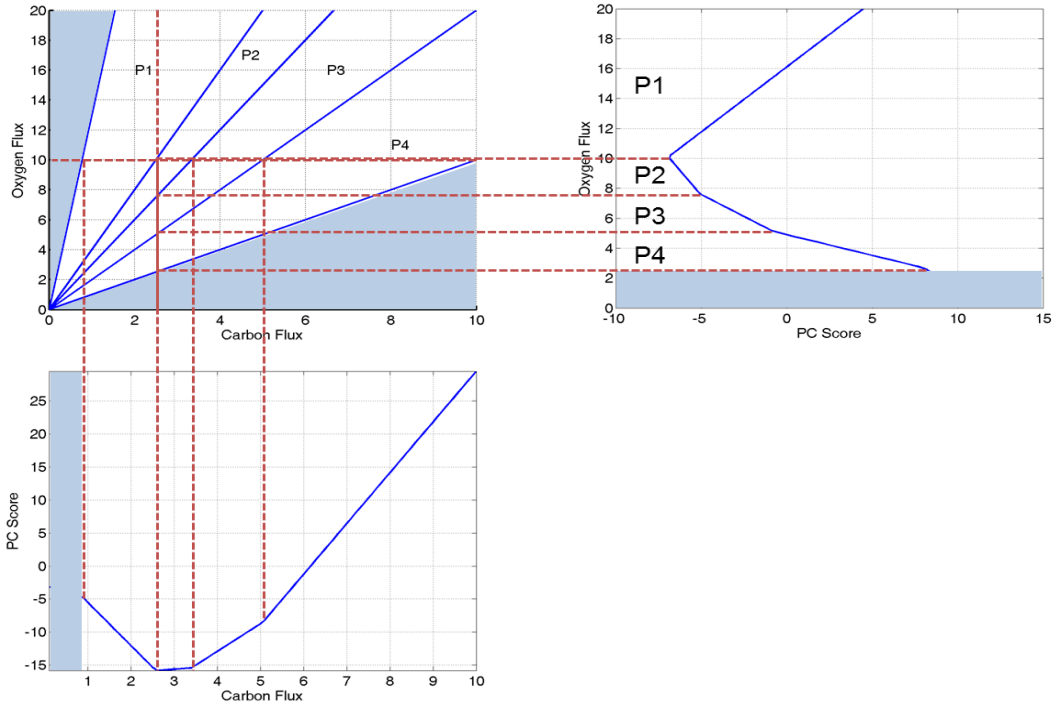

Figure 6.5: Prediction of phenotypes using SID enhanced PhPP analysis.

P1, LO, and P2 is investigated together, because they provide the most crucial results, since from the literature has shown that the biomass growth operates either on or very close to the LO (Edwards et al., 2001). Table 6.1 displays the shadow prices for P1, LO, and P2, where a negative shadow price means that by adding a unit of a metabolite the objective function would increase, while on contrary for a positive shadow price would cause a decrease in the objective function. A zero shadow price means that the metabolite is secreted from the system. For P1, there is positive shadow price of oxygen, meaning that oxygen is in excess. Oxygen is only consumed in Rx8 for the production of ATP, thus ATP is in excess and is secreted from the system using the ATP dissipation reaction (Rx9), which is why the shadow price is zero. The shadow prices for the LO are all negative. For P2, shadow price is zero for D, meaning that it is secreted from the system. The only clear analysis that was taken from the shadow prices was if the shadow prices had a value of zero or was positive. It is very difficult just to look at the shadow prices and determine the distinct characteristics of each phase.

Table 6.1: Shadow prices of P1, LO, and P2

	A	B	C	D	E	O_2	NADH	ATP
P1	-1.30	-1.30	-1.00	-0.20	-0.40	0.10	-0.10	0.00
LO	-1.20	-1.20	-0.93	-0.18	-0.27	-0.01	-0.07	-0.09
P2	-0.21	-0.30	-0.09	0.00	-0.02	-0.01	-0.01	-0.09

Figure 6.6 shows the active and non-active reactions, which are shown in black and gray respectively, for P1, LO, and P2. There are distinct reactions that are active for each phenotype. The reactions that are similar between P1, LO, and P2 are Rx1, Rx2, Rx3 Rx4, Rx5, Rx8, and Rx10. P1 has Rx9 (ATP dissipation reaction), while P2 has Rx6 and Rx12 turned on, which represents the production of byproduct D. For the LO, neither of these reactions is utilized, meaning that these reactions Rx2, Rx6, and Rx9 do not provide highest biomass production when activated.

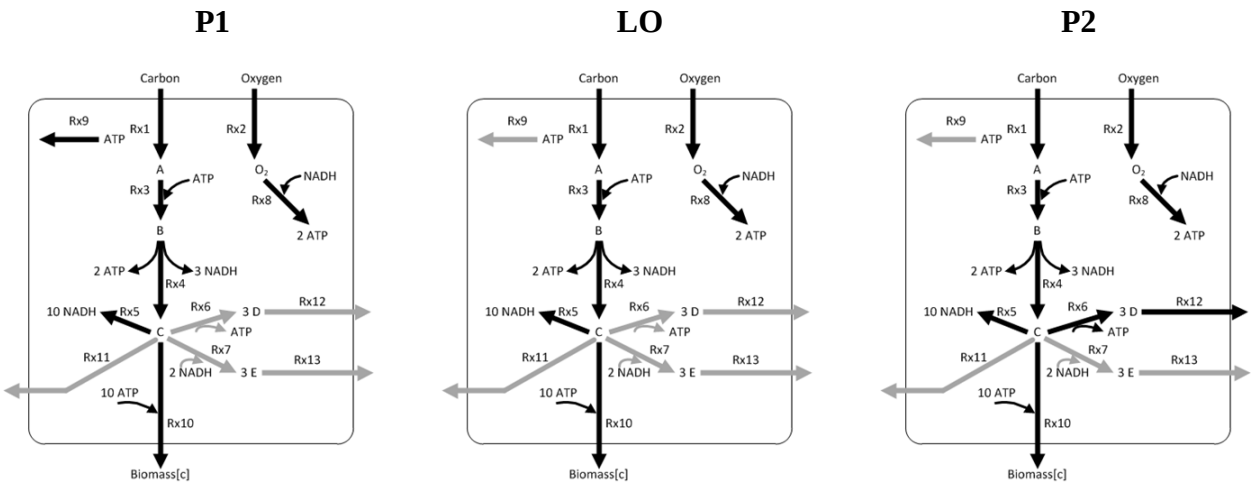

Figure 6.6: Active and non-active reactions for P1, LO, and P2

Figure 6.7 shows the step by step process for the SID enhanced PhPP analysis for P1. The figures to the left and right represent when the carbon and oxygen uptake flux is solely varied, respectively Figure 6.7 (a) and (b). Here the variation of carbon and oxygen occurs in the

region that represents P1, which is represented by the red arrows. SID framework is then applied to the flux data, where the loadings were that calculated through PCA, which is shown in Figure 6.7 (c) and (d). For the variation of carbon uptake, Rx9 is a standout reaction, where it is heavily negatively correlated with carbon uptake. Using the shadow prices, a similar conclusion was made it that ATP was being secreted from the system; however shadow price analysis failed to reveal the degree it was impacted compared to the other reactions. Still observing the changes due to carbon uptake, Rx5 is negatively correlated, which could not be detected by shadow price analysis. The shadow price of NADH was asserting that adding a unit of NADH would result in an increase in the objective function, which is a global claim for the metabolite of NADH. However, it is more essential that we find out what reactions are being affected the most to better understand the model network. This model network only has three reactions where NADH is either being consumed or produced, but when you get to larger models there can be over 100 reactions that utilize NADH. Therefore, the shadow price value alone cannot depict the importance of what NADH reactions and the degree of the impact. Now looking at the variation of oxygen uptake, Rx9, now it has a positive correlative, thus it is upregulated. An upregulation of this reaction tells us that the model network is "wasting" energy, because ATP is being unused in the system and has to be secreted out. An explanation for this is that the oxygen uptake is going away from the line of optimality meaning that the model network is unable to handle the oxygen levels, therefore pathways that are less efficient are being used to offset the oxygen levels, which cause the biomass reaction to decline. These are results are visualized in Figure 6.7 (e) and (f).

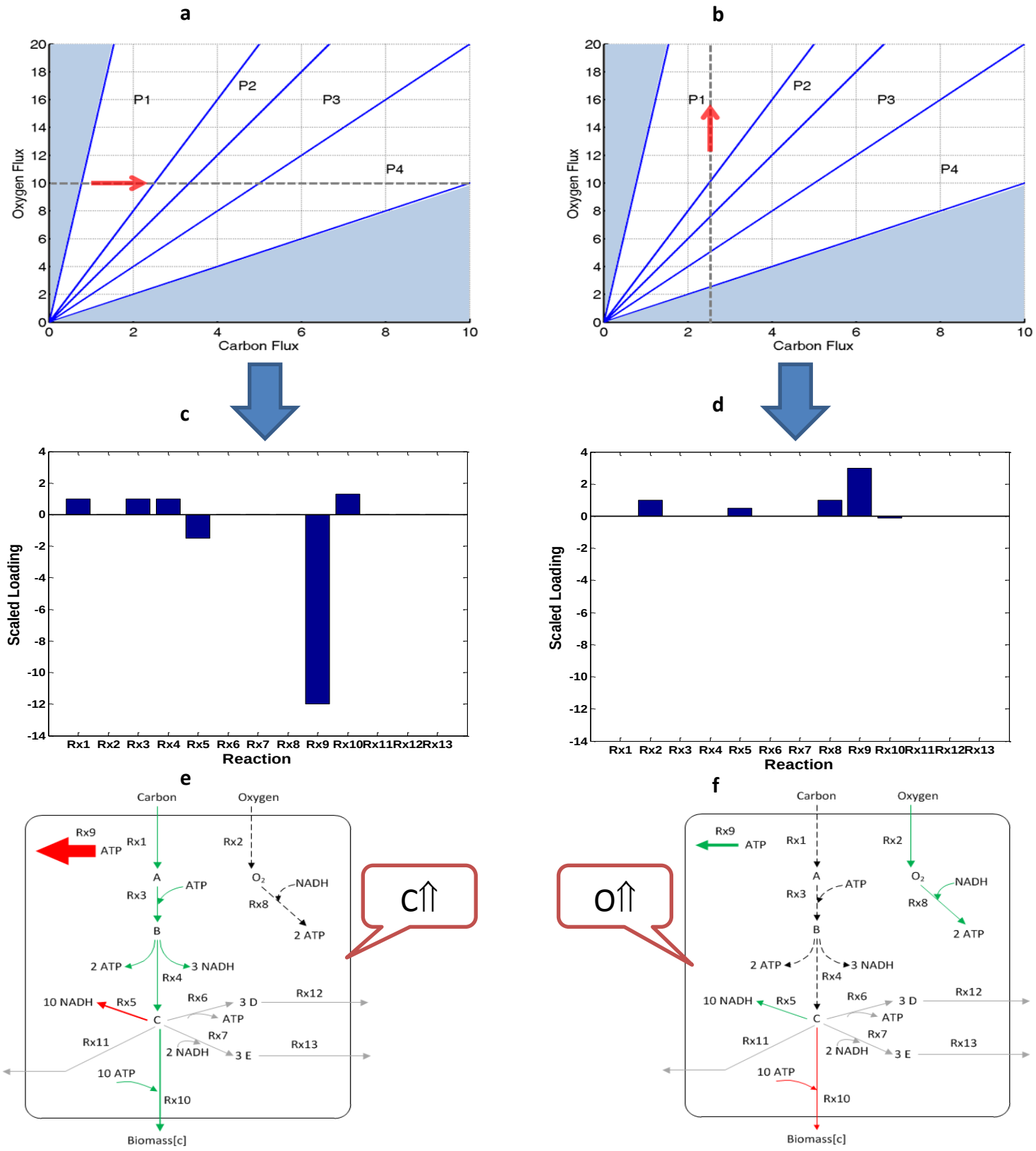

Figure 6.7: SID enhanced PhPP analysis for P1. (a) Variation of carbon in 2D phenotype plot, (b) Variation of oxygen in 2D phenotype plot, (c) Loadings for variation of carbon, (d) Loadings for variation of oxygen, (e) Visualization of P1 when varying carbon, (f) Visualization of P1 when varying oxygen

When the flux increases (green), decreases (red), and stays the same (gray) and weighting the line, which is the magnitude of the loading. This provides a very clear breakdown of the results in the metabolic network.

This same analysis was performed on LO and P2, where these results are shown in Figures 6.8 and 6.9. The LO does not activate inefficient reactions like ATP dissipation and byproduct production, because neither the carbon or oxygen uptake is in excess. Both of these uptakes are perfectly being utilized to maximize the cellular growth. The ratio between oxygen and carbon was determined to be 4:1. Examining P2, Rx5 is still being utilized, and now instead of utilizing the ATP dissipation reaction, the model selects the usage of producing D (Rx6).

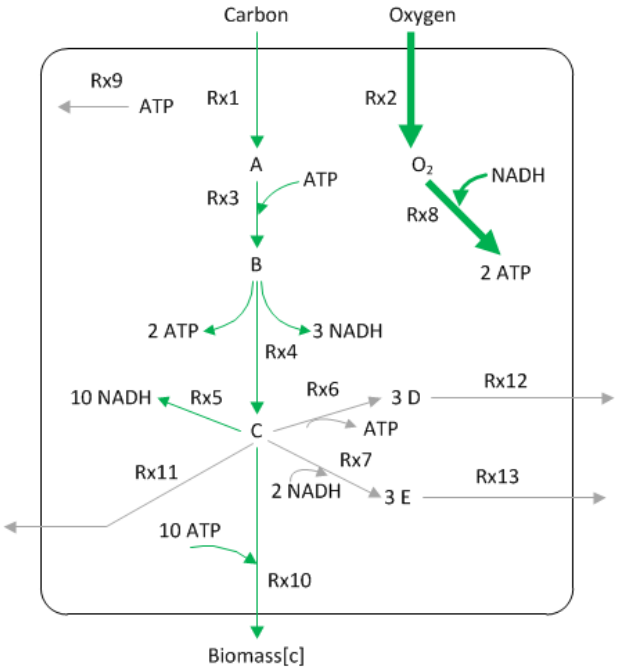

Figure 6.8: SID enhanced PhPP for LO

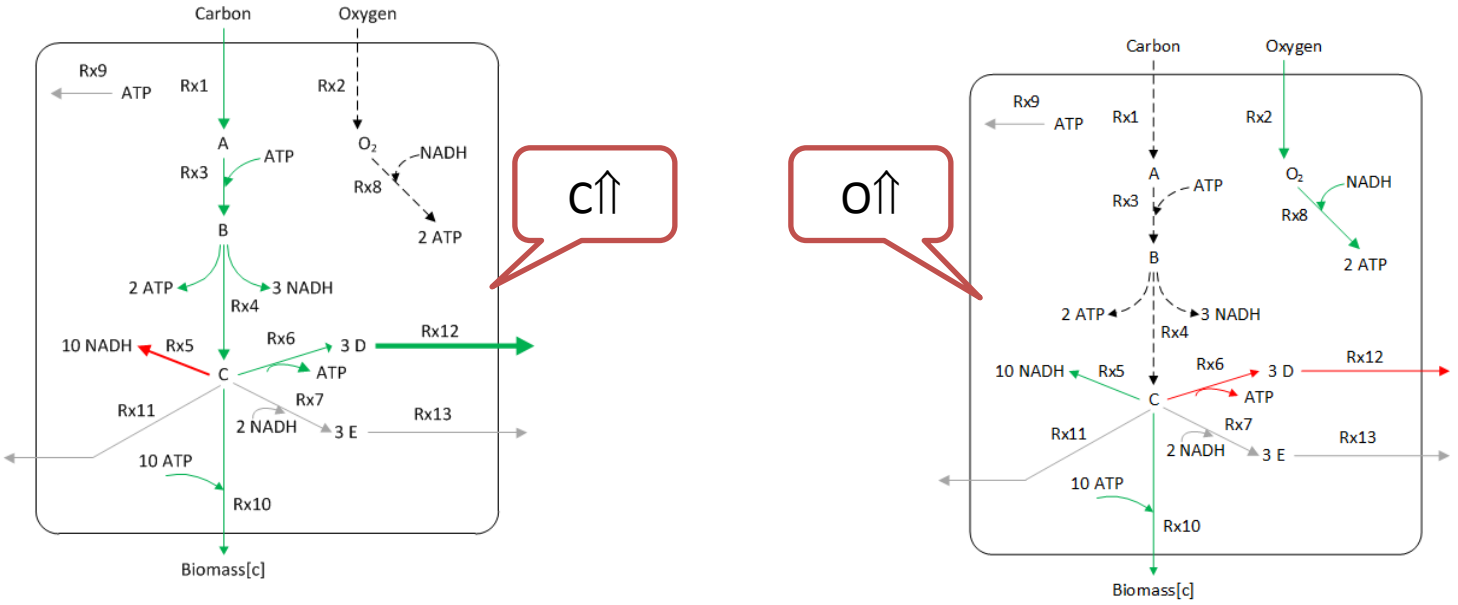

Figure 6.9: SID enhanced PhPP for P2

Figure 6.10 shows the comparison of P1, LO, and P2 as carbon is varied, and emphasizing the differences between the phenotypes.

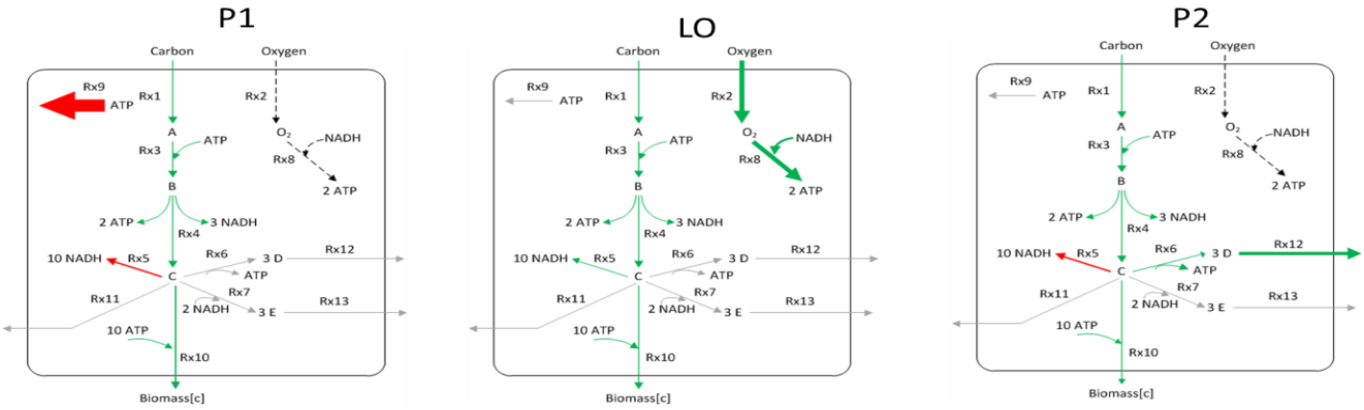

Figure 6.10: Comparison of P1, LO, and P2

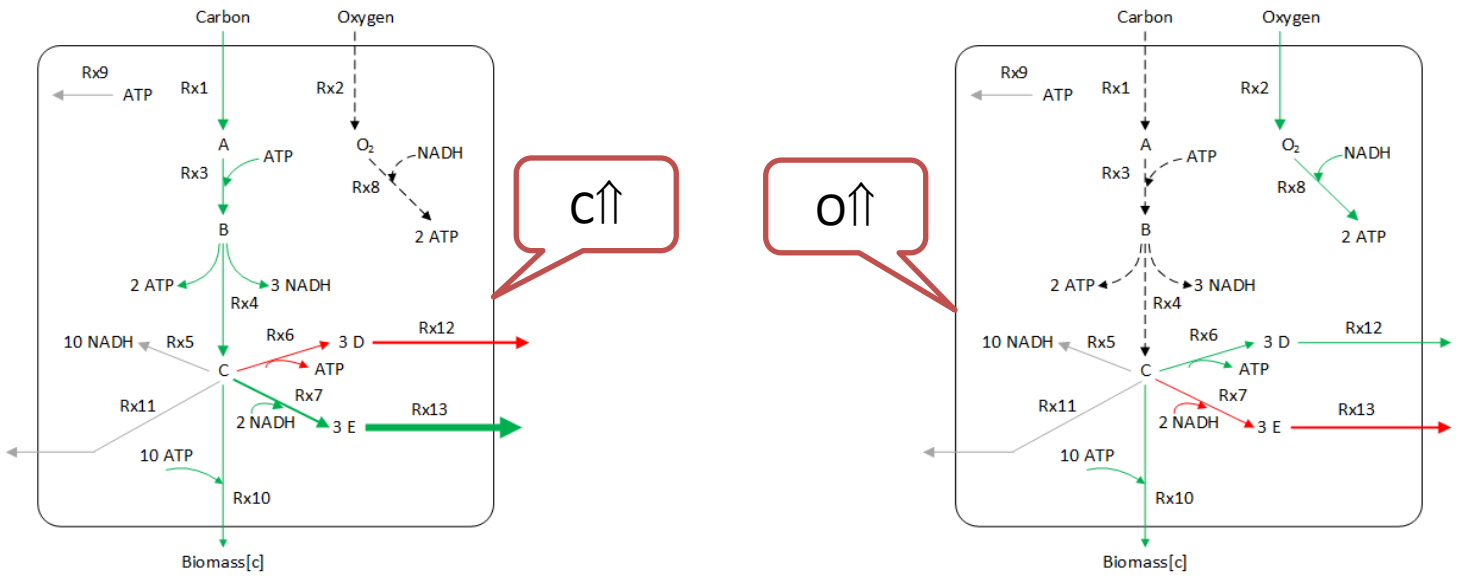

Figure 6.11: SID enhanced PhPP for P3

Figure 6.11 displays the visualization results for P3, when carbon and oxygen pickup rates were being varied. Rx5 is turned off, and now the byproduct E is generated by Rx7. The byproduct D is still being produced and this is negatively correlated with byproduct E, where the direction depends on whether carbon or oxygen uptake is varied. Table 6.2 shows the shadow prices for P3 and P4. Again, shadow prices that are either zero or positive are easy to interpret, but the others do not give much information. D and E are zero, meaning that they are expelled from the model network and NADH is positive, which entails that it is in excess. This explains why Rx5 was shut off, due to not needing anymore NADH.

Table 6.2: Shadow prices of P3 and P4

Phenotypes	A	B	C	D	E	O_2	NADH	ATP
P3	-0.05	-0.14	-0.09	0	0	-0.23	0.05	-0.09
P4	0.50	0.50	-1.00	-0.33	0	-0.50	-0.50	0

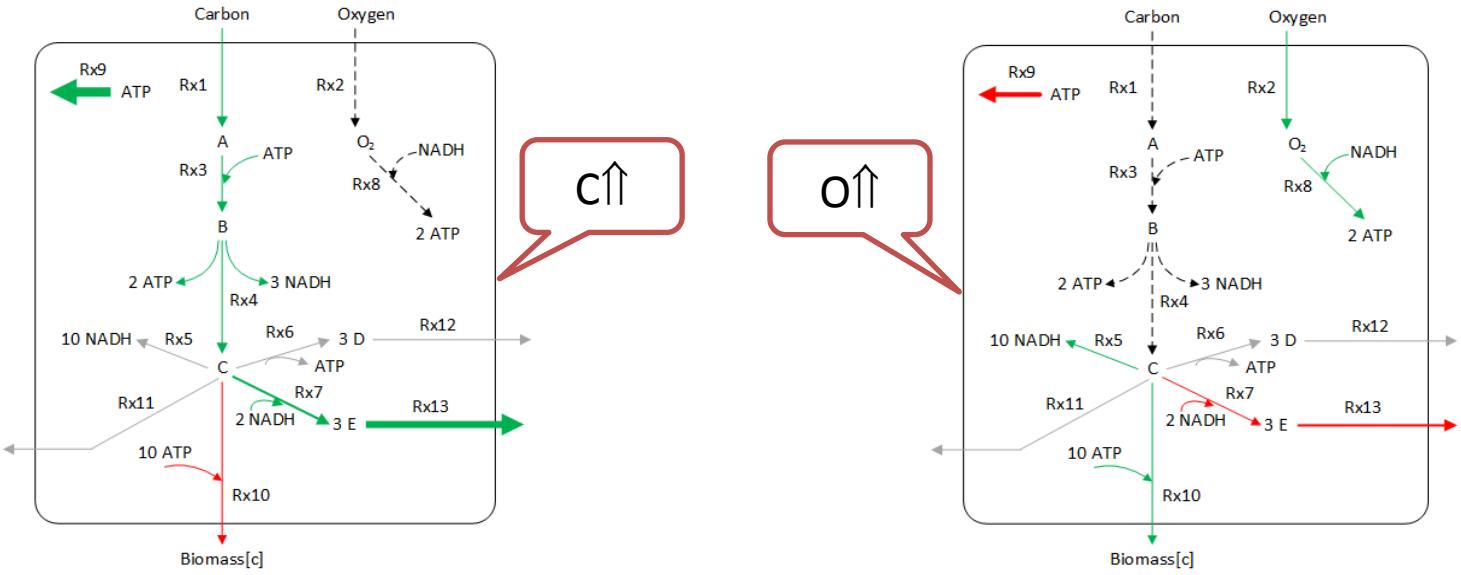

Figure 6.12: SID enhanced PhPP for P4

Figure 6.12 displays the SID enhanced PhPP analysis results for the final phenotype P4. This phenotype is characterized by carbon being in excess, which is why ATP dissipation reaction is activated. Also when the carbon uptake rate is increased this causes the biomass reaction to decrease. The byproduct D is not being produced, but the byproduct E is still in production. The shadow prices of A and B are positive meaning that they are in excess that is translated to an excess of carbon. E and ATP are zero, where this is agreement with SID enhanced PhPP analysis.

In summary, with this simple model network, the newly developed approach of SID enhanced PhPP analysis supersedes the commonly method of PhPP analysis. Shadow prices alone cannot extract the fine details of the model network. Although shadow prices can exert information about whether metabolites are being secreted or if a metabolite is in excess, but it cannot depict the magnitude of how each reaction is being affected. Overall, SID enhanced PhPP analysis extracts embedded metabolic information that is known from examining the shadow prices.

6.3.2 *E. coli* core model

The next example is a central carbon metabolism model of *E. coli* which contains 95 reactions and 72 metabolites, where the metabolism is shown in Figure 6.13. The *E. coli* model is a lot more complex than the previous model discussed. Instead of one reaction representing a whole subsystem, now the proper reactions are instilled into each central carbon metabolism subsystem. A quick overview of the metabolism is that there is the glycolysis, both branches of the pentose phosphate pathway (PPP), TCA cycle, and electron transport chain. The two substrates that were chosen for this study were glucose and oxygen. There were five byproducts that were examined: CO_2, lactate, formate, ethanol, and acetate. The biomass reaction was used as the objective function.

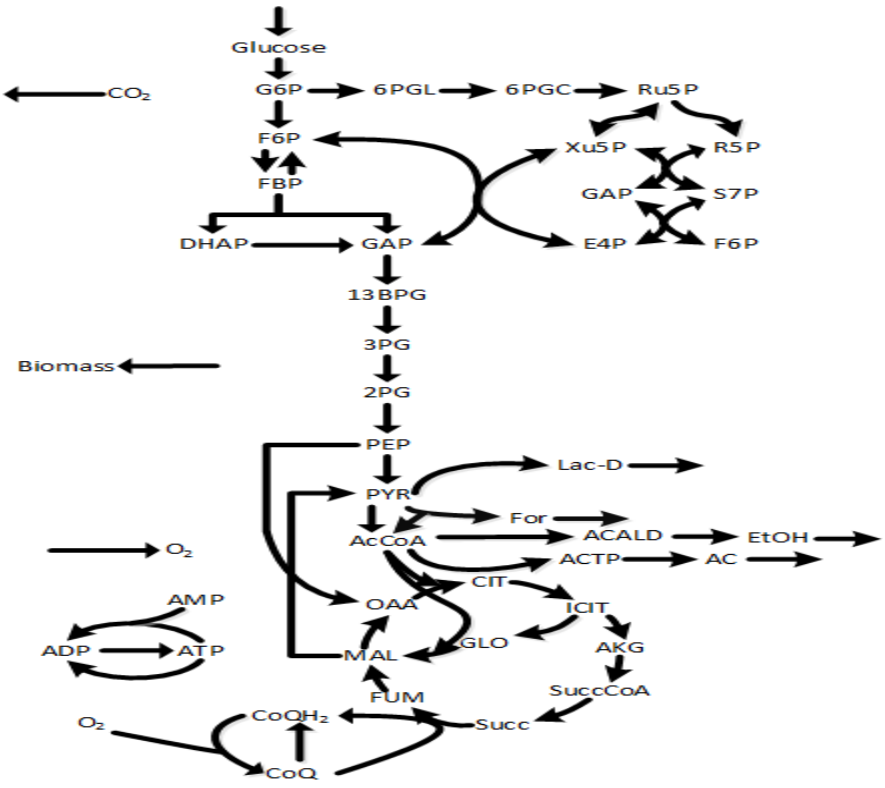

Figure 6.13: Central carbon metabolism of *E. coli* model

PhPP analysis was conducted on the *E. coli* model, where 4 phenotypes were uncovered, P1, P2, P3, and P4, which is shown in Figure 6.14 (a). When SID enhanced PhPP analysis was carried out, there was additional phenotypes that was discovered, naming them P3' and P3", which is shown in Figure 6.14 (b). PhPP analysis condenses P3' and P3'' into one phenotype (P3), where the green region in Figure 6.14 emphasizes the differences. The phenotypes P3' and P3'' were detected from the PC scores, which are shown in Figure 6.15.

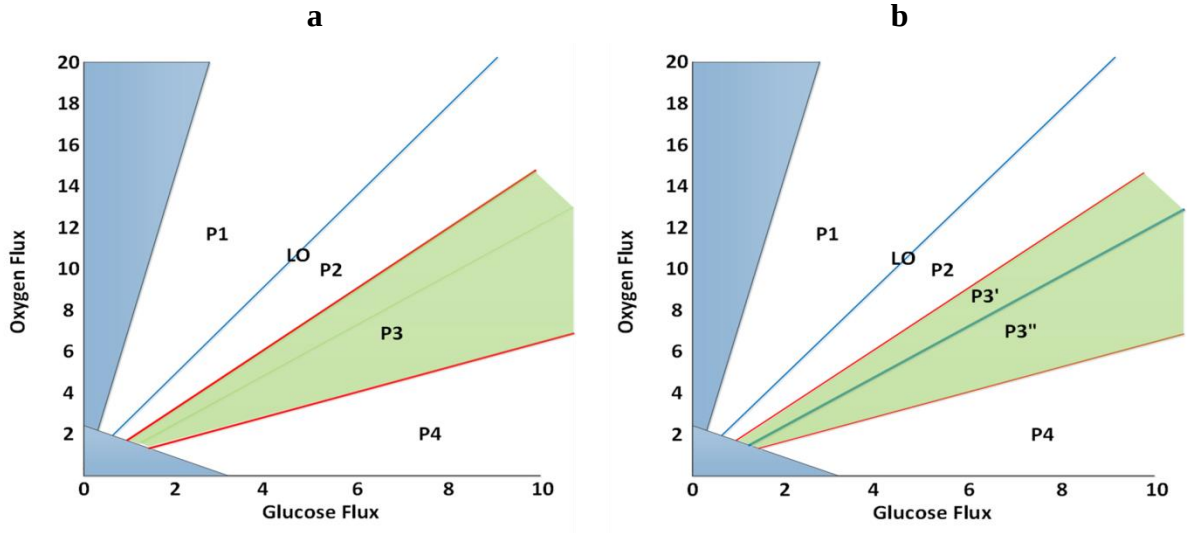

Figure 6.14: Comparison of phenotypes from PhPP analysis and SID enhanced PhPP analysis. (a) Phenotypes generated through PhPP analysis and (b) Phenotypes generated through SID enhanced PhPP analysis.

Figure 6.15 (a) displays the cuts that were made in both the glucose and oxygen uptake direction. The red arrow represents as glucose uptake is varying, where Figure 6.15 (b) shows the PC score plot showing the two separate phases, which is due to the break in the linear segment of P3'. The same is true for the oxygen uptake, which is the blue arrow and Figure 6.15 (c) exhibits the two different phases. The reason that PhPP analysis was unable to distinguish between P3' and P3", was because the shadow prices are the same in the two phenotypes. It is evident from Figure 6.15 that the PC score is a more reliable measurement to identify the phenotypes.

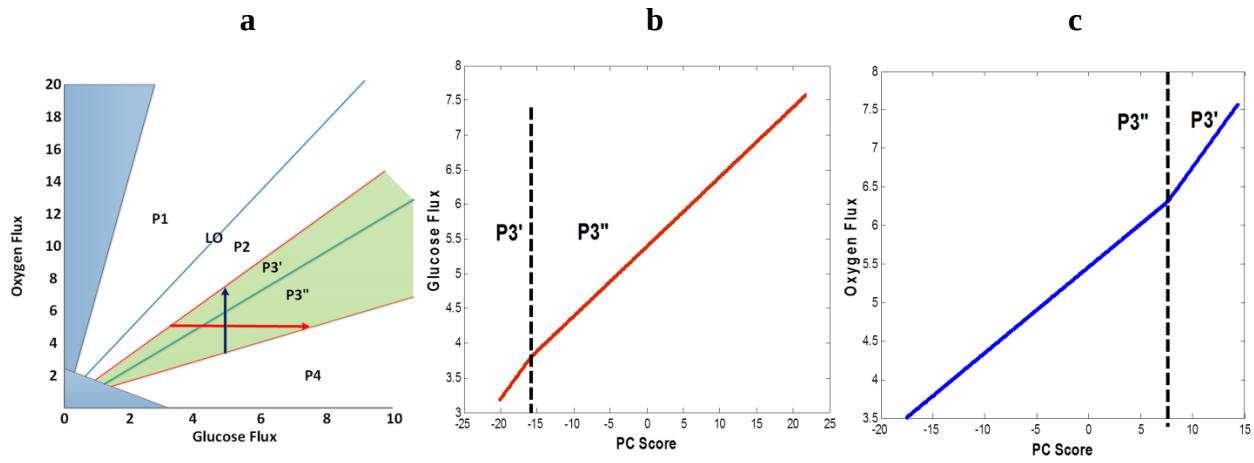

Figure 6.15 SID enhanced PhPP analysis P3' and P3''. (a) Cuts in glucose and oxygen direction in P3' and P3'', (b) Disctinction of phenotypes when varying glucose, (c) Disctinction of phenotypes when varying oxygen.

Figure 6.16 shows the results from SID enhanced PhPP analysis for P3' and P3'' when oxygen is being varied, where the blue dots correspond to reactions that differ in terms of being active or not active. There are a plethora of differences between the two phenotypes.

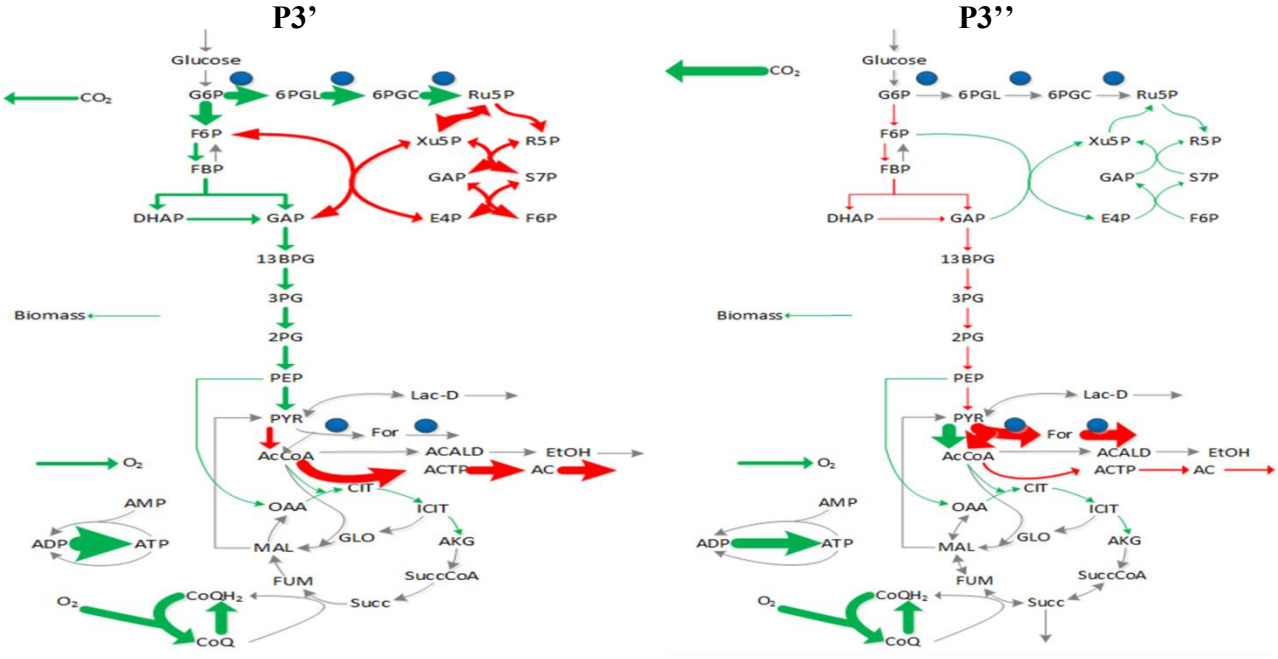

Figure 6.16: Comparison of SID enhanced PhPP results of P3' and P3''-1. Oxygen uptake is being varied.

Firstly, the glycolysis and non-oxidative branch of PPP is in opposing directions in P3' and P3''. Secondly, the oxidative branch PPP is heavily upregulated in P3', but in P3'' it is not active. Thirdly, formate is not produced in P3', but in P3'' formate production route is heavily downregulated. Finally, acetate production is heavily downregulated in P3' compared to P3''.

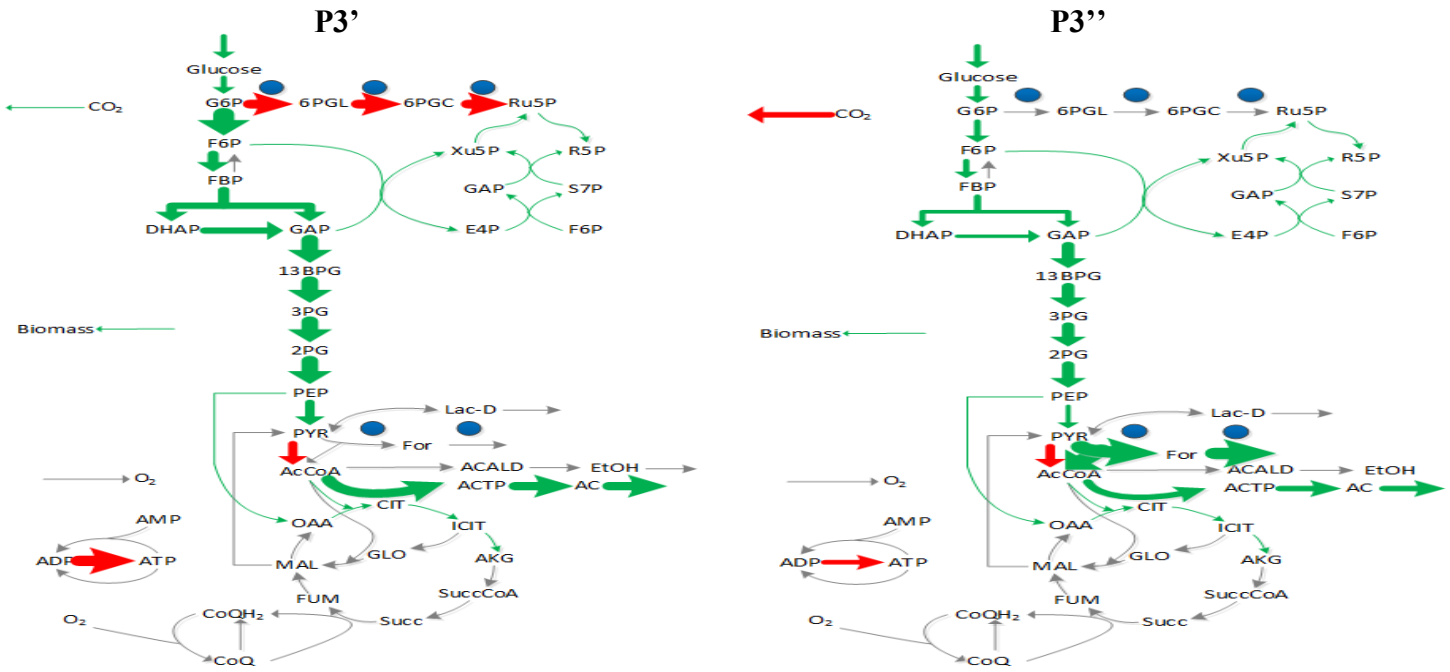

Figure 6.17: Comparison of SID enhanced PhPP results of P3' and P3''-2. Glucose uptake is being varied.

The other case to examine for P3' and P3'' was when glucose pickup rate is being changed, where the results are shown in Figure 6.17. For this case the results are very similar, the only discrepancy between the phenotypes is the reactions that are different in the active reactions, which are shown again in blue dots.

Figure 6.18 shows the phenotypes of P2 and P4, where the blue square shows that formate exchange is being unaffected in P2, while in P4 formate exchange is downregulated. Table 6.3 displays the shadow prices for all phenotypes for the substates and products, where the shadow price of P2 for formate is zero. By definition this means that formate should be secreted

from the sytem, which is the case for P4, however in P2 formate is not being secreted from the system. The other products, such as ethanol and acetate obey this rule for shadow prices, since ethanol is non-zero and acetate is zero in P2, where ethanol is not produced and acetate is produced. The other phenotypes also adhere to the shadow price rules. Therefore, again shadow prices can be unreliable in extracting information from the model network.

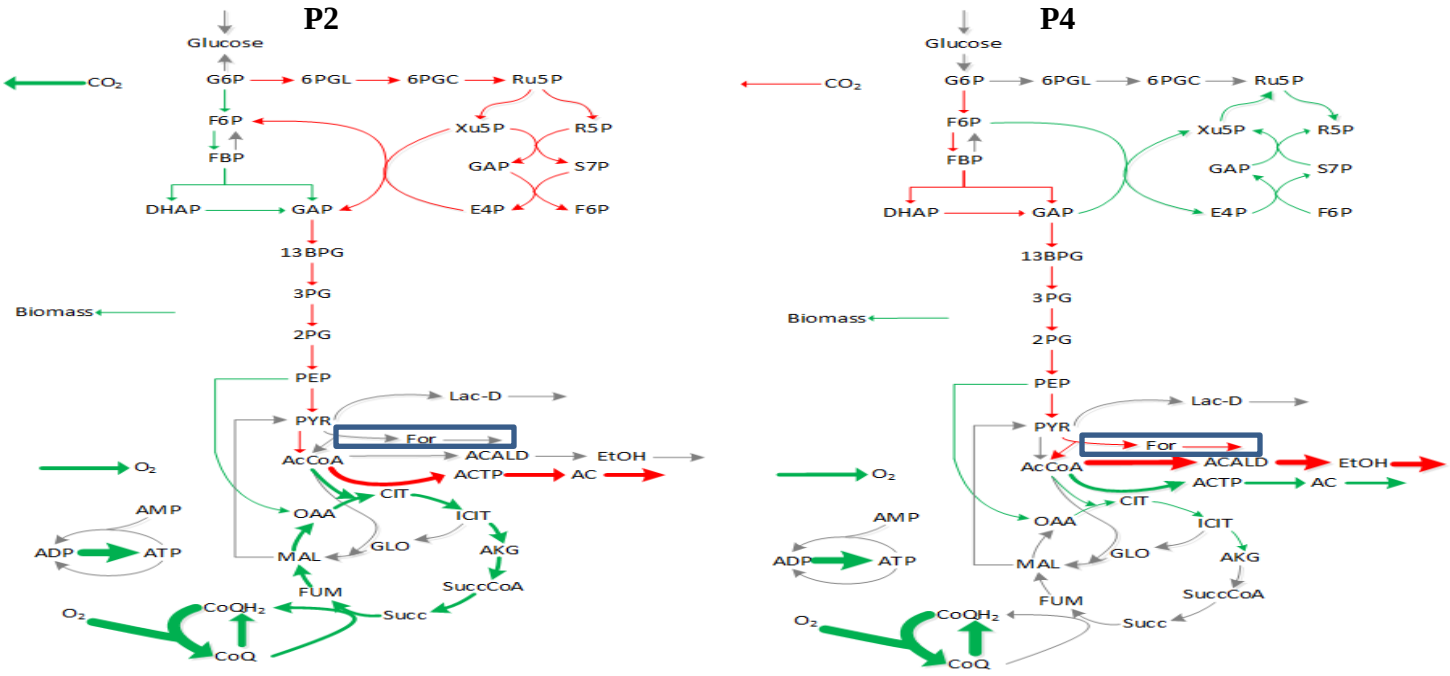

Figure 6.18: Comparison of SID enhanced PhPP results of P2 and P4. Oxygen uptake is being varied.

Another shortcoming of shadow prices is that it does not portray the metabolic details of what is happening in each phenotype. Table 6.4 shows some of the shadow prices of the key intermediate metabolites. Examining P2 and P4, there are significant differences metabolically; however the shadow prices do not have the same conclusion. For the metabolite G6P, there is a very small difference between P2 and P4, which encompasses both the glycolysis and oxidative branch of PPP, where there are significant differences in these pathways among P2 and P4.

Table 6.3: Shadow prices of the substrates and products for all phenotypes for *E. coli*.

Metabolites	P1	P2	P3	P4
Glucose	-0.10	-0.034	-0.033	-0.033
Oxygen	0.023	-0.023	-0.033	-0.036
Acetate	-0.046	0	0	0
Ethanol	-0.069	-0.010	-0.0027	0
Formate	0	0	0	0
Lactate	-0.069	-0.013	-0.0054	-0.0042

This is also seen in the E4P, which is a metabolite in the non-oxidative branch of PPP. Investigating the behavior of the TCA cycle between P2 and P4, we see that the TCA cycle in P2 is fully activated and in P4 it is branched. The metabolite AKG in the TCA cycle shows that the shadow prices between P2 and P4 are very analogous. Lastly, pyruvate (PYR) has a lot of interconnections between subsystems, the again the shadow prices of PYR between P2 and P4 are very similar. Looking at the SID enhanced PhPP analysis results there are substantial differences that are connected to pyruvate. Pyruvate dehydrogenase is the reaction that converts pyruvate to acetyl-CoA, in P2 this reaction is downregulated, while in P4 this reaction is not active. Pyruvate is alo involved in for the production of formate, in P4 formate exchange is downregulated and in P2 formate exchange is non-active.

Table 6.4: Shadow prices of the intermediate metabolites for all phenotypes for *E. coli*.

Metabolites	P1	P2	P3	P4
3PG	-0.057	-0.027	-0.024	-0.025
AcCoA	0	0	0	0
AKG	-0.092	-0.033	-0.033	-0.035
E4P	-0.092	-0.043	-0.035	-0.034
G6P	-0.14	-0.056	-0.046	-0.044
PYR	-0.057	-0.014	-0.011	-0.011

The next type of analysis that was performed was identifying the metabolic details between the phenotypes when oxygen was varied. Figure 6.19 displays the phenotypes of P4, P3'', P3', and P2, which are arranged in oxygen increasing order. Starting at P4, the key details

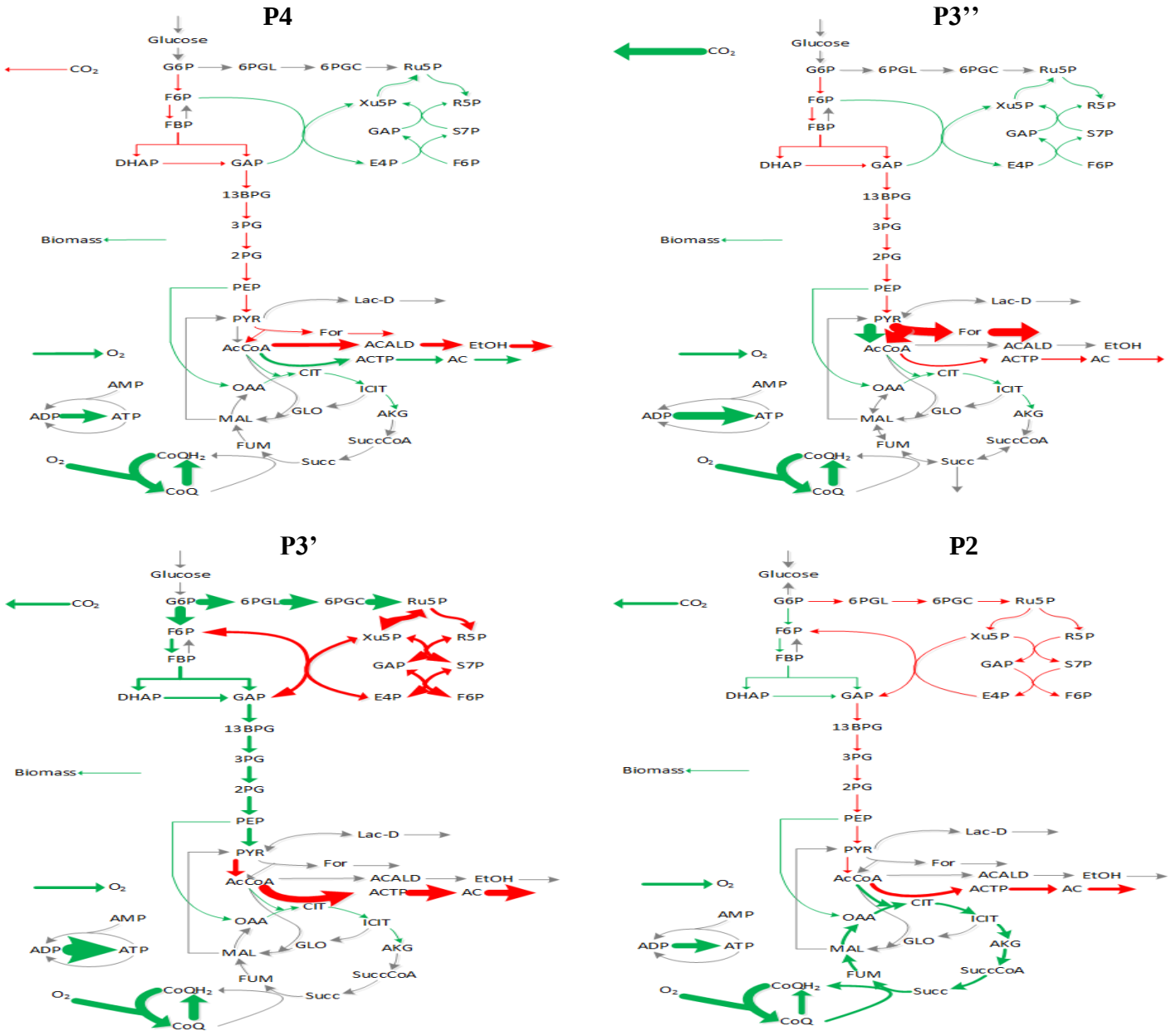

Figure 6.19: Comparison of SID enhanced PhPP results of P4, P3'', P3', and P2 as oxygen pickup is varied.

is that the oxidative branch of PPP is non-active. Glycolysis is downregulated and the non-oxidative branch of PPP is upregulated. Being a lower oxygen phenotype this caused the TCA cycle to be branched. There are 4 byproducts being generated: formate, ethanol, and CO_2 are downregulated, while acetate is upregulated. Moving to P3'', glycolysis, both branches of the PPP, and the TCA cycle are in the same direction. Ethanol production has now halted, formate is heavily downregulated, and acetate has switched production direction. Pyruvate dehydrogenase is now active. In P3', major changes occur; now the oxidative branch of PPP is activated, which causes the glycolysis pathway and non-oxidative branch of PPP to be shifted in a different direction than the previous phenotypes. Formate production has ceased and acetate is now heavily down regulated. The one similarity between the previous phenotypes is the TCA cycle is branched. Pyruvate dehydrogenase is now downregulated. Finally in P2, glycolysis and the non-oxidative branch of PPP is reverted back to the directions of P3''and P4. The oxidative branch of PPP is downregulated. The TCA cycle is fully activated denoted that is now in an aerobic phase. Some similarities between P2 and the previous phenotype of P3' is that pyruvate dehydrogenase and acetate production are in the same direction.

6.4 Conclusion

PhPP analysis is a constraint-based tool to characterize different phenotype phases based on genome-scale models, but its interpretation of different phases based on shadow price is not straight forward. The SID enhanced PhPP analysis reduces required computation, improves accuracy, as well as automate the analysis procedure. The key differences between different phenotype phases can be easily identified through the system identification enhanced approach. The illustrative example provided a simple model system of how system identification enhanced PhPP analysis infers the metabolic differences between phases. The *E. coli* core model was a

larger model that shows that only looking at the shadow prices of the metabolites is makes it very difficult to extract the key metabolic details. The system identification enhanced PhPP analysis was able to uncover the essential metabolic information for each phase and come up with correlation between the metabolic pathways.

Chapter 7: Conclusion and Outlook

7.1 Conclusion

With the constriction that fossil fuels play on the world wide economy and environment, alternative fuels are generated to alleviate these growing worries. Renewable energy in the form of lignocellulosic bioethanol offers a promising substitute, because the feedstock does not compete with food quantity and there is an abundance supply. However, there are main problem that needs to be resolved is improving the biological conversion of pentose sugars, most importantly xylose into bioethanol.

S. stipitis is the most effective strain for native xylose fermentation. Instead of studying the strain through the commonly used reductionist approach that examines individual elements one at a time, a system biology approach was taken that investigates the metabolism holistically. In order to achieve a clear perspective of the relationship between genotypic and phenotypic behaviors, constraint-based modeling was used to try to dissect this relationship via the utilization of genome-scale metabolic models. The computational that was employed to the GSMMs was flux balance analysis.

Once validated, GSMMs provide a platform to effectively interrogate cellular metabolism, such as characterizing metabolic resource allocation, predicting phenotype, designing experiments to verify model predictions, as well as designing mutant strains with desired properties. More importantly, GSMMs allow systematic assessment of how a genetic or environmental perturbation would affect the organism as a whole.

Validation and evaluation of GSMMs is one of the most challenging tasks in systems biology, due to the scale and complexity involved in genome-scale metabolisms. The

conventional GSMM validation relies on a "point-matching" approach by comparing model predictions with experimental measurements (usually substrate pickup rates, product secretion rates and cell growth rate) under different conditions. Due to the scale and complexity involved in GSMMs, combinations of multiple errors in a model could produce good agreement between predicted and measured fluxes over different points. In addition, it is very difficult to pinpoint the potential root cause (e.g., specific reactions) if erroneous model predictions occur, and model refinement requires significant effort from the modeler to manually examine hundreds or thousands of reactions

A novel system identification based (SID-based) framework was developed in order to enable a knowledge-matching approach for GSMM validation. In essence, a high-quality GSMMs is a comprehensive and well-annotated knowledge base of the strain's cellular metabolism. In the SID-based framework, the knowledge embedded in a GSMM is extracted through designed *in silico* experiments, and model validation is done by matching the extracted knowledge with the existing knowledge. We have applied the SID-based framework to conduct a comprehensive evaluation of the two published models, iSS884 and iBB814, and concluded that although both models contain multiple errors, biological knowledge captured by iBB814 agree better with existing knowledge on *S. stiptis.*

Regarding GSMM refinement, one major challenge is how to identify what reactions in the model should be modified, what reactions should be added to the model and what reactions should be deleted from the model, in order to obtain desired model behavior. Because the interconnectivity in the metabolic networks, many times seemingly unrelated reactions located far away from the "problematic" reactions, i.e., reactions that are not carried out in the way as expected, play a key role in changing model behavior. As a result, most of the time GSMM

refinement is through trial-and-error, and relies heavily on the modeler's knowledge and capability to sort out clues from various simulation results; and model refine is usually labor intensive and time consuming. In this work, we extend the SID-based framework to guide model refinement, and report an improved GSMM on *S. stipitis*, iAD828. The improved model predicts the production of an important byproduct, xylitol, under oxygen-limited conditions, which agrees with experimental observations. Note that both iSS884 and iBB814 fails in predicting xylitol production under such conditions. In addition, the analysis performed using the SID-based framework confirms that iAD828 offer better agreement with existing knowledge on *S. stipitis* than iSS884 and iBB814.

Due to the metabolic advancements of iAD828, cofactor engineering strategies was applied in order to force carbon flux toward ethanol overproduction. The cofactor preference of xylose reductase was varied and an optimal phenotype was determined. Analysis from this guided metabolic engineering *in silico* strategies, which resulted in elevated production of ethanol.

The SID framework was not only used for validation and refinement of GSMMs, but was used to enhance phenotype phase plane analysis. SID enhanced PhPP analysis was a methodology that was developed and applied to an illustrated example and *E. coli* core model in order to show the power of uncovering the metabolic information that the traditional PhPP analysis fails to do. The traditional PhPP analysis used shadow prices to determine the different phenotypes, which showed to be problematic for the *E. coli* core model. SID enhanced PhPP analysis was able to detect a "missing" phenotype that PhPP analysis failed to uncover. Also as the size of the metabolic model increases, the shadow price from PhPP analysis now provided

miniscule meaning. Error was shown in the shadow price of the formate exchange flux. SID enhanced PhPP analysis provides a powerful tool for understanding metabolic phenotypes.

7.2 Outlook

Even though advancements were made to iAD828, there are still limitations that hinder the performance:

Acetic Acid production: Wet lab experiments show that acetic acid was produced simultaneously with xylitol under oxygen-limited condition. There is a redox balance issue here, but in order for this to happen there might need to be regulation schemes implemented.

Robustness: iAD828 did add improvement, but there were additional phenotypes added under both oxygen-limited and aerobic condition. The number of phenotypes on both sides of the spectrum for oxygen needs to be cut back.

Biomass/Objective function: The biomass formation equation from iBB814 was used as the objective function. Additionally experiments could be done to make the biomass formation equation more accurate. iSS884 showed a lot of fatty acids that were absent from iBB814 biomass equation. Also does the biomass formation equation change with oxygen level. Metabolic engineering for ethanol overproduction is performed under oxygen-limited condition, collect data under this condition for biomass for be very helpful. Another part of this is to try different objective functions, such as the redox power, but also combine objective functions together.

Metabolic engineering: There are numerous of tools that have developed for overproduction of a desired metabolite. Use these to develop metabolic engineering strategies, these could allow biologist with ways to increase xylose fermentation.

Anaerobic growth: *S. stipitis* fails to grow under anaerobic conditions, thus it would be very advantageous to discover the reason(s) for this.

Dynamic modeling: The modeling used here employs the steady state assumption, using kinetic modeling or optimal control approaches would be very beneficial to model dynamic processes such as batch and fed batch, which is the majority of the operations scheme in industry.

Bibliography

Global Status Report - REN21. (2014). Retrieved October 19, 2015.

IEA. World energy outlook world energy outlook. Paris: International Energy Agency; 2007.

Iowa State Univeristy. Thrust 2: Microbial Metabolic Engineering. (2008). Retrieved October 1, 2015: http://www.cbirc.iastate.edu/research/thrust2/

Aderem, A. (2005). Systems biology: its practice and challenges. *Cell*, *121*(4), 511-513

Agbogbo, F. K., & Coward-Kelly, G. (2008). Cellulosic ethanol production using the naturally occurring xylose-fermenting yeast, Pichia stipitis. *Biotechnology letters*, *30*(9), 1515-1524.

Anesiadis, N., Cluett, W. R., & Mahadevan, R. (2008). Dynamic metabolic engineering for increasing bioprocess productivity. Metabolic engineering, 10(5), 255-266.

Antoniewicz, M. R. (2013). Dynamic metabolic flux analysis—tools for probing transient states of metabolic networks. *Current opinion in biotechnology*, *24*(6), 973-978.

Balagurunathan, B., Jonnalagadda, S., Tan, L., & Srinivasan, R. (2012). Reconstruction and analysis of a genome-scale metabolic model for Scheffersomyces stipitis. *Microb Cell Fact*, *11*(1), 27.

Balan, V. (2014). Current Challenges in Commercially Producing Biofuels from Lignocellulosic Biomass. *ISRN Biotechnology*, 1-31.

Balat, M., & Balat, H. (2009). Recent trends in global production and utilization of bio-ethanol fuel. *Applied Energy*, 2273-2282.

Balkema, A., & Pols, A. (2015). Biofuels: Sustainable Innovation or Gold Rush? Identifying Responsibilities for Biofuel Innovations. *Responsible Innovation 2*, 283-303.

Barabasi, A. L., & Oltvai, Z. N. (2004). Network biology: understanding the cell's functional organization. *Nature reviews genetics*, *5*(2), 101-113.

Becker, S. A., Feist, A. M., Mo, M. L., Hannum, G., Palsson, B. Ø., & Herrgard, M. J. (2007). Quantitative prediction of cellular metabolism with constraint-based models: the COBRA Toolbox. *Nature protocols*, *2*(3), 727-738.

Bell, S. L., & Palsson, B. Ø. (2005). Phenotype phase plane analysis using interior point methods. *Computers & chemical engineering*, *29*(3), 481-486.

Berezina, O. V., Zakharova, N. V., Brandt, A., Yarotsky, S. V., Schwarz, W. H., & Zverlov, V. (2010). Reconstructing the clostridial n-butanol metabolic pathway in Lactobacillus brevis. Applied microbiology and biotechnology, 87(2), 635-646.

Berg C, World bioethanol production, the distillery and bioethanol network. Available from: http://www.distill.com/worldethanolproduction.htm; 2001.

Bjerre, A., Olesen, A., Fernqvist, T., Plöger, A., & Schmidt, A. (1996). Pretreatment of wheat straw using combined wet oxidation and alkaline hydrolysis resulting in convertible cellulose and hemicellulose. *Biotechnol. Bioeng. Biotechnology and Bioengineering,* 568-577.

Bordbar, A., Monk, J. M., King, Z. A., & Palsson, B. O. (2014). Constraint-based models predict metabolic and associated cellular functions. *Nature Reviews Genetics, 15*(2), 107-120.

Bruinenberg, P. M., de Bot, P. H., van Dijken, J. P., & Scheffers, W. A. (1984). NADH-linked aldose reductase: the key to anaerobic alcoholic fermentation of xylose by yeasts. *Applied microbiology and biotechnology*, *19*(4), 256-260.

Borden, J. R., Jones, S. W., Indurthi, D., Chen, Y., & Papoutsakis, E. T. (2010). A genomic-library based discovery of a novel, possibly synthetic, acid-tolerance mechanism in Clostridium acetobutylicum involving non-coding RNAs and ribosomal RNA processing. *Metabolic engineering*, *12*(3), 268-281.

Bro, C., Regenberg, B., Förster, J., & Nielsen, J. (2006). In silico aided metabolic engineering of Saccharomyces cerevisiae for improved bioethanol production. *Metabolic engineering*, *8*(2), 102-111.

Bruinenberg, P. M., Van Dijken, J. P., & Scheffers, W. A. (1983). An enzymic analysis of NADPH production and consumption in Candida utilis. *Journal of General Microbiology*, *129*(4), 965-971.

Burgard, A. P., Pharkya, P., & Maranas, C. D. (2003). Optknock: a bilevel programming framework for identifying gene knockout strategies for microbial strain optimization. *Biotechnology and bioengineering*, *84*(6), 647-657.

Caspeta, L., Shoaie, S., Agren, R., Nookaew, I., & Nielsen, J. (2012). Genome-scale metabolic reconstructions of Pichia stipitis and Pichia pastoris and in silico evaluation of their potentials. *BMC systems biology*, *6*(1), 24.

Cherubini, F. (2010). The biorefinery concept: Using biomass instead of oil for producing energy and chemicals. *Energy Conversion and Management*, *51*(7), 1412–1421.

Cho, J. Y., & Jeffries, T. W. (1998). Pichia stipitis genes for alcohol dehydrogenase with fermentative and respiratory functions. *Applied and environmental microbiology*, *64*(4), 1350-1358.

Cho, J. Y., & Jeffries, T. W. (1999). Transcriptional control of ADH genes in the xylose-fermenting yeast Pichia stipitis. *Applied and environmental microbiology*, *65*(6), 2363-2368.

Collins K (2007). The new world of biofuels: implications for agriculture and energy. Energy Information Administration (United States Department of Energy) Energy Outlook, Modeling, and Data Conference. 28 March.

Covert, M. W., Schilling, C. H., Famili, I., Edwards, J. S., Goryanin, I. I., Selkov, E., & Palsson, B. O. (2001). Metabolic modeling of microbial strains in silico. *Trends in biochemical sciences*, *26*(3), 179-186.

Cvijovic, M., Olivares-Hernández, R., Agren, R., Dahr, N., Vongsangnak, W., Nookaew, I., & Nielsen, J. (2010). BioMet Toolbox: genome-wide analysis of metabolism. *Nucleic acids research*, *38*(suppl 2), W144-W149

Dahn, K. M., Davis, B. P., Pittman, P. E., Kenealy, W. R., & Jeffries, T. W. (1996, January). Increased xylose reductase activity in the xylose-fermenting yeast Pichia stipitis by overexpression of XYL1. In *Seventeenth Symposium on Biotechnology for Fuels and Chemicals* (pp. 267-276). Humana Press.

Damiani, A. L., He, Q. P., Jeffries, T. W., & Wang, J. (2015). Comprehensive evaluation of two genome-scale metabolic network models for Scheffersomyces stipitis. *Biotechnology and bioengineering*, *112*(6), 1250-1262.

Daran-Lapujade, P., Rossell, S., van Gulik, W. M., Luttik, M. A., de Groot, M. J., Slijper, M., & Bakker, B. M. (2007). The fluxes through glycolytic enzymes in Saccharomyces cerevisiae are predominantly regulated at posttranscriptional levels. *Proceedings of the National Academy of Sciences*, *104*(40), 15753-15758.

De Deken, R. H. (1966). The Crabtree effect and its relation to the petite mutation. *Journal of general microbiology*, *44*(2), 157-165

Du Preez, J. C., Van Driessel, B., & Prior, B. A. (1989). Effect of aerobiosis on fermentation and key enzyme levels during growth of Pichia stipitis, Candida shehatae and Candida tenuis on D-xylose. *Archives of microbiology*, *152*(2), 143-147.

Du Preez, J. C., Van Driessel, B., & Prior, B. A. (1989). Ethanol tolerance of Pichia stipitis and Candida shehatae strains in fed-batch cultures at controlled low dissolved oxygen levels. *Applied microbiology and biotechnology*, *30*(1), 53-58.

Duarte, N. C., Palsson, B. Ø., & Fu, P. (2004). Integrated analysis of metabolic phenotypes in Saccharomyces cerevisiae. *BMC genomics*, *5*(1), 63.

Edwards, J. S., & Palsson, B. O. (2000). Robustness analysis of the escherichiacoli metabolic network. *Biotechnology Progress*, *16*(6), 927-939.

Edwards, J. S., Ibarra, R. U., & Palsson, B. O. (2001). In silico predictions of Escherichia coli metabolic capabilities are consistent with experimental data. *Nature biotechnology*, *19*(2), 125-130.

Edwards, J. S., Covert, M., & Palsson, B. (2002a). Metabolic modelling of microbes: the flux-balance approach. *Environmental microbiology*, *4*(3), 133-140.

Edwards, J. S., Ramakrishna, R., & Palsson, B. O. (2002b). Characterizing the metabolic phenotype: a phenotype phase plane analysis. *Biotechnology and bioengineering*, *77*(1), 27-36.

Eisentraut, A. (2010). Sustainable Production of Second-Generation Biofuels. *IEA Energy Papers*.

Eliasson, A., Christensson, C., Wahlbom, C. F., & Hahn-Hägerdal, B. (2000). Anaerobic xylose fermentation by recombinant Saccharomyces cerevisiae carrying XYL1, XYL2, andXKS1 in mineral medium chemostat cultures. *Applied and Environmental Microbiology*, *66*(8), 3381-3386

Evans, M. (1997). *The economic impact of the demand for ethanol*. Lombard, Ill.: Midwestern Governors' Conference.

Famili, I., Mahadevan, R., & Palsson, B. O. (2005). k-Cone analysis: determining all candidate values for kinetic parameters on a network scale. *Biophysical journal*, *88*(3), 1616-1625

Feist, A. M., Herrgård, M. J., Thiele, I., Reed, J. L., & Palsson, B. Ø. (2009). Reconstruction of biochemical networks in microorganisms. *Nature Reviews Microbiology*, *7*(2), 129-143.

Feist, A. M., & Palsson, B. O. (2010). The biomass objective function. *Current opinion in microbiology*, *13*(3), 344-349.

Fell, D. A., & Small, J. R. (1986). Fat synthesis in adipose tissue. An examination of stoichiometric constraints. *Biochem. J*, *238*, 781-786.

Galitski, T. (2012, March 15). Reductionism Gives Way to Systems Biology | GEN Magazine Articles | GEN. Retrieved September 29, 2015.

Gallagher, R., Appenzeller, T., & Normile, D. (1999). Beyond reductionism. *Science*, *284*(5411), 79.

Gianchandani, E. P., Chavali, A. K., & Papin, J. A. (2010). The application of flux balance analysis in systems biology. *Wiley Interdisciplinary Reviews: Systems Biology and Medicine*, *2*(3), 372-382.

Gírio, F., Fonseca, C., Carvalheiro, F., Duarte, L., Marques, S., & Bogel-Łukasik, R. (2010). Hemicelluloses for fuel ethanol: A review. *Bioresource Technology*, 4775-4800.

Grootjen, D. R. J., Van der Lans, R. G. J. M., & Luyben, K. C. A. (1990). Effects of the aeration rate on the fermentation of glucose and xylose by Pichia stipitis CBS 5773. *Enzyme and microbial technology*, *12*(1), 20-23.

Grootjen, D. R. J., van Der Lans, R. G. J. M., & Luyben, K. C. A. (1991). Conversion of glucose/xylose mixtures by Pichia stipitis under oxygen-limited conditions. *Enzyme and microbial technology*, *13*(8), 648-654.

Gstaiger, M., & Aebersold, R. (2009). Applying mass spectrometry-based proteomics to genetics, genomics and network biology. *Nature Reviews Genetics*, *10*(9), 617-627

Gudmundsson, S., & Thiele, I. (2010). Computationally efficient flux variability analysis. *BMC bioinformatics*, *11*(1), 489.

Gupta, A., & Verma, J. P. (2015). Sustainable bio-ethanol production from agro-residues: A review. *Renewable and Sustainable Energy Reviews*, *41*, 550–567.

Ideker, T., Galitski, T., & Hood, L. (2001). A new approach to decoding life: systems biology. *Annual review of genomics and human genetics*, *2*(1), 343-372.

Hahn-Hägerdal, B., & Pamment, N. (2004). Special session A microbial pentose metabolism. Applied biochemistry and biotechnology, 116(1), 1207-1209.

Hahn-Hägerdal, B., Karhumaa, K., Fonseca, C., Spencer-Martins, I., & Gorwa-Grauslund, M. F. (2007). Towards industrial pentose-fermenting yeast strains. *Applied microbiology and biotechnology*, *74*(5), 937-953.

Hakeem, K. (2014). *Biomass and bioenergy: Applications*.

Hanly, T. J., & Henson, M. A. (2011). Dynamic flux balance modeling of microbial co-cultures for efficient batch fermentation of glucose and xylose mixtures. *Biotechnology and bioengineering*, *108*(2), 376-385.

Harhangi, H. R., Akhmanova, A. S., Emmens, R., van der Drift, C., de Laat, W. T., van Dijken, J. P., & den Camp, H. J. O. (2003). Xylose metabolism in the anaerobic fungus Piromyces sp. strain E2 follows the bacterial pathway. *Archives of Microbiology*, *180*(2), 134-141.

Hearst, M. A., Dumais, S. T., Osman, E., Platt, J., & Scholkopf, B. (1998). Support vector machines. Intelligent Systems and their Applications, IEEE, 13(4), 18-28.

Henry, C. S., DeJongh, M., Best, A. A., Frybarger, P. M., Linsay, B., & Stevens, R. L. (2010). High-throughput generation, optimization and analysis of genome-scale metabolic models. Nature biotechnology, 28(9), 977-982.

Heux, S., Cachon, R., & Dequin, S. (2006). Cofactor engineering in Saccharomyces cerevisiae: expression of a H 2 O-forming NADH oxidase and impact on redox metabolism. *Metabolic engineering*, *8*(4), 303-314.

Hjersted, J. L., & Henson, M. A. (2009). Steady-state and dynamic flux balance analysis of ethanol production by Saccharomyces cerevisiae. *IET systems biology*, *3*(3), 167-179.

Hou, J., Lages, N. F., Oldiges, M., & Vemuri, G. N. (2009). Metabolic impact of redox cofactor perturbations in Saccharomyces cerevisiae. *Metabolic engineering*, *11*(4), 253-261.

Hufbauer, G., & Charnovitz, S. (2009). *Global warming and the world trading system* (pp. 6-8). Washington, D.C.: Peterson Institute for International Economics.

Jamshidi, N., & Palsson, B. Ø. (2008). Formulating genome-scale kinetic models in the post-genome era. *Molecular systems biology*, *4*(1), 171.

Jeffries, T. W., & Shi, N. Q. (1999). Genetic engineering for improved xylose fermentation by yeasts. In *Recent progress in bioconversion of lignocellulosics* (pp. 117-161). Springer Berlin Heidelberg.

Jeffries, T. W. (2006). Engineering yeasts for xylose metabolism. *Current opinion in biotechnology*, *17*(3), 320-326.

Jeffries, T. W., Grigoriev, I. V., Grimwood, J., Laplaza, J. M., Aerts, A., Salamov, A., & Richardson, P. M. (2007). Genome sequence of the lignocellulose-bioconverting and xylose-fermenting yeast Pichia stipitis. *Nature biotechnology*, *25*(3), 319-326.

Jeffries, T. W., & Van Vleet, J. R. H. (2009). Pichia stipitis genomics, transcriptomics, and gene clusters. FEMS yeast research, 9(6), 793-807.

Jeppsson, M., Johansson, B., Hahn-Hägerdal, B., & Gorwa-Grauslund, M. F. (2002). Reduced oxidative pentose phosphate pathway flux in recombinant xylose-utilizing Saccharomyces cerevisiae strains improves the ethanol yield from xylose. *Applied and environmental microbiology*, *68*(4), 1604-1609.

Joachimsthal, E., & Rogers, P. (2000). Characterization of a High-Productivity Recombinant Strain of Zymomonas mobilis for Ethanol Production from Glucose/Xylose Mixtures. *Twenty-First Symposium on Biotechnology for Fuels and Chemicals*, 343-356.

Johansson, B., & Hahn-Hägerdal, B. (2002). The non-oxidative pentose phosphate pathway controls the fermentation rate of xylulose but not of xylose in Saccharomyces cerevisiae TMB3001. *FEMS yeast research*, *2*(3), 277-282

Joseph-Horne, T., & Hollomon, D. W. (2000). Functional diversity within the mitochondrial electron transport chain of plant pathogenic fungi. *Pest Management Science*, *56*(1), 24-30.

Kanehisa, M., & Goto, S. (2000). KEGG: kyoto encyclopedia of genes and genomes. Nucleic acids research, 28(1), 27-30.

Karhumaa, K., Hahn-Hägerdal, B., & Gorwa-Grauslund, M. F. (2005). Investigation of limiting metabolic steps in the utilization of xylose by recombinant Saccharomyces cerevisiae using metabolic engineering. *Yeast*, *22*(5), 359-368

Karhumaa, K., Sanchez, R. G., Hahn-Hägerdal, B., & Gorwa-Grauslund, M. F. (2007). Comparison of the xylose reductase-xylitol dehydrogenase and the xylose isomerase pathways for xylose fermentation by recombinant Saccharomyces cerevisiae. *Microbial Cell Factories*, *6*(1), 5.

Karp, P. D., Riley, M., Paley, S. M., & Pellegrini-Toole, A. (2002). The metacyc database. Nucleic acids research, 30(1), 59-61.

Karr, J. R., Sanghvi, J. C., Macklin, D. N., Gutschow, M. V., Jacobs, J. M., Bolival, B., & Covert, M. W. (2012). A whole-cell computational model predicts phenotype from genotype. *Cell*, *150*(2), 389-401.

Katahira, S., Ito, M., Takema, H., Fujita, Y., Tanino, T., Tanaka, T., ... & Kondo, A. (2008). Improvement of ethanol productivity during xylose and glucose co-fermentation by xylose-assimilating *S. cerevisiae* via expression of glucose transporter Sut1. *Enzyme and Microbial Technology*, *43*(2), 115-119.

Kauffman, K. J., Prakash, P., & Edwards, J. S. (2003). Advances in flux balance analysis. *Current opinion in biotechnology*, *14*(5), 491-496.

Kim, Y., Ingram, L., & Shanmugam, K. (2007). Construction of an Escherichia coli K-12 Mutant for Homoethanologenic Fermentation of Glucose or Xylose without Foreign Genes. *APPLIED AND ENVIRONMENTAL MICROBIOLOGY*, 1766-1771.

Kim, T. Y., Sohn, S. B., Kim, Y. B., Kim, W. J., & Lee, S. Y. (2012). Recent advances in reconstruction and applications of genome-scale metabolic models. *Current opinion in biotechnology*, *23*(4), 617-623.

Kim, M. H. (2015). *New Experimental and Modeling Approaches to Study the Dynamics of Xylose Fermenta-tion with Scheffersomyces stipitis* (Doctoral dissertation, Auburn University).

King, Z. A., Lloyd, C. J., Feist, A. M., & Palsson, B. O. (2015). Next-generation genome-scale models for metabolic engineering. *Current opinion in biotechnology*, *35*, 23-29.

Kitano, H. (2002). Systems Biology: A Brief Overview. *Science,* 1662-1664.

Klamt, S., & Stelling, J. (2003). Two approaches for metabolic pathway analysis?. *Trends in biotechnology*, *21*(2), 64-69.

Klapa, M. I., & Stephanopoulos, G. (2000). Metabolic flux analysis. In *Bioreaction Engineering* (pp. 106-124). Springer Berlin Heidelberg.

Klinner, U., Fluthgraf, S., Freese, S., & Passoth, V. (2005). Aerobic induction of respiro-fermentative growth by decreasing oxygen tensions in the respiratory yeast Pichia stipitis. *Applied microbiology and biotechnology*, *67*(2), 247-253.

Kompala, D. S., Ramkrishna, D., & Tsao, G. T. (1984). Cybernetic modeling of microbial growth on multiple substrates. *Biotechnology and bioengineering*, *26*(11), 1272-1281.

Knorr, A. L., Jain, R., & Srivastava, R. (2007). Bayesian-based selection of metabolic objective functions. *Bioinformatics*, *23*(3), 351-357.

Kötter, P., & Ciriacy, M. (1993). Xylose fermentation by Saccharomyces cerevisiae. *Applied microbiology and biotechnology*, *38*(6), 776-783.

Kreutz, C., & Timmer, J. (2009). Systems biology: experimental design. *FEBS journal*, *276*(4), 923-942.

Krömer, J., Quek, L. E., & Nielsen, L. (2009). 13C-Fluxomics: a tool for measuring metabolic phenotypes. *Aust Biochem*, *40*(3), 17-20.

Krömer, J. O., Nielsen, L. K., & Blank, L. M. (Eds.). (2014). *Metabolic Flux Analysis: Methods and Protocols*. Humana Press.

Kuyper, M., Hartog, M. M., Toirkens, M. J., Almering, M. J., Winkler, A. A., Dijken, J. P., & Pronk, J. T. (2005). Metabolic engineering of a xylose-isomerase-expressing Saccharomyces cerevisiae strain for rapid anaerobic xylose fermentation. *FEMS yeast research*, *5*(4-5), 399-409.

Llaneras, F., & Picó, J. (2010). Which metabolic pathways generate and characterize the flux space? A comparison among elementary modes, extreme pathways and minimal generators. *BioMed Research International*, *2010*.

Lee, J. M., Gianchandani, E. P., & Papin, J. A. (2006). Flux balance analysis in the era of metabolomics. *Briefings in bioinformatics*, *7*(2), 140-150.

Lee, K. Y., Park, J. M., Kim, T. Y., Yun, H., & Lee, S. Y. (2010). The genome-scale metabolic network analysis of Zymomonas mobilis ZM4 explains physiological features and suggests ethanol and succinic acid production strategies. *Microbial cell factories*, *9*(1), 94.

Lee, J. Y., Yang, K. S., Jang, S. A., Sung, B. H., & Kim, S. C. (2011). Engineering butanol-tolerance in escherichia coli with artificial transcription factor libraries. *Biotechnology and bioengineering*, *108*(4), 742-749.

Lewis, N. E., Nagarajan, H., & Palsson, B. O. (2012). Constraining the metabolic genotype–phenotype relationship using a phylogeny of in silico methods. *Nature Reviews Microbiology*, *10*(4), 291-305.

Li, P. Y. (2012). In silico metabolic network reconstruction of Scheffersomyces stipitis (Doctoral dissertation)

Liang, M., Damiani, A., He, Q. P., & Wang, J. (2013). Elucidating xylose metabolism of Scheffersomyces stipitis for lignocellulosic ethanol production. *ACS Sustainable Chemistry & Engineering*, *2*(1), 38-48.

Licht, F.O., (2006). World Ethanol Market: The Outlook to 2015, Tunbridge Wells, Agra Europe Special Report, UK.

Licht, F. O. (2013). Renewable fuels association. Ethanol industry outlook 2008–2013 reports.

Liu, L., Agren, R., Bordel, S., & Nielsen, J. (2010). Use of genome-scale metabolic models for understanding microbial physiology. *FEBS letters*, *584*(12), 2556-2564.

Liu, T., Zou, W., Liu, L., & Chen, J. (2012). A constraint-based model of Scheffersomyces stipitis for improved ethanol production. *Biotechnol Biofuels*, *5*(1), 72.

Lütke-Eversloh, T., & Bahl, H. (2011). Metabolic engineering of Clostridium acetobutylicum: recent advances to improve butanol production. *Current opinion in biotechnology*, *22*(5), 634-647.

Mahadevan, R., & Schilling, C. H. (2003). The effects of alternate optimal solutions in constraint-based genome-scale metabolic models. *Metabolic engineering*, *5*(4), 264-276.

Mahadevan, R., & Henson, M. A. (2007). Genome-scale analysis of Saccharomyces cerevisiae metabolism and ethanol production in fed-batch culture. Biotechnology and bioengineering, 97(5), 1190-1204

Mansfield, Betty Kay et al. (2006). Breaking the Biological barriers to Cellulosic Ethanol: A Joint Research Agenda. Tech. rep. Germantown, MD, USA: US DOE

Margeot, A., Hahn-Hagerdal, B., Edlund, M., Slade, R., & Monot, F. (2009). New improvements for lignocellulosic ethanol. *Current opinion in biotechnology*, *20*(3), 372-380.

Marioni, J. C., Mason, C. E., Mane, S. M., Stephens, M., & Gilad, Y. (2008). RNA-seq: an assessment of technical reproducibility and comparison with gene expression arrays. *Genome research*, *18*(9), 1509-1517.

Marris, E. (2006). Sugar cane and ethanol: Drink the best and drive the rest. *Nature News@nature*, 670-672.

Martín, C., Galbe, M., Wahlbom, C. F., Hahn-Hägerdal, B., & Jönsson, L. J. (2002). Ethanol production from enzymatic hydrolysates of sugarcane bagasse using recombinant xylose-utilising Saccharomyces cerevisiae. *Enzyme and Microbial Technology*, *31*(3), 274-282.

Matsushika, A., Watanabe, S., Kodaki, T., Makino, K., Inoue, H., Murakami, K., & Sawayama, S. (2008). Expression of protein engineered NADP+-dependent xylitol dehydrogenase increases ethanol production from xylose in recombinant Saccharomyces cerevisiae. *Applied microbiology and biotechnology*, *81*(2), 243-255.

Matsushika, A., Inoue, H., Kodaki, T., & Sawayama, S. (2009a). Ethanol production from xylose in engineered Saccharomyces cerevisiae strains: current state and perspectives. *Applied Microbiology and Biotechnology*, *84*(1), 37-53.

Matsushika, A., Inoue, H., Murakami, K., Takimura, O., & Sawayama, S. (2009b). Bioethanol production performance of five recombinant strains of laboratory and industrial xylose-fermenting Saccharomyces cerevisiae. *Bioresource Technology*, *100*(8), 2392-2398.

Mavrovouniotis, M., & Stephanopoulos, G. (1992). Synthesis of biochemical production routes. Computers & chemical engineering, 16(6), 605-619.

Mckendry, P. (2002). Energy production from biomass (part 2): Conversion technologies. *Bioresource Technology*, 47-54.

Mockler, T. C., & Ecker, J. R. (2005). Applications of DNA tiling arrays for whole-genome analysis. *Genomics*, *85*(1), 1-15.

Montagud, A., Navarro, E., de Córdoba, P. F., Urchueguía, J. F., & Patil, K. R. (2010). Reconstruction and analysis of genome-scale metabolic model of a photosynthetic bacterium. *BMC systems biology*, *4*(1), 156.

Mousdale, D. (2008). *Biofuels: Biotechnology, chemistry, and sustainable development*. Boca Raton: CRC Press.

Naik, S., Goud, V., Rout, P., & Dalai, A. (2009). Production of first and second generation biofuels: A comprehensive review. *Renewable and Sustainable Energy Reviews*, 578-597.

Nemutlu, E., Zhang, S., Juranic, N. O., Terzic, A., Macura, S., & Dzeja, P. (2012). 18 O-assisted dynamic metabolomics for individualized diagnostics and treatment of human diseases. *Croatian medical journal*, *53*(6), 529-534.

Oberhardt, M. A., Palsson, B. Ø., & Papin, J. A. (2009). Applications of genome-scale metabolic reconstructions. *Molecular systems biology*, *5*(1), 320

Ohgren, K., Bura, R., Saddler, J., & Zacchi, G. (2007). Effect of hemicellulose and lignin removal on enzymatic hydrolysis of steam pretreated corn stover. *Bioresource Technology*, 2503-2510.

Orth, J. D., Thiele, I., & Palsson, B. Ø. (2010a). What is flux balance analysis?. *Nature biotechnology*, *28*(3), 245-248.

Orth J.D., Fleming, R., & Palsson, B. Ø. (2010b) *Reconstruction and Use of Microbial Metabolic Networks: the Core* Escherichia coli *Metabolic Model as an Educational Guide* by Orth, Fleming, and Palsson

Orth, J. D., Conrad, T. M., Na, J., Lerman, J. A., Nam, H., Feist, A. M., & Palsson, B. Ø. (2011). A comprehensive genome-scale reconstruction of Escherichia coli metabolism—2011. *Molecular systems biology*, *7*(1), 535.

Österlund, T., Nookaew, I., & Nielsen, J. (2012). Fifteen years of large scale metabolic modeling of yeast: developments and impacts. *Biotechnology advances*, *30*(5), 979-988.

Paley, S. M., Latendresse, M., & Karp, P. D. (2012). Regulatory network operations in the pathway tools software. *BMC bioinformatics*, *13*(1), 243

Palsson, B. (2000). The challenges of in silico biology. *Nature biotechnology*, *18*(11), 1147-1150.

Passoth, V., Zimmermann, M., & Klinner, U. (1996, January). Peculiarities of the regulation of fermentation and respiration in the Crabtree-negative, xylose-fermenting yeast Pichia stipitis. In *Seventeenth Symposium on Biotechnology for Fuels and Chemicals* (pp. 201-212). Humana Press.

Patil, K. R., Rocha, I., Förster, J., & Nielsen, J. (2005). Evolutionary programming as a platform for in silico metabolic engineering. *BMC bioinformatics*, *6*(1), 308.

Patiño, C. E. H., Jaime-Muñoz, G., & Resendis-Antonio, O. (2012). Systems biology of cancer: moving toward the integrative study of the metabolic alterations in cancer cells. *Frontiers in physiology*, *3*.

Pharkya, P., Burgard, A. P., & Maranas, C. D. (2004). OptStrain: a computational framework for redesign of microbial production systems. Genome research, 14(11), 2367-2376.

Pramanik, J., & Keasling, J. D. (1997). Stoichiometric model of Escherichia coli metabolism: incorporation of growth-rate dependent biomass composition and mechanistic energy requirements. *Biotechnology and bioengineering*, *56*(4), 398-421.

Price, N. D., Reed, J. L., & Palsson, B. Ø. (2004). Genome-scale models of microbial cells: evaluating the consequences of constraints. *Nature Reviews Microbiology*, *2*(11), 886-897.

Ramakrishna, R., Edwards, J. S., McCulloch, A., & Palsson, B. O. (2001). Flux-balance analysis of mitochondrial energy metabolism: consequences of systemic stoichiometric constraints. American Journal of Physiology-Regulatory, Integrative and Comparative Physiology, 280(3), R695-R704.

Raman, K., & Chandra, N. (2009). Flux balance analysis of biological systems: applications and challenges. *Briefings in bioinformatics*, *10*(4), 435-449.

Ranganathan, S., Suthers, P. F., & Maranas, C. D. (2010). OptForce: an optimization procedure for identifying all genetic manipulations leading to targeted overproductions. PLoS Comput Biol, 6(4), e1000744.

Reed, J. L. (2012). Shrinking the metabolic solution space using experimental datasets. *PLoS Comput Biol*, *8*(8), e1002662.

Rizzi, M., Baltes, M., Theobald, U., & Reuss, M. (1997). In vivo analysis of metabolic dynamics in Saccharomyces cerevisiae: II. mathematical model. Biotechnology and bioengineering, 55(4), 592-608

Roca, C., Nielsen, J., & Olsson, L. (2003). Metabolic engineering of ammonium assimilation in xylose-fermenting Saccharomyces cerevisiae improves ethanol production. *Applied and environmental microbiology*, *69*(8), 4732-4736.

Rocha, I., Maia, P., Rocha, M., & Ferreira, E. C. (2008). OptGene: a framework for in silico metabolic engineering.

Sabido, E., Selevsek, N., & Aebersold, R. (2012). Mass spectrometry-based proteomics for systems biology. *Current opinion in biotechnology*, *23*(4), 591-597.

Sanford, K., Soucaille, P., Whited, G., & Chotani, G. (2002). Genomics to fluxomics and physiomics—pathway engineering. *Current opinion in microbiology*, *5*(3), 318-322.

Sauer, U. (2006). Metabolic networks in motion: 13C-based flux analysis. *Molecular systems biology*, *2*(1), 62.

Sauer, U., Heinemann, M., & Zamboni, N. (2007). Getting closer to the whole picture. *Science(Washington)*, *316*(5824), 550-551.

Savinell, J. M., & Palsson, B. O. (1992). Network analysis of intermediary metabolism using linear optimization. I. Development of mathematical formalism. *Journal of theoretical biology*, *154*(4), 421-454.

Scalbert, A., Brennan, L., Fiehn, O., Hankemeier, T., Kristal, B. S., van Ommen, B., ... & Wopereis, S. (2009). Mass-spectrometry-based metabolomics: limitations and recommendations for future progress with particular focus on nutrition research. *Metabolomics*, *5*(4), 435-458.

Schellenberger, J., Que, R., Fleming, R. M., Thiele, I., Orth, J. D., Feist, A. M., ... & Palsson, B. Ø. (2011). Quantitative prediction of cellular metabolism with constraint-based models: the COBRA Toolbox v2. 0. *Nature protocols*, *6*(9), 1290-1307.

Schilling, C. H., Schuster, S., Palsson, B. O., & Heinrich, R. (1999). Metabolic pathway analysis: basic concepts and scientific applications in the post-genomic era. Biotechnology progress, 15(3), 296-303

Schilling, C. H., & Palsson, B. Ø. (2000). Assessment of the metabolic capabilities of Haemophilus influenzae Rd through a genome-scale pathway analysis. Journal of theoretical biology, 203(3), 249-283

Scholkopft, B., & Mullert, K. R. (1999). Fisher discriminant analysis with kernels. *Neural networks for signal processing IX*, *1*, 1

Schomburg, I., Chang, A., & Schomburg, D. (2002). BRENDA, enzyme data and metabolic information. *Nucleic acids research*, *30*(1), 47-49.

Schuetz, R., Kuepfer, L., & Sauer, U. (2007). Systematic evaluation of objective functions for predicting intracellular fluxes in Escherichia coli. Molecular systems biology, 3(1), 119.

Schuster, S., Dandekar, T., & Fell, D. A. (1999). Detection of elementary flux modes in biochemical networks: a promising tool for pathway analysis and metabolic engineering. *Trends in biotechnology*, *17*(2), 53-60.

Sedlak, M., & Ho, N. (2004). Characterization of the effectiveness of hexose transporters for transporting xylose during glucose and xylose co-fermentation by a recombinantSaccharomyces yeast. *Yeast*, 671-684.

Segrè, D., Vitkup, D., & Church, G. M. (2002). Analysis of optimality in natural and perturbed metabolic networks. *Proceedings of the National Academy of Sciences*, *99*(23), 15112-15117.

Segrè, D., Zucker, J., Katz, J., Lin, X., D'Haeseleer, P., Rindone, W. P., ... & Church, G. M. (2003). From annotated genomes to metabolic flux models and kinetic parameter fitting. *OMICS A Journal of Integrative Biology*, *7*(3), 301-316.

Service, R. (2007). CELLULOSIC ETHANOL: Biofuel Researchers Prepare to Reap a New Harvest. *Science*, 1488-1491.

Shi, N. Q., & Jeffries, T. W. (1998). Anaerobic growth and improved fermentation of Pichia stipitis bearing a URA1 gene from Saccharomyces cerevisiae. *Applied microbiology and biotechnology*, *50*(3), 339-345

Shi, N. Q., Cruz, J., Sherman, F., & Jeffries, T. W. (2002). SHAM-sensitive alternative respiration in the xylose-metabolizing yeast Pichia stipitis. *Yeast*, *19*(14), 1203-1220.

Shlomi, T., Berkman, O., & Ruppin, E. (2005). Regulatory on/off minimization of metabolic flux changes after genetic perturbations. Proceedings of the National Academy of Sciences of the United States of America, 102(21), 7695-7700

Sindhu, R., Binod, P., & Pandey, A. (n.d.). Biological pretreatment of lignocellulosic biomass – An overview. *Bioresource Technology*.

Skoog, K., & Hahn-Hägerdal, B. (1990). Effect of oxygenation on xylose fermentation by Pichia stipitis. *Applied and environmental microbiology*, *56*(11), 3389-3394.

Skoog, K., Hahn-Hägerdal, B., Degn, H., Jacobsen, J. P., & Jacobsen, H. S. (1992). Ethanol reassimilation and ethanol tolerance in Pichia stipitis CBS 6054 as studied by 13C nuclear magnetic resonance spectroscopy. *Applied and environmental microbiology*, *58*(8), 2552-2558.

Slininger, P. J., Bothast, R. J., Okos, M. R., & Ladisch, M. R. (1985). Comparative evaluation of ethanol production by xylose-fermenting yeasts presented high xylose concentrations. Biotechnology letters, 7(6), 431-436.

Slininger, P. J., Branstrator, L. E., Bothast, R. J., Okos, M. R., & Ladisch, M. R. (1991). Growth, death, and oxygen uptake kinetics of Pichia stipitis on xylose. *Biotechnology and bioengineering*, *37*(10), 973-980.

Slininger, P. J., Dien, B. S., Gorsich, S. W., & Liu, Z. L. (2006). Nitrogen source and mineral optimization enhance D-xylose conversion to ethanol by the yeast Pichia stipitis NRRL Y-7124. *Applied microbiology and biotechnology*, *72*(6), 1285-1296.

Slininger, P. J., Thompson, S. R., Weber, S., Liu, Z. L., & Moon, J. (2011). Repression of xylose-specific enzymes by ethanol in Scheffersomyces (Pichia) stipitis and utility of repitching xylose-grown populations to eliminate diauxic lag. Biotechnology and bioengineering, 108(8), 1801-1815.

Smallbone, K., Simeonidis, E., Swainston, N., & Mendes, P. (2010). Towards a genome-scale kinetic model of cellular metabolism. *BMC Systems Biology*, *4*(1), 6.

Sobrino, F., & Monroy, C. (2010). Critical analysis of the European Union directive which regulates the use of biofuels: An approach to the Spanish case. *Renewable and Sustainable Energy Reviews*, 2675-2681.

Sonderegger, M., Jeppsson, M., Hahn-Hägerdal, B., & Sauer, U. (2004). Molecular basis for anaerobic growth of Saccharomyces cerevisiae on xylose, investigated by global gene expression and metabolic flux analysis. *Applied and environmental microbiology*, *70*(4), 2307-2317.

Spencer, T. E., Sandra, O., & Wolf, E. (2008). Genes involved in conceptus–endometrial interactions in ruminants: insights from reductionism and thoughts on holistic approaches. *Reproduction*, *135*(2), 165-179

Stelling, J. (2004). Mathematical models in microbial systems biology. *Current opinion in microbiology*, *7*(5), 513-518.

Stephanopoulos, G., Aristidou, A. A., & Nielsen, J. (1998). *Metabolic engineering: principles and methodologies*. Academic press.

Takuma, S., Nakashima, N., Tantirungkij, M., Kinoshita, S., Okada, H., Sew, T., & Yoshida, T. (1991). Isolation of xylose reductase gene ofPichia stipitis and its expression inSaccharomyces cerevisiae. *Applied biochemistry and biotechnology*, *28*(1), 327-340.

Tang, H., & Wang, Y. (2005). Metabonomics: a revolution in progress. *Sheng wu hua xue yu sheng wu wu li jin zhan*, *33*(5), 401-417.

Teusink, B., Passarge, J., Reijenga, C. A., Esgalhado, E., van der Weijden, C. C., Schepper, M., & Snoep, J. L. (2000). Can yeast glycolysis be understood in terms of in vitro kinetics of the constituent enzymes? Testing biochemistry. *European Journal of Biochemistry*, *267*(17), 5313-5329.

Thiele, I., & Palsson, B. Ø. (2010). A protocol for generating a high-quality genome-scale metabolic reconstruction. *Nature protocols*, *5*(1), 93-121.

Trinh, C. T., Wlaschin, A., & Srienc, F. (2009). Elementary mode analysis: a useful metabolic pathway analysis tool for characterizing cellular metabolism. *Applied microbiology and biotechnology*, *81*(5), 813-826.

Van Dijken, J. P., & Scheffers, W. A. (1986). Redox balances in the metabolism of sugars by yeasts. *FEMS Microbiol Rev*, *32*(3-4), 199-224.

Van Maris, A. J., Winkler, A. A., Kuyper, M., De Laat, W. T., Van Dijken, J. P., & Pronk, J. T. (2007). Development of efficient xylose fermentation in Saccharomyces cerevisiae: xylose isomerase as a key component. In *Biofuels* (pp. 179-204). Springer Berlin Heidelberg.

Van Urk, H., Voll, W. L., Scheffers, W. A., & Van Dijken, J. P. (1990). Transient-state analysis of metabolic fluxes in Crabtree-positive and Crabtree-negative yeasts. *Applied and environmental microbiology*, *56*(1), 281-287.

Varma, A., Boesch, B. W., & Palsson, B. O. (1993). Stoichiometric interpretation of Escherichia coli glucose catabolism under various oxygenation rates. *Applied and environmental microbiology*, *59*(8), 2465-2473.

Varma, A., & Palsson, B. O. (1994). Metabolic Flux Balancing: Basic Concepts, Scientific and Practical Use. Bio/technology, 12.

Vaseghi, S., Baumeister, A., Rizzi, M., & Reuss, M. (1999). In VivoDynamics of the Pentose Phosphate Pathway inSaccharomyces cerevisiae. *Metabolic engineering*, *1*(2), 128-140.

Verho, R., Londesborough, J., Penttilä, M., & Richard, P. (2003). Engineering redox cofactor regeneration for improved pentose fermentation in Saccharomyces cerevisiae. *Applied and environmental microbiology*, *69*(10), 5892-5897.

Vo, T. D., Greenberg, H. J., & Palsson, B. O. (2004). Reconstruction and functional characterization of the human mitochondrial metabolic network based on proteomic and biochemical data. *Journal of Biological Chemistry*.

Walfridsson, M., Hallborn, J., Penttilä, M. E. R. J. A., Keränen, S. I. R. K. K. A., & Hahn-Hägerdal, B. (1995). Xylose-metabolizing Saccharomyces cerevisiae strains overexpressing the TKL1 and TAL1 genes encoding the pentose phosphate pathway enzymes transketolase and transaldolase. Applied and environmental microbiology, 61(12), 4184-4190.

Wandrey, C. (2004). Biochemical reaction engineering for redox reactions. *The Chemical Record*, *4*(4), 254-265.

Wang, Z., Gerstein, M., & Snyder, M. (2009). RNA-Seq: a revolutionary tool for transcriptomics. *Nature Reviews Genetics*, *10*(1), 57-63.

Watanabe, S., Saleh, A. A., Pack, S. P., Annaluru, N., Kodaki, T., & Makino, K. (2007). Ethanol production from xylose by recombinant Saccharomyces cerevisiae expressing protein engineered NADP+-dependent xylitol dehydrogenase. *Journal of biotechnology*, *130*(3), 316-319.

Wiechert, W. (2001). 13 C metabolic flux analysis. *Metabolic engineering*, *3*(3), 195-206.

Wold, H. (1985). Partial least squares. *Encyclopedia of statistical sciences*.

Wold, S., Esbensen, K., & Geladi, P. (1987). Principal component analysis. *Chemometrics and intelligent laboratory systems*, *2*(1), 37-52.

Wright, B. E., & Kelly, P. J. (1981). Kinetic models of metabolism in intact cells, tissues, and organisms. *Current topics in cellular regulation*, *19*, 103.

Yablochkova, E. N., Bolotnikova, O. I., Mikhailova, N. P., Nemova, N. N., & Ginak, A. I. (2004). The activity of key enzymes in xylose-assimilating yeasts at different rates of oxygen transfer to the fermentation medium. *Microbiology*, *73*(2), 129-133.

Young, J. D., Henne, K. L., Morgan, J. A., Konopka, A. E., & Ramkrishna, D. (2008). Integrating cybernetic modeling with pathway analysis provides a dynamic, systems-level description of metabolic control. *Biotechnology and bioengineering*, *100*(3), 542-559.

Zhao, X., Kong, X., Hua, Y., Feng, B., & Zhao, Z. (2008). Medium optimization for lipid production through co-fermentation of glucose and xylose by the oleaginous yeastLipomyces starkeyi. *European Journal of Lipid Science and Technology Eur. J. Lipid Sci. Technol.*, 405-412.

Zomorrodi, A. R., Suthers, P. F., Ranganathan, S., & Maranas, C. D. (2012). Mathematical optimization applications in metabolic networks. *Metabolic engineering*, *14*(6), 672-686.

Appendices

A1 Overall comparison of iSS884 & iBB814

Table A1. Breadown of iSS884 and iBB814

Specification	iSS884	iBB814
Approach	Semi-Automatic	Manual
Reactions	1332	1371
Cytosol	824	757
Mitochondria	207	125
Peroxisome	60	N/A
Transport	239	489
Metabolites	922	644
Genes	884	814
Percent of Genome (%)	15.1	14.4
Compartment	Cytosol, Exchange, Mitochondria, Peroxisome	Cytosol, Exchange Mitochondria

A2 Fatty Acid Biosynthesis

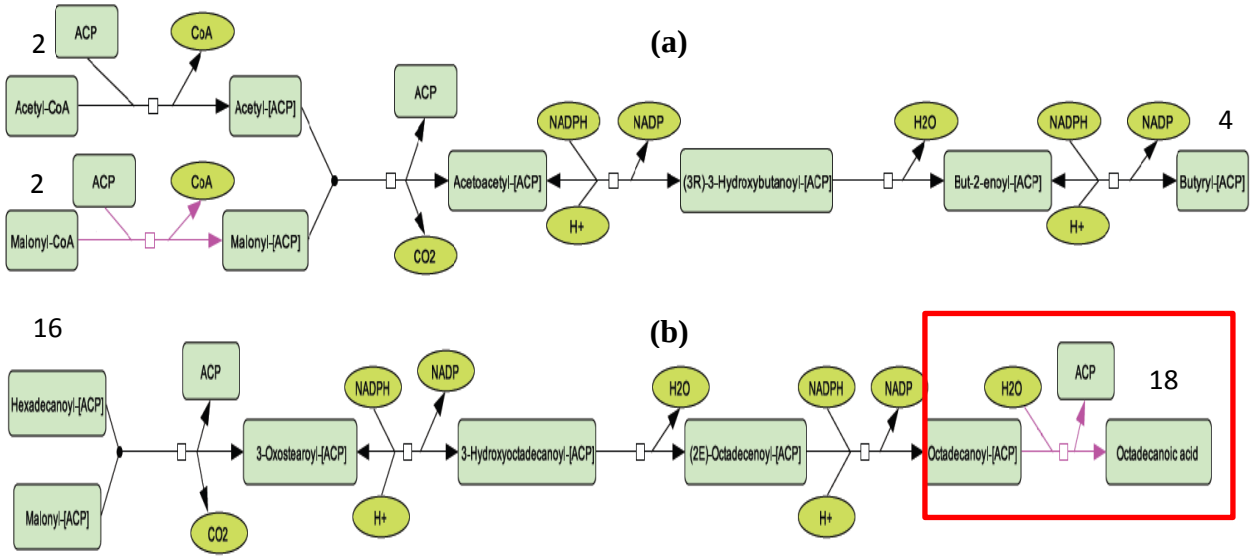

Figure A2.1 Fatty acid biosynthesis for iSS884: (a) saturated fatty acids, (b) end product of a saturated fatty acid

The saturated fatty acid biosynthesis for iSS884 is illustrated in Figure A2.1. For the synthesis of saturated fatty acid, each time the length of the fatty acid chain increases by 2 as shown in Figure A2.1 (a), where two examples are given, one is the production of butyryl-[ACP] (4 carbons) from acetyl-CoA (2 carbons), and the other is the production of ocetadecanoyl-[ACP] and octadecanoic acid (both with 18 carbons) from hexadecanoyl-[ACP] (with 16 carbons). It is worth noting that 8 synthesis reactions exist in iSS884 to produce ACP bounded fatty acids with length 4 up to 18, and they exist both in cytosol and mitochondrial . However, there are only 4 hydrolysis reactions that remove the ACP group to produce fatty acids (as shown in the red frame in Figure A2.1 (b)) for carbon length 12 up to 18. This means that the saturated fatty acid

with carbon chain length less than 12 are not available (as they are all ACP bounded) in the cell. In iBB814, production of saturated, unsaturated, and odd chain length fatty acids happen. Below we examine fatty acid synthesis in detail. Figure A2.2 (a) shows how decanoate (10 carbons) is produced from octanoate (8 carbons). At the same time, a similar reaction exists, as shown in Figure A2.2 (b), to produce decanoyl-CoA from octanoyl-CoA. Reactions similar to these two exist in cytosol to synthesize fatty acids with length from 4 up to 26. Note that the reactions in iBB814 are somewhat simplified, as they skip all the intermediate steps and the intermediate metabolites that all involved in iSS884, and all of the synthesis reactions in iBB814 have the hydrolysis step, therefore no ACP bounded fatty acids are produced in cytosol. Instead, ACP bounded fatty acids are produced in the mitochondria only, as shown in Figure A2.2 (c), where decanoyl-[ACP] is produced from octanoyl-[ACP]. The ACP bounded fatty acids are then transported to the cytosol, where the ACP group is removed through hydrolysis, as shown in Figure A2.2 (d).

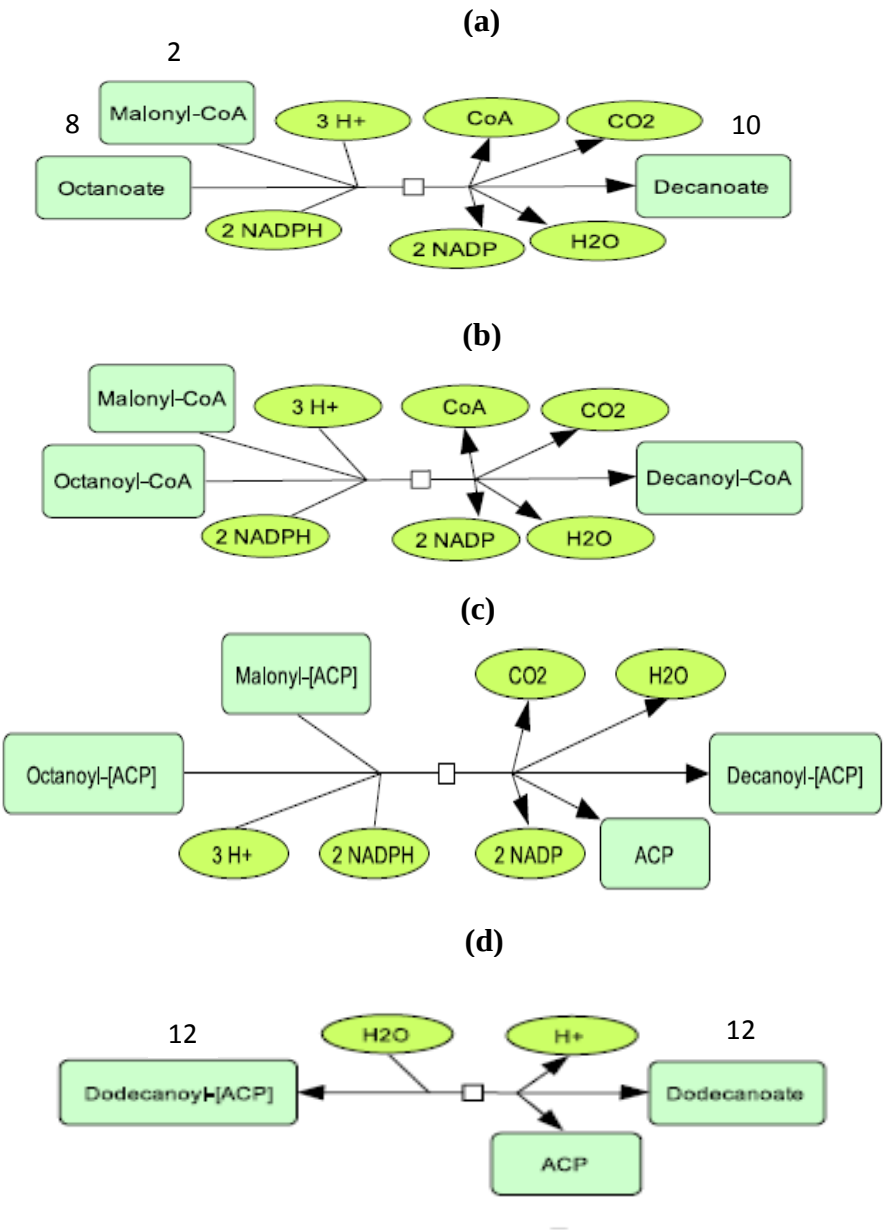

Figure A2.2 Fatty acid biosynthesis for iBB814: (a) Non-CoA group, (b) CoA group, (c) ACP group (d) Hydrolysis of ACP group

A3 Biomass Composition

Amino acids

Amino Acid	iSS884	iBB814	Amino Acid	iSS884	iBB814
ala-L[c]	0.496	0.4735	lys-L[c]	0.200	0.2624
arg-L[c]	0.1783	0.1821	met-L[c]	0.1577	0.0559
asn-L[c]	0.0719	0.1511	L-orn[c]	0.0258	Not Present
asp-L[c]	0.100	0.1566	phe-L[c]	0.0315	0.1147
cys-L[c]	0.0415	0.0511	pro-L[c]	0.141	0.1592
gln-L[c]	0.447	0.1817	ser-L[c]	0.1359	0.2330
glu-L[c]	0.447	0.3190	thr-L[c]	0.128	0.1809
gly[c]	0.186	0.4724	trp-L[c]	0.0483	0.0248
his-L[c]	0.143	0.1005	tyr-L[c]	0.033	0.0741
ile-L[c]	0.138	0.1454	val-L[c]	0.166	0.2201
leu-L[c]	0.0799	0.251			

Carbohydrates

Carbohydrates	iSS884	iBB814
13BDglcn[c]	1.798	0.6107
chitin[c]	Not Present	0.4528
glycogen[c]	0.178	0.2714
mannan[c]	Not Present	0.7156
tre[c]	0.0102	0.076

Fatty Acids

Fatty Acids	iSS884	iBB814	Fatty Acids	iSS884	iBB814
clpn[c]	0.002	Not Present	pe[c]	0.064	4.1×10^{-5}
eig3p[c]	0.0007	Not Present	ps[c]	0.001	Not Present
ergst[c]	0.0388	0.0560	ptd1ino[c]	0.003	1.5 x 10-5
fecost[c]	0.0007	Not Present	9ZHexdece[c]	0.0043	Not Present
hdca[c]	0.0119	Not Present	9ZOctadece[c]	0.0199	Not Present
lanost[c]	0.0002	Not Present	9Z12ZOctadecad[c]	0.0218	Not Present
ocdca[c]	0.0029	Not Present	(9Z,12Z,15Z)-Ocdeat[c]	0.0179	Not Present
pa[c]	0.001	Not Present	(9Z,12Z,15Z)-Ocdeat[c]	0.0179	Not Present
pc[c]		2.55×10^{-3}	zymst[c]	0.002	Not Present

Nucleotides

Nucleotides	iSS884	iBB814
atp[c]	39.92	44.4
amp[c]	0.078	0.0444
cmp[c]	0.0545	0.0388
gmp[c]	0.05469	0.0361
ump[c]	0.0781	0.0522
damp[c]	0.009	0.0112
dcmp[c]	0.0063	0.0084
dgmp[c]	0.0063	0.0084
dtmp[c]	0.009	Not Present

Other metabolites

Other	iSS884	iBB814
h2o[c]	39.92	44.4
dp[c] (right hand side)	39.92	44.4
pi[c] (right hand side)	39.92	44.4
h[c] (right hand side)	39.92	44.4

A4 Reaction list in iAD828

Rxn description	Formula	Subsystem
Argininosuccinate synthase	atp[c] + asp-L[c] + citr-L[c] <=> h[c] + amp[c] + argsuc[c] + ppi[c]	Alanine, aspartate and glutamate metabolism
Glutamate Decarboxylase	h[c] + glu-L[c] -> 4abut[c] + co2[c]	Alanine, aspartate and glutamate metabolism
Succinate Semialdehyde Dehydrogenase	nadp[c] + h2o[c] + succsal[c] -> succ[c] + 2 h[c] + nadph[c]	Alanine, aspartate and glutamate metabolism
4-aminobutyrate aminotransferase	4abut[c] + akg[c] <=> glu-L[c] + succsal[c]	Alanine, aspartate and glutamate metabolism
Aspartate transaminase	akg[m] + asp-L[m] <=> glu-L[m] + oaa[m]	Alanine, aspartate and glutamate metabolism
D-Alanine oxidase	h2o[c] + ala-D[c] + o2[c] -> pyr[c] + nh4[c] + h2o2[c]	Alanine, aspartate and glutamate metabolism
Argininosuccinate lyase	argsuc[c] <=> fum[c] + arg-L[c]	Alanine, aspartate and glutamate metabolism
Aspartate transaminase	asp-L[c] + akg[c] <=> glu-L[c] + oaa[c]	Alanine, aspartate and glutamate metabolism
L-Alanine transaminase	akg[m] + ala-L[m] <=> glu-L[m] + pyr[m]	Alanine, aspartate and glutamate metabolism
Carbamoyl-phosphate synthase	h2o[c] + 2 atp[c] + gln-L[c] + hco3[c] -> 2 h[c] + 2 adp[c] + pi[c] + glu-L[c] + cbp[c]	Alanine, aspartate and glutamate metabolism
L-Asparaginase	asn-L[e] + h2o[e] -> asp-L[e] + nh4[e]	Alanine, aspartate and glutamate metabolism
Glutamine synthetase	atp[c] + glu-L[c] + nh4[c] -> h[c] + adp[c] + pi[c] + gln-L[c]	Alanine, aspartate and glutamate metabolism
Glutamate dehydrogenase (NAD)	h2o[c] + nad[c] + glu-L[c] <=> h[c] + nadh[c] + akg[c] + nh4[c]	Alanine, aspartate and glutamate metabolism
Asparagine synthase	h2o[c] + atp[c] + asp-L[c] + gln-L[c] -> h[c] + amp[c] + ppi[c] + glu-L[c] + asn-L[c]	Alanine, aspartate and glutamate metabolism
Glutamate synthase (NADH)	h[c] + nadh[c] + akg[c] + gln-L[c] -> nad[c] + 2 glu-L[c]	Alanine, aspartate and glutamate metabolism
Glutamine phosphoribosyldiphosphate amidotransferase	h2o[c] + gln-L[c] + prpp[c] -> ppi[c] + glu-L[c] + pram[c]	Alanine, aspartate and glutamate metabolism
L-Alanine:2-oxoglutarate aminotransferase	ala-L[c] + akg[c] <=> pyr[c] + glu-L[c]	Alanine, aspartate and glutamate metabolism
Glutamate Decarboxylase	glu-L[m] + h[m] -> co2[m] + 4abut[m]	Alanine, aspartate and glutamate metabolism

4-aminobutyrate aminotransferase (4abut transaminase)	akg[m] + 4abut[m] <=> glu-L[m] + succsal[m]	Alanine, aspartate and glutamate metabolism
Succinate Semialdehyde Dehydrogenase	h2o[m] + nadp[m] + succsal[m] -> succ[m] + 2 h[m] + nadph[m]	Alanine, aspartate and glutamate metabolism
Transport mal-L-akg	akg[m] + mal-L[c] <=> akg[c] + mal-L[m]	alanine, aspartate and glutamate metabolism
Glutamate dehydrogenase (NADP)	nadp[c] + h2o[c] + glu-L[c] <=> h[c] + nadph[c] + akg[c] + nh4[c]	Alanine, aspartate and glutamate metabolism
N- Acetyl Glucosamine Kinase	atp[c] + acgam[c] -> h[c] + adp[c] + acgam6p[c]	Amino Sugar Metabolism
Chitin synthase	uacgam[c] -> h[c] + chitin[c] + udp[c]	Amino Sugar Metabolism
Chitinase/ beta-N-Acetylhexosaminidase	h2o[c] + chitin[c] -> acgam[c]	Amino Sugar Metabolism
Chitin deacetylase	h2o[c] + chitin[c] -> h[c] + ac[c] + chitos[c]	Amino Sugar Metabolism
Cytochrome B5 Reductase	nadh[c] + 2 ficytb5[c] <=> h[c] + nad[c] + 2 focytb5[c]	Amino Sugar Metabolism
N-acetylglucosamine-6-phosphate deacetylase	h2o[c] + acgam6p[c] -> ac[c] + gam6p[c]	Amino Sugar Metabolism
UDP-N-acetylglucosamine pyrophosphorylase	h[c] + acgam1p[c] + utp[c] <=> ppi[c] + uacgam[c]	Amino Sugar Metabolism
Glucosamine-6-phosphate deaminase	h2o[c] + gam6p[c] -> nh4[c] + f6p[c]	Amino Sugar Metabolism
Glutamine-fructose-6-phosphate transaminase	gln-L[c] + f6p[c] -> glu-L[c] + gam6p[c]	Amino Sugar Metabolism
N-acetylglucosamine-6-phosphate synthase	gam6p[c] + accoa[c] <=> h[c] + acgam6p[c] + coa[c]	Amino Sugar Metabolism
Phosphoacetylglucosamine mutase	acgam6p[c] <=> acgam1p[c]	Amino Sugar Metabolism
Aconitase, mitochondrial	2mcit[m] <=> micit[m]	Anaplerotic reactions
Methylisocitrate lyase	micit[m] -> succ[m] + pyr[m]	Anaplerotic reactions
Allophanate hydrolase	3 h[c] + h2o[c] + allphn[c] -> 2 co2[c] + 2 nh4[c]	Arginine and Proline Metabolism
Urea carboxylase	atp[c] + hco3[c] + urea[c] <=> h[c] + adp[c] + pi[c] + allphn[c]	Arginine and Proline Metabolism
Glutamate 5-kinase	atp[c] + glu-L[c] -> adp[c] + glu5p[c]	Arginine and Proline Metabolism
Agmatinase	h2o[c] + agm[c] -> urea[c] + ptrc[c]	Arginine and Proline Metabolism

Pyrroline-5-carboxylate reductase	2 h[c] + nadph[c] + 1pyr5c[c] -> nadp[c] + pro-L[c]	Arginine and Proline Metabolism
Ornithine carbamoyltransferase	cbp[c] + orn[c] -> h[c] + pi[c] + citr-L[c]	Arginine and Proline Metabolism
Acetamidase	h2o[c] + acetm[c] -> nh4[c] + ac[c]	Arginine and Proline Metabolism
Amidase	h2o[c] + pad[c] -> nh4[c] + pac[c]	Arginine and Proline Metabolism
N-acteylglutamate synthase	glu-L[c] + accoa[c] -> h[c] + coa[c] + acglu[c]	Arginine and Proline Metabolism
L-erythro-4-Hydroxyglutamate:2-oxoglutarate aminotransferase, mitochondrial	akg[m] + e4hglu[m] -> glu-L[m] + 4h2oglt[m]	Arginine and Proline Metabolism
Acetylornithine transaminase, mitochondrial	glu-L[m] + acg5sa[m] -> akg[m] + acorn[m]	Arginine and Proline Metabolism
Acetylglutamate kinase, mitochondrial	atp[m] + acglu[m] -> adp[m] + acg5p[m]	Arginine and Proline Metabolism
N-acetyl-g-glutamyl-phosphate reductase, mitochondrial	h[m] + nadph[m] + acg5p[m] -> pi[m] + acg5sa[m] + nadp[m]	Arginine and Proline Metabolism
N-acteylglutamate synthase	glu-L[m] + accoa[m] -> coa[m] + h[m] + acglu[m]	Arginine and Proline Metabolism
ornithine transacetylase, irreversible, mitochondrial	glu-L[m] + acorn[m] -> acglu[m] + orn[m]	Arginine and Proline Metabolism
L-erythro-4-Hydroxyglutamate:2-oxoglutarate aminotransferase	akg[c] + e4hglu[c] -> glu-L[c] + 4h2oglt[c]	Arginine and Proline Metabolism
Ornithine transaminase	akg[c] + orn[c] -> glu-L[c] + glu5sa[c]	Arginine and Proline Metabolism
Arginase	h2o[c] + arg-L[c] -> urea[c] + orn[c]	Arginine and Proline Metabolism
Proline oxidase (NAD), mitochondrial	nad[m] + pro-L[m] -> 2 h[m] + 1pyr5c[m] + nadh[m]	Arginine and Proline Metabolism
Ornithine Decarboxylase	h[c] + orn[c] -> co2[c] + ptrc[c]	Arginine and Proline Metabolism
Glutamate-5-semialdehyde dehydrogenase	h[c] + nadph[c] + glu5p[c] -> nadp[c] + pi[c] + glu5sa[c]	Arginine and Proline Metabolism
Glutamate-5-semialdehyde dehydrogenase	h[c] + nadh[c] + glu5p[c] -> nad[c] + pi[c] + glu5sa[c]	Arginine and Proline Metabolism
L-glutamate 5-semialdehyde dehydratase	glu5sa[c] <=> h[c] + h2o[c] + 1pyr5c[c]	Arginine and Proline Metabolism
L-glutamate 5-semialdehyde dehydratase, mitochondrial	glu5sa[m] <=> h2o[m] + h[m] + 1pyr5c[m]	Arginine and Proline Metabolism

1-Pyrroline-5-carboxylate dehydrogenase	h[c] + nadh[c] + glu-L[c] <=> 2 h2o[c] + nad[c] + 1pyr5c[c]	Arginine and Proline Metabolism
1-Pyrroline-5-carboxylate dehydrogenase	glu-L[m] + h[m] + nadh[m] <=> 2 h2o[m] + nad[m] + 1pyr5c[m]	Arginine and Proline Metabolism
Aldehyde dehydrogenase (3-aminopropanal, NAD)	h2o[c] + nad[c] + aproa[c] -> 2 h[c] + nadh[c] + ala-B[c]	beta-Alanine metabolism
Aspartate 1 decarboxylase	h[c] + asp-L[c] -> co2[c] + ala-B[c]	beta-Alanine metabolism
Biomass Formation reaction	0.4735 ala-L[c] + 0.2201 val-L[c] + 44.4 h2o[c] + 0.1566 asp-L[c] + 0.0444 amp[c] + 0.319 glu-L[c] + 0.1821 arg-L[c] + 0.1817 gln-L[c] + 0.1511 asn-L[c] + 0.4528 chitin[c] + 0.1592 pro-L[c] + 0.0559 met-L[c] + 0.0511 cys-L[c] + 0.233 ser-L[c] + 0.4724 gly[c] + 0.1005 his-L[c] + 0.1809 thr-L[c] + 0.7156 mannan[c] + 0.000255 pc[c] + 4.1e-05 pe[c] + 0.0388 cmp[c] + 1.5e-05 ptd1ino[c] + 0.2624 lys-L[c] + 0.0361 gmp[c] + 0.0112 dtmp[c] + 0.0741 tyr-L[c] + 0.1147 phe-L[c] + 0.0248 trp-L[c] + 0.0522 ump[c] + 0.0084 dcmp[c] + 0.0112 damp[c] + 0.0084 dgmp[c] + 0.056 ergst[c] + 0.0022 zymst[c] + 0.2714 glycogen[c] + 0.6107 13BDglcn[c] + 0.076 tre[c] + 0.1454 ile-L[c] + 0.2451 leu-L[c] -> .00001 h[c]	Biomass
Biotin synthase	dtbt[c] + s[c] <=> 2 h[c] + btn[c]	Biotin Metabolism
Adenosylmethionine-8-amino-7-oxononanoate transaminase	8aonn[c] + amet[c] <=> amob[c] + dann[c]	Biotin Metabolism
Dethiobiotin synthase	atp[c] + co2[c] + dann[c] <=> 3 h[c] + adp[c] + pi[c] + dtbt[c]	Biotin Metabolism
(R,R)-butanediol dehydrogenase	nad[c] + btd-RR[c] <=> h[c] + nadh[c] + actn-R[c]	Butanoate Metabolism
Succinate-CoA ligase (ATP-forming)	adp[m] + pi[m] + succoa[m] <=> succ[m] + atp[m] + coa[m]	Citrate cycle (TCA cycle)
Succinate-CoA ligase (GDP-forming)	pi[m] + succoa[m] + gdp[m] <=> succ[m] + coa[m] + gtp[m]	Citrate cycle (TCA cycle)
Succinate Dehydrogenase (Flavoprotein) Mitochondrial	succ[m] + fad[m] <=> fadh2[m] + fum[m]	Citrate cycle (TCA cycle)

Malate dehydrogenase, mitochondrial	nad[m] + mal-L[m] <=> oaa[m] + h[m] + nadh[m]	Citrate cycle (TCA cycle)
Isocitrate dehydrogenase (NAD+), mitochondrial	nad[m] + icit[m] -> akg[m] + nadh[m] + co2[m]	Citrate cycle (TCA cycle)
isocitrate dehydrogenase (NADP+) Mitochondrial	nadp[m] + icit[m] -> akg[m] + nadph[m] + co2[m]	Citrate cycle (TCA cycle)
2-Oxoglutarate Dehydrogenase (Mitochondrial)	coa[m] + akg[m] + nad[m] -> succoa[m] + nadh[m] + co2[m]	Citrate cycle (TCA cycle)
Aconitate Hydratase	cit[m] <=> icit[m]	Citrate cycle (TCA cycle)
Citrate Synthetase	oaa[m] + h2o[m] + accoa[m] -> coa[m] + h[m] + cit[m]	Citrate cycle (TCA cycle)
Fumarase, mitochondrial	h2o[m] + fum[m] -> mal-L[m]	Citrate cycle (TCA cycle)
Isocitrate dehydrogenase	nad[c] + icit[c] -> nadh[c] + co2[c] + akg[c]	Citrate cycle (TCA cycle)
Homocysteine S-methyltransferase	amet[c] + hcys-L[c] -> h[c] + ahcys[c] + met-L[c]	Cysteine and Methionine Metabolism
O-succinylhomoserine lyase (L-cysteine)	cys-L[c] + suchms[c] -> succ[c] + h[c] + cyst-L[c]	Cysteine and Methionine Metabolism
O-succinylhomoserine lyase	h2o[c] + suchms[c] <=> succ[c] + h[c] + nh4[c] + 2obut[c]	Cysteine and Methionine Metabolism
2,3-diketo-5-methylthio-1-phosphopentane degradation reaction	3 h2o[c] + dkmpp[c] -> 6 h[c] + pi[c] + 2kmb[c] + for[c]	Cysteine and Methionine Metabolism
3-Sulfo-L-alanine carboxy-lyase	lcyst[c] -> co2[c] + taur[c]	Cysteine and Methionine Metabolism
5-Methylthio-5-deoxy-D-ribulose 1-phosphate dehydratase	5mdru1p[c] -> h2o[c] + dkmpp[c]	Cysteine and Methionine Metabolism
Homoserine dehydrogenase (NAD)	h[c] + nadh[c] + aspsa[c] -> nad[c] + hom-L[c]	Cysteine and methionine metabolism
Methionine adenosyltransferase	h2o[c] + atp[c] + met-L[c] -> pi[c] + ppi[c] + amet[c]	Cysteine and Methionine Metabolism
5'-methylthioadenosine phosphorylase	pi[c] + 5mta[c] -> 5mdr1p[c] + ade[c]	Cysteine and Methionine Metabolism
2-keto-4-methylthiobutyrate transamination	glu-L[c] + 2kmb[c] -> akg[c] + met-L[c]	Cysteine and Methionine Metabolism
Aspartate kinase	atp[c] + asp-L[c] -> adp[c] + 4pasp[c]	Cysteine and methionine metabolism
Adenosylhomocysteinase	h2o[c] + ahcys[c] -> hcys-L[c] + adn[c]	Cysteine and Methionine Metabolism
Methionine synthase	hcys-L[c] + 5mthf[c] -> met-L[c] + thf[c]	Cysteine and Methionine Metabolism

5-methyltetrahydropteroyltriglutamate-homocysteine S-methyltransferase	hcys-L[c] + mhpglu[c] -> met-L[c] + hpglu[c]	Cysteine and Methionine Metabolism
Spermidine synthase	ptrc[c] + ametam[c] -> h[c] + 5mta[c] + spmd[c]	Cysteine and methionine metabolism
Spermine synthase	ametam[c] + spmd[c] -> h[c] + 5mta[c] + sprm[c]	Cysteine and methionine metabolism
Adenosylmethionine decarboxylase	h[c] + amet[c] -> co2[c] + ametam[c]	Cysteine and methionine metabolism
Aspartate-semialdehyde dehydrogenase	h[c] + nadph[c] + 4pasp[c] -> nadp[c] + pi[c] + aspsa[c]	Cysteine and methionine metabolism
5-methylthioribose-1-phosphate isomerase	5mdr1p[c] <=> 5mdru1p[c]	Cysteine and Methionine Metabolism
Serine O-acetyltransferase, irreversible	accoa[c] + ser-L[c] -> coa[c] + acser[c]	Cysteine and Methionine Metabolism
Cysteine synthase	acser[c] + h2s[c] -> h[c] + ac[c] + cys-L[c]	Cysteine and methionine metabolism
Homoserine O-trans-acetylase	accoa[c] + hom-L[c] <=> coa[c] + achms[c]	Cysteine and methionine metabolism
O-acetylhomoserine (thiol)-lyase	achms[c] + ch4s[c] -> h[c] + ac[c] + met-L[c]	Cysteine and methionine metabolism
Cystathionine b-lyase	h2o[c] + cyst-L[c] -> pyr[c] + nh4[c] + hcys-L[c]	Cysteine and methionine metabolism
Cystathionine g-lyase	h2o[c] + cyst-L[c] -> nh4[c] + cys-L[c] + 2obut[c]	Cysteine and methionine metabolism
Non-Specific Peptidase	h2o[c] + alaasp[c] -> ala-L[c] + asp-L[c]	Dipeptide metabolism
Non-Specific Peptidase	h2o[c] + glyglu[c] -> glu-L[c] + gly[c]	Dipeptide metabolism
Non-Specific Peptidase	h2o[c] + glymet[c] -> met-L[c] + gly[c]	Dipeptide metabolism
Non-Specific Peptidase	h2o[c] + metala[c] -> ala-L[c] + met-L[c]	Dipeptide metabolism
Non-Specific Peptidase	h2o[c] + glyasp[c] -> asp-L[c] + gly[c]	Dipeptide metabolism
Non-Specific Peptidase	h2o[c] + glypro[c] -> pro-L[c] + gly[c]	Dipeptide metabolism
Non-Specific Peptidase	h2o[c] + gluala[c] -> ala-L[c] + glu-L[c]	Dipeptide metabolism
Non-Specific Peptidase	h2o[c] + alagln[c] -> ala-L[c] + gln-L[c]	Dipeptide metabolism

Non-Specific Peptidase	h2o[c] + alaglu[c] -> ala-L[c] + glu-L[c]	Dipeptide metabolism
Non-Specific Peptidase	h2o[c] + alagly[c] -> ala-L[c] + gly[c]	Dipeptide metabolism
Non-Specific Peptidase	h2o[c] + alahis[c] -> ala-L[c] + his-L[c]	Dipeptide metabolism
Non-Specific Peptidase	alaleu[c] -> ala-L[c] + h2o[c]	Dipeptide metabolism
Non-Specific Peptidase	h2o[c] + alathr[c] -> ala-L[c] + thr-L[c]	Dipeptide metabolism
Non-Specific Peptidase	h2o[c] + glyasn[c] -> asn-L[c] + gly[c]	Dipeptide metabolism
Non-Specific Peptidase	h2o[c] + glygln[c] -> gln-L[c] + gly[c]	Dipeptide metabolism
1,3-beta-D-Glucan exchange	13BDglcn[e] <=>	Exchange Reaction
2-methylbutyraldehyde exchange	2mbald[e] <=>	Exchange Reaction
2-methyl-1-butanol exchange	2mbtoh[e] <=>	Exchange Reaction
2-methylpropanal exchange	2mppal[e] <=>	Exchange Reaction
2-oxobutanoate exchange	2obut[e] ->	Exchange Reaction
2-Phosphoglycerate Exchange	2pg[e] <=>	Exchange Reaction
2-Phosphoglycolate Exchange	2pglyc[e] <=>	Exchange Reaction
2-phenylethanol exchange	2phetoh[e] <=>	Exchange Reaction
3-Carboxy-3-hydroxy-4-methylpentanoate exchange	3c3hmp[e] <=>	Exchange Reaction
3-Methylbutanal exchange	3mbald[e] <=>	Exchange Reaction
3-Methyl-2-oxopentanoate exchange	3mop[e] <=>	Exchange Reaction
3-Phosphoglycerate Exchange	3pg[e] <=>	Exchange Reaction
4-Aminobutanoate exchange	4abut[e] <=>	Exchange Reaction
4-Aminobenzoate exchange	4abz[e] <=>	Exchange Reaction
hydroxyproline exchange	4hpro-LT[e] ->	Exchange Reaction
5-Amino-4-oxopentanoate exchange	5aop[e] <=>	Exchange Reaction
6-Phospho Gluconate Exchange	6pgc[e] <=>	Exchange Reaction
8-Amino-7-oxononanoate exchange	8aonn[e] <=>	Exchange Reaction
Acetate exchange	ac[e] <=>	Exchange Reaction
Acetoacetate exchange	acac[e] ->	Exchange Reaction
Acetaldehyde exchange	acald[e] <=>	Exchange Reaction
Acetamide exchange	acetm[e] ->	Exchange Reaction
Adenine exchange	ade[e] <=>	Exchange Reaction
Adenosine exchange	adn[e] <=>	Exchange Reaction
Agmatine exchange	agm[e] ->	Exchange Reaction
2-Oxoglutarate exchange	akg[e] <=>	Exchange Reaction
Ala-Asp Exchange	alaasp[e] ->	Exchange Reaction
D-Alanine exchange	ala-D[e] ->	Exchange Reaction

Ala-Gln Exchange	alagln[e] ->	Exchange Reaction
Ala-Glu Exchange	alaglu[e] ->	Exchange Reaction
Ala-Gly Exchange	alagly[e] ->	Exchange Reaction
Ala-His Exchange	alahis[e] ->	Exchange Reaction
L-Alanine exchange	ala-L[e] <=>	Exchange Reaction
Ala-Leu Exchange	alaleu[e] ->	Exchange Reaction
Allantoin exchange	alltn[e] ->	Exchange Reaction
Ala-Thr Exchange	alathr[e] ->	Exchange Reaction
S-Adenosyl-L-methionine exchange	amet[e] <=>	Exchange Reaction
AMP exchange	amp[e] ->	Exchange Reaction
D-arabinose exchange	arab-D[e] ->	Exchange Reaction
L-arabinose exchange	arab-L[e] ->	Exchange Reaction
L-Arginine exchange	arg-L[e] <=>	Exchange Reaction
L-Asparagine exchange	asn-L[e] <=>	Exchange Reaction
L-Aspartate exchange	asp-L[e] <=>	Exchange Reaction
(R,R)-2,3-Butanediol exchange	btd-RR[e] <=>	Exchange Reaction
Biotin exchange	btn[e] <=>	Exchange Reaction
Cellobiose exchange	cellb[e] <=>	Exchange Reaction
Cys-Gly Exchange	cgly[e] <=>	Exchange Reaction
Methanethiol Exchange	ch4s[e] <=>	Exchange Reaction
Choline exchange	chol[e] <=>	Exchange Reaction
Citrate exchange	cit[e] <=>	Exchange Reaction
L-Citruline exchange	citr-L[e] ->	Exchange Reaction
CMP Exchange	cmp[e] <=>	Exchange Reaction
CO2 exchange	co2[e] <=>	Exchange Reaction
Cytosine exchange	csn[e] <=>	Exchange Reaction
L-Cysteine exchange	cys-L[e] <=>	Exchange Reaction
Cystathione Exchange	cyst-L[e] <=>	Exchange Reaction
Cytidine exchange	cytd[e] <=>	Exchange Reaction
Deoxyadenosine exchange	dad-2[e] <=>	Exchange Reaction
7,8-Diaminononanoate exchange	dann[e] <=>	Exchange Reaction
Decanoate (n-C10:0) exchange	dca[e] <=>	Exchange Reaction
Deoxycytidine exchange	dcyt[e] <=>	Exchange Reaction
Dodecanoate (n-C12:0) exchange	ddca[e] <=>	Exchange Reaction
Deoxyguanosine exchange	dgsn[e] <=>	Exchange Reaction
Dihydroxy acetone exchange	dha[e] ->	Exchange Reaction
Deoxyinosine exchange	din[e] <=>	Exchange Reaction
Docosanoic acid, Exchange	docosa[e] <=>	Exchange Reaction

Thymidine 5 Phosphate Exchange	dtmp[e] <=>	Exchange Reaction
dTTP exchange	dttp[e] <=>	Exchange Reaction
Deoxyuridine exchange	duri[e] <=>	Exchange Reaction
Eicosapentaenoate, Exchange	eicosapen[e] <=>	Exchange Reaction
Episterol exchange	epist[e] <=>	Exchange Reaction
Ergosterol exchange	ergst[e] <=>	Exchange Reaction
Ethanolamine exchange	etha[e] <=>	Exchange Reaction
Ethanol exchange	etoh[e] <=>	Exchange Reaction
F6P exchange	f6p[e] ->	Exchange Reaction
Fe2+ exchange	fe2[e] <=>	Exchange Reaction
fecosterol exchange	fecost[e] <=>	Exchange Reaction
FMN exchange	fmn[e] <=>	Exchange Reaction
Formate exchange	for[e] <=>	Exchange Reaction
Formamide exchange	frmd[e] ->	Exchange Reaction
D-Fructose exchange	fru[e] <=>	Exchange Reaction
Fumarate exchange	fum[e] <=>	Exchange Reaction
G1P exchange	g1p[e] ->	Exchange Reaction
sn-Glycero-3-phosphocholine exchange	g3pc[e] <=>	Exchange Reaction
sn-Glycero-3-phospho-1-inositol exchange	g3pi[e] <=>	Exchange Reaction
G6P Exchange	g6p[e] ->	Exchange Reaction
D-Galactose exchange	gal[e] <=>	Exchange Reaction
D-Glucosamine 6-phosphate exchange	gam6p[e] <=>	Exchange Reaction
Glycolaldehyde exchange	gcald[e] <=>	Exchange Reaction
D-Glucose exchange	glc-D[e] <=>	Exchange Reaction
Gluconate exchange	glcn-D[e] ->	Exchange Reaction
L-Glutamine exchange	gln-L[e] <=>	Exchange Reaction
Glu-Ala Exchange	gluala[e] <=>	Exchange Reaction
L-Glutamate exchange	glu-L[e] <=>	Exchange Reaction
Glyoxylate exchange	glx[e] <=>	Exchange Reaction
Glycine exchange	gly[e] <=>	Exchange Reaction
Gly-Asn Exchange	glyasn[e] ->	Exchange Reaction
Gly-Asp Exchange	glyasp[e] ->	Exchange Reaction
Glycerol exchange	glyc[e] <=>	Exchange Reaction
Glycerol-3-Phosphate exchange	glyc3p[e] <=>	Exchange Reaction
Glycolate Exchange	glyclt[e] <=>	Exchange Reaction
Gly-Gln Exchange	glygln[e] ->	Exchange Reaction
Gly-Glu Exchange	glyglu[e] ->	Exchange Reaction

Gly-Met Exchange	glymet[e] ->	Exchange Reaction
Gly-Pro Exchange	glypro[e] ->	Exchange Reaction
GMP Exchange	gmp[e] <=>	Exchange Reaction
Guanosine exchange	gsn[e] <=>	Exchange Reaction
Oxidized glutathione exchange	gthox[e] <=>	Exchange Reaction
Reduced glutathione exchange	gthrd[e] <=>	Exchange Reaction
Guanine exchange	gua[e] <=>	Exchange Reaction
H+ exchange	h[e] <=>	Exchange Reaction
H2O exchange	h2o[e] <=>	Exchange Reaction
Hexadecanoate (n-C16:0) exchange	hdca[e] <=>	Exchange Reaction
hexadecenoate (n-C16:1) exchange	hdcea[e] <=>	Exchange Reaction
Heptadecenoate, Exchange	hepdcea[e] <=>	Exchange Reaction
hexanoate (n-C6:0) exchange	hexa[e] <=>	Exchange Reaction
hexacosanoate (n-C26:0) exchange	hexc[e] <=>	Exchange Reaction
L-Histidine exchange	his-L[e] <=>	Exchange Reaction
Homoserine exchange	hom-L[e] ->	Exchange Reaction
Isoamyl alcohol exchange	iamoh[e] <=>	Exchange Reaction
Isobutyl alcohol exchange	ibutoh[e] <=>	Exchange Reaction
L-Isoleucine exchange	ile-L[e] <=>	Exchange Reaction
Tryptophol Exchange	ind3eth[e] ->	Exchange Reaction
Myo-Inositol exchange	inost[e] <=>	Exchange Reaction
Inosine exchange	ins[e] <=>	Exchange Reaction
K+ exchange	k[e] <=>	Exchange Reaction
D-lactate exchange	lac-D[e] <=>	Exchange Reaction
L-Lactate exchange	lac-L[e] <=>	Exchange Reaction
Lanosterol exchange	lanost[e] <=>	Exchange Reaction
L-cysteate exchange	lcyst[e] <=>	Exchange Reaction
L-Leucine exchange	leu-L[e] <=>	Exchange Reaction
L-Lysine exchange	lys-L[e] <=>	Exchange Reaction
Alpha Methylglucoside exchange	madg[e] ->	Exchange Reaction
L-Malate exchange	mal-L[e] <=>	Exchange Reaction
Maltose exchange	malt[e] <=>	Exchange Reaction
Maltotriose Exchange	maltr[e] ->	Exchange Reaction
D-Mannose exchange	man[e] <=>	Exchange Reaction
Mannose 1 Phosphate Exchange	man1p[e] <=>	Exchange Reaction
Mannose 6 Phosphate Exchange	man6p[e] <=>	Exchange Reaction
D-Mannitol exchange	mnl[e] ->	Exchange Reaction

Beta Methylglucoside exchange	mbdg[e] ->	Exchange Reaction
Methanol exchange	meoh[e] ->	Exchange Reaction
Met-Ala Exchange	metala[e] ->	Exchange Reaction
L-Methionine exchange	met-L[e] <=>	Exchange Reaction
Sodium exchange	Na[e] <=>	Exchange Reaction
Nicotinate exchange	nac[e] <=>	Exchange Reaction
N-Acetyl Glucosamine exchange	acgam[e] ->	Exchange Reaction
Nicotinamide adenine dinucleotide phosphate exchange	nadp[e] <=>	Exchange Reaction
Ammonia exchange	nh4[e] <=>	Exchange Reaction
NMN exchange	nmn[e] <=>	Exchange Reaction
O2 exchange	o2[e] <=>	Exchange Reaction
Oxaloacetate exchange	oaa[e] <=>	Exchange Reaction
Octadecanoate (n-C18:0) exchange	ocdca[e] <=>	Exchange Reaction
Octadecenoate (n-C18:1) exchange	ocdcea[e] <=>	Exchange Reaction
Octadecatrienoate, Exchange	ocdcta[e] <=>	Exchange Reaction
Octadecynoate (n-C18:2) exchange	ocdcya[e] <=>	Exchange Reaction
5-oxoproline exchange	opro-L[e] ->	Exchange Reaction
Ornithine exchange	orn[e] <=>	Exchange Reaction
Phenylacetaldehyde exchange	pacald[e] <=>	Exchange Reaction
Adenosine 3',5'-bisphosphate exchange	pap[e] <=>	Exchange Reaction
Phosphatidylcholine, exchange	pc[e] <=>	Exchange Reaction
Phosphoenolpyruvate Exchange	pep[e] <=>	Exchange Reaction
L-Phenylalanine exchange	phe-L[e] <=>	Exchange Reaction
Phosphate exchange	pi[e] <=>	Exchange Reaction
(R)-Pantothenate exchange	pnto-R[e] <=>	Exchange Reaction
Diphosphate exchange	ppi[e] ->	Exchange Reaction
L-Proline exchange	pro-L[e] <=>	Exchange Reaction
O-Phospho-L-serine Exchange	pser-L[e] <=>	Exchange Reaction
Phosphatidyl-1D-myo-inositol, exchange	ptd1ino[e] <=>	Exchange Reaction
Putrescine exchange	ptrc[e] <=>	Exchange Reaction
Pyruvate exchange	pyr[e] <=>	Exchange Reaction
Ribitol exchange	rbt[e] ->	Exchange Reaction
L-Rhamnose exchange	rham-L[e] ->	Exchange Reaction
D-Ribose exchange	rib-D[e] <=>	Exchange Reaction
Riboflavin exchange	ribflv[e] <=>	Exchange Reaction

D-Sorbitol exchange	sbt-D[e] <=>	Exchange Reaction
L-Sorbitol exchange	sbt-L[e] <=>	Exchange Reaction
L-Serine exchange	ser-L[e] <=>	Exchange Reaction
Sulfite exchange	so3[e] <=>	Exchange Reaction
Sulfate exchange	so4[e] <=>	Exchange Reaction
Spermidine exchange	spmd[e] <=>	Exchange Reaction
Spermine Exchange	sprm[e] <=>	Exchange Reaction
L-Sorbose exchange	srb-L[e] <=>	Exchange Reaction
Succinate exchange	succ[e] <=>	Exchange Reaction
Sucrose exchange	sucr[e] <=>	Exchange Reaction
Taurine Exchange	taur[e] <=>	Exchange Reaction
Thiamin exchange	thm[e] <=>	Exchange Reaction
Thiamin monophosphate exchange	thmmp[e] <=>	Exchange Reaction
Thiamine diphosphate exchange	thmpp[e] <=>	Exchange Reaction
L-Threonine exchange	thr-L[e] <=>	Exchange Reaction
Thymine Exchange	thym[e] <=>	Exchange Reaction
Thymidine exchange	thymd[e] <=>	Exchange Reaction
Trimetaphosphate exchange	tmp[e] ->	Exchange Reaction
Trehalose exchange	tre[e] <=>	Exchange Reaction
L-Tryptophan exchange	trp-L[e] <=>	Exchange Reaction
Tetradecanoate (n-C14:0) exchange	ttdca[e] <=>	Exchange Reaction
L-Tyrosine exchange	tyr-L[e] <=>	Exchange Reaction
Uridine Monophosphate exchange	ump[e] <=>	Exchange Reaction
Uracil exchange	ura[e] <=>	Exchange Reaction
Uric acid exchange	urate[e] ->	Exchange Reaction
Urea exchange	urea[e] <=>	Exchange Reaction
Uridine exchange	uri[e] <=>	Exchange Reaction
L-Valine exchange	val-L[e] <=>	Exchange Reaction
Xanthine exchange	xan[e] <=>	Exchange Reaction
Xanthosine exchange	xtsn[e] <=>	Exchange Reaction
D-Xylose exchange	xyl-D[e] <=>	Exchange Reaction
Xylitol exchange	xylt[e] <=>	Exchange Reaction
Zymosterol exchange	zymst[e] <=>	Exchange Reaction
Hexacoa exchange	hexacoa[e] ->	Exchange Reaction
Fatty-acid--CoA ligase (decanoate)	atp[c] + coa[c] + dca[c] <=> amp[c] + ppi[c] + dcacoa[c]	Fatty acid Biosynthesis
Fatty-acid--CoA ligase (tetradecanoate)	atp[c] + coa[c] + ttdca[c] <=> amp[c] + ppi[c] + tdcoa[c]	Fatty acid Biosynthesis

Fatty-acid--CoA ligase (hexadecanoate)	atp[c] + coa[c] + hdca[c] <=> amp[c] + ppi[c] + pmtcoa[c]	Fatty acid Biosynthesis
Fatty-acid--CoA ligase (hexadecenoate)	atp[c] + coa[c] + hdcea[c] <=> amp[c] + ppi[c] + hdceacoa[c]	Fatty acid Biosynthesis
Fatty-acid--CoA ligase (eicosapentaenoate)	atp[c] + coa[c] + hepdca[c] <=> amp[c] + ppi[c] + hepdcacoa[c]	Fatty acid Biosynthesis
Fatty-acid--CoA ligase (eicosapentaenoate)	atp[c] + coa[c] + hepdcea[c] <=> amp[c] + ppi[c] + hepdceacoa[c]	Fatty acid Biosynthesis
Fatty-acid--CoA ligase (octadecanoate)	atp[c] + coa[c] + ocdca[c] <=> amp[c] + ppi[c] + stcoa[c]	Fatty acid Biosynthesis
Fatty-acid--CoA ligase (octadecenoate)	atp[c] + coa[c] + ocdcea[c] <=> amp[c] + ppi[c] + ocdceacoa[c]	Fatty acid Biosynthesis
Fatty-acid--CoA ligase (octadecynoate)	atp[c] + coa[c] + ocdcya[c] <=> amp[c] + ppi[c] + ocdcyacoa[c]	Fatty acid Biosynthesis
Fatty-acid--CoA ligase (octadecatrieonoate)	atp[c] + coa[c] + ocdcta[c] <=> amp[c] + ppi[c] + ocdctacoa[c]	Fatty acid Biosynthesis
Fatty-acid--CoA ligase (eicosapentaenoate)	atp[c] + coa[c] + eicosapen[c] <=> amp[c] + ppi[c] + eicosapencoa[c]	Fatty acid Biosynthesis
Fatty-acid--CoA ligase (octanoate)	atp[c] + coa[c] + hexa[c] <=> amp[c] + ppi[c] + hexacoa[c]	Fatty acid Biosynthesis
Fatty-acyl-ACP synthase (n-C10:0ACP), mitochondrial	3 h[m] + 2 nadph[m] + malACP[m] + octaACP[m] -> h2o[m] + 2 nadp[m] + co2[m] + ACP[m] + dcaACP[m]	Fatty acid Biosynthesis
Fatty-acyl-ACP synthase (n-C12:0ACP), mitochondrial	3 h[m] + 2 nadph[m] + malACP[m] + dcaACP[m] -> h2o[m] + 2 nadp[m] + co2[m] + ACP[m] + ddcaACP[m]	Fatty acid Biosynthesis
Fatty-acyl-ACP synthase (n-C14:0ACP), mitochondrial	3 h[m] + 2 nadph[m] + malACP[m] + ddcaACP[m] -> h2o[m] + 2 nadp[m] + co2[m] + ACP[m] + myrsACP[m]	Fatty acid Biosynthesis
Fatty-acyl-ACP synthase (n-C16:0ACP), mitochondrial	3 h[m] + 2 nadph[m] + malACP[m] + myrsACP[m] -> h2o[m] + 2 nadp[m] + co2[m] + ACP[m] + palmACP[m]	Fatty acid Biosynthesis
Fatty-acyl-ACP synthase (n-C16:1ACP), mitochondrial	4 h[m] + 3 nadph[m] + malACP[m] + myrsACP[m] + o2[m] -> 3 h2o[m] + 3 nadp[m] + co2[m] + ACP[m] + hdceaACP[m]	Fatty acid Biosynthesis
Fatty acyl-ACP synthase (n-C17:0ACP), mitochondrial, lumped reaction	21 h[m] + 14 nadph[m] + 7 malACP[m] + ppACP[m] -> 7 h2o[m] + 14 nadp[m] + 7 co2[m] + 7 ACP[m] + hepdcaACP[m]	Fatty acid Biosynthesis

Fatty-acyl-ACP synthase (n-C17:1ACP), mitochondrial	h[m] + nadph[m] + o2[m] + hepdcaACP[m] -> 2 h2o[m] + nadp[m] + co2[m] + ACP[m] + hepdceaACP[m]	Fatty acid Biosynthesis
Fatty acyl-ACP synthase (n-C17:1 ACP), mitochondrial, lumped reaction	22 h[m] + 15 nadph[m] + 7 malACP[m] + o2[m] + ppACP[m] -> 9 h2o[m] + 15 nadp[m] + 7 co2[m] + 7 ACP[m] + hepdceaACP[m]	Fatty acid Biosynthesis
fatty-acyl-ACP synthase (n-C18:0ACP), mitochondrial	3 h[m] + 2 nadph[m] + malACP[m] + palmACP[m] -> h2o[m] + 2 nadp[m] + co2[m] + ACP[m] + ocdcaACP[m]	Fatty acid Biosynthesis
fatty-acyl-ACP synthase (n-C18:1ACP), mitochondrial	4 h[m] + 3 nadph[m] + malACP[m] + palmACP[m] + o2[m] -> 3 h2o[m] + 3 nadp[m] + co2[m] + ACP[m] + ocdceaACP[m]	Fatty acid Biosynthesis
fatty-acyl-ACP synthase (n-C18:2ACP), mitochondrial	5 h[m] + 4 nadph[m] + malACP[m] + palmACP[m] + 2 o2[m] -> 5 h2o[m] + 4 nadp[m] + co2[m] + ACP[m] + ocdcyaACP[m]	Fatty acid Biosynthesis
fatty-acyl-ACP synthase (n-C18:3ACP), mitochondrial	6 h[m] + 5 nadph[m] + malACP[m] + palmACP[m] + 3 o2[m] -> 7 h2o[m] + 5 nadp[m] + co2[m] + ACP[m] + ocdctaACP[m]	Fatty acid Biosynthesis
fatty-acyl-ACP synthase (n-C20:0ACP), mitochondrial	3 h[m] + 2 nadph[m] + malACP[m] + ocdcaACP[m] -> h2o[m] + 2 nadp[m] + co2[m] + ACP[m] + eicosaACP[m]	Fatty acid Biosynthesis
fatty-acyl-ACP synthase (n-C20:5ACP), mitochondrial	8 h[m] + 7 nadph[m] + malACP[m] + 5 o2[m] + ocdcaACP[m] -> 11 h2o[m] + 7 nadp[m] + co2[m] + ACP[m] + eicosapenACP[m]	Fatty acid Biosynthesis
fatty-acyl-ACP synthase (n-C22:0ACP), mitochondrial	3 h[m] + 2 nadph[m] + malACP[m] + eicosaACP[m] -> h2o[m] + 2 nadp[m] + co2[m] + ACP[m] + docosaACP[m]	Fatty acid Biosynthesis
fatty-acyl-ACP synthase (n-C24:0ACP), mitochondrial	3 h[m] + 2 nadph[m] + malACP[m] + docosaACP[m] -> h2o[m] + 2 nadp[m] + co2[m] + ACP[m] + ttcACP[m]	Fatty acid Biosynthesis
fatty-acyl-ACP synthase (n-C26:0ACP), mitochondrial	3 h[m] + 2 nadph[m] + malACP[m] + ttcACP[m] -> h2o[m] + 2 nadp[m] + co2[m] + ACP[m] + hexcACP[m]	Fatty acid Biosynthesis

fatty acyl-ACP synthase (n-C6:0ACP), mitochondrial, lumped reaction	6 h[m] + 4 nadph[m] + 2 malACP[m] + acACP[m] -> 2 h2o[m] + 4 nadp[m] + 2 co2[m] + 2 ACP[m] + hexaACP[m]	Fatty acid Biosynthesis
fatty acyl-ACP synthase (n-C8:0ACP), mitochondrial, lumped reaction	9 h[m] + 6 nadph[m] + 3 malACP[m] + acACP[m] -> 3 h2o[m] + 6 nadp[m] + 3 co2[m] + octaACP[m] + 3 ACP[m]	Fatty acid Biosynthesis
Malonyl-CoA-ACP transacylase	ACP[m] + malcoa[m] <=> coa[m] + malACP[m]	Fatty acid Biosynthesis
Palmitoyl-CoA desaturase (n-C16:0CoA -> n-C16:1CoA)	2 h[c] + o2[c] + 2 focytb5[c] + pmtcoa[c] -> 2 h2o[c] + 2 ficytb5[c] + hdceacoa[c]	Fatty acid Biosynthesis
Hepdca-CoA desaturase (n-C17:0CoA -> n-C17:1CoA)	2 h[c] + o2[c] + 2 focytb5[c] + hepdcacoa[c] -> 2 h2o[c] + 2 ficytb5[c] + hepdceacoa[c]	Fatty acid Biosynthesis
stearoyl-CoA desaturase (n-C18:0CoA -> n-C18:1CoA)	2 h[c] + o2[c] + 2 focytb5[c] + stcoa[c] -> 2 h2o[c] + 2 ficytb5[c] + ocdceacoa[c]	Fatty acid Biosynthesis
Acetyl-CoA ACP transacylase	accoa[c] + ACP[c] <=> coa[c] + acACP[c]	Fatty acid Biosynthesis
Acetyl-CoA ACP transacylase, mitochondrial	accoa[m] + ACP[m] <=> coa[m] + acACP[m]	Fatty acid Biosynthesis
fatty-acyl-ACP hydrolase	h2o[c] + dcaACP[c] <=> h[c] + dca[c] + ACP[c]	Fatty acid Biosynthesis
fatty-acyl-ACP hydrolase	h2o[c] + ddcaACP[c] <=> h[c] + ACP[c] + ddca[c]	Fatty acid Biosynthesis
fatty-acyl-ACP hydrolase	h2o[c] + myrsACP[c] <=> h[c] + ttdca[c] + ACP[c]	Fatty acid Biosynthesis
fatty-acyl-ACP hydrolase	h2o[c] + palmACP[c] <=> h[c] + hdca[c] + ACP[c]	Fatty acid Biosynthesis
fatty-acyl-ACP hydrolase	h2o[c] + hdceaACP[c] <=> h[c] + hdcea[c] + ACP[c]	Fatty acid Biosynthesis
fatty-acyl-ACP hydrolase	h2o[c] + hepdcaACP[c] <=> h[c] + hepdca[c] + ACP[c]	Fatty acid Biosynthesis
fatty-acyl-ACP hydrolase	h2o[c] + hepdceaACP[c] <=> h[c] + hepdcea[c] + ACP[c]	Fatty acid Biosynthesis
fatty-acyl-ACP hydrolase	h2o[c] + ocdcaACP[c] <=> h[c] + ocdca[c] + ACP[c]	Fatty acid Biosynthesis
fatty-acyl-ACP hydrolase	h2o[c] + ocdceaACP[c] <=> h[c] + ocdcea[c] + ACP[c]	Fatty acid Biosynthesis
fatty-acyl-ACP hydrolase	h2o[c] + ocdcyaACP[c] <=> h[c] + ocdcya[c] + ACP[c]	Fatty acid Biosynthesis

fatty-acyl-ACP hydrolase	h2o[c] + ocdctaACP[c] <=> h[c] + ocdcta[c] + ACP[c]	Fatty acid Biosynthesis
fatty-acyl-ACP hydrolase	h2o[c] + eicosaACP[c] <=> h[c] + ACP[c] + eicosa[c]	Fatty acid Biosynthesis
fatty-acyl-ACP hydrolase	h2o[c] + eicosapenACP[c] <=> h[c] + eicosapen[c] + ACP[c]	Fatty acid Biosynthesis
fatty-acyl-ACP hydrolase	h2o[c] + docosaACP[c] <=> h[c] + ACP[c] + docosa[c]	Fatty acid Biosynthesis
fatty-acyl-ACP hydrolase	h2o[c] + ttcACP[c] <=> h[c] + ACP[c] + ttc[c]	Fatty acid Biosynthesis
fatty-acyl-ACP hydrolase	h2o[c] + hexcACP[c] <=> h[c] + ACP[c] + hexc[c]	Fatty acid Biosynthesis
fatty-acyl-ACP hydrolase	h2o[c] + hexaACP[c] <=> h[c] + hexa[c] + ACP[c]	Fatty acid Biosynthesis
fatty-acyl-ACP hydrolase	h2o[c] + octaACP[c] <=> h[c] + ACP[c] + octa[c]	Fatty acid Biosynthesis
fatty acid synthase (n-C10:0)	3 h[c] + 2 nadph[c] + octa[c] + malcoa[c] -> 2 nadp[c] + h2o[c] + co2[c] + coa[c] + dca[c]	Fatty acid Biosynthesis
fatty acyl-CoA synthase (n-C10:0CoA)	3 h[c] + 2 nadph[c] + malcoa[c] + octacoa[c] -> 2 nadp[c] + h2o[c] + co2[c] + coa[c] + dcacoa[c]	Fatty acid Biosynthesis
fatty acid synthase (n-C12:0)	3 h[c] + 2 nadph[c] + dca[c] + malcoa[c] -> 2 nadp[c] + h2o[c] + co2[c] + coa[c] + ddca[c]	Fatty acid Biosynthesis
fatty-acyl-CoA synthase (n-C12:0CoA)	3 h[c] + 2 nadph[c] + dcacoa[c] + malcoa[c] -> 2 nadp[c] + h2o[c] + co2[c] + coa[c] + ddcacoa[c]	Fatty acid Biosynthesis
fatty acid synthase (n-C14:0)	3 h[c] + 2 nadph[c] + ddca[c] + malcoa[c] -> 2 nadp[c] + h2o[c] + co2[c] + coa[c] + ttdca[c]	Fatty acid Biosynthesis
fatty-acyl-CoA synthase (n-C14:0CoA)	3 h[c] + 2 nadph[c] + malcoa[c] + ddcacoa[c] -> 2 nadp[c] + h2o[c] + co2[c] + coa[c] + tdcoa[c]	Fatty acid Biosynthesis
fatty acid synthase (n-C16:0)	3 h[c] + 2 nadph[c] + ttdca[c] + malcoa[c] -> 2 nadp[c] + h2o[c] + co2[c] + coa[c] + hdca[c]	Fatty acid Biosynthesis
fatty-acyl-CoA synthase (n-C16:0CoA)	3 h[c] + 2 nadph[c] + tdcoa[c] + malcoa[c] -> 2 nadp[c] + h2o[c] + co2[c] + coa[c] + pmtcoa[c]	Fatty acid Biosynthesis

fatty acid synthase (n-C16:1)	4 h[c] + 3 nadph[c] + o2[c] + ttdca[c] + malcoa[c] -> 3 nadp[c] + 3 h2o[c] + co2[c] + coa[c] + hdcea[c]	Fatty acid Biosynthesis
Fatty acid synthase (n-C17:0), lumped reaction	20 h[c] + 14 nadph[c] + 7 malcoa[c] + ppcoa[c] -> 14 nadp[c] + 6 h2o[c] + 7 co2[c] + 8 coa[c] + hepdca[c]	Fatty acid Biosynthesis
Fatty acyl-CoA synthase (n-C17:0CoA), lumped reaction	21 h[c] + 14 nadph[c] + 7 malcoa[c] + ppcoa[c] -> 14 nadp[c] + 7 h2o[c] + 7 co2[c] + 7 coa[c] + hepdcacoa[c]	Fatty acid Biosynthesis
Fatty acid synthase (n-C17:1), lumped reaction	21 h[c] + 15 nadph[c] + o2[c] + 7 malcoa[c] + ppcoa[c] -> 15 nadp[c] + 8 h2o[c] + 7 co2[c] + 8 coa[c] + hepdcea[c]	Fatty acid Biosynthesis
Fatty acyl-CoA synthase (n-C17:1CoA), lumped reaction	22 h[c] + 15 nadph[c] + o2[c] + 7 malcoa[c] + ppcoa[c] -> 15 nadp[c] + 9 h2o[c] + 7 co2[c] + 7 coa[c] + hepdceacoa[c]	Fatty acid Biosynthesis
fatty acid synthase (n-C18:0)	3 h[c] + 2 nadph[c] + hdca[c] + malcoa[c] -> 2 nadp[c] + h2o[c] + co2[c] + coa[c] + ocdca[c]	Fatty acid Biosynthesis
fatty-acyl-CoA synthase (n-C18:0CoA)	3 h[c] + 2 nadph[c] + pmtcoa[c] + malcoa[c] -> 2 nadp[c] + h2o[c] + co2[c] + coa[c] + stcoa[c]	Fatty acid Biosynthesis
fatty acid synthase (n-C18:1)	4 h[c] + 3 nadph[c] + o2[c] + hdca[c] + malcoa[c] -> 3 nadp[c] + 3 h2o[c] + co2[c] + coa[c] + ocdcea[c]	Fatty acid Biosynthesis
fatty acid synthase (n-C18:2)	5 h[c] + 4 nadph[c] + 2 o2[c] + hdca[c] + malcoa[c] -> 4 nadp[c] + 5 h2o[c] + co2[c] + coa[c] + ocdcya[c]	Fatty acid Biosynthesis
fatty acid synthase (n-C18:3)	6 h[c] + 5 nadph[c] + 3 o2[c] + hdca[c] + malcoa[c] -> 5 nadp[c] + 7 h2o[c] + co2[c] + coa[c] + ocdcta[c]	Fatty acid Biosynthesis
fatty acid synthase (n-C20:0)	3 h[c] + 2 nadph[c] + ocdca[c] + malcoa[c] -> 2 nadp[c] + h2o[c] + co2[c] + coa[c] + eicosa[c]	Fatty acid Biosynthesis
fatty-acyl-CoA synthase (n-C20:0CoA)	3 h[c] + 2 nadph[c] + stcoa[c] + malcoa[c] -> 2 nadp[c] + h2o[c] + co2[c] + coa[c] + eicosacoa[c]	Fatty acid Biosynthesis

fatty acid synthase (n-C20:5)	8 h[c] + 7 nadph[c] + 5 o2[c] + ocdca[c] + malcoa[c] -> 7 nadp[c] + 11 h2o[c] + co2[c] + coa[c] + eicosapen[c]	Fatty acid Biosynthesis
fatty acid synthase (n-C22:0)	3 h[c] + 2 nadph[c] + eicosa[c] + malcoa[c] -> 2 nadp[c] + h2o[c] + co2[c] + coa[c] + docosa[c]	Fatty acid Biosynthesis
fatty-acyl-CoA synthase (n-C22:0CoA)	3 h[c] + 2 nadph[c] + malcoa[c] + eicosacoa[c] -> 2 nadp[c] + h2o[c] + co2[c] + coa[c] + docosacoa[c]	Fatty acid Biosynthesis
fatty acid synthase (n-C24:0)	3 h[c] + 2 nadph[c] + docosa[c] + malcoa[c] -> 2 nadp[c] + h2o[c] + co2[c] + coa[c] + ttc[c]	Fatty acid Biosynthesis
fatty-acyl-CoA synthase (n-C24:0CoA)	3 h[c] + 2 nadph[c] + malcoa[c] + docosacoa[c] -> 2 nadp[c] + h2o[c] + co2[c] + coa[c] + ttccoa[c]	Fatty acid Biosynthesis
fatty acid synthase (n-C26:0)	3 h[c] + 2 nadph[c] + ttc[c] + malcoa[c] -> 2 nadp[c] + h2o[c] + co2[c] + coa[c] + hexc[c]	Fatty acid Biosynthesis
fatty-acyl-CoA synthase (n-C26:0CoA)	3 h[c] + 2 nadph[c] + malcoa[c] + ttccoa[c] -> 2 nadp[c] + h2o[c] + co2[c] + coa[c] + hexccoa[c]	Fatty acid Biosynthesis
Fatty acid synthase (n-C6:0), lumped reaction	5 h[c] + 4 nadph[c] + accoa[c] + 2 malcoa[c] -> 4 nadp[c] + h2o[c] + 2 co2[c] + 3 coa[c] + hexa[c]	Fatty acid Biosynthesis
Fatty acyl-CoA synthase (n-C6:0CoA), lumped reaction	6 h[c] + 4 nadph[c] + accoa[c] + 2 malcoa[c] -> 4 nadp[c] + 2 h2o[c] + 2 co2[c] + 2 coa[c] + hexacoa[c]	Fatty acid Biosynthesis
fatty acid synthase (n-C8:0), lumped reaction	8 h[c] + 6 nadph[c] + accoa[c] + 3 malcoa[c] -> 6 nadp[c] + 2 h2o[c] + 3 co2[c] + 4 coa[c] + octa[c]	Fatty acid Biosynthesis
fatty acyl-CoA synthase (n-C8:0CoA), lumped reaction	9 h[c] + 6 nadph[c] + accoa[c] + 3 malcoa[c] -> 6 nadp[c] + 3 h2o[c] + 3 co2[c] + 3 coa[c] + octacoa[c]	Fatty acid Biosynthesis
Propanoyl-CoA ACP transacylase	ACP[c] + ppcoa[c] <=> coa[c] + ppACP[c]	Fatty acid Biosynthesis
Propanoyl-CoA ACP transacylase, mitochondrial	ACP[m] + ppcoa[m] <=> coa[m] + ppACP[m]	Fatty acid Biosynthesis
Linoeyl-CoA desaturase (n-C18:2CoA -> n-C18:2CoA)	h[c] + nadph[c] + o2[c] + ocdcyacoa[c] -> nadp[c] + 2 h2o[c] + ocdctacoa[c]	Fatty acid Biosynthesis

Eicosa-CoA desaturase (n-C20:0CoA -> n-C20:5CoA)	5 h[c] + 5 nadph[c] + 5 o2[c] + eicosacoa[c] -> 5 nadp[c] + 10 h2o[c] + eicosapencoa[c]	Fatty acid Biosynthesis
Fatty acid Oxidation Pathway2, Lumped	4 h2o[c] + 4 nad[c] + 4 coa[c] + dcacoa[c] + 4 fad[c] -> 4 h[c] + 4 nadh[c] + 5 accoa[c] + 4 fadh2[c]	Fatty Acid Metabolism
Fatty acid Oxidation Pathway2, Lumped	5 h2o[c] + 5 nad[c] + 5 coa[c] + ddcacoa[c] + 5 fad[c] -> 5 h[c] + 5 nadh[c] + 6 accoa[c] + 5 fadh2[c]	Fatty Acid Metabolism
Fatty acid Oxidation Pathway2, Lumped	6 h2o[c] + 6 nad[c] + 6 coa[c] + tdcoa[c] + 6 fad[c] -> 6 h[c] + 6 nadh[c] + 7 accoa[c] + 6 fadh2[c]	Fatty Acid Metabolism
Fatty acid Oxidation Pathway2, Lumped	7 h2o[c] + 7 nad[c] + 7 coa[c] + pmtcoa[c] + 7 fad[c] -> 7 h[c] + 7 nadh[c] + 8 accoa[c] + 7 fadh2[c]	Fatty Acid Metabolism
Fatty acid Oxidation Pathway2, Lumped	6 h2o[c] + 6 nad[c] + 6 coa[c] + hepdcacoa[c] + 6 fad[c] -> 6 h[c] + 6 nadh[c] + 7 accoa[c] + ppcoa[c] + 6 fadh2[c]	Fatty Acid Metabolism
Fatty acid Oxidation Pathway2, Lumped	8 h2o[c] + 8 nad[c] + 8 coa[c] + stcoa[c] + 8 fad[c] -> 8 h[c] + 8 nadh[c] + 9 accoa[c] + 8 fadh2[c]	Fatty Acid Metabolism
Fatty acid Oxidation Pathway2, Lumped	9 h2o[c] + 9 nad[c] + 9 coa[c] + eicosacoa[c] + 9 fad[c] -> 9 h[c] + 9 nadh[c] + 10 accoa[c] + 9 fadh2[c]	Fatty Acid Metabolism
Fatty acid Oxidation Pathway2, Lumped	10 h2o[c] + 10 nad[c] + 10 coa[c] + docosacoa[c] + 10 fad[c] -> 10 h[c] + 10 nadh[c] + 11 accoa[c] + 10 fadh2[c]	Fatty Acid Metabolism
Fatty acid Oxidation Pathway2, Lumped	11 h2o[c] + 11 nad[c] + 11 coa[c] + ttccoa[c] + 11 fad[c] -> 11 h[c] + 11 nadh[c] + 12 accoa[c] + 11 fadh2[c]	Fatty Acid Metabolism
Fatty acid Oxidation Pathway2, Lumped	12 h2o[c] + 12 nad[c] + 12 coa[c] + hexccoa[c] + 12 fad[c] -> 12 h[c] + 12 nadh[c] + 13 accoa[c] + 12 fadh2[c]	Fatty Acid Metabolism
Fatty acid Oxidation Pathway2, Lumped	2 h2o[c] + 2 nad[c] + 2 coa[c] + hexacoa[c] + 2 fad[c] -> 2 h[c] + 2 nadh[c] + 3 accoa[c] + 2 fadh2[c]	Fatty Acid Metabolism
Fatty acid Oxidation Pathway2, Lumped	3 h2o[c] + 3 nad[c] + 3 coa[c] + octacoa[c] + 3 fad[c] -> 3 h[c] + 3 nadh[c] + 4 accoa[c] + 3 fadh2[c]	Fatty Acid Metabolism

Fatty acid Oxidation Pathway1, Lumped	4 h2o[c] + 4 nad[c] + 4 o2[c] + 4 coa[c] + dcacoa[c] -> 4 h[c] + 4 nadh[c] + 4 h2o2[c] + 5 accoa[c]	Fatty Acid Metabolism
Fatty acid Oxidation Pathway1, Lumped	5 h2o[c] + 5 nad[c] + 5 o2[c] + 5 coa[c] + ddcacoa[c] -> 5 h[c] + 5 nadh[c] + 5 h2o2[c] + 6 accoa[c]	Fatty Acid Metabolism
Fatty acid Oxidation Pathway1, Lumped	6 h2o[c] + 6 nad[c] + 6 o2[c] + 6 coa[c] + tdcoa[c] -> 6 h[c] + 6 nadh[c] + 6 h2o2[c] + 7 accoa[c]	Fatty Acid Metabolism
Fatty acid Oxidation Pathway1, Lumped	7 h2o[c] + 7 nad[c] + 7 o2[c] + 7 coa[c] + pmtcoa[c] -> 7 h[c] + 7 nadh[c] + 7 h2o2[c] + 8 accoa[c]	Fatty Acid Metabolism
Fatty acid oxidation	nadph[c] + 7 h2o[c] + 7 nad[c] + 7 o2[c] + 7 coa[c] + hdceacoa[c] -> nadp[c] + 6 h[c] + 7 nadh[c] + 7 h2o2[c] + 8 accoa[c]	Fatty Acid Metabolism
Fatty acid oxidation	7 h2o[c] + 7 nad[c] + 6 o2[c] + 7 coa[c] + hdceacoa[c] -> 7 h[c] + 7 nadh[c] + 6 h2o2[c] + 8 accoa[c]	Fatty Acid Metabolism
Fatty acid Oxidation Pathway1, Lumped	6 h2o[c] + 6 nad[c] + 6 o2[c] + 6 coa[c] + hepdcacoa[c] -> 6 h[c] + 6 nadh[c] + 6 h2o2[c] + 7 accoa[c] + ppcoa[c]	Fatty Acid Metabolism
Fatty acid oxidation	nadph[c] + 7 h2o[c] + 7 nad[c] + 7 o2[c] + 7 coa[c] + hepdceacoa[c] -> nadp[c] + 6 h[c] + 7 nadh[c] + 7 h2o2[c] + 7 accoa[c] + ppcoa[c]	Fatty Acid Metabolism
Fatty acid oxidation	7 h2o[c] + 7 nad[c] + 6 o2[c] + 7 coa[c] + hepdceacoa[c] -> 7 h[c] + 7 nadh[c] + 6 h2o2[c] + 7 accoa[c] + ppcoa[c]	Fatty Acid Metabolism
Fatty acid Oxidation Pathway1, Lumped	8 h2o[c] + 8 nad[c] + 8 o2[c] + 8 coa[c] + stcoa[c] -> 8 h[c] + 8 nadh[c] + 8 h2o2[c] + 9 accoa[c]	Fatty Acid Metabolism
Fatty acid oxidation	nadph[c] + 8 h2o[c] + 8 nad[c] + 8 o2[c] + 8 coa[c] + ocdceacoa[c] -> nadp[c] + 7 h[c] + 8 nadh[c] + 8 h2o2[c] + 9 accoa[c]	Fatty Acid Metabolism
Fatty acid oxidation	8 h2o[c] + 8 nad[c] + 7 o2[c] + 8 coa[c] + ocdceacoa[c] -> 8 h[c] + 8 nadh[c] + 7 h2o2[c] + 9 accoa[c]	Fatty Acid Metabolism

Fatty acid oxidation	2 nadph[c] + 8 h2o[c] + 8 nad[c] + 8 o2[c] + 8 coa[c] + ocdcyacoa[c] -> 2 nadp[c] + 6 h[c] + 8 nadh[c] + 8 h2o2[c] + 9 accoa[c]	Fatty Acid Metabolism
Fatty acid oxidation	nadph[c] + 8 h2o[c] + 8 nad[c] + 7 o2[c] + 8 coa[c] + ocdcyacoa[c] -> nadp[c] + 7 h[c] + 8 nadh[c] + 7 h2o2[c] + 9 accoa[c]	Fatty Acid Metabolism
Fatty acid oxidation	8 h2o[c] + 8 nad[c] + 6 o2[c] + 8 coa[c] + ocdcyacoa[c] -> 8 h[c] + 8 nadh[c] + 6 h2o2[c] + 9 accoa[c]	Fatty Acid Metabolism
Fatty acid oxidation	3 nadph[c] + 8 h2o[c] + 8 nad[c] + 9 o2[c] + 8 coa[c] + ocdctacoa[c] -> 3 nadp[c] + 5 h[c] + 8 nadh[c] + 9 h2o2[c] + 9 accoa[c]	Fatty Acid Metabolism
Fatty acid Oxidation Pathway1, Lumped	9 h2o[c] + 9 nad[c] + 9 o2[c] + 9 coa[c] + eicosacoa[c] -> 9 h[c] + 9 nadh[c] + 9 h2o2[c] + 10 accoa[c]	Fatty Acid Metabolism
Fatty acid oxidation	5 nadph[c] + 9 h2o[c] + 9 nad[c] + 14 o2[c] + 9 coa[c] + eicosapencoa[c] -> 5 nadp[c] + 4 h[c] + 9 nadh[c] + 14 h2o2[c] + 10 accoa[c]	Fatty Acid Metabolism
Fatty acid Oxidation Pathway1, Lumped	10 h2o[c] + 10 nad[c] + 10 o2[c] + 10 coa[c] + docosacoa[c] -> 10 h[c] + 10 nadh[c] + 10 h2o2[c] + 11 accoa[c]	Fatty Acid Metabolism
Fatty acid Oxidation Pathway1, Lumped	11 h2o[c] + 11 nad[c] + 11 o2[c] + 11 coa[c] + ttccoa[c] -> 11 h[c] + 11 nadh[c] + 11 h2o2[c] + 12 accoa[c]	Fatty Acid Metabolism
Fatty acid Oxidation Pathway1, Lumped	12 h2o[c] + 12 nad[c] + 12 o2[c] + 12 coa[c] + hexccoa[c] -> 12 h[c] + 12 nadh[c] + 12 h2o2[c] + 13 accoa[c]	Fatty Acid Metabolism
Fatty acid Oxidation Pathway1, Lumped	2 h2o[c] + 2 nad[c] + 2 o2[c] + 2 coa[c] + hexacoa[c] -> 2 h[c] + 2 nadh[c] + 2 h2o2[c] + 3 accoa[c]	Fatty Acid Metabolism
Fatty acid Oxidation Pathway1, Lumped	3 h2o[c] + 3 nad[c] + 3 o2[c] + 3 coa[c] + octacoa[c] -> 3 h[c] + 3 nadh[c] + 3 h2o2[c] + 4 accoa[c]	Fatty Acid Metabolism
fatty-acid--CoA ligase (dodecanoate)	atp[c] + coa[c] + ddca[c] <=> amp[c] + ppi[c] + ddcacoa[c]	Fatty Acid Metabolism
fatty-acid--CoA ligase (eicosanoate)	atp[c] + coa[c] + eicosa[c] <=> amp[c] + ppi[c] + eicosacoa[c]	Fatty Acid Metabolism

fatty-acid--CoA ligase (docosanoate)	atp[c] + coa[c] + docosa[c] <=> amp[c] + ppi[c] + docosacoa[c]	Fatty Acid Metabolism
fatty-acid--CoA ligase (ttc)	atp[c] + coa[c] + ttc[c] <=> amp[c] + ppi[c] + ttccoa[c]	Fatty Acid Metabolism
fatty-acid--CoA ligase (hexc)	atp[c] + coa[c] + hexc[c] <=> amp[c] + ppi[c] + hexccoa[c]	Fatty Acid Metabolism
fatty-acid--CoA ligase (octanoate)	atp[c] + coa[c] + octa[c] <=> amp[c] + ppi[c] + octacoa[c]	Fatty Acid Metabolism
Oleoyl-CoA desaturase (n-C18:1CoA -> n-C18:2CoA)	h[c] + nadph[c] + o2[c] + ocdceacoa[c] -> nadp[c] + 2 h2o[c] + ocdcyacoa[c]	Fatty Acid Metabolism
GTP cyclohydrolase I	h2o[c] + gtp[c] -> h[c] + for[c] + ahdt[c]	Folate Metabolism
5-formethyltetrahydrofolate cyclo-ligase	atp[c] + 5fthf[c] -> adp[c] + pi[c] + methf[c]	Folate Metabolism
dihydrofolate reductase (irreversible)	h[c] + nadph[c] + dhf[c] -> nadp[c] + thf[c]	Folate Metabolism
4-aminobenzoate synthase	4adcho[c] -> h[c] + pyr[c] + 4abz[c]	Folate Metabolism
alkaline phosphatase (Dihydroneopterin)	3 h2o[c] + ahdt[c] -> 2 h[c] + 3 pi[c] + dhnpt[c]	Folate Metabolism
Tetrahydrofolate:L-glutamate gamma-ligase (ADP-forming)	atp[c] + glu-L[c] + thf[c] <=> h[c] + adp[c] + pi[c] + thfglu[c]	Folate Metabolism
dihydroneopterin aldolase	dhnpt[c] -> h[c] + 2ahhmp[c] + gcald[c]	Folate Metabolism
dihydropteroate synthase	4abz[c] + 2ahhmp[c] -> h2o[c] + dhpt[c]	Folate Metabolism
dihydropteroate synthase	4abz[c] + 2ahhmd[c] -> ppi[c] + dhpt[c]	Folate Metabolism
2-amino-4-hydroxy-6-hydroxymethyldihydropteridine diphosphokinase, mitochondrial	atp[c] + 2ahhmp[c] -> h[c] + amp[c] + 2ahhmd[c]	Folate Metabolism
5,10-methylenetetrahydrofolate reductase	2 h[c] + nadph[c] + mlthf[c] -> nadp[c] + 5mthf[c]	Folate Metabolism
methylenetetrahydrofolate dehydrogenase (NAD)	nad[c] + mlthf[c] -> nadh[c] + methf[c]	Folate Metabolism
4-amino-4-deoxychorismate synthase	gln-L[c] + chor[c] -> glu-L[c] + 4adcho[c]	Folate Metabolism
formate-tetrahydrofolate ligase, mitochondrial	atp[m] + for[m] + thf[m] -> adp[m] + pi[m] + 10fthf[m]	Folate Metabolism
methenyltetrahydrifikate cyclohydrolase, mitochondrial	h2o[m] + methf[m] <=> h[m] + 10fthf[m]	Folate Metabolism

methylenetetrahydrofolate dehydrogenase (NADP), mitochondrial	nadp[m] + mlthf[m] <=> nadph[m] + methf[m]	Folate Metabolism
Methylenetetrahydrofolate dehydrogenase (NADP)	nadp[c] + mlthf[c] <=> nadph[c] + methf[c]	Folate Metabolism
tetrahydrofolate aminomethyltransferase, mitochondrial	h2o[m] + methf[m] -> h[m] + 5fthf[m]	Folate Metabolism
formate-tetrahydrofolate ligase	atp[c] + for[c] + thf[c] -> adp[c] + pi[c] + 10fthf[c]	Folate Metabolism
methenyltetrahydrofolate cyclohydrolase	h2o[c] + methf[c] <=> h[c] + 10fthf[c]	Folate Metabolism
aspartate oxidase	fad[m] + asp-L[c] -> fadh2[m] + h[c] + iasp[c]	Folate Metabolism
dihydrofolate synthase	atp[c] + glu-L[c] + dhpt[c] -> h[c] + adp[c] + pi[c] + dhf[c]	Folate Metabolism
5-formethyltetrahydrofolate cyclo-ligase, mitochondrial	atp[m] + 5fthf[m] -> adp[m] + pi[m] + methf[m]	Folate Metabolism
L-Fuculose Phosphate Aldolase	fuc1p[c] <=> dhap[c] + lald-S[c]	Fructose and Mannose Metabolism
hexokinase (D-mannose:ATP)	atp[c] + man[c] -> h[c] + adp[c] + man6p[c]	Fructose and mannose metabolism
hexokinase (D-fructose:ATP)	atp[c] + fru[c] -> h[c] + adp[c] + f6p[c]	Fructose and mannose metabolism
hexokinase (beta D-fructose:ATP)	atp[c] + fru[c] -> h[c] + adp[c] + bf6p[c]	Fructose and mannose metabolism
D-sorbitol dehydrogenase (D-fructose producing)	nad[c] + sbt-D[c] -> h[c] + nadh[c] + fru[c]	Fructose and Mannose Metabolism
L-sorbitol dehydrogenase (L-sorbose-producing)	nad[c] + sbt-L[c] -> h[c] + nadh[c] + srb-L[c]	Fructose and Mannose Metabolism
Fructose-2,6-bisphosphatase	h2o[c] + bf26p[c] -> pi[c] + bf6p[c]	Fructose and mannose metabolism
Fructose-2,6-bisphosphatase 1	h2o[c] + bf26p[c] -> pi[c] + f6p[c]	Fructose and mannose metabolism
6-Phosphofructo-2-Kinase	atp[c] + bf6p[c] <=> h[c] + adp[c] + bf26p[c]	Fructose and Mannose Metabolism
Mannose-6-phosphate isomerase	man6p[c] <=> f6p[c]	Fructose and Mannose Metabolism
Mannose-1-phosphate guanylyltransferase	h[c] + gtp[c] + man1p[c] -> ppi[c] + gdpmann[c]	Fructose and Mannose Metabolism
Phosphomannomutase	man1p[c] <=> man6p[c]	Fructose and Mannose Metabolism

L-KDR aldolase	23drhamn[c] -> pyr[c] + lald-S[c]	Fructose and Mannose Metabolism
Lactaldehyde Dehydrogenase	nad[c] + lald-S[c] <=> h[c] + nadh[c] + lac-L[c]	Fructose and Mannose Metabolism
Mannitol dehydrogenase	nad[c] + mnl[c] -> h[c] + nadh[c] + fru[c]	Fructose and Mannose Metabolism
L-Rhamnonate dehydratase	rhamn[c] -> h2o[c] + 23drhamn[c]	Fructose and Mannose Metabolism
Rhamnose dehydrogenase	nad[c] + rham-L[c] -> h[c] + nadh[c] + rhamlac[c]	Fructose and Mannose Metabolism
L-Rhamnono-lactonase	h2o[c] + rhamlac[c] -> rhamn[c]	Fructose and Mannose Metabolism
D-sorbitol reductase	h[c] + nadph[c] + glc-D[c] -> nadp[c] + sbt-D[c]	Fructose and mannose metabolism
Lactase (Beta- Galactosidase)	h2o[c] + lact[c] -> glc-D[c] + gal[c]	Galactose Metabolism
UDPglucose--hexose-1-phosphate uridylyltransferase	gal1p[c] + udpg[c] <=> g1p[c] + udpgal[c]	Galactose Metabolism
Galactokinase	atp[c] + gal[c] -> h[c] + adp[c] + gal1p[c]	Galactose Metabolism
Galactose Dehydrogenase	nad[c] + gal[c] <=> h[c] + nadh[c] + gal14lac[c]	Galactose metabolism
Alpha Glucosidase Maltase	h2o[c] + maltr[c] -> glc-D[c] + malt[c]	Galactose metabolism
UDPglucose 4-epimerase	udpg[c] <=> udpgal[c]	Galactose metabolism
glutathione peridoxase	h2o2[c] + 2 gthrd[c] <=> 2 h2o[c] + gthox[c]	Glutathione Metabolism
Non-Specific Peptidase	h2o[c] + cgly[c] -> cys-L[c] + gly[c]	Glutathione metabolism
glutathione oxidoreductase	h[c] + nadph[c] + gthox[c] -> nadp[c] + 2 gthrd[c]	Glutathione Metabolism
glutathione synthetase	atp[c] + gly[c] + glucys[c] -> h[c] + adp[c] + pi[c] + gthrd[c]	Glutathione Metabolism
g-glutamyltransferase	ala-L[c] + gthrd[c] -> gluala[c] + cgly[c]	Glutathione Metabolism
gamma-glutamylcysteine synthetase	atp[c] + glu-L[c] + cys-L[c] -> h[c] + adp[c] + pi[c] + glucys[c]	Glutathione Metabolism
Oxoprolinase	2 h2o[c] + atp[c] + opro-L[c] <=> adp[c] + pi[c] + glu-L[c]	Glutathione Metabolism
Dolichyl phosphate mannose protein mannosyltransferase endoplasmic reticular	dolmanp[c] -> h[c] + dolp[c] + mannan[c]	glycan
Dolichol kinase	ctp[c] + dolichol[c] -> h[c] + dolp[c] + cdp[c]	glycan

Dolichyl-phosphate D-mannosyltransferase	gdpmann[c] + dolp[c] -> dolmanp[c] + gdp[c]	glycan
Triacylglycerol lipase	h2o[c] + 0.01 triglyc[c] -> 0.019 dca[c] + 0.058 ttdca[c] + 0.18 hdca[c] + 0.078 hdcea[c] + 0.035 ocdca[c] + 0.315 ocdcea[c] + 0.094 ocdcya[c] + 0.012 ocdcta[c] + 0.011 eicosapen[c] + 0.028 hexa[c] + 0.115 ddca[c] + 0.01 docosa[c] + 0.023 octa[c] + 0.01 12dgr[c]	Glycerolipid Metabolism
Dihydroxyacetone kinase	atp[c] + dha[c] -> h[c] + adp[c] + dhap[c]	Glycerolipid Metabolism
Glycerol-3-phosphatase	h2o[c] + glyc3p[c] -> pi[c] + glyc[c]	Glycerolipid Metabolism
Glycerol 3 phosphate acyltransferase - glycerol 3 phosphate	0.019 dcacoa[c] + 0.058 tdcoa[c] + 0.18 pmtcoa[c] + 0.078 hdceacoa[c] + 0.035 stcoa[c] + 0.315 ocdceacoa[c] + 0.094 ocdcyacoa[c] + 0.012 ocdctacoa[c] + 0.011 eicosapencoa[c] + 0.028 hexacoa[c] + 0.023 octacoa[c] + 0.115 ddcacoa[c] + 0.01 docosacoa[c] + glyc3p[c] -> coa[c] + 0.01 1ag3p[c]	Glycerolipid Metabolism
Glycerol 3 phosphate acyltransferase - glycerone phosphate	0.019 dcacoa[c] + 0.058 tdcoa[c] + 0.18 pmtcoa[c] + 0.078 hdceacoa[c] + 0.035 stcoa[c] + 0.315 ocdceacoa[c] + 0.094 ocdcyacoa[c] + 0.012 ocdctacoa[c] + 0.011 eicosapencoa[c] + 0.028 hexacoa[c] + 0.023 octacoa[c] + 0.115 ddcacoa[c] + 0.01 docosacoa[c] + dhap[c] -> coa[c] + 0.01 1agly3p[c]	Glycerolipid Metabolism
1-Acyl-glycerol-3-phosphate acyltransferase,	0.019 dcacoa[c] + 0.058 tdcoa[c] + 0.18 pmtcoa[c] + 0.078 hdceacoa[c] + 0.035 stcoa[c] + 0.315 ocdceacoa[c] + 0.094 ocdcyacoa[c] + 0.012 ocdctacoa[c] + 0.011 eicosapencoa[c] + 0.028 hexacoa[c] + 0.023 octacoa[c] + 0.115 ddcacoa[c] + 0.01 docosacoa[c] + 0.01 1ag3p[c] -> coa[c] + 0.01 pa[c]	Glycerolipid Metabolism
Glycerol kinase	atp[c] + glyc[c] -> h[c] + adp[c] + glyc3p[c]	Glycerolipid Metabolism

Diacylglycerol pyrophosphate phosphatase	h2o[c] + 0.01 pa[c] -> pi[c] + 0.01 12dgr[c]	Glycerolipid Metabolism
Phosphatidylcholine-diacylglycerol acyltransferase	12dgr[c] + pc[c] -> triglyc[c] + 1agpc[c]	Glycerolipid Metabolism
Phospholipase D	h2o[c] + 0.01 pc[c] -> h[c] + chol[c] + 0.01 pa[c]	Glycerolipid Metabolism
Triglycerol synthesis	0.019 dcacoa[c] + 0.058 tdcoa[c] + 0.18 pmtcoa[c] + 0.078 hdceacoa[c] + 0.035 stcoa[c] + 0.315 ocdceacoa[c] + 0.094 ocdcyacoa[c] + 0.012 ocdctacoa[c] + 0.011 eicosapencoa[c] + 0.028 hexacoa[c] + 0.023 octacoa[c] + 0.115 ddcacoa[c] + 0.01 docosacoa[c] + 0.01 12dgr[c] -> coa[c] + 0.01 triglyc[c]	Glycerolipid Metabolism
Phospholipase D	chol[c] + cdpdag[c] <=> pc[c] + cmp[c]	Glycerolipid Metabolism
glycerol-3-phosphate dehydrogenase (NAD)	h[c] + nadh[c] + dhap[c] -> nad[c] + glyc3p[c]	Glycerophospholipid metabolism
glycerol-3-phosphate dehydrogenase (FAD), mitochondrial	fad[m] + glyc3p[m] -> fadh2[m] + dhap[m]	Glycerophospholipid metabolism
Phosphatidylserine decarboxylase Mitochondrial	h[m] + 0.01 ps[m] -> co2[m] + 0.01 pe[m]	Glycerophospholipid metabolism
Phosphatidylserine decarboxylase	h[c] + 0.01 ps[c] -> co2[c] + 0.01 pe[c]	Glycerophospholipid metabolism
Phosphatidylserine synthase, mitochondrial	0.01 cdpdag[m] + ser-L[m] <=> h[m] + 0.01 ps[m] + cmp[m]	Glycerophospholipid metabolism
Ethanolamine kinase	atp[c] + etha[c] -> h[c] + adp[c] + ethamp[c]	Glycerophospholipid metabolism
Phosphoethanolamine cytidyltransferase	h[c] + ctp[c] + ethamp[c] -> ppi[c] + cdpea[c]	Glycerophospholipid metabolism
methylene-fatty-acyl-phospholipid synthase,	amet[c] + 0.01 ptdmeeta[c] -> h[c] + ahcys[c] + 0.01 ptd2meeta[c]	Glycerophospholipid metabolism
Choline kinase	chol[c] + atp[c] -> h[c] + adp[c] + cholp[c]	Glycerophospholipid metabolism
Choline phosphate cytididyltransferase	h[c] + ctp[c] + cholp[c] -> ppi[c] + cdpchol[c]	Glycerophospholipid metabolism
CDP diacylglycerol serine O phosphatidyltransferase mitochondrial	glyc3p[m] + 0.01 cdpdag[m] <=> h[m] + cmp[m] + 0.01 pgp[m]	Glycerophospholipid metabolism
phosphatidylglycerol phosphate phosphatase A, , mitochondrial	h2o[m] + 0.01 pgp[m] -> pi[m] + 0.01 pg[m]	Glycerophospholipid metabolism

Phosphatidyl-N-methylethanolamine N-methyltransferase,	amet[c] + 0.01 ptd2meeta[c] -> h[c] + ahcys[c] + 0.01 pc[c]	Glycerophospholipid metabolism
1-Phosphatidyl-D-myo-inositol inositolphosphohydrolase	h2o[c] + ptd1ino[c] <=> 12dgr[c] + mi1p-D[c]	Glycerophospholipid metabolism
CDP-diacylglycerol:L-serine 3-phosphatidyltransferase	ser-L[c] + 0.01 cdpdag[c] <=> 0.01 ps[c] + cmp[c]	Glycerophospholipid metabolism
Phosphoserine transaminase	glu-L[c] + 3php[c] -> akg[c] + pser-L[c]	Glycine, serine and threonine metabolism
Phosphoserine phosphatase (L-serine)	h2o[c] + pser-L[c] -> pi[c] + ser-L[c]	Glycine, serine and threonine metabolism
Alanine glyoxylate aminotransferase (irreversible)	ala-L[c] + glx[c] -> pyr[c] + gly[c]	Glycine, serine and threonine metabolism
Homoserine dehydrogenase (NADP)	h[c] + nadph[c] + aspsa[c] -> nadp[c] + hom-L[c]	Glycine, serine and threonine metabolism
Threonine synthase	h2o[c] + phom[c] -> pi[c] + thr-L[c]	Glycine, serine and threonine metabolism
Threonine aldolase	acald[c] + gly[c] -> thr-L[c]	Glycine, serine and threonine metabolism
Glycine-cleavage complex (lipoamide), mitochondrial	h[m] + gly[m] + lpam[m] <=> co2[m] + alpam[m]	Glycine, serine and threonine metabolism
Glycine-cleavage system (lipoamide) irreversible, mitochondrial	thf[m] + alpam[m] -> mlthf[m] + dhlam[m] + nh4[m]	Glycine, serine and threonine metabolism
Glycine-cleavage complex (lipoamide), mitochondrial	nad[m] + dhlam[m] <=> h[m] + nadh[m] + lpam[m]	Glycine, serine and threonine metabolism
Cystathionine beta-synthase	hcys-L[c] + ser-L[c] -> h2o[c] + cyst-L[c]	Glycine, serine and threonine metabolism
L-threonine deaminase	thr-L[c] -> nh4[c] + 2obut[c]	Glycine, serine and threonine metabolism
Homoserine kinase	atp[c] + hom-L[c] -> h[c] + adp[c] + phom[c]	Glycine, serine and threonine metabolism
Phosphoglycerate dehydrogenase	nad[c] + 3pg[c] -> h[c] + nadh[c] + 3php[c]	Glycine, serine and threonine metabolism
5-aminolevulinate synthase, mitochondrial	succoa[m] + h[m] + gly[m] -> coa[m] + co2[m] + 5aop[m]	Glycine, serine and threonine metabolism
hexokinase (D-glucose:ATP)	atp[c] + glc-D[c] -> h[c] + adp[c] + g6p[c]	Glycolysis/Gluconeogenesis
Diphosphoglycerate mutase	13dpg[c] <=> h[c] + 23dph[c]	Glycolysis/Gluconeogenesis
Phosphoglycerate mutase	2pg[c] <=> 3pg[c]	Glycolysis/Gluconeogenesis

Fructose-1,6-bisphosphatase	h2o[c] + fdp[c] -> pi[c] + f6p[c]	Glycolysis/Gluconeogenesis
Phosphofructokinase	atp[c] + f6p[c] -> h[c] + adp[c] + fdp[c]	Glycolysis/Gluconeogenesis
Enolase	2pg[c] <=> h2o[c] + pep[c]	Glycolysis/Gluconeogenesis
Glyceraldehyde-3-phosphate dehydrogenase	nad[c] + pi[c] + g3p[c] <=> h[c] + nadh[c] + 13dpg[c]	Glycolysis/Gluconeogenesis
Phosphoglycerate kinase	atp[c] + 3pg[c] <=> adp[c] + 13dpg[c]	Glycolysis/Gluconeogenesis
Pyruvate kinase	h[c] + adp[c] + pep[c] -> pyr[c] + atp[c]	Glycolysis/Gluconeogenesis
Glucose-6-phosphate isomerase	g6p[c] <=> f6p[c]	Glycolysis/Gluconeogenesis
Fructose-bisphosphate aldolase	fdp[c] <=> dhap[c] + g3p[c]	Glycolysis/Gluconeogenesis
Triose-phosphate isomerase	dhap[c] <=> g3p[c]	Glycolysis/Gluconeogenesis
Formamidase	h2o[c] + frmd[c] -> nh4[c] + for[c]	Glyoxalate and Dicarboxylate Metabolism
Formate dehydrogenase	nad[c] + for[c] -> nadh[c] + co2[c]	Glyoxalate and Dicarboxylate Metabolism
Isocitrate lyase	icit[c] -> succ[c] + glx[c]	Glyoxalate and Dicarboxylate Metabolism
Phosphoglycolate phosphatase	h2o[c] + 2pglyc[c] -> pi[c] + glyclt[c]	Glyoxalate and Dicarboxylate Metabolism
Histidinol-phosphatase	h2o[c] + hisp[c] -> pi[c] + histd[c]	Histidine Metabolism
Imidazole-4-carboxamide isomerase	prfp[c] -> prlp[c]	Histidine Metabolism
Imidazole-glycerol-3-phosphate synthase	gln-L[c] + prlp[c] -> h[c] + glu-L[c] + aicar[c] + eig3p[c]	Histidine Metabolism
ATP phosphoribosyltransferase	atp[c] + prpp[c] -> ppi[c] + prbatp[c]	Histidine Metabolism
Histidinol dehydrogenase	h2o[c] + 2 nad[c] + histd[c] -> 3 h[c] + 2 nadh[c] + his-L[c]	Histidine Metabolism
Phosphoribosyl-AMP cyclohydrolase	h2o[c] + prbamp[c] -> prfp[c]	Histidine Metabolism
Phosphoribosyl-ATP pyrophosphatase	h2o[c] + prbatp[c] -> h[c] + ppi[c] + prbamp[c]	Histidine Metabolism
Imidazoleglycerol-phosphate dehydratase	eig3p[c] -> h2o[c] + imacp[c]	Histidine Metabolism

Histidinol-phosphate transaminase	glu-L[c] + imacp[c] -> akg[c] + hisp[c]	Histidine metabolism
Phosphatidylinositol synthase	0.01 cdpdag[c] + inost[c] -> h[c] + cmp[c] + 0.01 ptd1ino[c]	Inositol Phosphate Metabolism
Myo-Inositol-1-phosphate synthase	g6p[c] -> mi1p-D[c]	Inositol Phosphate Metabolism
1-phosphatidylinositol 3-kinase	atp[c] + 0.01 ptd1ino[c] -> h[c] + adp[c] + 0.01 ptd3ino[c]	Inositol Phosphate Metabolism
1-phosphatidylinositol-4,5-bisphosphate phosphodiesterase	h2o[c] + 0.01 ptd145bp[c] -> h[c] + 0.01 12dgr[c] + mi145tp-D[c]	Inositol Phosphate Metabolism
Phosphatidylinositol 4-kinase	atp[c] + 0.01 ptd1ino[c] -> h[c] + adp[c] + 0.01 ptd4ino[c]	Inositol Phosphate Metabolism
Inositol-1,4,5-trisphosphate 5-phosphatase	h2o[c] + mi145tp-D[c] -> pi[c] + mi14bp-D[c]	Inositol Phosphate Metabolism
Phosphatidylinositol-3-phosphate 4-kinase	atp[c] + 0.01 ptd3ino[c] -> h[c] + adp[c] + 0.01 ptd134bp[c]	Inositol Phosphate Metabolism
Inositol 2-dehydrogenase	nad[c] + inost[c] -> h[c] + nadh[c] + 2ins[c]	Inositol Phosphate Metabolism
Phosphatidylinositol-4-phosphate 5-kinase	atp[c] + 0.01 ptd4ino[c] -> h[c] + adp[c] + 0.01 ptd145bp[c]	Inositol Phosphate Metabolism
Homoisocitrate dehydrogenase, mitochondrial	nad[m] + hicit[m] <=> h[m] + nadh[m] + oxag[m]	Lysine Biosynthesis
Dihydrodipicolinate synthase	pyr[c] + aspsa[c] -> h[c] + 2 h2o[c] + 23dhdp[c]	Lysine Biosynthesis
2-aminoadipate transaminase	glu-L[c] + 2oxoadp[c] <=> akg[c] + L2aadp[c]	Lysine Biosynthesis
L-aminoadipate-semialdehyde dehydrogenase (NADPH)	h[c] + nadph[c] + atp[c] + L2aadp[c] -> nadp[c] + amp[c] + ppi[c] + L2aadp6sa[c]	Lysine Biosynthesis
L-aminoadipate-semialdehyde dehydrogenase (NADH)	h[c] + nadh[c] + atp[c] + L2aadp[c] -> nad[c] + amp[c] + ppi[c] + L2aadp6sa[c]	Lysine Biosynthesis
Saccharopine dehydrogenase (NADP, L-glutamate forming)	h[c] + nadph[c] + glu-L[c] + L2aadp6sa[c] <=> nadp[c] + h2o[c] + saccrp-L[c]	Lysine Biosynthesis
2-oxoadipate dehydrogenase	coa[m] + nad[m] + oxag[m] <=> h[m] + nadh[m] + co2[m] + glucoa[m]	Lysine Biosynthesis
Saccharopine dehydrogenase (NAD, L-lysine forming)	h2o[c] + nad[c] + saccrp-L[c] <=> h[c] + nadh[c] + akg[c] + lys-L[c]	Lysine Biosynthesis
Homoacontinate hydratase, mitochondrial	h2o[m] + b124tc[m] <=> hicit[m]	Lysine Biosynthesis
non-enzymatic reaction, mitochondrial	h[m] + oxag[m] <=> co2[m] + 2oxoadp[m]	Lysine Biosynthesis

ribosylnicotinamide kinase	atp[c] + rnam[c] -> h[c] + adp[c] + nmn[c]	NAD Biosynthesis
NAD nucleosidase	h2o[c] + nad[c] -> h[c] + adprib[c] + ncam[c]	NAD Biosynthesis
NAD nucleosidase, mitochondrial	h2o[m] + nad[m] -> h[m] + adprib[m] + ncam[m]	NAD Biosynthesis
nicotinamidase, reversible, mitochondrial	h2o[m] + ncam[m] <=> nh4[m] + nac[m]	NAD Biosynthesis
purine-nucleoside phosphorylase	pi[c] + rnam[c] <=> h[c] + ncam[c] + r1p[c]	NAD Biosynthesis
quinolinate synthase	iasp[c] + dhap[c] -> 2 h2o[c] + pi[c] + quln[c]	Nicotinate and nicotinamide metabolism
Nicotinamidase, reversible	h2o[c] + ncam[c] <=> nh4[c] + nac[c]	Nicotinate and nicotinamide metabolism
Nicotinate-nucleotide diphosphorylase (carboxylating)	2 h[c] + prpp[c] + quln[c] -> ppi[c] + co2[c] + nicrnt[c]	Nicotinate and nicotinamide metabolism
NAD synthase (nh4)	atp[c] + nh4[c] + dnad[c] -> h[c] + nad[c] + amp[c] + ppi[c]	Nicotinate and nicotinamide metabolism
NAD synthase (glutamine)	h2o[c] + atp[c] + gln-L[c] + dnad[c] -> nad[c] + amp[c] + ppi[c] + glu-L[c]	Nicotinate and nicotinamide metabolism
NAD kinase	nad[c] + atp[c] -> nadp[c] + h[c] + adp[c]	Nicotinate and nicotinamide metabolism
Nicotinate-nucleotide adenylyltransferase	h[c] + atp[c] + nicrnt[c] -> ppi[c] + dnad[c]	Nicotinate and nicotinamide metabolism
Nicotinamide-nucleotide adenylyltransferase, mitochondrial	h[c] + atp[c] + nmn[c] -> nad[c] + ppi[c]	Nicotinate and nicotinamide metabolism
NAPRTase	h[c] + prpp[c] + nac[c] -> ppi[c] + nicrnt[c]	Nicotinate and nicotinamide metabolism
Nitrilase	2 h2o[c] + aprop[c] -> ala-L[c] + nh4[c]	Nitrogen Metabolism
Nitrilase	2 h2o[c] + acybut[c] -> glu-L[c] + nh4[c]	Nitrogen Metabolism
ribonucleoside-triphosphate reductase (ATP)	atp[c] + trdrd[c] -> h2o[c] + datp[c] + trdox[c]	Nucleotide Salvage Pathway
ribonucleoside-triphosphate reductase (GTP)	gtp[c] + trdrd[c] -> h2o[c] + trdox[c] + dgtp[c]	Nucleotide Salvage Pathway
ribonucleoside-triphosphate reductase (CTP)	ctp[c] + trdrd[c] -> h2o[c] + trdox[c] + dctp[c]	Nucleotide Salvage Pathway
ribonucleoside-triphosphate reductase (UTP)	utp[c] + trdrd[c] -> h2o[c] + trdox[c] + dutp[c]	Nucleotide Salvage Pathway

Adenine Deaminase	h[c] + h2o[c] + ade[c] -> nh4[c] + hxan[c]	Nucleotide Salvage Pathway
Phosphopentomutase	2dr1p[c] <=> 2dr5p[c]	Nucleotide Salvage Pathway
CMP nucleosidase	h2o[c] + cmp[c] -> csn[c] + r5p[c]	Nucleotide Salvage Pathway
Deoxyribose-phosphate aldolase	2dr5p[c] <=> acald[c] + g3p[c]	Nucleotide Salvage Pathway
guanosine kinase	atp[c] + gsn[c] -> h[c] + adp[c] + gmp[c]	Nucleotide Salvage Pathway
insosine kinase	atp[c] + ins[c] -> h[c] + adp[c] + imp[c]	Nucleotide Salvage Pathway
thymidine kinase (ATP:thymidine)	atp[c] + thymd[c] -> h[c] + adp[c] + dtmp[c]	Nucleotide Salvage Pathway
Thymidine phosphorylase	pi[c] + thymd[c] <=> 2dr1p[c] + thym[c]	Nucleotide Salvage Pathway
Glycine hydroxymethyltransferase, reversible, mitochondrial	thf[m] + ser-L[m] <=> h2o[m] + mlthf[m] + gly[m]	One carbon pool by folate
Glycine hydroxymethyltransferase, reversible	thf[c] + ser-L[c] <=> h2o[c] + gly[c] + mlthf[c]	One carbon pool by folate
Adenosinetriphosphatase	h2o[c] + atp[c] -> h[c] + adp[c] + pi[c]	Oxidative phosphorylation
Succinate Dehydrogenase (Ubiquinone) Mitochondrial	succ[m] + q6[m] <=> fum[m] + q6h2[m]	Oxidative Phosphorylation
NADPH dehydrogenase	h[c] + nadph[c] + q6[m] -> nadp[c] + q6h2[m]	Oxidative Phosphorylation
Ubiquinol-6 cytochrome c reductase	2 h[m] + q6h2[m] + 2 ficytc[m] -> 4 h[c] + q6[m] + 2 focytc[m]	Oxidative Phosphorylation
NADPH Quinone reductase	h[m] + nadph[m] + q6[m] -> nadp[m] + q6h2[m]	Oxidative Phosphorylation
NADH dehydrogenase, with proton transport	5 h[m] + nadh[m] + q6[m] -> 4 h[c] + nad[m] + q6h2[m]	Oxidative Phosphorylation
NADPH-ferrihemoprotein reductase	nadph[c] + 2 ficytc[c] -> nadp[c] + h[c] + 2 focytc[c]	Oxidative Phosphorylation
Inorganic diphosphatase, mitochondrial	h2o[m] + ppi[m] -> 2 pi[m] + h[m]	Oxidative Phosphorylation
NADH dehydrogenase, cytoplasmic	h[c] + nadh[c] + q6[m] -> nad[c] + q6h2[m]	Oxidative Phosphorylation
Na+/K+-exchanging ATPase	h[c] + h2o[c] + atp[c] + k[e] -> adp[c] + pi[c] + h[e] + k[c]	Oxidative Phosphorylation

Na+/K+-exchanging ATPase	h[c] + h2o[c] + atp[c] + Na[e] -> adp[c] + pi[c] + h[e] + Na[c]	Oxidative Phosphorylation
Na+/K+-exchanging ATPase	h2o[c] + atp[c] + k[e] + Na[c] -> adp[c] + pi[c] + Na[e] + k[c]	Oxidative Phosphorylation
Succinate Dehydrogenase (Ubiquinone) Mitochondrial	fadh2[m] + q6[m] -> fad[m] + q6h2[m]	Oxidative phosphorylation
NADH dehydrogenase, mitochondrial	h[m] + nadh[m] + q6[m] -> nad[m] + q6h2[m]	Oxidative Phosphorylation
Cytochrome c peroxidase, mitochondrial	h2o2[c] + 2 focytc[c] -> 2 h2o[c] + 2 ficytc[c]	Oxidative Phosphorylation
Alternative oxidase	0.5 o2[m] + q6h2[m] -> h2o[m] + q6[m]	Oxidative Phosphorylation
ATP synthase, mitochondrial	adp[m] + pi[m] + 4 h[c] -> atp[m] + h2o[m] + 4 h[m]	Oxidative Phosphorylation
cytochrome c oxidase, mitochondrial	8 h[m] + o2[m] + 4 focytc[m] -> 4 h[c] + 2 h2o[m] + 4 ficytc[m]	Oxidative Phosphorylation
Inorganic diphosphatase	h2o[c] + ppi[c] -> h[c] + 2 pi[c]	Oxidative Phosphorylation
ATPase, cytosolic	h[c] + h2o[c] + atp[c] -> adp[c] + pi[c] + h[e]	Oxidative Phosphorylation
adenylate kinase (Inorganic triphosphate)	amp[c] + pppi[c] <=> adp[c] + ppi[c]	Oxidative Phosphorylation
Trimetaphosphate hydrolase	h2o[c] + tmp[c] <=> h[c] + pppi[c]	Oxidative Phosphorylation
GUANPRIBOSYLTRAN-RXN	prpp[c] + gua[c] <=> ppi[c] + gmp[c]	Oxidative Phosphorylation
purine nucleosidase	h2o[c] + gsn[c] <=> rib-D[c] + gua[c]	Oxidative Phosphorylation
polyamine oxidase	h2o[c] + o2[c] + N1aspmd[c] -> h2o2[c] + aproa[c] + aprut[c]	Pantothenate and CoA Biosynthesis
poylamine oxidase	h2o[c] + o2[c] + N1sprm[c] -> h2o2[c] + aproa[c] + N1aspmd[c]	Pantothenate and CoA Biosynthesis
poylamine oxidase	h2o[c] + o2[c] + sprm[c] -> h2o2[c] + aproa[c] + spmd[c]	Pantothenate and CoA Biosynthesis
3-methyl-2-oxobutanoate hydroxymethyltransferase	3mob[c] + h2o[c] + mlthf[c] -> thf[c] + 2dhp[c]	Pantotheonate and CoA metabolism
Dephospho-CoA kinase	atp[c] + dpcoa[c] -> h[c] + adp[c] + coa[c]	Pantotheonate and CoA metabolism
Pantetheine-phosphate adenylyltransferase	h[c] + atp[c] + pan4p[c] -> ppi[c] + dpcoa[c]	Pantotheonate and CoA metabolism
Phosphopantothenate-cysteine ligase	cys-L[c] + ctp[c] + 4ppan[c] -> h[c] + ppi[c] + cmp[c] + 4ppcys[c]	Pantotheonate and CoA metabolism
2-dehydropantoate 2-reductase, mitochondrial	h[m] + nadph[m] + 2dhp[m] -> nadp[m] + pant-R[m]	Pantotheonate and CoA metabolism
Pantothenate kinase	atp[c] + pnto-R[c] -> h[c] + adp[c] + 4ppan[c]	Pantotheonate and CoA metabolism

Pantothenate synthase	atp[c] + ala-B[c] + pant-R[c] -> h[c] + amp[c] + ppi[c] + pnto-R[c]	Pantotheonate and CoA metabolism
Phosphopantothenoylcysteine decarboxylase	h[c] + 4ppcys[c] -> co2[c] + pan4p[c]	Pantotheonate and CoA metabolism
Dihydroxy-acid dehydratase (2,3-dihydroxy-3-methylbutanoate), mitochondrial	23dhmb[m] -> h2o[m] + 3mob[m]	Pantotheonate and CoA metabolism
Acetohydroxy acid isomeroreductase, mitochondrial	h[m] + nadph[m] + alac-S[m] -> nadp[m] + 23dhmb[m]	Pantotheonate and CoA metabolism
Ribitol-2-Dehydrogenase	nad[c] + rbt[c] <=> h[c] + nadh[c] + rbl-D[c]	Pentose and glucuronate interconversions
Xylulokinase	atp[c] + xylu-D[c] -> h[c] + adp[c] + xu5p-D[c]	Pentose and glucuronate interconversions
D-Xylulose Reductase	h[c] + nadh[c] + xylu-D[c] <=> nad[c] + xylt[c]	Pentose and glucuronate interconversions
Xylose reductase	h[c] + nadph[c] + xyl-D[c] -> nadp[c] + xylt[c]	Pentose and glucuronate interconversions
Xylose reductase NADH	h[c] + nadh[c] + xyl-D[c] -> nad[c] + xylt[c]	Pentose and glucuronate interconversions
Xylose reductase Mixed	h[c] + 0.284 nadph[c] + 0.716 nadh[c] + xyl-D[c] -> 0.284 nadp[c] + 0.716 nad[c] + xylt[c]	Pentose and glucuronate interconversions
D-Arabinose reductase	h[c] + nadph[c] + arab-D[c] -> nadp[c] + abt-D[c]	Pentose and glucuronate interconversions
L-Arabinose reductase	h[c] + nadph[c] + arab-L[c] -> nadp[c] + abt-L[c]	Pentose and glucuronate interconversions
D-Ribose reductase	h[c] + nadh[c] + rbt[c] <=> nad[c] + rib-D[c]	Pentose and glucuronate interconversions
L-Xylulose reductase	h[c] + nadh[c] + xylu-L[c] <=> nad[c] + xylt[c]	Pentose and glucuronate interconversions
D-arabinitol dehydrogenase	h[c] + nadh[c] + xylu-D[c] <=> abt-D[c] + nad[c]	Pentose and glucuronate interconversions
L-arabinitol dehydrogenase	h[c] + nadh[c] + ribu-D[c] <=> nad[c] + rbt[c]	Pentose and glucuronate interconversions
L-arabinitol dehydrogenase	h[c] + nadh[c] + xylu-L[c] <=> nad[c] + abt-L[c]	Pentose and glucuronate interconversions
Ribulokinase	rbl-D[c] + atp[c] -> h[c] + adp[c] + ru5p-D[c]	Pentose and glucuronate interconversions
Ribulokinase	atp[c] + ribu-D[c] -> h[c] + adp[c] + ru5p-D[c]	Pentose and glucuronate interconversions
Gluconolactonase	h2o[c] + g15lac[c] <=> glcn-D[c]	Pentose Phosphate Pathway

Phosphoribosylpyrophosphate synthetase	atp[c] + r5p[c] <=> h[c] + amp[c] + prpp[c]	Pentose Phosphate Pathway
Gluconate Dehydrogenase	nadp[c] + glcn-D[c] <=> h[c] + nadph[c] + 2glcna[c]	Pentose Phosphate Pathway
Ribulose 5-phosphate 3-epimerase	ru5p-D[c] <=> xu5p-D[c]	Pentose Phosphate Pathway
Transketolase 1	xu5p-D[c] + e4p[c] <=> f6p[c] + g3p[c]	Pentose Phosphate Pathway
Transketolase 2	r5p[c] + xu5p-D[c] <=> g3p[c] + s7p[c]	Pentose Phosphate Pathway
6-phosphogluconolactonase	h2o[c] + 6pgl[c] -> h[c] + 6pgc[c]	Pentose Phosphate Pathway
Phosphogluconate dehydrogenase	nadp[c] + 6pgc[c] -> nadph[c] + co2[c] + ru5p-D[c]	Pentose Phosphate Pathway
Transaldolase	g3p[c] + s7p[c] <=> f6p[c] + e4p[c]	Pentose Phosphate Pathway
Ribokinase	atp[c] + rib-D[c] -> h[c] + adp[c] + r5p[c]	Pentose Phosphate Pathway
Ribose-5-phosphate isomerase	r5p[c] <=> ru5p-D[c]	Pentose Phosphate Pathway
Gluconokinase	atp[c] + glcn-D[c] <=> h[c] + adp[c] + 6pgc[c]	Pentose Phosphate Pathway
Glucose 6-phosphate dehydrogenase	nadp[c] + g6p[c] -> h[c] + nadph[c] + 6pgl[c]	Pentose Phosphate Pathway
Phosphopentomutase	r1p[c] <=> r5p[c]	Pentose phosphate pathway
Aldehyde dehydrogenase (phenylacetaldehyde, NAD)	h2o[c] + nad[c] + pacald[c] -> 2 h[c] + nadh[c] + pac[c]	Phenylalanine Metabolism
Indole 3-pyruvate decarboxylase	h[c] + indpyr[c] -> co2[c] + id3acald[c]	Phenylalanine Metabolism
Phenylpyruvate decarboxylase	h[c] + phpyr[c] -> co2[c] + pacald[c]	Phenylalanine Metabolism
Prephenate dehydratase	h[c] + pphn[c] -> h2o[c] + co2[c] + phpyr[c]	Phenylalanine, Tyrosine and Trytophan Biosynthesis
Anthranilate phosphoribosyltransferase	prpp[c] + anth[c] -> ppi[c] + pran[c]	Phenylalanine, Tyrosine and Trytophan Biosynthesis
Phosphoribosylanthranilate isomerase	pran[c] -> 2cpr5p[c]	Phenylalanine, Tyrosine and Trytophan Biosynthesis

Tyrosine transaminase, mitochondrial	akg[m] + tyr-L[m] <=> glu-L[m] + 34hpp[m]	Phenylalanine, Tyrosine and Trytophan Biosynthesis
Prephenate dehydrogenase (NADP)	nadp[c] + pphn[c] -> nadph[c] + co2[c] + 34hpp[c]	Phenylalanine, Tyrosine and Trytophan Biosynthesis
3-dehydroquinate dehydratase	3dhq[c] -> h2o[c] + 3dhsk[c]	Phenylalanine, Tyrosine and Trytophan Biosynthesis
Tyrosine transaminase	akg[c] + tyr-L[c] <=> glu-L[c] + 34hpp[c]	Phenylalanine, Tyrosine and Trytophan Biosynthesis
Phenylalanine transaminase	akg[c] + phe-L[c] <=> glu-L[c] + phpyr[c]	Phenylalanine, Tyrosine and Trytophan Biosynthesis
tryptophan transaminase	akg[c] + trp-L[c] <=> glu-L[c] + indpyr[c]	Phenylalanine, Tyrosine and Trytophan Biosynthesis
Tyrosine transaminase	glu-L[c] + 34hpp[c] -> akg[c] + tyr-L[c]	Phenylalanine, Tyrosine and Trytophan Biosynthesis
Tryptophan synthase (indoleglycerol phosphate)	ser-L[c] + 3ig3p[c] -> h2o[c] + g3p[c] + trp-L[c]	Phenylalanine, Tyrosine and Trytophan Biosynthesis
Chorismate mutase	chor[c] -> pphn[c]	Phenylalanine, Tyrosine and Trytophan Biosynthesis
Anthranilate synthase	gln-L[c] + chor[c] -> h[c] + pyr[c] + glu-L[c] + anth[c]	Phenylalanine, Tyrosine and Trytophan Biosynthesis
3-deoxy-D-arabino-heptulosonate 7-phosphate synthetase	h2o[c] + pep[c] + e4p[c] -> pi[c] + 2dda7p[c]	Phenylalanine, Tyrosine and Trytophan Biosynthesis
3-dehydroquinate synthase	2dda7p[c] -> pi[c] + 3dhq[c]	Phenylalanine, Tyrosine and Trytophan Biosynthesis
3-phosphoshikimate 1-carboxyvinyltransferase	pep[c] + skm5p[c] -> pi[c] + 3psme[c]	Phenylalanine, Tyrosine and Trytophan Biosynthesis
shikimate dehydrogenase	h[c] + nadph[c] + 3dhsk[c] -> nadp[c] + skm[c]	Phenylalanine, Tyrosine and Trytophan Biosynthesis

shikimate kinase	atp[c] + skm[c] -> h[c] + adp[c] + skm5p[c]	Phenylalanine, Tyrosine and Trytophan Biosynthesis
Chorismate synthase	3psme[c] -> pi[c] + chor[c]	Phenylalanine, Tyrosine and Trytophan Biosynthesis
Indole-3-glycerol-phosphate synthase	h[c] + 2cpr5p[c] -> h2o[c] + co2[c] + 3ig3p[c]	Phenylalanine, Tyrosine and Trytophan Biosynthesis
diacylglycerol cholinephosphotransferase,	0.01 12dgr[c] + cdpchol[c] -> h[c] + 0.01 pc[c] + cmp[c]	Phospholipid Biosynthesis
myo-inositol 1-phosphatase	h2o[c] + mi1p-D[c] -> pi[c] + inost[c]	Phospholipid Biosynthesis
Lyso-phosphatidylcholine acyltransferase acyltransferase	0.019 dcacoa[c] + 0.058 tdcoa[c] + 0.18 pmtcoa[c] + 0.078 hdceacoa[c] + 0.035 stcoa[c] + 0.315 ocdceacoa[c] + 0.094 ocdcyacoa[c] + 0.012 ocdctacoa[c] + 0.011 eicosapencoa[c] + 0.028 hexacoa[c] + 0.023 octacoa[c] + 0.115 ddcacoa[c] + 0.01 docosacoa[c] + 0.01 1agpc[c] -> coa[c] + 0.01 pc[c]	Phospholipid Biosynthesis
phospholipase B (phosphatidylcholine)	h2o[c] + 0.01 pc[c] -> 0.019 dca[c] + 0.058 ttdca[c] + 0.18 hdca[c] + 0.078 hdcea[c] + 0.025 hepdcea[c] + 0.035 ocdca[c] + 0.315 ocdcea[c] + 0.094 ocdcya[c] + 0.012 ocdcta[c] + 0.011 eicosapen[c] + 0.028 hexa[c] + 0.115 ddca[c] + 0.01 docosa[c] + 0.023 octa[c] + 0.5 g3pc[c]	Phospholipid Metabolism
Glycerophosphodiester phosphodiesterase (Glycerophosphocholine)	h2o[c] + g3pc[c] -> h[c] + chol[c] + glyc3p[c]	Phospholipid Metabolism
Ethanolaminephosphotransferase	0.01 12dgr[c] + cdpea[c] <=> h[c] + 0.01 pe[c] + cmp[c]	Phospholipid Metabolism

phospholipase B (phosphatidylinositol)	h2o[e] + 0.005 ptd1ino[e] -> 0.019 dca[e] + 0.115 ddca[e] + 0.01 docosa[e] + 0.011 eicosapen[e] + 0.5 g3pi[e] + 0.18 hdca[e] + 0.078 hdcea[e] + 0.025 hepdcea[e] + 0.028 hexa[e] + 0.035 ocdca[e] + 0.315 ocdcea[e] + 0.012 ocdcta[e] + 0.094 ocdcya[e] + 0.058 ttdca[e] + 0.023 octa[e]	Phospholipid Metabolism
phospholipase B (phosphatidylcholine)	h2o[e] + 0.005 pc[e] -> 0.019 dca[e] + 0.115 ddca[e] + 0.01 docosa[e] + 0.011 eicosapen[e] + 0.5 g3pc[e] + 0.18 hdca[e] + 0.078 hdcea[e] + 0.025 hepdcea[e] + 0.028 hexa[e] + 0.035 ocdca[e] + 0.315 ocdcea[e] + 0.012 ocdcta[e] + 0.094 ocdcya[e] + 0.058 ttdca[e] + 0.023 octa[e]	Phospholipid Metabolism
Cardiolipin synthase, mitochondrial	0.01 cdpdag[m] + 0.01 pg[m] -> h[m] + cmp[m] + 0.01 clpn[m]	Phospholipid Metabolism
Phosphatidylethanolamine N methyltransferase	amet[c] + 0.01 pe[c] -> h[c] + ahcys[c] + 0.01 ptdmeeta[c]	Phospholipid Metabolism
CDP Diacylglycerol synthetase	h[c] + ctp[c] + 0.01 pa[c] <=> ppi[c] + 0.01 cdpdag[c]	Phospholipid Metabolism
CDP Diacylglycerol synthetase, Mitochondrial	h[m] + ctp[m] + 0.01 pa[m] <=> 0.01 cdpdag[m] + ppi[m]	Phospholipid Metabolism
uroporphyrinogen methyltransferase	2 amet[c] + uppg3[c] -> h[c] + 2 ahcys[c] + dscl[c]	Porphyrin and chlorophyll metabolism
Ferrochelatase, mitochondrial	fe2[m] + ppp9[m] -> 2 h[m] + pheme[m]	Porphyrin and chlorophyll metabolism
uroporphyrinogen decarboxylase (uroporphyrinogen III)	4 h[c] + uppg3[c] -> 4 co2[c] + cpppg3[c]	Porphyrin and chlorophyll metabolism
hydroxymethylbilane synthase	h2o[c] + 4 ppbng[c] -> 4 nh4[c] + hmbil[c]	Porphyrin and chlorophyll metabolism
Heme O synthase, mitochondrial	h2o[m] + pheme[m] + frdp[m] -> ppi[m] + hemeO[m]	Porphyrin and chlorophyll metabolism
porphobilinogen synthase	2 5aop[c] -> h[c] + 2 h2o[c] + ppbng[c]	Porphyrin and chlorophyll metabolism
protoporphyrinogen oxidase, mitochondrial	3 o2[m] + 2 pppg9[m] -> 6 h2o[m] + 2 ppp9[m]	Porphyrin and chlorophyll metabolism

uroporphyrinogen-III synthase	hmbil[c] -> h2o[c] + uppg3[c]	Porphyrin and chlorophyll metabolism
sirohydrochlorin dehydrogenase	nadp[c] + dscl[c] -> h[c] + nadph[c] + scl[c]	Porphyrin and chlorophyll metabolism
sirohydrochlorin ferrochetalase	scl[c] + fe2[c] -> 3 h[c] + sheme[c]	Porphyrin and chlorophyll metabolism
coproporphyrinogen oxidase (O2 required)	2 h[c] + o2[c] + cpppg3[c] -> 2 h2o[c] + 2 co2[c] + pppg9[c]	Porphyrin and chlorophyll metabolism
Heme O monooxygenase, mitochondrial	nadh[m] + o2[m] + hemeO[m] -> h2o[m] + nad[m] + hemeA[m]	Porphyrin and chlorophyll metabolism
2-methylcitrate synthase	oaa[m] + h2o[m] + ppcoa[m] -> coa[m] + 2mcit[m] + h[m]	Propanoate metabolism
3-Hydroxypropionyl-CoA hydro-lyase	h2o[c] + ppcoa[c] <=> hppcoa[c]	Propanoate Metabolism
Acyl-CoA Dehydrogenase	ppcoa[c] + fad[c] <=> fadh2[c] + ppecoa[c]	Propanoate Metabolism
Beta-alanine:2-oxoglutarate aminotransferase	akg[c] + ala-B[c] <=> glu-L[c] + msa[c]	Propanoate Metabolism
Methylmalonate-semialdehyde dehydrogenase, Mitochondrial	coa[m] + nad[m] + 2mop[m] -> nadh[m] + co2[m] + ppcoa[m]	Propanoate Metabolism
Adenine phosphoribosyltransferase	prpp[c] + ade[c] -> amp[c] + ppi[c]	Purine Metabolism
Ribonucleoside-diphosphate reductase (ADP)	adp[c] + trdrd[c] -> h2o[c] + trdox[c] + dadp[c]	Purine Metabolism
Ribonucleoside-diphosphate reductase (GDP)	gdp[c] + trdrd[c] -> h2o[c] + trdox[c] + dgdp[c]	Purine Metabolism
5'-nucleotidase (XMP)	h2o[c] + xmp[c] -> pi[c] + xtsn[c]	Purine Metabolism
5'-nucleotidase (UMP)	h2o[c] + ump[c] -> pi[c] + uri[c]	Purine Metabolism
5'-nucleotidase (dCMP)	h2o[c] + dcmp[c] -> pi[c] + dcyt[c]	Purine Metabolism
5'-nucleotidase (dTMP)	h2o[c] + dtmp[c] -> pi[c] + thymd[c]	Purine Metabolism
5'-nucleotidase (dAMP)	h2o[c] + damp[c] -> pi[c] + dad-2[c]	Purine Metabolism
5'-nucleotidase (AMP)	h2o[c] + amp[c] -> pi[c] + adn[c]	Purine Metabolism
5'-nucleotidase (dGMP)	h2o[c] + dgmp[c] -> pi[c] + dgsn[c]	Purine Metabolism

5'-nucleotidase (GMP)	h2o[c] + gmp[c] -> pi[c] + gsn[c]	Purine Metabolism
Phosphoribosylglycinamide formyltransferase	10fthf[c] + gar[c] -> h[c] + thf[c] + fgam[c]	Purine Metabolism
Allantoinase	h2o[c] + alltn[c] -> alltt[c]	Purine Metabolism
Guanine deaminase	h[c] + h2o[c] + gua[c] -> nh4[c] + xan[c]	Purine Metabolism
Uricase	2 h2o[c] + o2[c] + urate[c] -> co2[c] + h2o2[c] + alltn[c]	Purine Metabolism
Adenosine monophosphate deaminase	h[c] + h2o[c] + amp[c] -> nh4[c] + imp[c]	Purine Metabolism
Bis(5'-adenosyl)-tetraphosphatase	h2o[c] + ap4a[c] -> atp[c] + amp[c]	Purine Metabolism
Bis(5'-Guanosyl)-tetraphosphatase	h2o[c] + gp4g[c] -> gtp[c] + gmp[c]	Purine Metabolism
Bis(5'-Uridyl)-tetraphosphatase	h2o[c] + up4u[c] -> utp[c] + ump[c]	Purine Metabolism
Bis(5'-Xanthosyl)-tetraphosphatase	h2o[c] + xp4x[c] -> xmp[c] + xtp[c]	Purine Metabolism
Ureidoglycolate hydrolase	h2o[c] + urdglyc[c] -> co2[c] + 2 nh4[c] + glx[c]	Purine Metabolism
ATP adenylyltransferase	h[c] + adp[c] + gtp[c] -> pi[c] + ap4g[c]	Purine Metabolism
ATP adenylyltransferase	h[c] + gtp[c] + gdp[c] -> pi[c] + gp4g[c]	Purine Metabolism
Phosphoribosyl aminoimidazole succinocarboxamide synthase	atp[c] + asp-L[c] + 5aizc[c] <=> h[c] + adp[c] + pi[c] + 25aics[c]	Purine Metabolism
Allantoate aminohydrolase	h2o[c] + alltt[c] <=> urea[c] + urdglyc[c]	Purine Metabolism
Adenosine kinase	atp[c] + adn[c] -> h[c] + adp[c] + amp[c]	Purine Metabolism
Adenosine deaminase	h[c] + h2o[c] + adn[c] -> nh4[c] + ins[c]	Purine Metabolism
Ap4A hydrolase	h2o[c] + ap4a[c] -> 2 h[c] + 2 adp[c]	Purine Metabolism
adenylate kinase, mitochondrial	atp[m] + amp[m] <=> 2 adp[m]	Purine Metabolism
adenylate kinase	atp[c] + amp[c] <=> 2 adp[c]	Purine Metabolism
IMP dehydrogenase	h2o[c] + nad[c] + imp[c] -> h[c] + nadh[c] + xmp[c]	Purine Metabolism

Adenylate cyclase	atp[c] -> ppi[c] + camp[c]	Purine Metabolism
nucleoside-diphosphate kinase (ATP:GDP)	atp[c] + gdp[c] <=> adp[c] + gtp[c]	Purine Metabolism
nucleoside-diphosphate kinase (ATP:dGDP)	atp[c] + dgdp[c] <=> adp[c] + dgtp[c]	Purine Metabolism
nucleoside-diphosphate kinase (ATP:dADP)	atp[c] + dadp[c] <=> adp[c] + datp[c]	Purine Metabolism
nucleoside-diphophate kinase (ATP:IDP)	atp[c] + idp[c] <=> adp[c] + itp[c]	Purine Metabolism
phosphoribosylaminoimidazolecarboxamide formyltransferase	10fthf[c] + aicar[c] <=> thf[c] + fprica[c]	Purine Metabolism
IMP cyclohydrolase	h2o[c] + imp[c] <=> fprica[c]	Purine Metabolism
GMP synthase	h2o[c] + atp[c] + gln-L[c] + xmp[c] -> 2 h[c] + amp[c] + ppi[c] + glu-L[c] + gmp[c]	Purine Metabolism
Guanylate kinase (GMP:ATP)	atp[c] + gmp[c] <=> adp[c] + gdp[c]	Purine Metabolism
Guanylate kinase (GMP:dATP)	datp[c] + gmp[c] <=> gdp[c] + dadp[c]	Purine Metabolism
Guanylate kinase (dGMP:ATP)	atp[c] + dgmp[c] <=> adp[c] + dgdp[c]	Purine Metabolism
nucleoside-diphosphatase (ADP)	h2o[c] + adp[c] -> h[c] + pi[c] + amp[c]	Purine Metabolism
nucleoside-diphosphatase (CDP)	h2o[c] + cdp[c] -> h[c] + pi[c] + cmp[c]	Purine Metabolism
nucleoside-triphosphatase (CTP)	h2o[c] + ctp[c] -> h[c] + pi[c] + cdp[c]	Purine Metabolism
nucleoside-triphosphatase (GTP)	h2o[c] + gtp[c] -> h[c] + pi[c] + gdp[c]	Purine Metabolism
nucleoside-diphosphatase (IDP)	h2o[c] + idp[c] -> h[c] + pi[c] + imp[c]	Purine Metabolism
nucleoside-triphosphatase (ITP)	h2o[c] + itp[c] -> h[c] + pi[c] + idp[c]	Purine Metabolism
Phosphoribosylformylglycinamidine synthase	h2o[c] + atp[c] + gln-L[c] + fgam[c] -> h[c] + adp[c] + pi[c] + glu-L[c] + fpram[c]	Purine Metabolism
Phosphoribosylglycinamide synthase	atp[c] + pram[c] + gly[c] <=> h[c] + adp[c] + pi[c] + gar[c]	Purine Metabolism
Phosphoribosylaminoimidazole synthase	atp[c] + fpram[c] -> 2 h[c] + adp[c] + pi[c] + air[c]	Purine Metabolism

3',5'-cyclic-nucleotide phosphodiesterase	h2o[c] + camp[c] -> h[c] + amp[c]	Purine Metabolism
Phosphoribosylaminoimidazole carboxylase	co2[c] + air[c] <=> h[c] + 5aizc[c]	Purine Metabolism
nucleoside-diphosphatase (GDP)	h2o[c] + gdp[c] -> h[c] + pi[c] + gmp[c]	Purine Metabolism
nucleoside-diphosphatase (UDP)	h2o[c] + udp[c] -> h[c] + pi[c] + ump[c]	Purine Metabolism
Pyruvate kinase GDP	h[c] + gdp[c] + pep[c] -> pyr[c] + gtp[c]	Purine Metabolism
Adenylsuccinate lyase	dcamp[c] <=> fum[c] + amp[c]	Purine Metabolism
Adenylosuccinate lyase	25aics[c] <=> fum[c] + aicar[c]	Purine Metabolism
Adenylosuccinate synthase	asp-L[c] + gtp[c] + imp[c] -> 2 h[c] + pi[c] + gdp[c] + dcamp[c]	Purine Metabolism
deoxyuridine kinase (ATP:Deoxyuridine)	atp[c] + duri[c] -> h[c] + adp[c] + dump[c]	Purine Metabolism
purine nucleoside phosphorylase Xanthosine	pi[c] + xtsn[c] <=> r1p[c] + xan[c]	Purine Metabolism
xanthine dehydrogenase	h2o[c] + nad[c] + hxan[c] -> h[c] + nadh[c] + xan[c]	Purine Metabolism
xanthine dehydrogenase	h2o[c] + nad[c] + xan[c] -> h[c] + nadh[c] + urate[c]	Purine Metabolism
Adenylyl-sulfate kinase	atp[c] + aps[c] -> h[c] + paps[c] + adp[c]	Purine Metabolism
Deoxyadenosine deaminase	h[c] + h2o[c] + dad-2[c] -> nh4[c] + din[c]	Purine Metabolism
deoxyadenylate kinase	atp[c] + damp[c] <=> adp[c] + dadp[c]	Purine Metabolism
purine nucleoside phosphorylase Adenosine	pi[c] + adn[c] <=> ade[c] + r1p[c]	Purine Metabolism
purine-nucleoside phosphorylase (Deoxyadenosine)	pi[c] + dad-2[c] <=> ade[c] + 2dr1p[c]	Purine Metabolism
purine nucleoside phosphorylase Guanosine	pi[c] + gsn[c] <=> r1p[c] + gua[c]	Purine Metabolism
purine-nucleoside phosphorylase (Deoxyguanosine)	pi[c] + dgsn[c] <=> 2dr1p[c] + gua[c]	Purine Metabolism
purine nucleoside phosphorylase Inosine	pi[c] + ins[c] <=> r1p[c] + hxan[c]	Purine Metabolism
purine-nucleoside phosphorylase (Deoxyinosine)	pi[c] + din[c] <=> hxan[c] + 2dr1p[c]	Purine Metabolism

guanine deaminase	h2o[c] + gsn[c] <=> nh4[c] + xtsn[c]	Purine Metabolism
uridine nucleosidase	h2o[c] + uri[c] <=> rib-D[c] + ura[c]	Purine Metabolism
5'-nucleotidase (CMP)	h2o[c] + cmp[c] -> pi[c] + cytd[c]	Pyrimidine metabolism
nucleoside-diphosphate kinase (ATP:dTDP)	atp[c] + dtdp[c] <=> adp[c] + dttp[c]	Pyrimidine metabolism
nucleoside-diphosphate kinase (ATP:dUDP)	atp[c] + dudp[c] <=> adp[c] + dutp[c]	Pyrimidine metabolism
nucleoside-diphosphate kinase (ATP:dCDP)	atp[c] + dcdp[c] <=> adp[c] + dctp[c]	Pyrimidine metabolism
Ribonucleoside-diphosphate reductase (CDP)	cdp[c] + trdrd[c] -> h2o[c] + trdox[c] + dcdp[c]	Pyrimidine metabolism
Ribonucleoside-diphosphate reductase (UDP)	udp[c] + trdrd[c] -> h2o[c] + trdox[c] + dudp[c]	Pyrimidine metabolism
Cytosine deaminase	h[c] + h2o[c] + csn[c] -> nh4[c] + ura[c]	Pyrimidine Metabolism
Dihydroorotase	h2o[c] + dhor-S[c] <=> h[c] + cbasp[c]	Pyrimidine Metabolism
dCMP deaminase	h[c] + h2o[c] + dcmp[c] <=> nh4[c] + dump[c]	Pyrimidine Metabolism
Thymidylate synthase	mlthf[c] + dump[c] -> dhf[c] + dtmp[c]	Pyrimidine Metabolism
Cytidine deaminase	h[c] + h2o[c] + cytd[c] -> nh4[c] + uri[c]	Pyrimidine Metabolism
Deoxycytidine deaminase	h[c] + h2o[c] + dcyt[c] -> nh4[c] + duri[c]	Pyrimidine Metabolism
Uracil phosphoribosyltransferase	prpp[c] + ura[c] -> ppi[c] + ump[c]	Pyrimidine Metabolism
Orotidine-5'-phosphate decarboxylase	h[c] + orot5p[c] -> co2[c] + ump[c]	Pyrimidine Metabolism
dTMP kinase	atp[c] + dtmp[c] <=> adp[c] + dtdp[c]	Pyrimidine Metabolism
Dihydoorotic acid dehydrogenase	o2[c] + dhor-S[c] -> h2o2[c] + orot[c]	Pyrimidine Metabolism
Thioredoxin reductase (NADPH)	h[c] + nadph[c] + trdox[c] -> nadp[c] + trdrd[c]	Pyrimidine Metabolism
dUTP diphosphatase	h2o[c] + dutp[c] -> h[c] + ppi[c] + dump[c]	Pyrimidine Metabolism
CTP synthase (NH3)	atp[c] + nh4[c] + utp[c] -> 2 h[c] + adp[c] + pi[c] + ctp[c]	Pyrimidine Metabolism

CTP synthase (glutamine)	h2o[c] + atp[c] + gln-L[c] + utp[c] -> 2 h[c] + adp[c] + pi[c] + glu-L[c] + ctp[c]	Pyrimidine Metabolism
Uridine kinase (ATP:Uridine)	atp[c] + uri[c] -> h[c] + adp[c] + ump[c]	Pyrimidine Metabolism
Uridine kinase (GTP:Uridine)	gtp[c] + uri[c] -> h[c] + gdp[c] + ump[c]	Pyrimidine Metabolism
Aspartate carbamoyltransferase	asp-L[c] + cbp[c] -> h[c] + pi[c] + cbasp[c]	Pyrimidine Metabolism
Cytidylate kinase (CMP)	atp[c] + cmp[c] <=> adp[c] + cdp[c]	Pyrimidine Metabolism
Cytidylate kinase (dCMP)	atp[c] + dcmp[c] <=> adp[c] + dcdp[c]	Pyrimidine Metabolism
UMP kinase	atp[c] + ump[c] <=> adp[c] + udp[c]	Pyrimidine Metabolism
uridylate kinase (dUMP)	atp[c] + dump[c] <=> adp[c] + dudp[c]	Pyrimidine Metabolism
Orotate phosphoribosyltransferase	ppi[c] + orot5p[c] <=> prpp[c] + orot[c]	Pyrimidine Metabolism
deoxyuridine phosphorylase	pi[c] + duri[c] <=> 2dr1p[c] + ura[c]	Pyrimidine Metabolism
5'-nucleotidase (dUMP)	h2o[c] + dump[c] -> pi[c] + duri[c]	Pyrimidine Metabolism
5'-nucleotidase (IMP)	h2o[c] + imp[c] -> pi[c] + ins[c]	Pyrimidine Metabolism
nucleoside-diphosphate kinase (ATP:UDP)	atp[c] + udp[c] <=> adp[c] + utp[c]	Pyrimidine Metabolism
nucleoside-diphosphate kinase (ATP:CDP)	atp[c] + cdp[c] <=> adp[c] + ctp[c]	Pyrimidine Metabolism
nucleoside-triphosphatase (UTP)	h2o[c] + utp[c] -> h[c] + pi[c] + udp[c]	Pyrimidine Metabolism
Alcohol dehydrogenase (ethanol) NADP	nadp[c] + etoh[c] <=> h[c] + nadph[c] + acald[c]	Pyruvate metabolism
methylglyoxal synthase	dhap[c] -> pi[c] + mthgxl[c]	Pyruvate metabolism
Alcohol dehydrogenase (ethanol)	etoh[c] + nad[c] <=> h[c] + acald[c] + nadh[c]	Pyruvate metabolism
Aldehyde Dehydrogenase	acald[c] + h2o[c] + nad[c] -> 2 h[c] + nadh[c] + ac[c]	Pyruvate metabolism
Homocitrate synthase	akg[m] + h2o[m] + accoa[m] -> coa[m] + h[m] + hicit[m]	Pyruvate Metabolism
Hydroxyacylglutathione hydrolase	h2o[c] + lgt-S[c] -> h[c] + gthrd[c] + lac-D[c]	Pyruvate Metabolism

Acetyl-CoA C-acetyltransferase	2 accoa[c] -> coa[c] + aacoa[c]	Pyruvate Metabolism
malic enzyme (NAD), mitochondrial	nad[m] + mal-L[m] -> pyr[m] + nadh[m] + co2[m]	Pyruvate metabolism
Aldehyde Dehydrogenase Mitochondrial	h2o[m] + nad[m] + acald[m] -> 2 h[m] + nadh[m] + ac[m]	Pyruvate metabolism
Acetolactate synthase, mitochondrial	2 pyr[m] + h[m] -> co2[m] + alac-S[m]	Pyruvate metabolism
L-Lactate dehydrogenase, mitochondrial	2 ficytc[m] + lac-L[m] -> pyr[m] + 2 focytc[m]	Pyruvate Metabolism
Malate synthase	h2o[c] + accoa[c] + glx[c] -> h[c] + coa[c] + mal-L[c]	Pyruvate Metabolism
Aldehyde Dehydrogenase NADP dependent	nadp[c] + acald[c] + h2o[c] -> 2 h[c] + nadph[c] + ac[c]	Pyruvate metabolism
Lactoylglutathione lyase	gthrd[c] + mthgxl[c] -> lgt-S[c]	Pyruvate Metabolism
Pyruvate decarboxylase	h[c] + pyr[c] -> acald[c] + co2[c]	Pyruvate Metabolism
2-isopropylmalate synthase	h2o[m] + accoa[m] + 3mob[m] -> coa[m] + h[m] + 3c3hmp[m]	Pyruvate Metabolism
Acetyl-CoA hydrolase	h2o[c] + accoa[c] -> h[c] + ac[c] + coa[c]	Pyruvate Metabolism
Acetyl-coA Synthetase Mitochondrial	atp[m] + coa[m] + ac[m] -> accoa[m] + ppi[m] + amp[m]	Pyruvate metabolism
Acetyl-coA Synthetase	atp[c] + ac[c] + coa[c] -> amp[c] + ppi[c] + accoa[c]	Pyruvate metabolism
Pyruvate dehydrogenase, mitochondrial	coa[m] + pyr[m] + nad[m] -> accoa[m] + nadh[m] + co2[m]	Pyruvate metabolism
Acetyl-CoA carboxylase	atp[c] + hco3[c] + accoa[c] <=> h[c] + adp[c] + pi[c] + malcoa[c]	Pyruvate Metabolism
Acetyl-Coa carboxylase, mitochondrial	atp[m] + accoa[m] + hco3[m] <=> adp[m] + pi[m] + h[m] + malcoa[m]	Pyruvate Metabolism
D-lactate dehydrogenase, mitochondrial	2 ficytc[m] + lac-D[m] -> pyr[m] + 2 focytc[m]	Pyruvate Metabolism
Malate dehydrogenase	nad[c] + mal-L[c] <=> h[c] + nadh[c] + oaa[c]	Pyruvate Metabolism
Pyruvate carboxylase	pyr[c] + atp[c] + hco3[c] -> h[c] + adp[c] + pi[c] + oaa[c]	Pyruvate metabolism
Phosphoenolpyruvate carboxykinase	atp[c] + oaa[c] -> adp[c] + co2[c] + pep[c]	Pyruvate metabolism

2-hexaprenyl-3-methyl-5-hydroxy-6-methoxy-1,4-benzoquinone methyltransferase, mitochondrial	2hpmhmbq[m] + amet[m] -> h[m] + q6[m] + ahcys[m]	Quinone Synthesis
S-adenosyl-L-methionine:3-hexaprenyl-4,5-dihydroxylate O-methyltransferase, mitochondrial	amet[m] + 3dh5hpb[m] -> h[m] + ahcys[m] + 3hph5mb[m]	Quinone Synthesis
2-Hexaprenyl-6-methoxyphenol monooxygenase, mitochondrial	o2[m] + 2hp6mp[m] -> h2o[m] + 2hp6mbq[m]	Quinone Synthesis
2-hexaprenyl-3-methyl-6-methoxy-1,4-benzoquinone monooxygenase, mitochondrial	0.5 o2[m] + 2hpmmbq[m] -> 2hpmhmbq[m]	Quinone Synthesis
2-hexaprenyl-6-methoxy-1,4-benzoquinone methyltransferase, mitochondrial	amet[m] + 2hp6mbq[m] -> h[m] + ahcys[m] + 2hpmmbq[m]	Quinone Synthesis
Trans-pentaprenyltranstransferase, mitochondrial	ipdp[m] + pendp[m] -> ppi[m] + hexdp[m]	Quinone Synthesis
Hydroxybenzoate octaprenyltransferase, mitochondrial	hexdp[m] + 4hbz[m] -> ppi[m] + 3ophb_5[m]	Quinone Synthesis
3-Hexaprenyl-4-hydroxy-5-methoxybenzoate decarboxylase, mitochondrial	3hph5mb[m] -> co2[m] + 2hp6mp[m]	Quinone Synthesis
3-Hexaprenyl-4,5-dihydroxybenzoate hydroxylase, mitochondrial	0.5 o2[m] + 3ophb_5[m] -> 3dh5hpb[m]	Quinone Synthesis
GTP cyclohydrolase II	3 h2o[c] + gtp[c] -> 2 h[c] + ppi[c] + for[c] + 25dhpp[c]	Riboflavin Metabolism
FMN adenylyltransferase	h[c] + atp[c] + fmn[c] -> ppi[c] + fad[c]	Riboflavin Metabolism
Riboflavin synthase alpha chain	4r5au[c] + db4p[c] -> 2 h2o[c] + pi[c] + dmlz[c]	Riboflavin Metabolism
Acid phosphatase, extracellular	h2o[e] + fmn[e] -> pi[e] + ribflv[e]	Riboflavin Metabolism
Riboflavin kinase	atp[c] + ribflv[c] -> h[c] + adp[c] + fmn[c]	Riboflavin Metabolism
Riboflavin synthase beta chain	2 dmlz[c] -> 4r5au[c] + ribflv[c]	Riboflavin Metabolism

5-amino-6-(5-phosphoribosylamino)uracil reductase	h[c] + nadph[c] + 5apru[c] -> nadp[c] + 5aprbu[c]	Riboflavin Metabolism
Diaminohydroxyphosphoribosylaminopyrimidine deaminase	h[c] + h2o[c] + 25dhpp[c] -> nh4[c] + 5apru[c]	Riboflavin Metabolism
3,4-Dihydroxy-2-butanone-4-phosphate	ru5p-D[c] -> h[c] + for[c] + db4p[c]	Riboflavin Metabolism
Pyrimidine phosphatase	h2o[c] + 5aprbu[c] -> pi[c] + 4r5au[c]	Riboflavin Metabolism
sphingoid base-phosphate phosphatase (sphinganine 1-phosphatase), endoplasmic reticulum	h2o[c] + sph1p[c] -> pi[c] + sphgn[c]	Sphingolipid Metabolism
sphingoid base-phosphate phosphatase (phytosphingosine 1-phosphate), endoplasmic reticulum	h2o[c] + psph1p[c] -> pi[c] + psphings[c]	Sphingolipid Metabolism
beta-galactosidase (Glucosyl ceramide)	udpgal[c] + gcylcer[c] -> udp[c] + lactcer[c]	Sphingolipid Metabolism
Ceramide-1 synthase (24C)	ttccoa[c] + sphgn[c] -> h[c] + coa[c] + cer1_24[c]	Sphingolipid Metabolism
Ceramide-1 synthase (26C)	hexccoa[c] + sphgn[c] -> h[c] + coa[c] + cer1_26[c]	Sphingolipid Metabolism
Ceramide-2 synthase (24C)	ttccoa[c] + psphings[c] -> h[c] + coa[c] + cer2_24[c]	Sphingolipid Metabolism
Ceramide-2 synthase (26C)	hexccoa[c] + psphings[c] -> h[c] + coa[c] + cer2_26[c]	Sphingolipid Metabolism
inositol phosphorylceramide, ceramide-1 (24C) phospholipase C	h2o[c] + 0.01 ipc124[c] -> h[c] + mi1p-D[c] + cer1_24[c]	Sphingolipid Metabolism
inositol phosphorylceramide, ceramide-1 (26C) phospholipase C	h2o[c] + 0.01 ipc126[c] -> h[c] + mi1p-D[c] + cer1_26[c]	Sphingolipid Metabolism
inositol phosphorylceramide, ceramide-2 (24C) phospholipase C	h2o[c] + 0.01 ipc224[c] -> h[c] + mi1p-D[c] + cer2_24[c]	Sphingolipid Metabolism
inositol phosphorylceramide, ceramide-2 (26C) phospholipase C	h2o[c] + 0.01 ipc226[c] -> h[c] + mi1p-D[c] + cer2_26[c]	Sphingolipid Metabolism
Mannose-(inositol-P)2-ceramide, ceramide-1 (24C) phospholipase C	h2o[c] + 0.01 mip2c124[c] -> h[c] + cer1_24[c] + man2mi1p-D[c]	Sphingolipid Metabolism

Mannose-(inositol-P)2-ceramide, ceramide-1 (26C) phospholipase C	h2o[c] + 0.01 mip2c126[c] -> h[c] + cer1_26[c] + man2mi1p-D[c]	Sphingolipid Metabolism
Mannose-(inositol-P)2-ceramide, ceramide-2 (24C) phospholipase C	h2o[c] + 0.01 mip2c224[c] -> h[c] + cer2_24[c] + man2mi1p-D[c]	Sphingolipid Metabolism
Mannose-(inositol-P)2-ceramide, ceramide-2 (26C) phospholipase C	h2o[c] + 0.01 mip2c226[c] -> h[c] + cer2_26[c] + man2mi1p-D[c]	Sphingolipid Metabolism
Mannose-inositol phosphorylceramide, ceramide-1 (24C) phospholipase C	h2o[c] + 0.01 mipc124[c] -> h[c] + cer1_24[c] + manmi1p-D[c]	Sphingolipid Metabolism
Mannose-inositol phosphorylceramide, ceramide-1 (26C) phospholipase C	h2o[c] + 0.01 mipc126[c] -> h[c] + cer1_26[c] + manmi1p-D[c]	Sphingolipid Metabolism
Mannose-inositol phosphorylceramide, ceramide-2 (24C) phospholipase C	h2o[c] + 0.01 mipc224[c] -> h[c] + cer2_24[c] + manmi1p-D[c]	Sphingolipid Metabolism
Mannose-inositol phosphorylceramide, ceramide-2 (26C) phospholipase C	h2o[c] + 0.01 mipc226[c] -> h[c] + cer2_26[c] + manmi1p-D[c]	Sphingolipid Metabolism
ceramide glucosyltransferase	udpg[c] + cer3[c] -> udp[c] + gcylcer[c]	Sphingolipid Metabolism
3 Dehydrosphinganine reductase	h[c] + nadph[c] + 3dsphgn[c] -> nadp[c] + sphgn[c]	Sphingolipid Metabolism
mannose-(inositol-P)2-ceramide synthase (ceramide-1, 24C),	0.01 ptd1ino[c] + 0.01 mipc124[c] -> 0.01 12dgr[c] + 0.01 mip2c124[c]	Sphingolipid Metabolism
mannose-(inositol-P)2-ceramide synthase (ceramide-1, 26C),	0.01 ptd1ino[c] + 0.01 mipc126[c] -> 0.01 12dgr[c] + 0.01 mip2c126[c]	Sphingolipid Metabolism
mannose-(inositol-P)2-ceramide synthase (ceramide-2, 26C), yeast specific	0.01 ptd1ino[c] + 0.01 mipc224[c] -> 0.01 12dgr[c] + 0.01 mip2c224[c]	Sphingolipid Metabolism
mannose-(inositol-P)2-ceramide synthase (ceramide-2, 24C),	0.01 ptd1ino[c] + 0.01 mipc226[c] -> 0.01 12dgr[c] + 0.01 mip2c226[c]	Sphingolipid Metabolism
Sphingomyelin phosphodiesterase	h2o[c] + spmylin[c] -> cholp[c] + cer3[c]	Sphingolipid Metabolism

sphingolipid long chain base kinase (sphinganine)	atp[c] + sphgn[c] -> h[c] + adp[c] + sph1p[c]	Sphingolipid Metabolism
sphingolipid long chain base kinase (phytosphingosine)	atp[c] + psphings[c] -> h[c] + adp[c] + psph1p[c]	Sphingolipid Metabolism
Fatty acid desaturase	cer1_24[c] -> cer3_24[c]	Sphingolipid Metabolism
Fatty acid desaturase	cer1_26[c] -> cer3_26[c]	Sphingolipid Metabolism
Alkaline ceramidase (ceramide-1)	h[c] + coa[c] + cer1_24[c] -> ttccoa[c] + sphgn[c]	Sphingolipid Metabolism
Alkaline ceramidase (ceramide-1)	h[c] + coa[c] + cer1_26[c] -> hexccoa[c] + sphgn[c]	Sphingolipid Metabolism
Alkaline ceramidase (ceramide-2)	h[c] + coa[c] + cer2_24[c] -> ttccoa[c] + psphings[c]	Sphingolipid Metabolism
Alkaline ceramidase (ceramide-2)	h[c] + coa[c] + cer2_26[c] -> hexccoa[c] + psphings[c]	Sphingolipid Metabolism
Ceramide-1 hydroxylase (24C)	h[c] + nadph[c] + o2[c] + cer1_24[c] -> nadp[c] + h2o[c] + cer2_24[c]	Sphingolipid Metabolism
Ceramide-1 hydroxylase (26C)	h[c] + nadph[c] + o2[c] + cer1_26[c] -> nadp[c] + h2o[c] + cer2_26[c]	Sphingolipid Metabolism
Phytosphingosine synthesis	h[c] + nadph[c] + o2[c] + sphgn[c] -> nadp[c] + h2o[c] + psphings[c]	Sphingolipid Metabolism
mannose-inositiol phophorylceramide synthase (ceramide-1, 24C),	gdpmann[c] + 0.01 ipc124[c] -> h[c] + gdp[c] + 0.01 mipc124[c]	Sphingolipid Metabolism
mannose-inositol phosphorylceramide synthase (ceramide-1, 26C),	gdpmann[c] + 0.01 ipc126[c] -> h[c] + gdp[c] + 0.01 mipc126[c]	Sphingolipid Metabolism
mannose-inositol phosphorylceramide synthase (ceramide-2, 24C),	gdpmann[c] + 0.01 ipc224[c] -> h[c] + gdp[c] + 0.01 mipc224[c]	Sphingolipid Metabolism

mannose-inositol phosphorylceramide synthase (ceramide-2, 26C),	gdpmann[c] + 0.01 ipc226[c] -> h[c] + gdp[c] + 0.01 mipc226[c]	Sphingolipid Metabolism
Serine C palmitoyltransferase	h[c] + ser-L[c] + pmtcoa[c] -> co2[c] + coa[c] + 3dsphgn[c]	Sphingolipid Metabolism
phytosphingosine phosphate lyase	psph1p[c] -> ethamp[c] + 2hhxdal[c]	Sphingolipid Metabolism
sphinganine phosphate lyase	sph1p[c] -> ethamp[c] + hxdcal[c]	Sphingolipid Metabolism
Inositol phosphorylceramide synthase (ceramide-1, 24C),	0.01 ptd1ino[c] + cer1_24[c] -> 0.01 12dgr[c] + 0.01 ipc124[c]	Sphingolipid Metabolism
Inositol phosphorylceramide synthase (ceramide-1, 26C),	0.01 ptd1ino[c] + cer1_26[c] -> 0.01 12dgr[c] + 0.01 ipc126[c]	Sphingolipid Metabolism
Inositol phosphorylceramide synthase (ceramide-2, 24C),	0.01 ptd1ino[c] + cer2_24[c] -> 0.01 12dgr[c] + 0.01 ipc224[c]	Sphingolipid Metabolism
Inositol phosphoryceramide synthase (ceramide-2, 26C),	0.01 ptd1ino[c] + cer2_26[c] -> 0.01 12dgr[c] + 0.01 ipc226[c]	Sphingolipid Metabolism
Ceramide synthase - model reaction	cer3_24[c] + cer3_26[c] <=> cer3[c]	Sphingolipid Metabolism
Alpha-glucosidase	h2o[c] + malt[c] -> 2 glc-D[c]	Starch and sucrose metabolism
Phosphoglucomutase	g1p[c] <=> g6p[c]	Starch and sucrose metabolism
UTP-glucose-1-phosphate uridylyltransferase	h[c] + utp[c] + g1p[c] <=> ppi[c] + udpg[c]	Starch and sucrose metabolism
C-5 sterol desaturase	h[c] + nadph[c] + o2[c] + epist[c] -> nadp[c] + 2 h2o[c] + ergtrol[c]	Sterol Biosynthesis
C-s24 sterol reductase	h[c] + nadph[c] + ergtetrol[c] -> nadp[c] + ergst[c]	Sterol Biosynthesis

C-14 sterol reductase	h[c] + nadph[c] + 44mctr[c] -> nadp[c] + 44mzym[c]	Sterol Biosynthesis
C-3 sterol keto reductase (4-methylzymosterol)	h[c] + nadph[c] + 4mzym_int2[c] -> nadp[c] + 4mzym[c]	Sterol Biosynthesis
C-3 sterol keto reductase (zymosterol)	h[c] + nadph[c] + zym_int2[c] -> nadp[c] + zymst[c]	Sterol Biosynthesis
Cytochrome P450 lanosterol 14-alpha-demethylase	2 h[c] + 3 nadph[c] + 3 o2[c] + lanost[c] -> 3 nadp[c] + 4 h2o[c] + for[c] + 44mctr[c]	Sterol Biosynthesis
Lanosterol synthase	Ssq23epx[c] -> lanost[c]	Sterol Biosynthesis
C-3 sterol dehydrogenase (4-methylzymosterol)	nad[c] + 4mzym_int1[c] -> h[c] + nadh[c] + co2[c] + 4mzym_int2[c]	Sterol Biosynthesis
C-3 sterol dehydrogenase (zymosterol)	nad[c] + zym_int1[c] -> h[c] + nadh[c] + co2[c] + zym_int2[c]	Sterol Biosynthesis
C-22 sterol desaturase (NADP)	h[c] + nadph[c] + o2[c] + ergtrol[c] -> nadp[c] + 2 h2o[c] + ergtetrol[c]	Sterol Biosynthesis
C-22 sterol desaturase (NAD)	h[c] + nadh[c] + o2[c] + ergtrol[c] -> 2 h2o[c] + nad[c] + ergtetrol[c]	Sterol Biosynthesis
C-8 sterol isomerase	fecost[c] -> epist[c]	Sterol Biosynthesis
C-4 sterol methyl oxidase (4,4-dimethylzymosterol)	3 h[c] + 3 nadph[c] + 3 o2[c] + 44mzym[c] -> 3 nadp[c] + 4 h2o[c] + 4mzym_int1[c]	Sterol Biosynthesis
C-4 sterol methyl oxidase (4-methylzymosterol)	3 h[c] + 3 nadph[c] + 3 o2[c] + 4mzym[c] -> 3 nadp[c] + 4 h2o[c] + zym_int1[c]	Sterol Biosynthesis
Squalene epoxidase	h[c] + nadph[c] + o2[c] + sql[c] -> nadp[c] + h2o[c] + Ssq23epx[c]	Sterol Biosynthesis
S-adenosyl-methionine delta-24-sterol-c-methyltransferase	amet[c] + zymst[c] -> h[c] + ahcys[c] + fecost[c]	Sterol Biosynthesis

Squalene synthase	h[c] + nadph[c] + 2 frdp[c] -> nadp[c] + 2 ppi[c] + sql[c]	Sterol Biosynthesis
Beta-glucosidase (cellobiose)	h2o[e] + cellb[e] -> 2 glc-D[e]	Sucrose and Starch Metabolism
Beta-glucosidase (MADG)	h2o[e] + madg[e] -> glc-D[e] + meoh[e]	Sucrose and Starch Metabolism
Beta-glucosidase(MBDG)	h2o[e] + mbdg[e] -> glc-D[e] + meoh[e]	Sucrose and Starch Metabolism
Glucan 1,4-alpha-glucosidase	h2o[c] + glycogen[c] -> glc-D[c]	Sucrose and Starch Metabolism
Endo-1,3-beta-glucan glucohydrase	h2o[c] + 13BDglcn[c] -> glc-D[c]	Sucrose and Starch Metabolism
Exo-1,3-beta-glucan glucohydrase, extracellular	h2o[e] + 13BDglcn[e] -> glc-D[e]	Sucrose and Starch Metabolism
Alpha-glucoside glucohydrolase	h2o[c] + sucr[c] -> fru[c] + glc-D[c]	Sucrose and Starch Metabolism
1,3-beta-glucan synthase	udpg[c] -> h[c] + udp[c] + 13BDglcn[c]	Sucrose and Starch Metabolism
Alpha,alpha-trehalose-phosphate synthase (UDP-forming)	udpg[c] + g6p[c] -> h[c] + udp[c] + tre6p[c]	Sucrose and Starch Metabolism
Alpha,alpha-trehalase	h2o[c] + tre[c] -> 2 glc-D[c]	Sucrose and Starch Metabolism
Glycogen phosphorylase	pi[c] + glycogen[c] -> g1p[c]	Sucrose and Starch Metabolism
Trehalose-phosphatase	h2o[c] + tre6p[c] -> pi[c] + tre[c]	Sucrose and Starch Metabolism
Glycogen synthase (UDPGlc)	udpg[c] -> h[c] + udp[c] + glycogen[c]	Sucrose and Starch Metabolism

Glycogen (starch) synthase	h2o[c] + udpg[c] -> h[c] + udp[c] + 14glun[c]	Sucrose and Starch Metabolism
1,4-alpha-glucan branching enzyme	14glun[c] -> h2o[c] + glycogen[c]	Sucrose and Starch Metabolism
3',5'-bisphosphate nucleotidase	pap[c] + h2o[c] -> pi[c] + amp[c]	Sulphur Metabolism
Phosphoadenylyl-sulfate reductase (thioredoxin)	paps[c] + trdrd[c] -> 2 h[c] + pap[c] + trdox[c] + so3[c]	Sulphur Metabolism
Sulfate adenylyltransferase	h[c] + so4[c] + atp[c] -> ppi[c] + aps[c]	Sulphur Metabolism
Sulfite reductase (NADPH)	3 nadp[c] + 3 h2o[c] + h2s[c] <=> 5 h[c] + 3 nadph[c] + so3[c]	Sulphur Metabolism
Hydroxymethylglutaryl CoA synthase	h[c] + coa[c] + hmgcoa[c] <=> h2o[c] + accoa[c] + aacoa[c]	Synthesis and degradation of ketone bodies
Taurine dioxygenase	akg[c] + o2[c] + taur[c] -> succ[c] + co2[c] + so3[c] + amacald[c]	Taurine and hypotaurine metabolism
Aldehyde dehydrogenase (aminoacetaldehyde, NAD)	h2o[c] + nad[c] + amacald[c] -> h[c] + nadh[c] + gly[c]	Taurine and hypotaurine metabolism
Geranylgeranyltranstransferase	ggdp[c] + ipdp[c] -> ppi[c] + pendp[c]	Terpenoid Backbone Synthesis
Mevalonate kinase (atp)	atp[c] + mev-R[c] -> h[c] + adp[c] + 5pmev[c]	Terpenoid Backbone Synthesis
Mevalonate kinase (ctp)	ctp[c] + mev-R[c] -> h[c] + cdp[c] + 5pmev[c]	Terpenoid Backbone Synthesis
Mevalonate kinase (gtp)	gtp[c] + mev-R[c] -> h[c] + gdp[c] + 5pmev[c]	Terpenoid Backbone Synthesis
Mevalonate kinase (utp)	utp[c] + mev-R[c] -> h[c] + udp[c] + 5pmev[c]	Terpenoid Backbone Synthesis

Farnesyltranstransferase	frdp[c] + ipdp[c] -> ppi[c] + ggdp[c]	Terpenoid Backbone Synthesis
Dimethylallyltranstransferase	ipdp[c] + dmpp[c] -> ppi[c] + grdp[c]	Terpenoid Backbone Synthesis
Geranyltranstransferase	ipdp[c] + grdp[c] -> ppi[c] + frdp[c]	Terpenoid Backbone Synthesis
Phosphomevalonate kinase	atp[c] + 5pmev[c] -> adp[c] + 5dpmev[c]	Terpenoid Backbone Synthesis
Isopentenyl-diphosphate D-isomerase	ipdp[c] <=> dmpp[c]	Terpenoid Backbone Synthesis
Hydroxymethylglutaryl CoA reductase	2 nadp[c] + coa[c] + mev-R[c] <=> 2 h[c] + 2 nadph[c] + hmgcoa[c]	Terpenoid Backbone Synthesis
Diphosphomevalonate decarboxylase	atp[c] + 5dpmev[c] -> adp[c] + pi[c] + co2[c] + ipdp[c]	Terpenoid Backbone Synthesis
Thiamine diphosphokinase	atp[c] + thm[c] -> h[c] + amp[c] + thmpp[c]	Thiamine Metabolism
Thiamine-diphosphate kinase	atp[c] + thmpp[c] -> adp[c] + thmtp[c]	Thiamine Metabolism
Thiazole phosphate synthesis (xylulose 5-phosphate),	h[c] + cys-L[c] + achms[c] + gly[c] + xu5p-D[c] -> pyr[c] + 3 h2o[c] + 4abut[c] + co2[c] + nh4[c] + ac[c] + 4mpetz[c]	Thiamine Metabolism
Thiazole phosphate synthesis (ribose 5-phosphate), yeast-specifc	h[c] + cys-L[c] + achms[c] + gly[c] + r5p[c] -> pyr[c] + 3 h2o[c] + 4abut[c] + co2[c] + nh4[c] + ac[c] + 4mpetz[c]	Thiamine Metabolism
Hydroxymethylpyrimidine kinase (ATP)	atp[c] + 4ahmmp[c] -> h[c] + adp[c] + 4ampm[c]	Thiamine Metabolism
Phosphomethylpyrimidine kinase	atp[c] + 4ampm[c] -> adp[c] + 2mahmp[c]	Thiamine Metabolism
Thiaminase	h2o[c] + thm[c] -> h[c] + 4ahmmp[c] + 4mhetz[c]	Thiamine Metabolism

Thiamin phosphatase	h2o[c] + thmmp[c] -> pi[c] + thm[c]	Thiamine Metabolism
Thiamin diphosphatase	2 h2o[c] + thmpp[c] -> h[c] + 2 pi[c] + thm[c]	Thiamine Metabolism
Hydroxyethylthiazole kinase	atp[c] + 4mhetz[c] -> h[c] + adp[c] + 4mpetz[c]	Thiamine Metabolism
Thiamine-phosphate diphosphorylase	h[c] + 4mpetz[c] + 2mahmp[c] -> ppi[c] + thmmp[c]	Thiamine Metabolism
4 amino 5 hydroxymethyl 2 methylpyrimidine synthetase	2 h[c] + air[c] -> pi[c] + gcald[c] + 4ahmmp[c]	Thiamine Metabolism
Thiamine-phosphate kinase	atp[c] + thmmp[c] <=> adp[c] + thmpp[c]	Thiamine Metabolism
citrate Transport Mitochondrial	mal-L[m] + cit[c] <=> cit[m] + mal-L[c]	Transport Mitochondrial
citrate Transport Mitochondrial	icit[m] + cit[c] <=> icit[c] + cit[m]	Transport Mitochondrial
Citrate Transport Mitochondrial3	cit[c] + pep[m] <=> cit[m] + pep[c]	Transport Mitochondrial
ADP/ATP transporter, mitochondrial	atp[m] + h[c] + adp[c] + pi[c] + h2o[m] -> adp[m] + pi[m] + h2o[c] + atp[c] + h[m]	Transport Mitochondrial
Succinate/fumarate mitochondrial transporter	succ[c] + fum[m] <=> succ[m] + fum[c]	Transport Mitochondrial
Aspartate-glutamate transporter	glu-L[c] + asp-L[m] -> asp-L[c] + glu-L[m]	Transport Mitochondrial
dicarboxylate transport mitochondrial	succ[m] + mal-L[c] <=> succ[c] + mal-L[m]	Transport Mitochondrial
malate Transport Mitochondrial	pi[m] + mal-L[c] <=> pi[c] + mal-L[m]	Transport Mitochondrial

Succinate Transport Mitochondrial	pi[m] + succ[c] <=> succ[m] + pi[c]	Transport Mitochondrial
CTP/CMP antiport	2 h[c] + ctp[c] + cmp[m] -> 2 h[m] + cmp[c] + ctp[m]	Transport Mitochondrial
2-Dehydropantoate mitochondrial transport	2dhp[c] <=> 2dhp[m]	Transport Mitochondrial
2-oxobutanoate transporter (mitochondrial)	2obut[c] <=> 2obut[m]	Transport Mitochondrial
2-oxoadipate transport out of mitochondria via diffusion	2oxoadp[m] -> 2oxoadp[c]	Transport Mitochondrial
3-(4-hydroxyphenyl)pyruvate mitochondrial transport via proton symport	h[c] + 34hpp[c] <=> h[m] + 34hpp[m]	Transport Mitochondrial
2-Isopropylmalate transport, diffusion, mitochondrial	3c3hmp[c] <=> 3c3hmp[m]	Transport Mitochondrial
3-Carboxy-4-methyl-2-oxopentanoate transport, diffusion, mitochondrial	3c4mop[c] <=> 3c4mop[m]	Transport Mitochondrial
3mob, diffusion, mitochondrial	3mob[m] -> 3mob[c]	Transport Mitochondrial
3-Methyl-2-oxopentanoate transport, diffusion, mitochondrial	3mop[c] <=> 3mop[m]	Transport Mitochondrial
trans-4-hydroxy-L-proline mitochondrial transport via diffusion	4hpro-LT[c] <=> 4hpro-LT[m]	Transport Mitochondrial
5-Aminolevulinate mitochondrial transport	5aop[c] <=> 5aop[m]	Transport Mitochondrial
Aceto acetate Transport Mitochondrial	acac[c] <=> acac[m]	Transport Mitochondrial
acetaldehyde mitochondrial diffusion	acald[m] <=> acald[c]	Transport Mitochondrial

Acyl carrier protein Transport Mitochondrial	ACP[m] <=> ACP[c]	Transport Mitochondrial
acetate Transport Mitochondrial	ac[c] <=> ac[m]	Transport Mitochondrial
S-adenosyl-L-homocysteine reversible Transport Mitochondrial	ahcys[c] <=> ahcys[m]	Transport Mitochondrial
Alanine transport from mitochondia to cytoplasm	ala-L[m] -> ala-L[c]	Transport Mitochondrial
S-Adenosyl-L-methionine reversible Transport Mitochondrial	amet[c] <=> amet[m]	Transport Mitochondrial
CO2 transport (diffusion), mitochondrial	co2[c] <=> co2[m]	Transport Mitochondrial
CoA transporter (mitochondrial), irreversible	coa[c] -> coa[m]	Transport Mitochondrial
dihydroxyacetone phosphate Transport Mitochondrial	dhap[m] -> dhap[c]	Transport Mitochondrial
D-lactate Transport Mitochondrial	h[c] + lac-D[c] <=> h[m] + lac-D[m]	Transport Mitochondrial
L-erythro-4-hydroxyglutamate mitochondrial transport via diffusion	e4hglu[c] <=> e4hglu[m]	Transport Mitochondrial
fatty-acyl-ACP mitochondrial transport	dcaACP[m] -> dcaACP[c]	Transport Mitochondrial
fatty-acyl-ACP mitochondrial transport	ddcaACP[m] -> ddcaACP[c]	Transport Mitochondrial
fatty-acyl-ACP mitochondrial transport	myrsACP[m] -> myrsACP[c]	Transport Mitochondrial
fatty-acyl-ACP mitochondrial transport	palmACP[m] -> palmACP[c]	Transport Mitochondrial

fatty-acyl-ACP mitochondrial transport	hdceaACP[m] -> hdceaACP[c]	Transport Mitochondrial
fatty-acyl-ACP mitochondrial transport	hepdcaACP[m] -> hepdcaACP[c]	Transport Mitochondrial
fatty-acyl-ACP mitochondrial transport	hepdceaACP[m] -> hepdceaACP[c]	Transport Mitochondrial
fatty-acyl-ACP mitochondrial transport	ocdcaACP[m] -> ocdcaACP[c]	Transport Mitochondrial
fatty-acyl-ACP mitochondrial transport	ocdceaACP[m] -> ocdceaACP[c]	Transport Mitochondrial
fatty-acyl-ACP mitochondrial transport	ocdcyaACP[m] -> ocdcyaACP[c]	Transport Mitochondrial
fatty-acyl-ACP mitochondrial transport	ocdctaACP[m] -> ocdctaACP[c]	Transport Mitochondrial
fatty-acyl-ACP mitochondrial transport	eicosaACP[m] -> eicosaACP[c]	Transport Mitochondrial
fatty-acyl-ACP mitochondrial transport	eicosapenACP[m] -> eicosapenACP[c]	Transport Mitochondrial
fatty-acyl-ACP mitochondrial transport	docosaACP[m] -> docosaACP[c]	Transport Mitochondrial
fatty-acyl-ACP mitochondrial transport	ttcACP[m] -> ttcACP[c]	Transport Mitochondrial
fatty-acyl-ACP mitochondrial transport	hexcACP[m] -> hexcACP[c]	Transport Mitochondrial
fatty-acyl-ACP mitochondrial transport	hexaACP[m] -> hexaACP[c]	Transport Mitochondrial
fatty-acyl-ACP mitochondrial transport	octaACP[m] -> octaACP[c]	Transport Mitochondrial

iron (II) uptake (mitochondrial)	fe2[c] -> fe2[m]	Transport Mitochondrial
iron (II) transport	fe2[m] -> fe2[c]	Transport Mitochondrial
formate mitochondrial transport	for[m] -> for[c]	Transport Mitochondrial
farnesyl diphosphate transport (mitochondrial)	frdp[c] <=> frdp[m]	Transport Mitochondrial
glycerol-3-phosphate shuttle	glyc3p[c] -> glyc3p[m]	Transport Mitochondrial
glycine mitochondrial transport via proton symport	h[c] + gly[c] <=> h[m] + gly[m]	Transport Mitochondrial
H2O Transport Mitochondrial	h2o[c] <=> h2o[m]	Transport Mitochondrial
Hydroxyisobutyrate Transport Mitochondrial	hibut[m] <=> hibut[c]	Transport Mitochondrial
Isobutyryl coA transport Mitochondrial	ibcoa[m] <=> ibcoa[c]	Transport Mitochondrial
Isoleucine transport from mitochondria to cytosol	ile-L[m] -> ile-L[c]	Transport Mitochondrial
Isopentenyl diphosphate Transport Mitochondrial	ipdp[c] <=> ipdp[m]	Transport Mitochondrial
Isovaleryl coA transport Mitochondrial	ivcoa[m] <=> ivcoa[c]	Transport Mitochondrial
L-lactate Transport Mitochondrial	h[c] + lac-L[c] <=> h[m] + lac-L[m]	Transport Mitochondrial
NH3 mitochondrial transport	nh4[c] <=> nh4[m]	Transport Mitochondrial

O2 transport (diffusion)	o2[c] <=> o2[m]	Transport Mitochondrial
oxaloacetate Transport Mitochondrial	h[c] + oaa[c] <=> oaa[m] + h[m]	Transport Mitochondrial
ornithine mitochondrial transport via proton antiport	h[c] + orn[m] <=> orn[c] + h[m]	Transport Mitochondrial
pantothenate mitochondrial transport	pant-R[c] <=> pant-R[m]	Transport Mitochondrial
phosphatidate reversible Transport Mitochondrial,	pa[c] <=> pa[m]	Transport Mitochondrial
all-trans-Pentaprenyl diphosphate Transport Mitochondrial	pendp[c] <=> pendp[m]	Transport Mitochondrial
phosphatidylethanolamine mitochondrial transport,	pe[c] <=> pe[m]	Transport Mitochondrial
Propanoyl coA Transport	ppcoa[m] <=> ppcoa[c]	Transport Mitochondrial
protoporphyrinogen IX mitochondrial transport	pppg9[c] <=> pppg9[m]	Transport Mitochondrial
L-proline Transport Mitochondrial	pro-L[c] <=> pro-L[m]	Transport Mitochondrial
phosphatidylserine mitochondrial transport,	ps[c] <=> ps[m]	Transport Mitochondrial
pyruvate mitochondrial transport via proton symport	h[c] + pyr[c] <=> pyr[m] + h[m]	Transport Mitochondrial
serine mitochondrial transport via proton symport	h[c] + ser-L[c] <=> h[m] + ser-L[m]	Transport Mitochondrial
threonine mitochondrial transport via proton symport	h[c] + thr-L[c] <=> h[m] + thr-L[m]	Transport Mitochondrial

tyrosine mitochondrial transport via proton symport	h[c] + tyr-L[c] <=> h[m] + tyr-L[m]	Transport Mitochondrial
Valine reversible mitochondrial transport via proton symport	h[c] + val-L[c] <=> h[m] + val-L[m]	Transport Mitochondrial
Transport akg-2oxoadp	akg[c] + 2oxoadp[m] <=> akg[m] + 2oxoadp[c]	Transport Mitochondrial
L-glutamine reversible transport via proton symport	gln-L[e] + h[e] <=> h[c] + gln-L[c]	Transport Reaction
L-histidine reversible transport via proton symport	h[e] + his-L[e] <=> h[c] + his-L[c]	Transport Reaction
Thiamine transport in via proton symport	h[e] + thm[e] -> h[c] + thm[c]	Transport Reaction
L-alanine reversible transport via proton symport	ala-L[e] + h[e] <=> h[c] + ala-L[c]	Transport Reaction
L-asparagine reversible transport via proton symport	asn-L[e] + h[e] <=> h[c] + asn-L[c]	Transport Reaction
L-aspartate reversible transport via proton symport	asp-L[e] + h[e] <=> h[c] + asp-L[c]	Transport Reaction
L-glutamate transport via proton symport, reversible	glu-L[e] + h[e] <=> h[c] + glu-L[c]	Transport Reaction
glycine reversible transport via proton symport	gly[e] + h[e] <=> h[c] + gly[c]	Transport Reaction
L-serine reversible transport via proton symport	h[e] + ser-L[e] <=> h[c] + ser-L[c]	Transport Reaction
L-cysteine reversible transport via proton symport	cys-L[e] + h[e] <=> h[c] + cys-L[c]	Transport Reaction
L-isoleucine reversible transport via proton symport	h[e] + ile-L[e] <=> h[c] + ile-L[c]	Transport Reaction

L-leucine reversible transport via proton symport	h[e] + leu-L[e] <=> h[c] + leu-L[c]	Transport Reaction
orntithine reversible transport in via proton symport	h[e] + orn[e] <=> h[c] + orn[c]	Transport Reaction
L-phenylalanine reversible transport via proton symport	h[e] + phe-L[e] <=> h[c] + phe-L[c]	Transport Reaction
L-threonine reversible transport via proton symport	h[e] + thr-L[e] <=> h[c] + thr-L[c]	Transport Reaction
L-tryptophan reversible transport via proton symport	h[e] + trp-L[e] <=> h[c] + trp-L[c]	Transport Reaction
L-tyrosine reversible transport via proton symport	h[e] + tyr-L[e] <=> h[c] + tyr-L[c]	Transport Reaction
L-valine reversible transport via proton symport	h[e] + val-L[e] <=> h[c] + val-L[c]	Transport Reaction
Allantoin transport	alltn[c] <=> alltn[e]	Transport Reaction
Uric acid transport	urate[c] <=> urate[e]	Transport Reaction
xanthine reversible transport	xan[e] <=> xan[c]	Transport Reaction
Pantothenate reversible transport via proton symport	h[e] + pnto-R[e] <=> h[c] + pnto-R[c]	Transport Reaction
Ala-Asp Transport	h2o[c] + atp[c] + alaasp[e] -> h[c] + adp[c] + pi[c] + alaasp[c]	Transport Reaction
Ala-Gln Transport	h2o[c] + atp[c] + alagln[e] -> h[c] + adp[c] + pi[c] + alagln[c]	Transport Reaction
Ala-Glu Transport	h2o[c] + atp[c] + alaglu[e] -> h[c] + adp[c] + pi[c] + alaglu[c]	Transport Reaction

Ala-Gly Transport	h2o[c] + atp[c] + alagly[e] -> h[c] + adp[c] + pi[c] + alagly[c]	Transport Reaction
Ala-His Transport	h2o[c] + atp[c] + alahis[e] -> h[c] + adp[c] + pi[c] + alahis[c]	Transport Reaction
Ala-Leu Transport	h2o[c] + atp[c] + alaleu[e] -> h[c] + adp[c] + pi[c] + alaleu[c]	Transport Reaction
Ala-Thr Transport	h2o[c] + atp[c] + alathr[e] -> h[c] + adp[c] + pi[c] + alathr[c]	Transport Reaction
Cys-Gly Transport	h2o[c] + atp[c] + cgly[e] <=> h[c] + adp[c] + pi[c] + cgly[c]	Transport Reaction
Glu-Ala Transport	h2o[c] + atp[c] + gluala[e] <=> h[c] + adp[c] + pi[c] + gluala[c]	Transport Reaction
Gly-Asn Transport	h2o[c] + atp[c] + glyasn[e] -> h[c] + adp[c] + pi[c] + glyasn[c]	Transport Reaction
Gly-Asp Transport	h2o[c] + atp[c] + glyasp[e] -> h[c] + adp[c] + pi[c] + glyasp[c]	Transport Reaction
Gly-Gln Transport	h2o[c] + atp[c] + glygln[e] -> h[c] + adp[c] + pi[c] + glygln[c]	Transport Reaction
Gly-Glu Transport	h2o[c] + atp[c] + glyglu[e] -> h[c] + adp[c] + pi[c] + glyglu[c]	Transport Reaction
Gly-Met Transport	h2o[c] + atp[c] + glymet[e] -> h[c] + adp[c] + pi[c] + glymet[c]	Transport Reaction
Gly-Pro Transport	h2o[c] + atp[c] + glypro[e] -> h[c] + adp[c] + pi[c] + glypro[c]	Transport Reaction
Met-Ala Transport	h2o[c] + atp[c] + metala[e] -> h[c] + adp[c] + pi[c] + metala[c]	Transport Reaction
glucose transport (uniport)	glc-D[e] -> glc-D[c]	Transport Reaction

Lactose transport in via proton symport	h[e] + lact[e] -> h[c] + lact[c]	Transport Reaction
4-aminobutyrate reversible transport in via proton symport	4abut[e] + h[e] <=> h[c] + 4abut[c]	Transport Reaction
D-xylose reversible transport	h[e] + xyl-D[e] <=> h[c] + xyl-D[c]	Transport Reaction
maltose transport in via proton symport	h[e] + malt[e] -> h[c] + malt[c]	Transport Reaction
D-fructose transport in via proton symport	fru[e] + h[e] -> h[c] + fru[c]	Transport Reaction
adenine transport in via proton symport	ade[e] + h[e] -> h[c] + ade[c]	Transport Reaction
L-proline reversible transport via proton symport	h[e] + pro-L[e] <=> h[c] + pro-L[c]	Transport Reaction
urea reversible transport via proton symport (2 H+)	2 h[e] + urea[e] <=> 2 h[c] + urea[c]	Transport Reaction
D-galactose transport in via proton symport	gal[e] + h[e] -> h[c] + gal[c]	Transport Reaction
cytidine transport in via proton symport	cytd[e] + h[e] -> h[c] + cytd[c]	Transport Reaction
guanine reversible transport via proton symport	gua[e] + h[e] -> h[c] + gua[c]	Transport Reaction
Nicotinic acid transport	nac[e] <=> nac[c]	Transport Reaction
phosphate reversible transport via symport	h[e] + pi[e] <=> h[c] + pi[c]	Transport Reaction
glycerol transport via symport	glyc[e] + h[e] -> h[c] + glyc[c]	Transport Reaction

L-methionine reversible transport via proton symport	h[e] + met-L[e] <=> h[c] + met-L[c]	Transport Reaction
cytosine transport in via proton symport	csn[e] + h[e] -> h[c] + csn[c]	Transport Reaction
inositol transport in via proton symport	h[e] + inost[e] -> h[c] + inost[c]	Transport Reaction
L-lysine reversible transport via proton symport	h[e] + lys-L[e] <=> h[c] + lys-L[c]	Transport Reaction
ammonia reversible transport	nh4[e] <=> nh4[c]	Transport Reaction
L-arganine reversible transport via proton symport	arg-L[e] + h[e] <=> h[c] + arg-L[c]	Transport Reaction
sulfate irreversible uniport	so4[e] -> so4[c]	Transport Reaction
D-Arabinose reversible transport	arab-D[e] <=> arab-D[c]	Transport Reaction
L-Arabinose reversible transport	arab-L[e] <=> arab-L[c]	Transport Reaction
2-Methylbutanal transport (extracellular)	2mbald[c] <=> 2mbald[e]	Transport Reaction
2-methyl-1-butanol transport (extracellular)	2mbtoh[c] <=> 2mbtoh[e]	Transport Reaction
2-methylpropanal transport (extracellular)	2mppal[c] <=> 2mppal[e]	Transport Reaction
2-oxobutanoate transport	2obut[c] <=> 2obut[e]	Transport Reaction
2-Phosphoglycolate transport in/out via proton symport	2pglyc[e] + h[e] <=> h[c] + 2pglyc[c]	Transport Reaction

D-Glycerate 2-phosphate transport in/out via proton symport	2pg[e] + h[e] -> h[c] + 2pg[c]	Transport Reaction
2-phenylethanol reversible transport	2phetoh[e] <=> 2phetoh[c]	Transport Reaction
2-Isopropylmalate transport, diffusion	3c3hmp[c] <=> 3c3hmp[e]	Transport Reaction
3-methylbutanal transport (extracellular)	3mbald[c] <=> 3mbald[e]	Transport Reaction
3mop reversible trasport	3mop[e] <=> 3mop[c]	Transport Reaction
3-Phospho-D-glycerate transport in/out via proton symport	3pg[e] + h[e] -> h[c] + 3pg[c]	Transport Reaction
4-Aminobenzoate mitochondrial transport via diffusion	4abz[c] <=> 4abz[e]	Transport Reaction
hydroxyproline transport	4hpro-LT[c] <=> 4hpro-LT[e]	Transport Reaction
5-Aminolevulinate transport in via proton symport	5aop[e] + h[e] -> h[c] + 5aop[c]	Transport Reaction
6-Phospho-D-gluconate transport in/out via proton symport	6pgc[e] + h[e] <=> h[c] + 6pgc[c]	Transport Reaction
8-Amino-7-oxononanoate reversible transport via proton symport	8aonn[e] + h[e] <=> h[c] + 8aonn[c]	Transport Reaction
Acetoacetate transport	acac[c] <=> acac[e]	Transport Reaction
acetaldehyde reversible transport	acald[e] <=> acald[c]	Transport Reaction
Acetamide transport	acetm[c] <=> acetm[e]	Transport Reaction

N-Acetyl Glucosamine reversible transport	acgam[e] <=> acgam[c]	Transport Reaction
acetate transporter	ac[e] <=> ac[c]	Transport Reaction
adenosine transport in via proton symport	adn[e] + h[e] -> h[c] + adn[c]	Transport Reaction
Agmatine transport	agm[c] <=> agm[e]	Transport Reaction
2-oxoglutarate reversible transport via symport	akg[e] + h[e] <=> h[c] + akg[c]	Transport Reaction
D-Alanine reversible transport	ala-D[e] <=> ala-D[c]	Transport Reaction
S-adenosyl-L-methionine transport in via proton symport	amet[e] + h[e] -> h[c] + amet[c]	Transport Reaction
AMP transport in/out via proton symport	amp[e] + h[e] <=> h[c] + amp[c]	Transport Reaction
D-Arabinitol reversible transport	abt-D[e] <=> abt-D[c]	Transport Reaction
L-Arabinitol reversible transport	abt-L[e] <=> abt-L[c]	Transport Reaction
(R,R)-butanediol transport	btd-RR[c] <=> btd-RR[e]	Transport Reaction
Biotin uptake	btn[e] + h[e] -> h[c] + btn[c]	Transport Reaction
Methanethiol Transport	ch4s[e] <=> ch4s[c]	Transport Reaction
choline transport via proton symport	chol[e] + h[e] <=> h[c] + chol[c]	Transport Reaction

L-Citruline transport	citr-L[c] <=> citr-L[e]	Transport Reaction
citrate reversible transport via symport	cit[e] + h[e] <=> h[c] + cit[c]	Transport Reaction
CMP transport in/out via proton symport	cmp[e] + h[e] <=> h[c] + cmp[c]	Transport Reaction
CO2 transporter via diffusion	co2[e] <=> co2[c]	Transport Reaction
Cystathione Transport	cyst-L[e] <=> cyst-L[c]	Transport Reaction
deoxyadenosine transport in via proton symport	dad-2[e] + h[e] -> h[c] + dad-2[c]	Transport Reaction
7,8-Diaminononanoate reversible transport via proton symport	dann[e] + h[e] <=> h[c] + dann[c]	Transport Reaction
Decanoate (n-C10:0), Transport	dca[e] <=> dca[c]	Transport Reaction
deoxycytidine transport in via proton symport	dcyt[e] + h[e] -> h[c] + dcyt[c]	Transport Reaction
Dodecanoate (n-C12:0), Transport	ddca[e] <=> ddca[c]	Transport Reaction
deoxyguanosine transport in via proton symport	dgsn[e] + h[e] -> h[c] + dgsn[c]	Transport Reaction
Dihydroxy acetone transport	dha[c] <=> dha[e]	Transport Reaction
deoxyinosine transport in via proton symport	din[e] + h[e] -> h[c] + din[c]	Transport Reaction
D-lactate transport via proton symport	h[e] + lac-D[e] <=> h[c] + lac-D[c]	Transport Reaction

Docosanoic acid, Transport	docosa[e] <=> docosa[c]	Transport Reaction
Thymidine 5 Phosphate Transport	dtmp[c] <=> dtmp[e]	Transport Reaction
dTTP reversible uniport	dttp[e] <=> dttp[c]	Transport Reaction
deoxyuridine transport in via proton symport	duri[e] + h[e] -> h[c] + duri[c]	Transport Reaction
Eicosapentaenoate, Transport	eicosapen[e] <=> eicosapen[c]	Transport Reaction
episterol reversible transport	epist[e] <=> epist[c]	Transport Reaction
ergosterol reversible transport	ergst[e] <=> ergst[c]	Transport Reaction
ethanolamine transport via diffusion (extracellular)	etha[e] <=> etha[c]	Transport Reaction
ethanol reversible transport	etoh[e] <=> etoh[c]	Transport Reaction
Lactose Exchange	lact[e] <=>	Transport Reaction
Fructose-6-phosphate transport via phosphate antiport	2 pi[c] + f6p[e] -> f6p[c] + 2 pi[e]	Transport Reaction
iron (II) transport	fe2[e] -> fe2[c]	Transport Reaction
fecosterol reversible transport	fecost[e] <=> fecost[c]	Transport Reaction
formate transport via diffusion	for[e] <=> for[c]	Transport Reaction

Formamide transport	frmd[c] <=> frmd[e]	Transport Reaction
fumarate reversible transport via symport	fum[e] + h[e] -> fum[c] + h[c]	Transport Reaction
Glucose-1-phosphate transport via phosphate antiport	2 pi[c] + g1p[e] -> 2 pi[e] + g1p[c]	Transport Reaction
glycero-3-phosphocholine transport (extracellular to cytosol)	g3pc[e] <=> g3pc[c]	Transport Reaction
glycero-3-phospho-1-inositol transport (extracellular to cytosol)	g3pi[e] <=> g3pi[c]	Transport Reaction
Glucose-6-phosphate transport via phosphate antiport	2 pi[c] + g6p[e] -> 2 pi[e] + g6p[c]	Transport Reaction
D-glucosamine 6-phosphate reversible uniport	gam6p[e] -> gam6p[c]	Transport Reaction
Glycoaldehydye reversible transport	gcald[e] <=> gcald[c]	Transport Reaction
Gluconate transport	glcn-D[c] <=> glcn-D[e]	Transport Reaction
glyoxylate transport	glx[c] <=> glx[e]	Transport Reaction
glycerol-3-phosphate transport in via proton symport	glyc3p[e] + h[e] -> h[c] + glyc3p[c]	Transport Reaction
glycolate transport via proton symport, reversible	glyclt[e] + h[e] <=> h[c] + glyclt[c]	Transport Reaction
glycerol transport via channel	glyc[c] <=> glyc[e]	Transport Reaction
GMP transport in/out via proton symport	gmp[e] + h[e] <=> h[c] + gmp[c]	Transport Reaction

guanosine transport in via proton symport	gsn[e] + h[e] -> h[c] + gsn[c]	Transport Reaction
oxidized glutathione irreversible uniport	gthox[e] -> gthox[c]	Transport Reaction
glutathione transport	gthrd[e] -> gthrd[c]	Transport Reaction
H2O transport via diffusion	h2o[e] <=> h2o[c]	Transport Reaction
HCO3 equilibration reaction	h2o[c] + co2[c] <=> h[c] + hco3[c]	Transport Reaction
HCO3 equilibration reaction	h2o[m] + co2[m] <=> h[m] + hco3[m]	Transport Reaction
Hexadecanoate (n-C16:0), Transport	hdca[e] <=> hdca[c]	Transport Reaction
Hexadecenoate (n-C16:1), Transport	hdcea[e] <=> hdcea[c]	Transport Reaction
Heptadecenoate, Transport	hepdcea[e] <=> hepdcea[c]	Transport Reaction
Hexanoate, Transport	hexa[e] <=> hexa[c]	Transport Reaction
Hexacoa Transport	hexacoa[c] <=> hexacoa[e]	Transport Reaction
hexacosanoate, Transport	hexc[e] <=> hexc[c]	Transport Reaction
homoserine transport	hom-L[c] <=> hom-L[e]	Transport Reaction
isoamyl alcohol transport (extracellular)	iamoh[c] <=> iamoh[e]	Transport Reaction

isobutyl alcohol transport (extracellular)	ibutoh[c] <=> ibutoh[e]	Transport Reaction
Tryptophol transport	ind3eth[c] <=> ind3eth[e]	Transport Reaction
inosine transport in via proton symport	h[e] + ins[e] -> h[c] + ins[c]	Transport Reaction
Potassium transport via proton symport	h[e] + k[e] -> h[c] + k[c]	Transport Reaction
lanosterol reversible transport	lanost[e] <=> lanost[c]	Transport Reaction
L-cysteate transport	h2o[c] + atp[c] + lcyst[e] -> h[c] + adp[c] + pi[c] + lcyst[c]	Transport Reaction
L-lactate reversible transport via proton symport	h[e] + lac-L[e] <=> h[c] + lac-L[c]	Transport Reaction
L-Rhamnose Transport	rham-L[c] <=> rham-L[e]	Transport Reaction
L-malate reversible transport via proton symport	h[e] + mal-L[e] <=> h[c] + mal-L[c]	Transport Reaction
Maltotriose transport	h[e] + maltr[e] <=> h[c] + maltr[c]	Transport Reaction
MAN1P transport in/out via proton symport	h[e] + man1p[e] -> h[c] + man1p[c]	Transport Reaction
MAN6P transport in/out via proton symport	h[e] + man6p[e] -> h[c] + man6p[c]	Transport Reaction
D-Mannitol Transport	mnl[c] <=> mnl[e]	Transport Reaction
D-mannose transport in via proton symport	h[e] + man[e] -> h[c] + man[c]	Transport Reaction

NADP transporter	nadp[c] <=> nadp[e]	Transport Reaction
nmntp	h[e] + nmn[e] -> h[c] + nmn[c]	Transport Reaction
o2 transport (diffusion)	o2[e] <=> o2[c]	Transport Reaction
Oxaloacetate transport	oaa[c] <=> oaa[e]	Transport Reaction
Octadecanoate (n-C18:0), Transport	ocdca[e] <=> ocdca[c]	Transport Reaction
Octadecenoate (n-C18:1), Transport	ocdcea[e] <=> ocdcea[c]	Transport Reaction
Octadecatrienoate, Transport	ocdcta[e] <=> ocdcta[c]	Transport Reaction
Octadecadienoate (n-C18:2), Transport	ocdcya[e] <=> ocdcya[c]	Transport Reaction
Octanoate (n-C8:0), Transport	octa[e] <=> octa[c]	Transport Reaction
5-oxoproline transport	opro-L[c] <=> opro-L[e]	Transport Reaction
Phenylacetaldehyde transport (extracellular)	pacald[c] <=> pacald[e]	Transport Reaction
PAP reversible uniport	pap[e] <=> pap[c]	Transport Reaction
Phosphoenolpyruvate transport in via proton symport	h[e] + pep[e] -> h[c] + pep[c]	Transport Reaction
diphosphate transport in via ABC system	h2o[c] + atp[c] + ppi[e] -> h[c] + adp[c] + pi[c] + ppi[c]	Transport Reaction

O-Phospho-L-serine transport in via proton symport	h[e] + pser-L[e] <=> h[c] + pser-L[c]	Transport Reaction
putrescine transport in via proton antiport, irreversible	h[c] + ptrc[e] -> ptrc[c] + h[e]	Transport Reaction
Pyruvate exchange, diffusion	pyr[c] -> pyr[e]	Transport Reaction
pyruvate transport in via proton symport	h[e] + pyr[e] -> h[c] + pyr[c]	Transport Reaction
riboflavin transport in via proton symport	h[e] + ribflv[e] -> h[c] + ribflv[c]	Transport Reaction
Ribitol reversible transport	rbt[e] <=> rbt[c]	Transport Reaction
ribose transport in via proton symporter	h[e] + rib-D[e] -> h[c] + rib-D[c]	Transport Reaction
D-sorbitol transport via passive diffusion	sbt-D[e] <=> sbt-D[c]	Transport Reaction
L-sorbitol transport via passive diffusion	sbt-L[e] <=> sbt-L[c]	Transport Reaction
sulfite transport (efflux, cytosol to extracellular)	so3[c] -> so3[e]	Transport Reaction
spermidine transport in via proton antiport	h[c] + spmd[e] -> spmd[c] + h[e]	Transport Reaction
Spermine transport via proton antiport	h[c] + sprm[e] -> sprm[c] + h[e]	Transport Reaction
L-sorbose reversible transport	srb-L[e] <=> srb-L[c]	Transport Reaction
succinate transport via proton symport	h[e] + succ[e] <=> succ[c] + h[c]	Transport Reaction

sucrose transport in via proton symport	h[e] + sucr[e] -> h[c] + sucr[c]	Transport Reaction
Taurine Transport	taur[c] <=> taur[e]	Transport Reaction
thiamin diphosphatase, extracellular	2 h2o[e] + thmpp[e] -> h[e] + 2 pi[e] + thm[e]	Transport Reaction
thymidine transport in via proton symport	h[e] + thymd[e] <=> h[c] + thymd[c]	Transport Reaction
thiamin phosphatase, extracellular	h2o[e] + thmmp[e] -> pi[e] + thm[e]	Transport Reaction
thymine reversible transport via proton antiport	h[e] + thym[c] <=> h[c] + thym[e]	Transport Reaction
Trimetaphosphate transport	tmp[c] <=> tmp[e]	Transport Reaction
trehalose transport in via proton symporter	h[e] + tre[e] -> h[c] + tre[c]	Transport Reaction
Tetradecanoate (n-C14:0), Transport	ttdca[e] <=> ttdca[c]	Transport Reaction
UMP transport in via proton symport	h[e] + ump[e] <=> h[c] + ump[c]	Transport Reaction
Uracil transport in via proton symport	h[e] + ura[e] <=> h[c] + ura[c]	Transport Reaction
uridine transport in via proton symport	h[e] + uri[e] -> h[c] + uri[c]	Transport Reaction
xanthosine transport in via proton symport	h[e] + xtsn[e] -> h[c] + xtsn[c]	Transport Reaction
Xylitol transport via passive diffusion	xylt[e] <=> xylt[c]	Transport Reaction

zymosterol reversible transport	zymst[e] <=> zymst[c]	Transport Reaction
Hydrogen transport	h[c] -> h[e]	Transport Reaction
Catalase	2 h2o2[c] -> 2 h2o[c] + o2[c]	Tryptophan Metabolism
kynurenine 3-monooxygenase	h[c] + nadph[c] + o2[c] + Lkynr[c] -> nadp[c] + h2o[c] + hLkynr[c]	Tryptophan Metabolism
Amidase	h2o[c] + iad[c] -> nh4[c] + ind3ac[c]	Tryptophan metabolism
N-Formyl-L-kynurenine amidohydrolase	h2o[c] + Lfmkynr[c] -> h[c] + for[c] + Lkynr[c]	Tryptophan Metabolism
3-Hydroxy-L-kynurenine hydrolase	h2o[c] + hLkynr[c] -> ala-L[c] + 3hanthrn[c]	Tryptophan Metabolism
kynureninase	h2o[c] + Lkynr[c] -> h[c] + ala-L[c] + anth[c]	Tryptophan Metabolism
3-hydroxyanthranilate 3,4-dioxygenase	o2[c] + 3hanthrn[c] -> h[c] + cmusa[c]	Tryptophan Metabolism
L-Tryptophan:oxygen 2,3-oxidoreductase (decyclizing)	o2[c] + trp-L[c] -> Lfmkynr[c]	Tryptophan Metabolism
aminomuconate semialdehyde dehydrogenase	h2o[c] + nad[c] + am6sa[c] -> 2 h[c] + nadh[c] + amuco[c]	Tryptophan Metabolism
Picolinic acid decarboxylase	h[c] + cmusa[c] -> co2[c] + am6sa[c]	Tryptophan Metabolism
Quinolinate Synthase (Eukaryotic)	cmusa[c] -> h[c] + h2o[c] + quln[c]	Tryptophan Metabolism
Nitrilase	2 h2o[c] + ind3acnl[c] -> nh4[c] + ind3ac[c]	Tryptophan Metabolism

Formaldehyde dehydrogenase - Glutathione dependent	nad[c] + hmgth[c] <=> h[c] + nadh[c] + Sfglutth[c]	Tyrosine Metabolism
4-Hydroxyphenylpyruvate:oxygen oxidoreductase	o2[c] + 34hpp[c] -> co2[c] + hgentis[c]	Tyrosine Metabolism
Fumarylacetoacetase	h2o[c] + 4fumacac[c] -> fum[c] + h[c] + acac[c]	Tyrosine Metabolism
Homogentisate:oxygen 1,2-oxidoreductase (decyclizing)	o2[c] + hgentis[c] -> h[c] + 4mlacac[c]	Tyrosine Metabolism
Maleylacetoacetate isomerase	4mlacac[c] -> 4fumacac[c]	Tyrosine Metabolism
Spermidine acetyltransferase	accoa[c] + spmd[c] -> h[c] + coa[c] + N1aspmd[c]	Tyrosine Metabolism
Spermine acetyltransferase	accoa[c] + sprm[c] -> h[c] + coa[c] + N1sprm[c]	Tyrosine Metabolism
2-aceto-2-hydroxybutanoate synthase, mitochondrial	pyr[m] + h[m] + 2obut[m] -> co2[m] + 2ahbut[m]	Valine, leucine and isoleucine Biosynthesis
3-isopropylmalate dehydrogenase	nad[c] + 3c2hmp[c] -> h[c] + nadh[c] + 3c4mop[c]	Valine, leucine and isoleucine Biosynthesis
3-isopropylmalate dehydratase	3c2hmp[c] <=> h2o[c] + 2ippm[c]	Valine, leucine and isoleucine Biosynthesis
2-isopropylmalate hydratase	h2o[c] + 2ippm[c] <=> 3c3hmp[c]	Valine, leucine and isoleucine Biosynthesis
Dihydroxy-acid dehydratase (2,3-dihydroxy-3-methylpentanoate), mitochondrial	23dhmp[m] -> h2o[m] + 3mop[m]	Valine, leucine and isoleucine Biosynthesis
Ketol-acid reductoisomerase (2-Aceto-2-hydroxybutanoate), mitochondrial	h[m] + nadph[m] + 2ahbut[m] -> nadp[m] + 23dhmp[m]	Valine, leucine and isoleucine Biosynthesis
L-threonine deaminase, mitochondrial	thr-L[m] -> nh4[m] + 2obut[m]	Valine, leucine and isoleucine Biosynthesis

Aldehyde dehydrogenase (Tryptophol, NAD)	h[c] + nadh[c] + id3acald[c] -> nad[c] + ind3eth[c]	Valine, leucine and isoleucine Metabolism
aldehyde dehydrogenase (2-methylbutanol, NAD)	h[c] + nadh[c] + 2mbald[c] -> nad[c] + 2mbtoh[c]	Valine, leucine and isoleucine Metabolism
aldehyde dehydrogenase (isoamyl alcohol, NAD)	h[c] + nadh[c] + 3mbald[c] -> nad[c] + iamoh[c]	Valine, leucine and isoleucine Metabolism
aldehyde dehydrogenase (isobutyl alcohol, NAD)	h[c] + nadh[c] + 2mppal[c] -> nad[c] + ibutoh[c]	Valine, leucine and isoleucine Metabolism
aldehyde dehydrogenase (2-phenylethanol, NAD)	h[c] + nadh[c] + pacald[c] -> nad[c] + 2phetoh[c]	Valine, leucine and isoleucine Metabolism
Urea Amidolyase	atp[c] + hco3[c] + mcrocoa[c] <=> 2 h[c] + adp[c] + pi[c] + mglutcoa[c]	Valine, leucine and isoleucine Metabolism
aldehyde dehydrogenase (2-methylbutanol, NADP)	h[c] + nadph[c] + 2mbald[c] -> nadp[c] + 2mbtoh[c]	Valine, leucine and isoleucine Metabolism
aldehyde dehydrogenase (isoamyl alcohol, NADP)	h[c] + nadph[c] + 3mbald[c] -> nadp[c] + iamoh[c]	Valine, leucine and isoleucine Metabolism
aldehyde dehydrogenase (isobutyl alcohol, NADP)	h[c] + nadph[c] + 2mppal[c] -> nadp[c] + ibutoh[c]	Valine, leucine and isoleucine Metabolism
aldehyde dehydrogenase (2-phenylethanol, NADP)	h[c] + nadph[c] + pacald[c] -> nadp[c] + 2phetoh[c]	Valine, leucine and isoleucine Metabolism
Aldehyde dehydrogenase (Tryptophol, NADP)	h[c] + nadph[c] + id3acald[c] -> nadp[c] + ind3eth[c]	Valine, leucine and isoleucine Metabolism
Hydroxy ButyrylcoA hydrolase	h2o[c] + hibcoa[c] <=> h[c] + coa[c] + hibut[c]	Valine, leucine and isoleucine Metabolism
Methyl acrylylcoA hydratase	h2o[c] + macrylcoa[c] <=> hibcoa[c]	Valine, leucine and isoleucine Metabolism
Methyl But2enoyl coA hydratase	h2o[c] + 2mb2coa[c] <=> 3hmbcoa[c]	Valine, leucine and isoleucine Metabolism

Methyl GlutaconylcoA hydratase	h2o[c] + mglutcoa[c] <=> hmgcoa[c]	Valine, leucine and isoleucine Metabolism
3-hydroxyacyl-CoA dehydrogenase (2-Methylacetoacetyl-CoA)	nad[c] + 3hmbcoa[c] <=> h[c] + nadh[c] + 2maacoa[c]	Valine, leucine and isoleucine Metabolism
acetyl-CoA C-acyltransferase (2-Methyl-3-acetoacetyl-CoA)	coa[c] + 2maacoa[c] <=> accoa[c] + ppcoa[c]	Valine, leucine and isoleucine Metabolism
Branced Chain acyl coA dehydrogenase	h[c] + fad[c] + ibcoa[c] <=> fadh2[c] + macrylcoa[c]	Valine, leucine and isoleucine Metabolism
Branced Chain acyl coA dehydrogenase	h[c] + fad[c] + ivcoa[c] <=> fadh2[c] + mcrocoa[c]	Valine, leucine and isoleucine Metabolism
Branced Chain acyl coA dehydrogenase	h[c] + fad[c] + 2mbcoa[c] <=> fadh2[c] + 2mb2coa[c]	Valine, leucine and isoleucine Metabolism
Oxo acid coA transferase	succoa[m] + acac[m] <=> succ[m] + aacoa[m]	Valine, leucine and isoleucine Metabolism
Isoleucine transaminase,mitochondrial	akg[m] + ile-L[m] <=> glu-L[m] + 3mop[m]	Valine, leucine and isoleucine Metabolism
Leucine transaminase,mitochondrial	akg[m] + leu-L[m] <=> glu-L[m] + 4mop[m]	Valine, leucine and isoleucine Metabolism
2-oxo-4-methyl-3-carboxypentanoate decarboxylation	h[m] + 3c4mop[m] -> co2[m] + 4mop[m]	Valine, leucine and isoleucine Metabolism
Valine transaminase,mitovhondrial	akg[m] + val-L[m] <=> glu-L[m] + 3mob[m]	Valine, leucine and isoleucine Metabolism
Hydroxy isobutyrate dehydrogenase	nad[m] + hibut[m] <=> h[m] + nadh[m] + 2mop[m]	Valine, leucine and isoleucine Metabolism
3-Methyl-2-oxobutanoate decarboxylase	h[c] + 3mob[c] -> co2[c] + 2mppal[c]	Valine, leucine and isoleucine Metabolism
3-Methyl-2-oxopentanoate decarboxylase	h[c] + 3mop[c] -> co2[c] + 2mbald[c]	Valine, leucine and isoleucine Metabolism

4-Methyl-2-oxopentanoate decarboxylase	h[c] + 4mop[c] -> co2[c] + 3mbald[c]	Valine, leucine and isoleucine Metabolism
2-oxoisovalerate dehydrogenase	nad[c] + coa[c] + 3mop[c] <=> nadh[c] + co2[c] + 2mbcoa[c]	Valine, leucine and isoleucine Metabolism
Keto-Isocaproate dehydrogenase	coa[m] + nad[m] + 4mop[m] <=> h[m] + nadh[m] + ivcoa[m]	Valine, leucine and isoleucine Metabolism
2-Oxovalerate dehydrogenase	coa[m] + nad[m] + 3mob[m] <=> h[m] + nadh[m] + ibcoa[m]	Valine, leucine and isoleucine Metabolism
Isoleucine transaminase	akg[c] + ile-L[c] <=> glu-L[c] + 3mop[c]	Valine, leucine and isoleucine Metabolism
Leucine transaminase	akg[c] + leu-L[c] <=> glu-L[c] + 4mop[c]	Valine, leucine and isoleucine Metabolism
2-Oxo-4-methyl-3-carboxypentanoate decarboxylation	h[c] + 3c4mop[c] -> co2[c] + 4mop[c]	Valine, leucine and isoleucine Metabolism
Valine transaminase	val-L[c] + akg[c] <=> 3mob[c] + glu-L[c]	Valine, leucine and isoleucine Metabolism
Pyridoxamine kinase	atp[c] + pydam[c] -> h[c] + adp[c] + pyam5p[c]	Vitamin B6 Metabolism
Pyridoxal kinase	atp[c] + pydx[c] -> h[c] + adp[c] + pydx5p[c]	Vitamin B6 Metabolism
Pyridoxine kinase	atp[c] + pydxn[c] -> h[c] + adp[c] + pdx5p[c]	Vitamin B6 Metabolism
Pyridoxine 5'-phosphate oxidase	o2[c] + pdx5p[c] <=> h2o2[c] + pydx5p[c]	Vitamin B6 Metabolism
Pyridoxamine 5'-phosphate oxidase	h2o[c] + o2[c] + pyam5p[c] -> nh4[c] + h2o2[c] + pydx5p[c]	Vitamin B6 Metabolism
Pyridoxine oxidase	o2[c] + pydxn[c] -> h2o2[c] + pydx[c]	Vitamin B6 Metabolism

Pyridoxal oxidase	2 h2o[c] + 0.5 o2[c] + nh4[c] + pydx[c] <=> 2 h2o2[c] + pydam[c]	Vitamin B6 Metabolism
Pyridoxal-5'-phosphate synthase	gln-L[c] + g3p[c] + r5p[c] -> glu-L[c] + pydx5p[c]	Vitamin B6 Metabolism
Pyridoxine Dehydrogenase	nadp[c] + pydxn[c] <=> h[c] + nadph[c] + pydx[c]	Vitamin B6 Metabolism

A5 Metabolite list in iAD828

Abbreviations	Full name
10ft	10-Formyltetrahydrofolate
12dgr	1,2-Diacylglycerol
13BDglcn	1,3-beta-D-Glucan
13dpg	3-Phospho-D-glyceroyl phosphate
14glun	(1,4-alpha-D-Glucosyl)n
1ag3p	1-Acyl-sn-glycerol 3-phosphate
1agly3p	1-Acyl-glycerone 3-phosphate
1agpc	acyl-glycerophosphocholine
1pyr5c	1-Pyrroline-5-carboxylate
23dhdp	2,3-Dihydrodipicolinate
23dhmb	(R)-2,3-Dihydroxy-3-methylbutanoate
23dph	2,3-Bisphospho-D-glycerate
23drhamn	2-Dehydro-3-deoxy-L-rhamnonate
25aics	(S)-2-[5-Amino-1-(5-phospho-D-ribosyl)imidazole-4-carboxamido]succinate
25dhpp	2,5-Diamino-6-hydroxy-4-(5-phosphoribosylamino)-pyrimidine
2ahbut	(S)-2-Aceto-2-hydroxybutanoate
2ahhmd	2-Amino-4-hydroxy-6-hydroxymethyl-7,8-dihydropteridine diphosphate
2ahhmp	2-Amino-4-hydroxy-6-hydroxymethyl-7,8-dihydropteridine
2cpr5p	1-(2-Carboxyphenylamino)-1-deoxy-D-ribulose 5-phosphate
2dda7p	2-Dehydro-3-deoxy-D-arabino-heptonate 7-phosphate
2dhp	2-Dehydropantoate
2dr1p	2-Deoxy-D-ribose 1-phosphate
2dr5p	2-Deoxy-D-ribose 5-phosphate
2glcna	2-Dehydro-D-gluconate
2hhxdal	2-Hydroxy-hexadecanal
2hp6mbq	2-Hexaprenyl-6-methoxy-1,4-benzoquinone
2hp6mp	2-Hexaprenyl-6-methoxyphenol
2hpmhmbq	2-Hexaprenyl-3-methyl-5-hydroxy-6-methoxy-1,4-benzoquinone
2hpmmbq	2-Hexaprenyl-3-methyl-6-methoxy-1,4-benzoquinone
2ins	2-Inosose
2ippm	2-Isopropylmaleate
2kmb	2-keto-4-methylthiobutyrate

2maacoa	2-Methyl-3-acetoacetyl-CoA
2mahmp	2-Methyl-4-amino-5-hydroxymethylpyrimidine diphosphate
2mb2coa	trans-2-Methylbut-2-enoyl-CoA
2mbald	2-Methylbutanal
2mbcoa	2-Methylbutanoyl-CoA
2mbtoh	2-Methyl Butanol
2mcit	2-Methylcitrate
2mop	2-Methyl-3-oxopropanoate
2mppal	2-Methyl 1- Propanal
2obut	2-Oxobutanoate
2oxoadp	2-Oxoadipate
2pg	D-Glycerate 2-phosphate
2pglyc	2-Phosphoglycolate
2phetoh	2-Phenylethanol
34hpp	3-(4-Hydroxyphenyl)pyruvate
3c2hmp	3-Carboxy-2-hydroxy-4-methylpentanoate
3c3hmp	3-Carboxy-3-hydroxy-4-methylpentanoate
3c4mop	3-Carboxy-4-methyl-2-oxopentanoate
3dh5hpb	3-Hexaprenyl-4,5-dihydroxybenzoate
3dhq	3-Dehydroquinate
3dhsk	3-Dehydroshikimate
3dsphgn	3-Dehydrosphinganine
3hanthrn	3-Hydroxyanthranilate
3hmbcoa	(S)-3-Hydroxy-2-methylbutyryl-CoA
3hph5mb	3-Hexaprenyl-4-hydroxy-5-methoxybenzoate
3ig3p	C-(3-Indolyl)-glycerol 3-phosphate
3mbald	3-Methylbutanal
3mob	3-Methyl-2-oxobutanoate
3mop	(S)-3-Methyl-2-oxopentanoate
3ophb_5	3-Hexaprenyl-4-hydroxybenzoate
3pg	3-Phospho-D-glycerate
3php	3-Phosphohydroxypyruvate
3psme	5-O-(1-Carboxyvinyl)-3-phosphoshikimate
44mctr	4,4-dimethylcholesta-8,14,24-trienol
44mzym	4,4-dimethyllanosterol
4abut	4-Aminobutanoate
4abz	4-Aminobenzoate
4adcho	4-amino-4-deoxychorismate

4ahmmp	4-Amino-5-hydroxymethyl-2-methylpyrimidine
4ampm	4-Amino-2-methyl-5-phosphomethylpyrimidine
4fumacac	4-Fumarylacetoacetate
4h2oglt	4-Hydroxy-2-oxoglutarate
4hbz	4-Hydroxybenzoate
4hpro-LT	trans-4-Hydroxy-L-proline
4mhetz	4-Methyl-5-(2-hydroxyethyl)-thiazole
4mlacac	4-Maleylacetoacetate
4mop	4-Methyl-2-oxopentanoate
4mpetz	4-Methyl-5-(2-phosphoethyl)-thiazole
4mzym	4-methylzymosterol
4mzym_int1	4alpha-Methylzymosterol-4-carboxylate
4mzym_int2	3-Keto-4-methylzymosterol
4pasp	4-Phospho-L-aspartate
4ppan	D-4-Phosphopantothenate
4ppcys	N-((R)-4-Phosphopantothenoyl)-L-cysteine
4r5au	4-(1-D-Ribitylamino)-5-aminouracil
5aizc	5-amino-1-(5-phospho-D-ribosyl)imidazole-4-carboxylate
5aop	5-Amino-4-oxopentanoate
5aprbu	5-Amino-6-(5-phosphoribitylamino)uracil
5apru	5-Amino-6-(5-phosphoribosylamino)uracil
5dpmev	(R)-5-Diphosphomevalonate
5fthf	5-Formyltetrahydrofolate
5mdr1p	5-Methylthio-5-deoxy-D-ribose 1-phosphate
5mdru1p	5-Methylthio-5-deoxy-D-ribulose 1-phosphate
5mta	5-Methylthioadenosine
5mthf	5-Methyltetrahydrofolate
5pmev	(R)-5-Phosphomevalonate
6pgc	6-Phospho-D-gluconate
6pgc	6-Phospho-D-gluconate
6pgl	6-phospho-D-glucono-1,5-lactone
8aonn	8-Amino-7-oxononanoate
aacoa	Acetoacetyl-CoA
abt-D	D- Arabitol
abt-L	L-Arabitol
ac	Acetate
acac	Acetoacetate
acACP	Acetyl-ACP

acald	Acetaldehyde
accoa	Acetyl-CoA
acetm	Acetamide
acg5p	N-Acetyl-L-glutamyl 5-phosphate
acg5sa	N-Acetyl-L-glutamate 5-semialdehyde
acgam	N-Acetyl-D-glucosamine
acgam1p	N-Acetyl-D-glucosamine 1-phosphate
acgam6p	N-Acetyl-D-glucosamine 6-phosphate
acglu	N-Acetyl-L-glutamate
achms	O-Acetyl-L-homoserine
acorn	N2-Acetyl-L-ornithine
ACP	acyl carrier protein
acser	O-Acetyl-L-serine
actn-R	(R)-Acetoin
acybut	gamma-Amino-gamma-cyanobutanoate
ade	Adenine
adn	Adenosine
adp	ADP
adprib	ADPribose
agm	Agmatine
ahcys	S-Adenosyl-L-homocysteine
ahdt	2-Amino-4-hydroxy-6-(erythro-1,2,3-trihydroxypropyl)dihydropteridine triphosphate
aicar	5-Amino-1-(5-Phospho-D-ribosyl)imidazole-4-carboxamide
air	5-amino-1-(5-phospho-D-ribosyl)imidazole
akg	2-Oxoglutarate
alaasp	L-Alanine-L-Aspartate
ala-B	beta-Alanine
alac-S	(S)-2-Acetolactate
ala-D	D-Alanine
alagln	L-Alanine -L-Glutamine
alaglu	L-alanine-L-glutamate
alagly	L-alanine-Glycine
alahis	L-alanine-L-Histidine
ala-L	L-Alanine
alaleu	L-alanine-L-Leucine
alathr	L-alanine-L-Threonine
allphn	Allophanate

alltn	Allantoin
alltt	Allantoate
alpam	S-aminomethyldihydrolipoamide
am6sa	2-Aminomuconate 6-semialdehyde
amacald	Aminoacetaldehyde
amet	S-Adenosyl-L-methionine
ametam	S-Adenosylmethioninamine
amob	S-Adenosyl-4-methylthio-2-oxobutanoate
amp	AMP
amuco	2-Aminomuconate
anth	Anthranilate
ap4g	P1-(5-adenosyl),P4-(5-guanosyl) tetraphosphate
aproa	3-Aminopropanal
aprop	alpha-Aminopropiononitrile
aprut	N-Acetylputrescine
aps	Adenosine 5-phosphosulfate
arab-D	D-Arabinose
arab-L	L-Arabinose
arg-L	L-Arginine
argsuc	N(omega)-(L-Arginino)succinate
asn-L	L-Asparagine
asp-L	L-Aspartate
aspsa	L-Aspartate 4-semialdehyde
atp	ATP
b124tc	But-1-ene-1,2,4-tricarboxylate
bf26p	beta-D-Fructose 2,6-phosphate
bf6p	beta-D-Fructose 6-bisphosphate
btd-RR	(R,R)-2,3-Butanediol
btn	Biotin
camp	cAMP
cbasp	N-Carbamoyl-L-aspartate
cbp	Carbamoyl phosphate
cdp	CDP
cdpchol	CDPcholine
cdpdag	CDPdiacylglycerol
cdpea	CDPethanolamine
cellb	Cellobiose
cer1_24	Ceramide-1 (Sphinganine:n-C24:0)

cer1_26	Ceramide-1 (Sphinganine:n-C26:0)
cer2_24	Ceramide-2 (Phytosphingosine:n-C24:0)
cer2_26	Ceramide-2 (Phytosphingosine:n-C26:0)
cer3	N-Acylsphingosine
cer3_24	Ceramide-3 (Phytosphingosine:n-C24:0OH)
cer3_26	Ceramide-3 (Phytosphingosine:n-C26:0OH)
cgly	Cys-Gly
ch4s	Methanethiol
chitin	Chitin (monomer)
chitos	Chitosan
chol	Choline
chor	chorismate
cit	Citrate
citr-L	L-Citrulline
citr-L	L-Citrulline
clpn	Cardiolipin
cmp	CMP
cmusa	2-Amino-3-carboxymuconate semialdehyde
co2	Carbon dioxide
coa	Coenzyme A
cpppg3	Coproporphyrinogen III
csn	Cytosine
ctp	CTP
cys-L	L-Cysteine
cyst-L	L-Cystathionine
cytd	Cytidine
dad-2	Deoxyadenosine
dadp	dADP
damp	dAMP
dann	7,8-Diaminononanoate
datp	dATP
db4p	3,4-dihydroxy-2-butanone 4-phosphate
dca	Decanoate (n-C10:0)
dcaACP	Decanoyl-ACP (n-C10:0ACP)
dcacoa	Decanoyl-CoA (n-C10:0CoA)
dcamp	N6-(1,2-Dicarboxyethyl)-AMP
dcdp	dCDP
dcmp	dCMP

dctp	dCTP
dcyt	Deoxycytidine
ddca	Dodecanoate (n-C12:0)
ddcaACP	Dodecanoyl-ACP (n-C12:0ACP)
ddcacoa	Dodecanoyl-CoA (n-C12:0CoA)
dgdp	dGDP
dgmp	dGMP
dgsn	Deoxyguanosine
dgtp	dGTP
dha	Dihydroxyacetone
dhap	Dihydroxyacetone phosphate
dhf	7,8-Dihydrofolate
dhlam	Dihydrolipoamide
dhnpt	Dihydroneopterin
dhor-S	(S)-Dihydroorotate
dhpt	Dihydropteroate
din	Deoxyinosine
dkmpp	2,3-diketo-5-methylthio-1-phosphopentane
dmlz	6,7-Dimethyl-8-(1-D-ribityl)lumazine
dmpp	Dimethylallyl diphosphate
dnad	Deamino-NAD+
docosa	Docosanoic acid
docosaACP	Docosanoyl-ACP
docosacoa	Docosanoyl-CoA
dolichol	Dolichol
dolmanp	Dolichyl phosphate D-mannose
dolp	Dolichol phosphate
dpcoa	Dephospho-CoA
dscl	dihydrosirohydrochlorin
dtbt	Dethiobiotin
dtdp	dTDP
dtmp	dTMP
dttp	dTTP
dudp	dUDP
dump	dUMP
duri	Deoxyuridine
dutp	dUTP
e4hglu	L-erythro-4-Hydroxyglutamate

e4p	D-Erythrose 4-phosphate
eicosa	Eicosanoic acid
eicosaACP	Eicosanoyl - ACP
eicosacoa	Eicosanoyl-CoA
eicosapen	Eicosapentaenoic acid
eicosapenACP	Eicosapentanoyl - ACP
eicosapencoa	Icosapentaenoyl-CoA
eig3p	D-erythro-1-(Imidazol-4-yl)glycerol 3-phosphate
epist	episterol
ergst	Ergosterol
ergtetrol	Ergosta-5,7,22,24,(28)-tetraen-3beta-ol
ergtrol	ergosta-5,7,24(28)-trienol
etha	Ethanolamine
ethamp	Ethanolamine phosphate
etoh	Ethanol
f6p	D-Fructose 6-phosphate
fad	Flavin adenine dinucleotide oxidized
fadh2	Flavin adenine dinucleotide reduced
fdp	D-Fructose 1,6-bisphosphate
fe2	Fe2+
fecost	fecosterol
fgam	N2-Formyl-N1-(5-phospho-D-ribosyl)glycinamide
ficytb5	Ferricytochrome b5
ficytc	Ferricytochrome c
fmn	FMN
focytb5	Ferrocytochrome b5
focytc	Ferrocytochrome c
for	Formate
fpram	2-(Formamido)-N1-(5-phospho-D-ribosyl)acetamidine
fprica	5-Formamido-1-(5-phospho-D-ribosyl)imidazole-4-carboxamide
frdp	Farnesyl diphosphate
frmd	Formamide
fru	D-Fructose
fuc1p	L-Fuculose 1-phosphate
fum	Fumarate
g15lac	D-Glucono-1,5-lactone
g1p	D-Glucose 1-phosphate

g3p	Glyceraldehyde 3-phosphate
g3pc	sn-Glycero-3-phosphocholine
g3pi	sn-Glycero-3-phospho-1-inositol
g6p	D-Glucose 6-phosphate
gal	D-Galactose
gal14lac	D-Galactono-1,4-lactone
gal1p	alpha-D-Galactose 1-phosphate
gam6p	D-Glucosamine 6-phosphate
gar	N1-(5-Phospho-D-ribosyl)glycinamide
gcald	Glycolaldehyde
gcylcer	Glucosylceramide
gdp	GDP
gdpmann	GDP-D-mannose
ggdp	Geranylgeranyl diphosphate
glc-D	D-Glucose
glcn-D	D-Gluconic acid
gln-L	L-Glutamine
glu5p	L-Glutamate 5-phosphate
glu5sa	L-Glutamate 5-semialdehyde
gluala	5-L-Glutamyl-L-alanine
glucoa	Glutaryl-CoA
glucys	gamma-L-Glutamyl-L-cysteine
glu-L	L-Glutamate
glx	Glyoxylate
gly	Glycine
glyasn	Glycyl Asparagine
glyasp	Glycyl Aspartate
glyc	Glycerol
glyc3p	Glycerol 3-phosphate
glyclt	Glycolate
glycogen	glycogen
glygln	Glycyl Glutamine
glyglu	Glycyl Glutamate
glymet	Glycyl Methionine
glypro	Glycyl Proline
gmp	GMP
gp4g	P1,P4-Bis(5-guanosyl) tetraphosphate
grdp	Geranyl diphosphate

gsn	Guanosine
gthox	Oxidized glutathione
gthrd	Reduced glutathione
gtp	GTP
gua	Guanine
h	H+
h2o	H2O
h2o2	Hydrogen peroxide
h2s	Hydrogen sulfide
hco3	Bicarbonate
hcys-L	L-Homocysteine
hdca	Hexadecanoate (n-C16:0)
hdcea	Hexadecenoate (n-C16:1)
hdceaACP	Hexadecenoyl ACP
hdceacoa	Hexadecenoyl coA
hemeA	Heme A
hemeO	Heme O
hepdca	Heptadecanoate
hepdcaACP	Heptadecanoyl-ACP
hepdcacoa	Heptadecanoyl-CoA
hepdcea	Heptadecenoate
hepdceaACP	Heptadecenoyl-ACP
hepdceacoa	Heptadecenoyl-CoA
hexa	Hexanoate
hexaACP	Hexanoyl-ACP
hexacoa	Hexanoyl-CoA
hexc	hexacosanoate (n-C26:0)
hexcACP	Hexacosanoyl-ACP
hexccoa	Hexacosanoyl-CoA (n-C26:0CoA)
hexdp	all-trans-Hexaprenyl diphosphate
hgentis	Homogentisate
hibcoa	(S)-3-Hydroxyisobutyryl-CoA
hibut	(S)-3-Hydroxyisobutyrate
hicit	Homoisocitrate
his-L	L-Histidine
hisp	L-Histidinol phosphate
histd	L-Histidinol
hLkynr	3-Hydroxy-L-kynurenine

hmbil	Hydroxymethylbilane
hmgcoa	Hydroxymethylglutaryl-CoA
hmgth	hydroxymethylglutathione
hom-L	L-Homoserine
hpglu	Tetrahydropteroyltri-L-glutamate
hppcoa	3-Hydroxypropionyl-CoA
hxan	Hypoxanthine
hxdcal	Hexadecanal
iad	Indole-3-acetamide
iamoh	3-Methylbutanol
iamoh	3-Methylbutanol
iasp	Iminoaspartate
ibcoa	Isobutyryl-CoA
ibutoh	Isobutyl alcohol
icit	Isocitrate
id3acald	Indole-3-acetaldehyde
idp	IDP
ile-L	L-Isoleucine
imacp	3-(Imidazol-4-yl)-2-oxopropyl phosphate
imp	IMP
ind3ac	Indole-3-acetate
ind3acnl	Indole-3-acetonitrile
ind3eth	Indole-3-ethanol
indpyr	Indolepyruvate
inost	myo-Inositol
ins	Inosine
ipc124	Inositol phosphorylceramide, ceramide-1 (24C) (IPC24C)
ipc126	Inositol phosphorylceramide, ceramide-1 (26C)
ipc224	Inositol-phosphorylceramide-ceramide-2-24C
ipc226	Inositol phosphorylceramide, ceramide-2 (26C)
ipdp	Isopentenyl diphosphate
itp	ITP
ivcoa	Isovaleryl-CoA
k	potassium
L2aadp	L-2-Aminoadipate
L2aadp6sa	L-2-Aminoadipate 6-semialdehyde
lac-D	D-Lactate
lac-L	L-Lactate

lact	Lactose
lact	Lactose
lactcer	Lactosylceramide
lald-S	(S)-Lactaldehyde
lanost	Lanosterol
lcyst	L-Cysteate
leu-L	L-Leucine
Lfmkynr	L-Formylkynurenine
lgt-S	(R)-S-Lactoylglutathione
Lkynr	L-Kynurenine
lpam	Lipoamide
lys-L	L-Lysine
macrylcoa	Methacrylyl-CoA
madg	alpha-Methyl-D-glucoside
malACP	Malonyl-[acyl-carrier protein]
malcoa	Malonyl-CoA
mal-L	L-Malate
malt	Maltose
maltr	Maltotriose
man	D-Mannose
man1p	D-Mannose 1-phosphate
man1p	D-Mannose 1-phosphate
man2mi1p-D	D-Mannose Inositol Phosphate 2
man6p	D-Mannose 6-phosphate
manmi1p-D	D-Mannose Inositol Phosphate
mannan	Mannan
mbdg	beta-Methylglucoside
mcrocoa	3-Methylcrotonyl-CoA
meoh	Methanol
metala	Methionine-Alanine
methf	5,10-Methenyltetrahydrofolate
methf	5,10-Methenyltetrahydrofolate
met-L	L-Methionine
met-L	L-Methionine
mev-R	(R)-Mevalonate
mglutcoa	3-Methylglutaconyl-CoA
mhpglu	5-Methyltetrahydropteroyltri-L-glutamate
mi145tp-D	D-myo-Inositol 1,4,5-trisphosphate

mi14bp-D	D-myo-Inositol 1,4-bisphosphate
mi1p-D	1D-myo-Inositol 1-phosphate
micit	methylisocitrate
mip2c124	mannose-(inositol-P)2-ceramide, ceramide-1 (24C)
mip2c126	mannose-(inositol-P)2-ceramide, ceramide-1 (26C)
mip2c224	mannose-(inositol-P)2-ceramide, ceramide-2 (24C)
mip2c226	mannose-(inositol-P)2-ceramide, ceramide-2 (26C)
mipc124	mannose-inositol phosphorylceramide, ceramide-1 (24C)
mipc126	mannose-inositol phosphorylceramide, ceramide-1 (26C)
mipc224	mannose-inositol phosphorylceramide, ceramide-2 (24C)
mipc226	mannose-inositol phosphorylceramide, ceramide-2 (26C)
mlthf	5,10-Methylenetetrahydrofolate
mnl	D-Mannitol
msa	Malonate semialdehyde
mthgxl	Methylglyoxal
myrsACP	Myristoyl-ACP (n-C14:0ACP)
N1aspmd	N1-Acetylspermidine
N1sprm	N1-Acetylspermine
Na	Sodium
nac	Nicotinate
nad	Nicotinamide adenine dinucleotide
nadh	Nicotinamide adenine dinucleotide - reduced
nadp	Nicotinamide adenine dinucleotide phosphate
nadph	Nicotinamide adenine dinucleotide phosphate - reduced
ncam	Nicotinamide
nh4	Ammonium
nicrnt	Nicotinate D-ribonucleotide
nmn	NMN
o2	O2
oaa	Oxaloacetate
ocdca	octadecanoate (n-C18:0)
ocdcaACP	Octadecanoyl-ACP (n-C18:0ACP)
ocdcea	octadecenoate (n-C18:1)
ocdceaACP	octadecenoyl-ACP
ocdceacoa	octadecenoyl-coA
ocdcta	Octadecatrienoate
ocdctaACP	Octadecatrienoyl-ACP
ocdctacoa	Octadecatrienoyl-CoA

ocdcya	octadecadienoate (n-C18:2)
ocdcyaACP	Octadecynoyl-ACP (n-C18:2ACP)
ocdcyacoa	Octadecynoyl-CoA-n-C182CoA
octa	octanoate (n-C8:0)
octaACP	Octanoyl-ACP
octacoa	Octanoyl-CoA
opro-L	5-Oxoproline
orn	Ornithine
orot	Orotate
orot5p	Orotidine 5-phosphate
oxag	Oxaloglutarate
pa	Phosphatidate
pac	Phenylacetic acid
pacald	Phenylacetaldehyde
pad	2-Phenylacetamide
palmACP	Palmitoyl-ACP (n-C16:0ACP)
pan4p	Pantetheine 4-phosphate
pant-R	(R)-Pantoate
pap	Adenosine 3,5-bisphosphate
paps	3-Phosphoadenylyl sulfate
pc	Phosphatidylcholine
pdx5p	Pyridoxine 5-phosphate
pe	phosphatidylethanolamine
pendp	all-trans-Pentaprenyl diphosphate
pep	Phosphoenolpyruvate
pg	Phosphatidylglycerol
pgp	Phosphatidylglycerophosphate
phe-L	L-Phenylalanine
pheme	Protoheme
phom	O-Phospho-L-homoserine
phpyr	Phenylpyruvate
pi	Phosphate
pmtcoa	Palmitoyl-CoA (n-C16:0CoA)
pnto-R	(R)-Pantothenate
ppACP	Propanoyl-ACP
ppbng	Porphobilinogen
ppcoa	Propanoyl-CoA
ppecoa	Propenoyl-CoA

pphn	Prephenate
ppi	Diphosphate
ppp9	Protoporphyrin
pppg9	Protoporphyrinogen IX
pppi	Inorganic triphosphate
pram	5-Phospho-beta-D-ribosylamine
pran	N-(5-Phospho-D-ribosyl)anthranilate
prbamp	1-(5-Phosphoribosyl)-AMP
prbatp	1-(5-Phosphoribosyl)-ATP
prfp	1-(5-Phosphoribosyl)-5-[(5-phosphoribosylamino)methylideneamino]imidazole-4-carboxamide
prlp	5-[(5-phospho-1-deoxyribulos-1-ylamino)methylideneamino]-1-(5-phosphoribosyl)imidazole-4-carboxamide
pro-L	L-Proline
prpp	5-Phospho-alpha-D-ribose 1-diphosphate
ps	phosphatidylserine
pser-L	O-Phospho-L-serine
psph1p	Phytosphingosine 1-phosphate
psphings	Phytosphingosine
ptd134bp	phosphatidyl-1D-myo-inositol 3,4-bisphosphate
ptd145bp	1-Phosphatidyl-D-myo-inositol 4,5-bisphosphate
ptd1ino	phosphatidyl-1D-myo-inositol
ptd2meeta	Phosphatidyl-N-dimethylethanolamine
ptd3ino	1-Phosphatidyl-1D-myo-inositol 3-phosphate
ptd4ino	1-Phosphatidyl-1D-myo-inositol 4-phosphate
ptdmeeta	Phosphatidyl-N-methylethanolamine
ptrc	Putrescine
pyam5p	Pyridoxamine 5-phosphate
pydam	Pyridoxamine
pydx	Pyridoxal
pydx5p	Pyridoxal 5-phosphate
pydxn	Pyridoxine
pyr	Pyruvate
q6	Ubiquinone-6
q6h2	Ubiquinol-6
quln	Quinolinate
r1p	alpha-D-Ribose 1-phosphate

r5p	alpha-D-Ribose 5-phosphate
rbl-D	D-Ribulose
rbt	Ribitol
rham-L	L-Rhamnose
rhamlac	L-Rhamnono-1,4-lactone
rhamn	L-Rhamnonate
rib-D	D-Ribose
ribflv	Riboflavin
ribu-D	D-Ribulose
rnam	N-Ribosylnicotinamide
ru5p-D	D-Ribulose 5-phosphate
s	Sulfur
s7p	Sedoheptulose 7-phosphate
saccrp-L	L-Saccharopine
sbt-D	D-Sorbitol
sbt-L	L-Sorbitol
scl	sirohydrochlorin
ser-L	L-Serine
Sfglutth	S-Formylglutathione
sheme	Siroheme
skm	Shikimate
skm5p	Shikimate 5-phosphate
so3	Sulfite
so4	Sulfate
sph1p	Sphinganine 1-phosphate
sphgn	Sphinganine
spmd	Spermidine
spmylin	Sphingomyelin
sprm	Spermine
sql	Squalene
srb-L	L-Sorbose
Ssq23epx	(S)-Squalene-2,3-epoxide
stcoa	Stearoyl-CoA (n-C18:0CoA)
succ	Succinate
succoa	Succinyl-CoA
succsal	succsal[m]
suchms	O-Succinyl-L-homoserine
sucr	Sucrose

taur	Taurine
tdcoa	Tetradecanoyl-CoA (n-C14:0CoA)
thf	5,6,7,8-Tetrahydrofolate
thfglu	Tetrahydrofolyl-[Glu](2)
thm	Thiamin
thmpp	Thiamine diphosphate
thmtp	Thiamin triphosphate
thr-L	L-Threonine
thym	Thymine
thymd	Thymidine
tmp	Trimetaphosphate
trdox	Oxidized thioredoxin
trdrd	Reduced thioredoxin
tre	Trehalose
tre6p	alpha,alpha-Trehalose 6-phosphate
triglyc	triglyceride
trp-L	L-Tryptophan
ttc	tetracosanoate (n-C24:0)
ttcACP	tetracosanoyl-ACP
ttccoa	tetracosanoyl-CoA (n-C24:0CoA)
ttdca	tetradecanoate (n-C14:0)
tyr-L	L-Tyrosine
uacgam	UDP-N-acetyl-D-glucosamine
udp	UDP
udpg	UDPglucose
udpgal	UDPgalactose
ump	UMP
up4u	P1,P4-Bis(5-uridyl) tetraphosphate
uppg3	Uroporphyrinogen III
ura	Uracil
urate	Uric acid
urdglyc	Ureidoglycolate
urea	Urea
uri	Uridine
utp	UTP
val-L	L-Valine
xan	Xanthine
xmp	Xanthosine 5-phosphate

xp4x	P1,P4-Bis(5-xanthosyl) tetraphosphate
xtp	XTP
xtsn	Xanthosine
xu5p-D	D-Xylulose 5-phosphate
xyl-D	D-Xylose
xylt	Xylitol
xylu-D	D-Xylulose
xylu-L	L-Xylulose
zym_int1	zymosterol intermediate 1
zym_int2	zymosterol intermediate 2
zymst	zymosterol